TECHNISCHE UNIVERSITÄT WIEN

Dissertation

Custom made Inclusion Bodies: Effects on Quality Attributes by Variation of Critical Process Parameters and Control Strategies

ausgeführt zur Erlangung des akademischen Grades eines Doktors der Technischen Wissenschaften unter der Leitung von

Prof. Dr. Christoph Herwig

am

Institut für Verfahrenstechnik, Umwelttechnik

und Technische Biowissenschaften (E-166)

eingereicht an der Technischen Universität Wien

Fakultät für Technische Chemie

von

Christoph Slouka

00425112

Mautner-Markhofgasse 58/405

1110 Wien

Wien, 31.10.2018

Erklärung zur Verfassung dieser Arbeit:

Hiermit erkläre ich, dass ich diese Arbeit selbstständig verfasst, alle verwendeten Quellen und Hilfsmittel vollständig angegeben habe und Stellen der Arbeit - einschließlich Tabellen, Karten und Abbildungen -, die andere Werken oder dem Internet im Wortlaut oder Sinn entnommen sind, auf jeden Fall unter Angabe der Quelle als Entlehnung kenntlich gemacht habe.

_____

Christoph Slouka

Abstract (en)

E. coli is the host of choice for about 30% of the worldwide production of recombinant pharmaceuticals. In a multitude of processes, recombinant proteins are expressed as inclusion bodies (IB) in *E. coli* - an (in)active aggregate of misfolded produced protein. Respective IB Quality attributes (QA) should ideally be modified by the cultivation conditions in the upstream process as they have severe impact on the performance of the subsequent process chain, like the centrifugation or refolding unit operations. However, only a very few studies deal with the general quality attributes of IBs.

The goal of this work was to create a process development platform for an industrial relevant recombinant produced protein, produced as IB in *E. coli*. The work followed a three-step approach according to the generally known and accepted process development cycle:

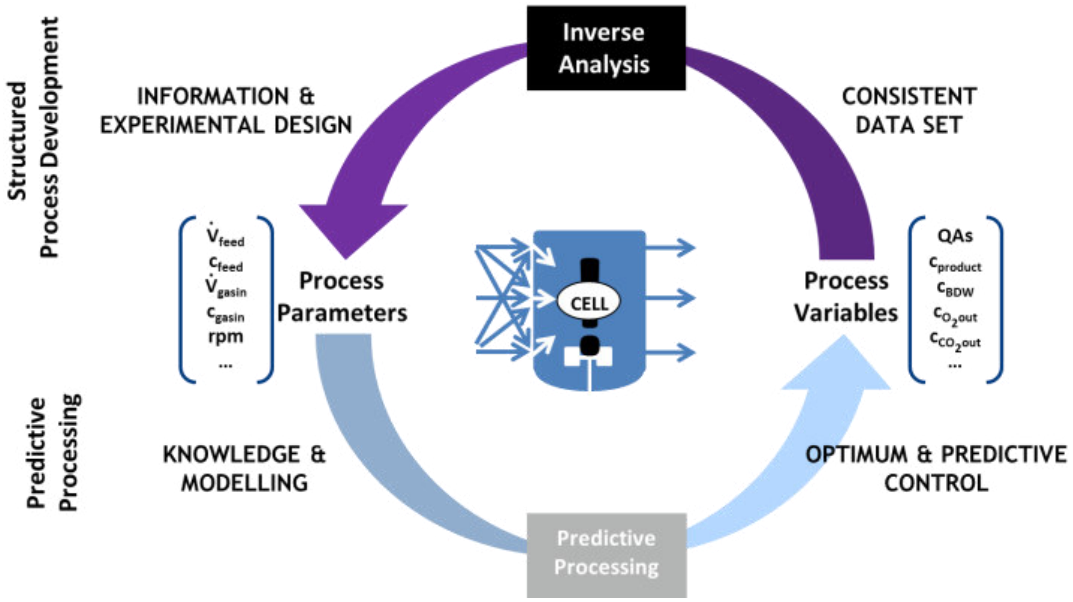

In the first step we aimed for understanding the impact of process parameters on different IB quality attributes. We performed a quantitative process development based on the interaction of different IB QAs like size, titer and purity and their interactions on critical process parameters temperature, pH and specific growth rate (q_s). These were altered using design of experiment (DoE) approaches and analyzed with different analytical techniques, like SEM, Bioanalyzer based chip technology and HPLC. QAs were monitored as a function of induction time and analyzed in

a time resolved manner. It was shown, that different QAs already showed a strong time dependence within a single cultivation run and were highly correlated to each other.

In the second step the knowledge on the interactions onto IB quality attributes was used to develop physiological control strategies to obtain optimized titer and size during the process. With trigger indicators like the cumulative sugar uptake, we were able to receive custom made IBs with optimized performance for further process steps.

In the third step we established a process analytical tool for stable processing. As product degradation in the investigated process was also accompanied or caused by decrease in viable cell concentration, we aimed for direct determination of the viable cell concentration during the cultivations. The developed sensor is based on electrochemical impedance spectroscopy in the low frequency regime and tested on different model microorganism like *E. coli* and *S. cerevisiae*.

The different parts - starting with analytical techniques for IB quality attribute determination, control of the IB production process and advances in process analytical tools - sum up to an overall closing of the process development cycle for the given product and could be seen as overall achievement of this work. The given platform knowledge of IB based cultivations may help to facilitate further process developments for new IB based products in *E. coli* and result in a robust downstream processing.

Abstract (de)

Das gram-negative Bakterium *E. coli* wird als Expressionssystem für ungefähr 30 % der weltweiten Produktion an biopharmazeutischen Wertstoffen genutzt. In einer Vielzahl an benutzen Prozessen wird das Protein in Form von Einschlusskörpern (Inclusion Bodies - IBs) exprimiert. IBs sind ungefaltete hydrophobe Aggregate an produziertem Protein. Eigenschaften von IBs können über Prozesssteuerung während der Kultivierung verändert werden und haben dementsprechend einen hohen Einfluss auf nachfolgende Prozessschritte in der Proteinreinigung und Veredelung. Bis dato wurden diese Einflüsse der Kultivierung auf die Eigenschaften der IBs nur rudimentär untersucht.

In dieser Arbeit wird eine Produktentwicklung für ein rekombinant produziertes Protein vorgestellt, welches in *E. coli* ausschließlich als IB exprimiert wird. Die Arbeit wurde in drei Arbeitspaketen durchgeführt, welche sich am allgemein bekannten Prozessentwicklungskreislauf orientieren.

Im ersten Teil wurde der Einfluss von klassischen und physiologischen Prozessparametern auf IB Qualitätsattribute (QA) behandelt. Größe, Menge und Reinheit wurden abhängig von pH und Temperatur und Substratfütterungsrate in einem Experimentaldesign (design of experiments - DoE) während der Produktionsphase adaptiert und mittels verschiedener analytischer Methoden (z.B REM, Bioanalyzer basierende Chip Technologien) gemessen. Es wird gezeigt das IB-QAs sich schon während der Kultivierungsdauer zeitabhängig stark verändern und eine hohe Korrelation aufweisen.

Diese Resultate wurden im zweiten Teil benutzt um eine physiologische Kontrollstrategie zu etablieren, vor allem um IB Größe und Titer zu optimieren. Mit abgeleitetem Parameter wie der kumulative Zuckeraufnahmewert war es möglich „maßgeschneiderte“ IBs zu produzieren.

Der dritte Teil basiert auf Etablierung Prozessanalytischer Werkzeuge (PAT) um stabile Prozessführung zu garantieren. Da Produktdegradation hauptsächlich auf die Reduktion der viablen Zellen zurückzuführen ist, wurde ein Sensor zu dessen Abschätzung entwickelt. Dieser funktioniert auf Basis elektrochemischer Impedanzspektroskopie im niederfrequenten Bereich und wurde für verschiedene Modellorganismen, *E. coli* und *S. cerevisiae*, getestet.

Die verschiedenen Teile – beginnend mit der Etablierung analytischer Techniken um IB Qualitätsattribute zu bestimmen, Kontrollstrategien um diese zu steuern und Neuerungen für Prozessanalytische Werkzeuge – schließen im Großen und Ganzen die verschieden Teile des Prozessentwicklungskreislaufs und können daher als grundlegende Leistung dieser Arbeit gesehen werden. Das so generierte Plattformwissen für IB basierende Prozesse hilft für neue Prozessentwicklungen in diesem Bereich maßgeblich zu vereinfachen und garantiert stabile Bedingungen für weiterführende Prozessschritte im Downstream.

Table of contents

1. Introduction 5

1.1. Applications of Inclusion Body based Technologies 7

Inactive vs active IBs for high value products 7

IB treatment by homogenisation and solubilization: Differences based on expression 9

Direct application of IBs 11

1.2. Analytics of IB quality attributes (IB-QAs) 12

Size and Purity as QAs for the downstream processing 12

Protein Activity as QA 14

Catalytic Activity as QA 14

1.3. Impact of the Upstream processing on IB QAs 15

Impact of induction system on IB QAs 15

QAs affected by Classical and Physiological Process parameters 16

Effects of process parameters on QA activity 18

1.4. Discussion 19

1.5. Conclusions 22

1.6. Industrial need and scientific questions of this thesis 24

2. Custom Made Inclusion Bodies: Impact of classical process parameters and physiological parameters on Inclusion Body quality attributes 26

2.1. Background 26

2.2. Methods 29

Strains 29

Bioreactor cultivations 29

Cultivation Analytics 32

Product Analytics 33

2.3. Results and Discussion 37

Impact of classical process parameters on IB QAs using strain 1 (N-Pro fused protein) 38

Secondary structure analysis of IBs exhibiting different size 44

Validation of the impact of classical process parameters on IB QAs using strain 2 45

Impact of the physiological process parameter $q_{s,Glu}$ on IB quality attributes of strain 1 (N-Pro fused protein) 48

2.4. Conclusions 50

2. Impact of glycerol as carbon source onto specific sugar and inducer uptake rates and inclusion body productivity in E. coli BL21(DE3) *52*

3.1. Introduction 52

3.2. Material and Methods 55

Bioreactor cultivations 55

Cultivation scheme and q_s screening procedure 56

Process analytics 57

3.3. Results and Discussion 60

Mechanistic correlations of glycerol onto specific lactose uptake rate 60

Productivity and physiology using glycerol as primary carbon source 67

3.4. Conclusions 70

4. Control Strategies for Production of Recombinant Proteins based on the Cumulative Sugar Uptake and the Oxygen Uptake rate *72*

4.1. Introduction for Titer as Key Performance Indicator 72

4.2. Material and Methods for Titer Determination 75

Bioreactor cultivations 75

Cultivation scheme and q_s adaption 76

Process analytics 77

Product Analytics 78

Modelling of process parameters and KPIs 79

4.3. Results and Discussion for Titer as KPI 80

Static $q_{s,C}$ feeding strategies 80

Offline dSn controlled feeding strategies 84

Oxygen Uptake Rate as online trigger for determination of transition for dSn controlled cultures 87

Model based approach for prediction of IB titer as KPI 89

4.4. Conclusion 92

4.5. Introduction Size as QA 94

4.6. Material and Methods Size as QA 97

4.7. Results and Discussion for Size as QA 98

Static $q_{s,C}$ feed forwards feeding for size determination 98

Model based approach for prediction of IB bead size 102

4.8. Conclusions 106

5. Determination of Viable Cell Concentrations (VCC) using Electrochemical Sensors in the Low Frequency Regime 107

5.1. Introduction 110

5.2. Materials and Methods 113

Expression host and Cultivation 113

Analytical procedures 114

Impedance Measurements 114

Inline probe construction 115

5.3. Results and Discussion 116

Aerobic and anaerobic batch cultivations in defined media monitored in online mode 116

Raw data and general considerations 117

Aerobic cultivations 119

Anaerobic cultivations _____ 120

Aerobic and anaerobic cultivations in defined media using the new inline probe _____ 123

Aerobic growth of yeast on complex malt extract medium _____ 126

5.4. Conclusions _____ 129

6. Conclusion and Outlook _____ 130

6.1. Scientific questions _____ 130

6.2. Outlook: Triggers to enable continuous upstream processing _____ 132

Supplementary Material _____ 133

Abbreviations _____ 137

Captions _____ 138

Literature _____ 144

Appendix: Original Manuscripts _____ 153

1. Introduction

This chapter is based on a minireview in Applied Microbiology and Biotechnology Journal. The chapter gives an overview to Inclusion Body based processes, the appropriate analytics and the impact on process design and should serve as introduction chapter to this thesis. It is submitted to **AMB journal** as **Mini-Review:**

The first steps for recombinant protein expression have been made back in 1973, where Stanley Cohen and Herbert Boyer invented the possibility of in vitro DNA-cloning (Cohen, et al., 1973, Baeshen, et al., 2014). This opened the door for the expression of multiple diverse molecules. The first recombinant pharmaceutical product was insulin, licensed back in 1982 (Baeshen, et al., 2014). Today the main focus of pharmaceutical market remains on the production of monoclonal antibodies, diverse hormones as well as growth factors, which turn out to be the majority of the pharmaceutical income (Walsh, 2004, Baeshen, et al., 2014, Baeshen, et al., 2015).

Although complex recombinant proteins are mainly produced in mammalian cells, a good number of proteins is still expressed in *E. coli* (Walsh, 2014). Production of proteins in eukaryotic cells such as mammalian cells and yeasts has the big advantage of enabling diverse proper post translational glycosylation patterns, while there is no glycosylation machinery in active *E.* coli cells (Gupta and Shukla, 2016). Recently published papers referred that the production of biopharmaceutical proteins in *E. coli* moved up to a number as high as 40 % (Walsh, 2010, Gupta and Shukla, 2016). Protein production in *E. coli* gained importance again as the demand in single chain antibody-fragments, which can be successfully expressed in *E. coli*, increased (Spadiut, et al., 2013). *E. coli* is most likely the cheapest organism to cultivate, though its products lack in quality and therefore take long durations and efforts when it comes to product purification (Berlec and Strukelj, 2013). However, the genome of *E. coli* is known very well (Huang, et al., 2012) and *E. coli* shows very fast replication rates, resulting in high cell densities (Murarka, et al., 2007, Sahdev, et al., 2007). Also cultivations can be carried out on comparatively cheap media, coupled

with little risk of contamination compared to other cultivation hosts (DeLisa, et al., 1999). In addition, scale-up can be quite easily performed in recombinant protein production, using *E. coli*, when compared to other organisms (Gupta and Shukla, 2016). Even secretion of a complete immune globulin G in *E. coli* has already been reported, though the antibody was lacking any glycosylation (Gupta and Shukla, 2016). Summing up, protein production using *E. coli* as a host, provides a very useful alternative to mammalian cell cultivations (Baeshen, et al., 2015), as yields up to 4 g/L of soluble antibody fragments have been referred already (Gupta and Shukla, 2016).

The vast majority of recombinant proteins in *E. coli* are expressed in Inclusion Bodies (IBs). Despite general benefits are given in the USP IB-processing, the DSP and especially the refolding unit operation is still creating the bottleneck in an IB - process. It suffers in robustness and relatively low product yields (Singh and Panda, 2005). The refolding operation is the most time-consuming step in gaining the correctly folded product from *E. coli* cultivations (García-Fruitós, et al., 2012, Palmer and Wingfield, 2012, Ramón, et al., 2014, Villaverde, et al., 2015). A high number of studies today deal with the refolding process and to improve performance using different methodological approaches (Altamirano, et al., 1997, Liu, et al., 2005, Yamamoto, et al., 2010, Palmer and Wingfield, 2012, Mollania, et al., 2013, Wingfield, 2014, Wingfield, et al., 2014, Yamaguchi and Miyazaki, 2014, Singh, et al., 2015, Eggenreich, et al., 2016, Gabrielczyk, et al., 2017).

Beside the classical aim to produce high amount of protein or even toxic intermediates, recent development showed that the application range of IBs is far wider than to be expected at first glance. New approaches towards usage as biocatalysts and as nanoparticulate matter are emerging. These developments make the production of active IBs and their physical properties even more important compared to the classical usage. In the last decade the term of non-classical IBs (ncIBs) – IBs with residual protein activity– was widely used in literature (García-Fruitós, 2010). However, many studies in the recent years show that there is no distinct borderline between classical and non-classical IBs anymore, especially visible during solubilization experiments. Different approaches during strain development and especially cultivation makes it

possible to adapt protein activity and other quality attributes in the respective IB to a certain extend. In this review we want to address the impact of process parameters on different quality attributes (QAs) of IBs. Different IB producing concepts are presented in the beginning and subsequently the used analytics is compared. Following topics are therefore addressed: i) An overview of the range of Inclusion Body applications; ii) analytical methods to determine quality attributes and iii) screws in process engineering to achieve the desired quality attributes for different Inclusion Body based applications.

1.1. Applications of Inclusion Body based Technologies

Inclusion bodies have originally been believed to be waste products by bacteria (García-Fruitós, et al., 2012), until it was realized that they are formed as a stress reaction by the cells resulting in a biologically inactive precipitated protein (Palmer and Wingfield, 2012, Ramón, et al., 2014, Villaverde, et al., 2015). Protein aggregation is a complex reaction, as aggregates are only formed within the same kind of proteins or highly similar proteins (Singh, et al., 2015). Figure 1 presents the general route of IB production with link to the downstream, respectively.

Inactive vs active IBs for high value products

Generally, approaches to express active soluble protein in *E. coli* yield a high amount of IBs as 'by-product'. In the last years the notion of IBs as unwanted by-product changed fundamentally in case of high value pharmaceutical products. *E. coli* attracted again notice as fragmented antibodies (fABs) could be successfully expressed in the periplasm or produced in high concentration as IBs (Spadiut, et al., 2014). IB based processes enable not only a high production of the desired pharmaceutical ingredient, but also makes it possible to express toxic proteins within the cell as no enzyme activity is given in classical IBs. Combined with the fact that IBs can

be produced in that high excess (so that the amount of generated product often outweighs the DSP efforts), IB based processes are believed to fundamentally boost time/space yields for recombinant protein production (García-Fruitós, et al., 2012, Berlec and Strukelj, 2013, Baeshen, et al., 2015, Gupta and Shukla, 2017). Many recent studies show that IBs consist of up to 50% correctly folded protein in contrast to the general perception of IBs as inactive structures (Jevševar, et al., 2005, Peternel, et al., 2008). Already in studies in the late 80ies IBs were already recognised to inherit residual activity when expressed at certain conditions (Worrall and Goss, 1989, Tokatlidis, et al., 1991). The mind-set in producing IBs changed, as it was shown in a multitude of studies that IBs have a high amount of active protein being highly functional (Hrabárová, et al., 2015). Enzyme tests within this study revealed, that IB-fraction provides high activity in classical enzyme assays when being compared to soluble (correctly folded) fractions. Trying to achieve high enzyme activity it was proposed to create highly dense and pure IB-fractions (García-Fruitós, 2010). Ling et al (Ling, et al., 2015) present approaches towards expression of papain-like cysteine proteases. Different protocols are compared in order to achieve high amounts of active protein. However, no satisfactory process could be established yet. Kischnick et al. (Kischnick, et al., 2006) produced major wasp allergen antigen 5 in an IB process for an industrial based application. Gundinger and Spadiut (Gundinger and Spadiut, 2017) produced recombinant HRP in *E. coli* with optimized conditions for soluble protein (pET39b$^+$ using SRP translocation pathway) and for IBs (pET21d$^+$). Yield and activity of the refolded IB product were outstanding better than the active translocated product (20 times in yield, 5 times in activity). A similar approach was performed by Jong et. al (Jong, et al., 2017) aiming for expression of a human epidermal growth factor (hEGF) into the periplasmic space. No translocation was observed but the construct of ssTorA/hEGF (including multiple repeats of TorA) boosts IB formation in the cytoplasmic space and resulted in high yields of the desired product in the cells. Fusion tags linked to the protein of interest often favour the expression of the desired protein as IB. The N^{Pro} fusion tag (N-terminal autoprotease derived from classical swine fever virus) by Achmüller et al. (Achmüller, et al., 2007) not only pulls the protein to IBs, put also

makes capture of the protein very easy. Furthermore, the fusion tag guarantees an authentic N-terminus of the protein after cleavage.

IB treatment by homogenisation and solubilization: Differences based on expression

The challenge of IBs in *E. coli* lies in cell disruption and inherent capture of the product IB and also effects QAs, respectively. High content of impurities (especially endotoxins of *E. coli*) make the DSP challenging and cost/time consuming. The key unit operations before the downstream processing lies in homogenization and solubilization (**Figure 1**). In general, a trade-off between purity, homogenization efficiency and loss of IB product titer has to be considered.

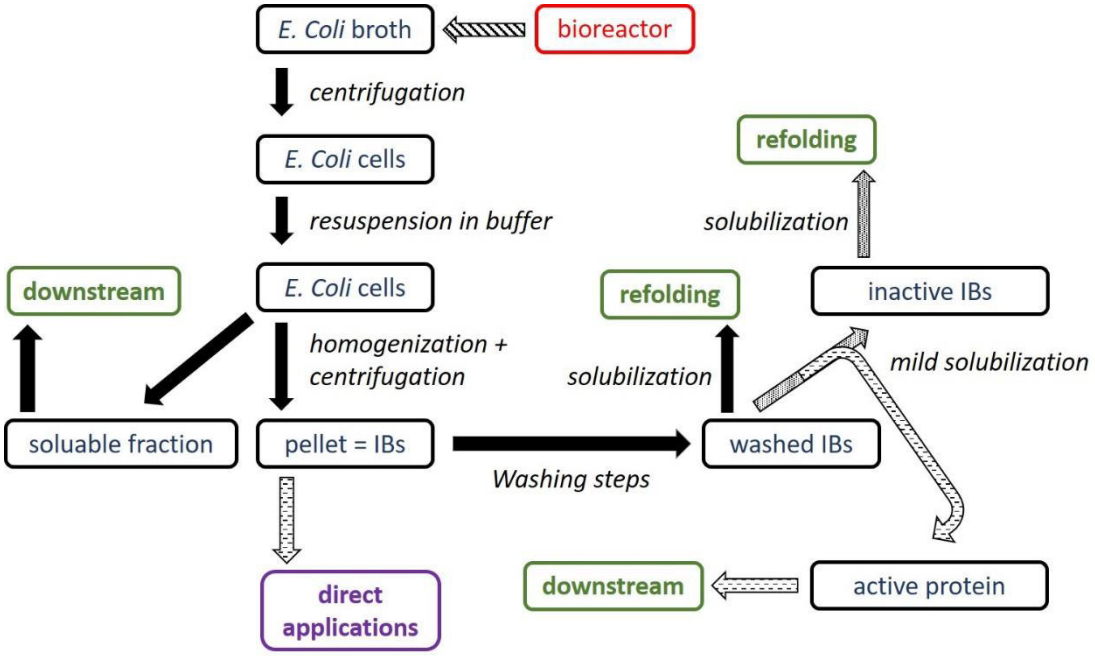

Figure 1: Workflow of IB production with link to different further used process steps during upstream and downstream.

The solubilization of the IB after cell disruption and washing is a key parameter for the refolding step. Cell disruption tends to be the main cause for impurities in recombinant protein, especially in IBs, since hydrophobic substances, especially membrane proteins, of the host cell tend to accumulate at the surface of these structures. A general overview of outer membrane proteins in

E. coli including mass, isoelectric point and hydrophobicity was measured with 2-D gel electrophoresis and subsequent MALDI-ToF SIMS (Molloy, et al., 2000). Rodriguez-Carmona et. al (Rodríguez-Carmona, et al., 2010) compared a multitude of different homogenization protocols for IB recovery, focused on the recovery of pure cell-free IBs. No single homogenization procedure was accordingly successful to disrupt all living bacterial cells. In this study a novel combination of sonication-lysozyme treatment with DNase and detergent washing steps was developed in order for direct use for IBs for biomaterials or biomedical applications. Effects of different cell disruption techniques on protein solubility were also studied by Peternel and Komel (Peternel and Komel, 2010). Enzymatic release using lysozyme (2.5 mg/mL) resulted in highly impure samples as lysozyme could not be removed from the surface of the IBs subsequently. Mechanical cell disruption using sonification and high-pressure homogenization yields better results than enzymatic release. However, a higher loss of protein is visible during sonication compared to high-pressure homogenization. Therefore, in industrial applications high pressure homogenization, with low loss of protein and lower amount of impurities, is the method of choice. In contrast to classical disruption technique alternative phage ϕX174-derived lysis system using protein E was investigated by Ehrgartner et. al. (Ehgartner, et al., 2017) producing the recombinant human bone morphogenetic protein 2 as IB. Best results could be obtained using low specific growth rate in the induction phase, yielding lysis values higher than 90 %. Purity is about 10 % lower compared to high pressure homogenization.

Active structures of IBs could be extracted by mild solubilization techniques recently presented in literature. While state of the art solubilization techniques generally use a high concentrated amount of chaotropic substances, like urea of guanidium hydrochloride to completely dissolve all protein structures for further processing steps, mild solubilization relies on different chemicals (Singh, et al., 2015). These mild solubilization techniques are able to extract this active amount and increase the recovery during the downstream process for highly pure protein. Jevševar et. al (Jevševar, et al., 2005) produced an human granulocyte-colony stimulating factor (hG-CSF) and isolated active fraction of the IBs by applying non-denaturating agents like 0.2% N-lauroyl-

sarcosine. Also, low concentrations of polar substances like DMSO are able to extract up to 45 % of the active inclusion body fraction. Qi et. al. (Qi, et al., 2015) combined mild solubilization at using a solubilization buffer containing 2 M urea at alkalic pH after freeze-thawing at -20°C. Activity of the mild solubilized protein was increased by a factor of 2 compared to the classical solubilization method. Wang et al. (Wang, et al., 2015) used a different method for receiving active protein out of IBs. The amino acid sequence consisted of a mutated intein performing self-cleavage on the N terminus upon addition of DTT. Two tested proteins lipA and AMA had a recovery of 58.6 % and 20.6 %. For AMA the majority of the protein stayed within the aggregate despite cleavage efficiency of about 60%. Since all QAs of IBs are affected by these steps' optimization is of utmost importance to guarantee product quality.

Direct application of IBs

Beside the pharmaceutical applications, IBs recently came into focus upon establishment of bio-scaffolds for mammalian cell orientation. Not only an improved adhesion of the cells is desired but also delivering active proteins to the cells is possible (Rodríguez-Carmona and Villaverde, 2010). Seras-Franzoso et al. (Seras-Franzoso, et al., 2013) used IBs based on human growth hormone or human chaperons for growth stimulation. These nano-active materials are supposed to release active substances in the cytoplasm and the nuclear compartments of the cells, referred as nanopills. After expression and washing steps catalytic active IBs could be directly used as catalysator for different synthesis steps often in combination with entrapment of the produced IBs. Sans et al. (Sans, et al., 2012) expressed fuculose-1-phosphate aldolase in E. coli. The produced IBs showed activity (in the best-case cultivation with optimized media and strain) similar to the soluble fraction. Entrapped IBs (Lentikat particles) could be successfully used as active immobilized biocatalysts. Nahálka et al. (Nahálka, et al., 2008) produced IBs fused to a cellulose binding domain of Clostridium cellulovorans for sialic acid synthesis. The fusion with CBM effectively promoted the aggregation of inclusion bodies in the place of soluble protein. A stable

catalytic activity over 20 circles was given using the immobilized encapsulated IB. Han et. al. (Han, et al., 2017) presented that IBs could be used as active centres for metabolic engineering in E. coli. Heterologous enzymes for production of 1-butanol in combination with carbon binding domain interacting through a leucine zipper motive (prey-bait system) yielded in active IB for 1-butanol production even in vivo. The yield of 1-butanol production in E. coli could be increased by 1.5-fold using batch fermentation approaches. Infrared measurements showed, that these IBs are consisted of a β-sheet region and generally show "amyloid-like structures" (García-Fruitós, et al., 2011, Villaverde, et al., 2015).

1.2. Analytics of IB quality attributes (IB-QAs)

Different industrial aims and applications impose very variable needs of the quality of the produced inclusion bodies. The quality of a pharmaceutical product has to be very high and the effects of the upstream on the downstream are an important factor. In contrast, IB for biocatalyst need to have a high activity combined with mechanical stability during the given process. We want to address differences in the quality attributes and their measurement based on the technological application.

Size and Purity as QAs for the downstream processing

Physiological parameters like size and morphology are of high importance for further processing steps in the downstream process (DSP) especially for the classical IB manufacturing chain. Quality attributes for IBs have already been defined in several studies (García-Fruitós, et al., 2012, Reichelt, et al., 2017, Reichelt, et al., 2017, Wurm, et al., 2017). First approaches towards IB sizing during the induction phase were already made by Reichelt et al. (Reichelt, et al., 2017) using transmission electron microscopy in combination with nanoparticle tracking analysis and

revealed general trends of IB growth during cultivation. Expression of GFP as IB by (Wurm, et al., 2017) showed a strong correlation between induction strength (specific lactose feeding rate) and IB size and IB titer. Increase in lactose amount drastically increased the IB size during cultivation. Generally, saturation in IB size is observed around 700 nm depicting the limit of IB growth inside *E. coli*. A maximum size of 600 nm was found for the GFP-model protein. Others report IB sizes between 502 nm for DnaK, IBs and 580 nm for ClpA-IBs (Díez-Gil, et al., 2010) and approximately 600 nm for G-CSF IBs (Peternel, et al., 2008). As inclusion body formation is a highly time-dependent process, IB-size can be triggered via harvest time point alteration (Rinas, et al., 2017). New results of our work show a strong dependence of quality attributes on pH, T and process time (Slouka Christoph, 2018).

High purity is generally found at large IB size, which indicates that the surface to volume ratio is very important in receiving purer products. It is believed that major concentration impurities are a result of host cell fragments upon cell disruption. As IB-formation is very specific process for each target protein, the purity patterns for IBs might be highly different. As aggregated proteins might contain different host cell proteins, as wells as RNA fragments, it is extremely important to purify theses contents of the desired protein (Singh, et al., 2015). As IBs show very bad solubility in water, polar washing procedures may help to increase purity patterns (Fahnert, et al., 2004). Addition of diverse detergence (such as Triton X-100) in low concentrations might additionally solubilize outer membrane proteins therefore increasing the IB-fraction (Clark, 2001). Such differentiation can generally made using attenuated total reflectance Fourier-transformed infrared spectroscopy (ATR-FTIR) measurements, SDS-PAGE gels or even using MALDI-ToF analysis (Molloy, et al., 2000).

Protein Activity as QA

Knowledge on the amount of active protein or enzymatic activity of the IB is of high interest for the cultivation and further processing steps. In general, GFP model proteins, known to inherit protein activity, are tested using fluorescence-based methods. These could be used as integral techniques measuring the entire fluorescence of an IB sample, e.g. on a plate reader-based technique, or using fluorescence microscopy-based techniques for detailed description of the IB inside the cell (García-Fruitós, et al., 2007, Govers, et al., 2014). García-Fruitós et al. (García-Fruitós, et al., 2007) showed based on confocal microscopy that protein activity is not homogenously distributed within the structure of an IB. Peternel et al. (Peternel, et al., 2009) used a multitude of different techniques for description of the overall IB quality and the activity. Purity of the soluble fraction as well as of the IB samples were measured using classical SDS-Page techniques. Folding quality was determined using circular dichroism (CD). Peternel et al. (Peternel, et al., 2008) used similar extraction buffers for mild homogenisation with 0.2% N-lauroyl-sarcosine for four different products and subsequently measured biological activity of all fractions with infrared spectroscopy (IR) in the amid I and amid II region. Jevševar et. al (Jevševar, et al., 2005) also used IR for determination of structural activity in their produced protein. Biological activity could be found in all IB samples but differed greatly depending on the protein. However, very low solubility of the active part of these proteins was observed using the described mild solubilization method (shortly presented in the previous chapter), indicating that solubilization and protein activity in ncIBs was highly dependent onto the product.

Catalytic Activity as QA

Enzymatic conversion activity can be used to show the activity of the IB as biocatalysts. Photometric analysis of IB activity was used by Sans et. al (Sans, et al., 2012) measuring the

dihydroxyacetone phosphate salt using an UV/VIS photometer. Other metabolites during the reaction were determined using online HPLC methods. Nahálka et al. (Nahálka, et al., 2008) measured conversion kinetics by means of flow calorimeter techniques. After calibration using HPLC the conversion efficiency could be directly detected via a voltage signal of the thermistor.

1.3. Impact of the Upstream processing on IB QAs

A very broad range of proteins is produced as IB for high concentrations of the desired product or due to the use of IBs as biomaterials or biocatalysts as also presented in the first part (Villaverde, et al., 2015, Rinas, et al., 2017). Generally, stress due to strong overexpression of foreign DNA (Fahnert, et al., 2004) in combination with a slow folding machinery is believed to lead to protein aggregation (Thomas and Baneyx, 1996) during the cultivation. Stress as high temperatures, pH-shifts or high feeding rates also favour IB-formation (Fahnert, et al., 2004). These factors tend to result in higher yields of product (Gupta and Shukla, 2017), which of course is advantageous combined with the possibility of expressing toxic proteins (Berlec and Strukelj, 2013). There are different screws for altering QAs of IBs starting with choice of the strain and the induction mechanism, classical process parameters like T and pH and finally physiological feeding control of the cultivation. We want to address different screws in cultivation technology to modify the most important IB QAs.

Impact of induction system on IB QAs

There are a multitude of promotor systems, which are regularly used in *E. coli*. The most important for therapeutic protein production are lac, lac-trc or T7 promotors, which are commenly induced by isopropyl β-D-1 thiogalactopyranoside (IPTG) (Neubauer and Hofmann, 1994, Wurm, et al., 2016). However, induction with IPTG stresses the cells, as in higher concentrations it is

known to be toxic at elevated induction times (Neubauer and Hofmann, 1994, Viitanen, et al., 2003, Marbach and Bettenbrock, 2012, Dvorak, et al., 2015). Alternative induction mechanisms are temperature shifts (λ-phage), phosphate depletion (phoA) (Huang, et al., 2012) and induction with L-rhamnose (rhaT). In contrast to most other promotor systems rhaT is tightly regulated and renders turnability of recombinant protein production possible (Giacalone, et al., 2006). This is most likely due to a positive-coupled feedback system, when compared to the commonly used T7-expression system (Wegerer, et al., 2008) and may be a powerful tool to modify IB QAs based on the induction strenth. Similar to the rham-BAD-system is induction performed with arabinose using an ara-BAD-System, hence suffering from the same drawbacks as the rhamnose induction system, (Khlebnikov, et al., 2002) being the usually high cost of L-rhamnose nad L-arabinose. Comparision of protein expression of eGFP based on induction with IPTG and lactose have been performed by Wurm et al. (Wurm, et al., 2017). Induction with lactose (using a pET vector system) gives the possibility to adapt the QAs size and purity for the given inclusion body based on the inducer concentration. Akbari et al. (Akbari, et al., 2015) studied effects on the inducer concentration using IPTG in a pTZ57R/T cloning vector. Changing the inducer concentration showed significant impact analysed in combination with temperature and induction time. Kischnick et. al. (Kischnick, et al., 2006) observed that a component of papain digested soy peptone mimics the effects of IPTG and may therefore be used as cheap alternative in complex media systems.

QAs affected by Classical and Physiological Process parameters

Classical process parameters like temperature and pH have a severe influence on the expression of IBs and/or soluble protein. However, many studies are only based on shake flasks experiments or only batch approaches, being far away from realistic biomass concentrations in industrial applications. Effects on quality attributes of IBs based on alterations in the culture pH was investigated by Castellanos-Mendoza et. al. (Castellanos-Mendoza, et al., 2014) producing

recombinant sphingomyelinase-D. The cells were cultivated in shake flask and batch approaches. Differences in size were detectable during the 24 h run based on the pH variances during the cultivation. Variance in temperature, induction time and IPTG inducer concentration was performed by Akbari et al. (Akbari, et al., 2015) producing a single chain antibody fragment. Optimized cultivation conditions were found at 37 °C, post-induction time of 10.45 h, and 0.75 mM IPTG producing up to 236 mg/L of product as IB. However, experiments were exclusively performed in shake flasks exhibiting cell densities below 2 g/L. Performed fed -batch based cultivations using an industrial protein fused to N^{Pro} exclusively expressing IBs (Slouka Christoph, 2018) showed high impact on IB QA based on classical process parameters tested in a DoE approach. Low pH of 6.7 and low temperature of 31.5°C during favour IB productivity in an exclusively IB producing strain. Beside specific titer, also QAs of size and purity were analysed and optimized within this study. Limited oxygen growth conditions yielded increased productivity and purity for an IB based process by Kischnik et al. (Kischnick, et al., 2006).

Beside the classical parameters, physiological control of the cultivation process is important for optimization of the performance. Physiological feeding strategies are based on the specific substrate feeding rate ($q_{s,C}$) of the respective C-source. Cell stress and reduction of cell viability during the induction lead to a reduced uptake of C-source and therefore to a possible overfeeding during induction (Reichelt, et al., 2016, Slouka Christoph, 2018). Adapting of $q_{s;C}$ based on the physiological state of the cell is essential for preventing cell death and IB degradation during cultivation. Furthermore, IPTG as inducer often imposes high cell stress during induction. Application of lactose as inducer is a method to prevent this high imposed stress, since lactose can be metabolized during induction. Further benefits of lactose is the possibility to adapt induction strength in a mixed feed approach varying $q_{s,C}$ of the C-source and lactose, respectively. Wurm et al. (Wurm, et al., 2017) tested different recombinant proteins for concomitant uptake of glucose and lactose. Results show that IBs are strongly dependent on the amount of the specific lactose uptake rate in the mixed feed and on the specific uptake rate of the primary carbon source. Furthermore, these cultivation techniques help to overcome the problem of cell stress caused by

harsh induction using IPTG and renders the possibility for tuning between soluble and IB production. Mixed feed could be applied for a multitude of products including antibody fragments (Looser, et al.) (Wurm, et al., 2017) and can be used to increase the production of soluble protein compared to the IB fraction (Wurm, et al., 2016), also valid for a GFP model protein, expressing IBs as well as soluble protein (Wurm, et al., 2017). Also, effects on activity of the produced GFP were visible within this study. Changing the primary carbon source from glucose to glycerol in mixed feed systems with lactose was performed by Kopp et. al (Kopp, et al., 2017). Though no major differences between glucose and glycerol uptake regarding the specific inducer uptake rate rates could be detected. However, the specific IB productivity is highly increased using glycerol as primary carbon source, which makes the cheap carbon source an ideal alternative for cultivation (Martínez-Gómez, et al., 2012).

Effects of process parameters on QA activity

Different process parameters were recently identified to increase the expression of active structures within the produced IBs. Castellanos-Mendoza et. al. (Castellanos-Mendoza, et al., 2014) showed that changes in the culture pH changed the IB characteristics of sphingomyelinase-D between the classical and active form. Uncontrolled pH results in a higher amount of active IBs analysed by means of solubilization and enzyme kinetic tests. To increase the amount of biological active inclusion bodies Wang et. al. (Wang, et al., 2015) tested for different hydrophobic self-assembling polypeptides fused to the C- terminus of two model proteins – *Bacillus subtilis* lipase A (LipA) or *Aspergillus fumigatus* amadoriase II (AMA). Results indicate that these protein-tags increase the amount of the insoluble fraction drastically, with remaining activity. Jevševar et. al (Jevševar, et al., 2005) increased the fraction of active IB in human granulocyte-colony stimulating factor (hG-CSF) by decreasing temperature to 25°C during induction. This yielded in an increased titer (higher than 2-fold) and an increase of biological activity up to 30%. Peternel et al. (Peternel, et al., 2009) produced GFP as model protein and

altered induction strategy and induction temperature. Higher titer could be found under conditions of delayed induction. As already shown in different studies lower temperature also increased the amount of active protein within in IB structure.

IBs for direct applications or catalytic purposes are up to now only produced in shake flask experiments or in small scale batch cultivations using only few controls. Process engineering approaches may be highly beneficial in production of distinct bead sizes for scaffolds and in boosting activity of catalytic active IB materials.

1.4. Discussion

The IB based applicational range widened remarkedly during the last decade, mainly based on the findings of enzymatic activity. Product design and expression are only one important part in the product development chain. **Figure 2** presents the general approaches for optimization of IB based production processes based on the presented chapters in this review. After conceptualization of the product and the expression system given in chapter 1, development of respective analytics for measurement of the critical QAs is of utmost importance. For pharmaceutical applied products titer and purity measurements during the downstream (chromatographic steps) are already implemented. However, without direct analysis - especially in a time dependent manner – in the upstream, control during the process is challenging. Several analytical methods presented in the literature were therefore summarized in chapter 2 and represent the most important pillar for process understanding.

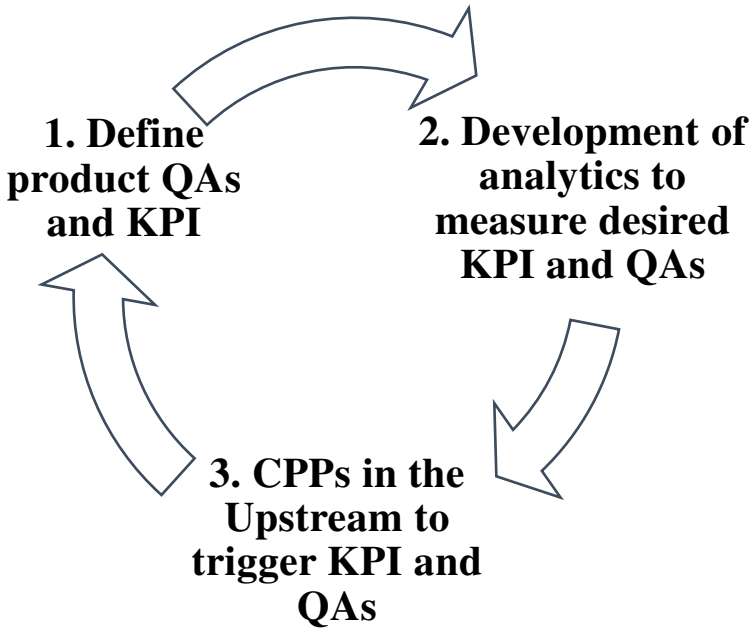

Figure 2: Product development chain for (IB) products and it's iterative optimization process.

Based on that, important QAs and KPIs for the upstream could be analysed yet. Important QAs for different IB based applications are summarized in Table 1. QAs like size and purity and KPIs like titer can be already well measured in the upstream process based on time dependent sampling. Enzyme/catalytic activity measurements of the product is also extensively researched. Model proteins like GFP enables us to get inside on effects of critical process parameters (CPP) on IB protein activity and its modification during the upstream. This would help to increase the number of direct applications of IB for enzymatic reactions in vitro, but also is believed to increase downstream recovery of the product. However, in several applications process engineering methods are not applied to a satisfying content, also seen in empty spaces in Table 1. The already used methods were presented in chapter 3, but are restricted primary to pharmaceutical products, leading the way to robust downstream. Despite knowledge of important QAs for new applications, upstream technological approaches are not engineered sufficiently in order to control KPIs and QAs.

Table 1**:** Differences in QA, and performance indicators for different IB based products. QAs can be influenced by process parameters in the USP.

product	Quality attributes (QA)	Key performance Indicator (KPI)	Screws in Critical Process Parameters (CPP)
IBs without protein activity	• Size (Peternel, et al., 2008, Díez-Gil, et al., 2010, Slouka Christoph, 2018) (Rinas, et al., 2017) • Purity (Kischnick, et al., 2006, Slouka Christoph, 2018)	• Time space yield/Titer • DSP performance	• Classical (pH,T,pO_2) (Castellanos-Mendoza, et al., 2014, Slouka Christoph, 2018) • Physiologcal ($q_{s,C}$) (Slouka Christoph, 2018) • Cell viability(Reichelt, et al., 2016, Slouka Christoph, 2018) • Inducer (e.g. IPTG vs lactose) (Neubauer and Hofmann, 1994, Akbari, et al., 2015, Wurm, et al., 2016, Wurm, et al., 2017) • C-source (Kopp, et al., 2017) • Induction time (Rinas, et al., 2017).
IBs with protein activity	• Size • Purity • Activity *(García-Fruitós, et al., 2007, Govers, et al., 2014) (Peternel, et al., 2009)*	• Recovery of mild solubilitzation performance • DSP performance	• Classical (pH,T) (Castellanos-Mendoza, et al., 2014) (Jevševar, et al., 2005) *(Peternel, et al., 2009)* • Fusion tags (Wang, et al., 2015) • Induction time
IBs as nonoparticulate matter	• Size • Cell penetration *(Seras-Franzoso, et al., 2013)* • Drug delivery *(Rodríguez-Carmona and Villaverde, 2010).*	• Mammalian cell growth	
IBs as biocatalysts	• Catalytic activity *(Nahálka, et al., 2008, Sans, et al., 2012)* • Recircilation number *(Nahálka, et al., 2008)* • Purity	• Turnover number	• Fusion tags *(Nahálka, et al., 2008)*
IBs for multienzyme cascades	• Catalytic activity (Han, et al., 2017)	• Metabolon activity	

One reason may be that diverse products are in the very early stage of development for several application. Optimization of the process is therefore not under investigation yet and desired at the current point as the efforts are too high. In case of industrial need for these IB based products,

based on competitive prices and quality, an emerging need for upstream screws will be given in the near future. A second reason may be investigations of IB properties intending a rather basic science claim. Industrial relevance may be not given and may not be seen to the current time and therefore no need is given to optimize production and properties of the product. Summing up, bio-engineering is a powerful tool not only to broaden the application range of IB based products in industry, but also improve product quality and magnitude. This further process understanding for a high variety of products with different applications also may pave the way for new benchmarks in the industry, e.g. continuous manufacturing in microbial processes.

1.5. Conclusions

IB processes experienced a new renaissance in the recent years, as the range of application of IBs increased considerably. Classical process parameter like temperature, pH and physiological feeding in combination with very different induction mechanism are powerful tools to trigger the properties of IBs in order to fit the desired quality. IBs are still widely exploited for production of pharmaceutical processes for high product titer and expression of toxic proteins, where no posttranslational modifications are required, e.g. fABs.

The differentiation between classical and non-classical IBs is not a distinct boarder anymore. Different process parameters in the upstream does highly affect the amount of active protein within the IB.

Process understanding during cultivation for different purpose in IB applications is still highly underestimated. Different screws are already identified for individual products to enhance or repress activity in the IB product. Desired QAs for different applications are already triggered by process technological based tools. While the analytical toolbox for determination is already developed to a high extend and applicable, quality by design criteria are not yet applied for multitude of products as no need for high production is given yet. Furthermore, we think that, if

further basic research is done for a number of products, distinct process understanding during production will help to improve product quality (and quality attributes) for these IB based products in the future.

1.6. Industrial need and scientific questions of this thesis

Control of the quality attributes of the IB product in the Upstream Process is of utmost importance to guarantee a stable Downstream Processing for pharmaceutical active products. As many factors affect these Quality Attributes – classical process parameters, physiological parameters and especially harvest timepoint – we wanted to create a knowledge platform for triggering these attributes during cultivation. This knowledge platform is formed using process engineering methods in a product development for an industrial relevant biopharmaceutical. Following workflow (**Figure 3**) was chosen to fulfil this task.

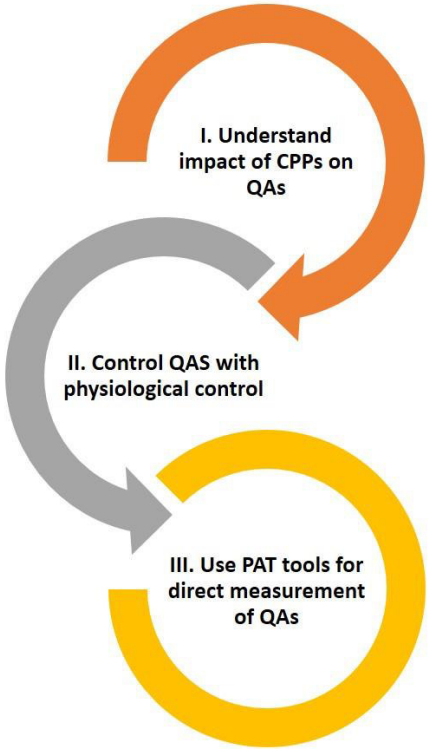

Figure 3: Workflow of this thesis to acquire process understanding during the given product development. Part I and II are presented in the following chapters. For part III first approaches will be presented for viable cell concentration as an important factor for PAT analytics.

The first part describes the impact of different critical process parameters (CPP) on the defined Inclusion Body quality attributes (QAs). This process knowledge is subsequently applied to

develop physiological feeding control for the developed process in the second part. In the third part process analytical tools for raising control strategies to the next level are approached.

Based on the workflow in **Figure 3** following scientific questions and aims were addressed during this thesis, with questions 1 and 2 governing the understanding of the impact on QAs, question 3 dealing with physiological control and question 4 trying to approach PAT based technologies:

I. **Are we able to detect variances in inclusion body quality attributes (size, purity) by means of analytical techniques? Can these quality attributes be changed based on the two classical process parameters pH and temperature in the induction phase?**

II. **Can product formation be boosted by usage of glycerol instead of glucose, overcoming the limitation of carbon catabolite repression when using lactose as inducer? Can cell stress be reduced by usage of lactose as inducer instead of IPTG?**

III. **As cell stress leads to reduction of viable cell concentration and subsequent product degradation, control strategies need to be applied to overcome these issues. Are there trigger parameters for determination of cell stress, and can control strategies be applied based on these?**

IV. **Viable cell concentration is the most important parameter during cultivations with microorganism as they are the catalysator or producer of the value product? Is it possible to determine viable cell concentration and/or the physiological state of the cell using hard sensor methods?**

2. Custom Made Inclusion Bodies: Impact of classical process parameters and physiological parameters on Inclusion Body quality attributes

Inclusion Body quality attributes were analyzed based on the process parameters triggered in the induction phase of fed-batch based cultivations using *E. coli* BL21(DE)3. This part deals with the understanding of the impact of CPP on IB-QAs. The results of this part were published in **Microbial Cell Factories Journal** (Slouka Christoph, 2018).

2.1. Background

The gram-negative bacterium *E. coli* is the expression host of choice for the production of 30% to 40% of recombinant drugs in industry (Walsh, 2010, Gupta and Shukla, 2017). As *E. coli* shows very fast replication rates (Meuris, et al., 2014, Wurm, et al., 2016) on comparatively inexpensive media (DeLisa, et al., 1999), the benefits often outweigh the numerous purification steps (Berlec and Strukelj, 2013, Gupta and Shukla, 2017) and the missing glycosylation pattern (Spadiut, et al., 2014, Baeshen, et al., 2015, Gupta and Shukla, 2017). Recombinant protein production in *E. coli* regained more interest as the demand in single chain antibody-fragments increased, which can be properly expressed in *E. coli* (Spadiut, et al., 2014, Gupta and Shukla, 2017). The strain BL21(DE3) created by F. Studier and B. Moffatt back in 1986 (Studier and Moffatt, 1986) is often used in an industrial scale, because of very low acetate formation, high replication rates (Steen, et al., 1986, Studier and Moffatt, 1986, Studier, et al., 1990, Dubendorff and Studier, 1991, Neubauer and Hofmann, 1994, Lyakhov, et al., 1998), as well as the possibility of protein secretion into the fermentation broth due to a type 2 secretion protein (Jeong, et al., 2009, Tseng, et al., 2009, Jeong, et al., 2015). For expression of the recombinant protein, the lac operon is still

one of the most favored promotors in pET-expression-systems using integrated T7-polymerase for high transcriptional rates (Dubendorff and Studier, 1991, Marbach and Bettenbrock, 2012, Wurm, et al., 2016). The repressor protein can only be blocked by allolactose or a structural analogue (Keiler, 2008), e.g. the well-known expensive inducer isopropyl β-D-1 thiogalactopyranoside (IPTG) (Neubauer and Hofmann, 1994, Wurm, et al., 2016). However, induction with IPTG stresses the cells, as IPTG in higher concentrations is known to be toxic (Neubauer and Hofmann, 1994, Viitanen, et al., 2003, Marbach and Bettenbrock, 2012).

Recombinant proteins are often expressed as Inclusion Bodies (Inada, et al.). IBs have originally been believed to be waste products by bacteria (García-Fruitós, et al., 2012), until it was realized that they are formed as a stress reaction by the cells resulting in a biologically inactive precipitated protein (Palmer and Wingfield, 2012, Ramón, et al., 2014, Villaverde, et al., 2015). Such stress reactions can be caused by high temperatures, pH-shifts or occur due to high feeding rates. These factors tend to result in higher yields of product (Gupta and Shukla, 2017), which of course is advantageous combined with the possibility of expressing toxic proteins (Berlec and Strukelj, 2013). Still, the DSP and especially the refolding unit operation suffers in robustness and is the most time-consuming step in gaining the correctly folded product from *E. coli* cultivations (García-Fruitós, et al., 2012, Palmer and Wingfield, 2012, Ramón, et al., 2014, Villaverde, et al., 2015), which requires significantly more technology and time, when purifying IBs (Palmer and Wingfield, 2012, Wingfield, 2014, Wingfield, et al., 2014).

Quality attributes (or key performance indicator) of IBs, such as titer and morphology changes during extraction procedures have already been studied and show that IBs are dynamic structures depending on the cultivation and extraction conditions (Peternel, et al., 2008, Peternel, et al., 2008, Díez-Gil, et al., 2010). First approaches towards IB sizing in the upstream process have already been made within our group by Reichelt et al. (Reichelt, et al., 2017) using transmission electron microscopy (Schwaighofer, et al.) in combination with nanoparticle tracking analysis (García-Fruitós, et al.) revealing general trends of IB growth during cultivation. Further studies show that IBs consist of up to 50% correctly folded protein in contrast to the general perception of

IBs as inactive structures (Jevševar, et al., 2005, Peternel, et al., 2008). Combined with the fact that IBs can be produced in high concentration (so that the amount of generated product often outweighs the additional downstream steps), IB based processes are believed to fundamentally boost time/space yields for recombinant protein production (García-Fruitós, et al., 2012, Berlec and Strukelj, 2013, Baeshen, et al., 2015, Gupta and Shukla, 2017). Knowledge about the state of IB QAs during a cultivation process is therefore of utmost importance. Three IB QAs are generally of importance: bead size, titer and purity, as those three quality attributes were already defined elsewhere (García-Fruitós, et al., 2012, Reichelt, et al., 2017, Reichelt, et al., 2017, Wurm, et al., 2017). It has been reported that inclusion body sizes can be measured with different methods, e.g. AFM (atomic force microscopy), TEM and NTA (García-Fruitós, et al., 2012, Reichelt, et al., 2017, Wurm, et al., 2017). SDS-pages and ELISA-methods have been often reported as tool to determine impurities and titer in the IB product samples (Kischnick, et al., 2006). The impact of single process parameters like pH on IB QAs has already been investigated in literature (Strandberg and Enfors, 1991, Castellanos-Mendoza, et al., 2014). Reichelt et al. (Reichelt, et al., 2017) showed that alterations of ($q_{s,glu}$) influence the behavior of common IB-processes, using IPTG as an inducer. The impact of the feeding rate onto product formation in *E. coli* BL21(DE3) has been investigated recently, though lactose was used as inducer instead of IPTG (Kopp, et al., 2017). However, no monitoring of all IB-QAs over induction time has been performed in any of the previous studies.

In this study we performed cultivations with a BL21(DE3) strain, producing a recombinant protein coupled to a N-pro-fusion protein (Achmüller, et al., 2007) – *strain 1* – and a non N-Pro fused protein – *strain 2* -, both exclusively expressing IBs, as the products are highly toxic for the cell. Classical process parameters were monitored as a function of induction time. The impact of process parameters on IB bead size in combination with purity and titer as a function of time has not been investigated in depth. Secondary structure of different IB sizes were analyzed using IR and showed no differences for IB beads of different size compared to the standard. Based on these

results, the physiological parameter of the specific substrate uptake rate ($q_{s,glu}$) is altered at constant pH and T for *strain 1* and QAs are analyzed time-dependently. In this current study we collected time resolved results, which are used to optimize the USP. In conclusion, it is demonstrated that low T and low pH in combination with high $q_{s,glu}$ are beneficial for increasing the productivity and robustness of IB based processes for the two tested proteins.

2.2. Methods

Strains

Strain 1 was an *E. coli* BL21(DE3) with the pET[30a] plasmid system (kanamycin resistance) for recombinant protein production. The target protein was linked to a N-pro fusion protein used for purification (Achmüller, et al., 2007). *Strain 2, E. coli* BL21(DE3), (kanamycin resistance) was used for testing the results obtained with *strain 1*. Expression of the protein occurs only as IB since the product is toxic to the cell. No N-Pro taq is fused to this product.

Bioreactor cultivations

Strain 1:

All bioreactor and preculture cultivations for *strain 1* were carried out using a defined minimal medium referred to DeLisa et al. (1999) (DeLisa, et al., 1999). Batch media and the preculture media had the same composition with different amounts of glucose respectively. The glucose concentrations for the phases were: 8 g/L for the preculture, 20

g/L for the batch phase. The feed for fed-batch and induction had a concentration of 300 g/L glucose.

Antibiotic was added throughout all fermentations, resulting in a final concentration of 0.02 g/L of kanamycin. All precultures were performed using 500 mL high yield flasks. They were inoculated with 1.5 mL of bacteria solution stored in cryos at -80°C and subsequently cultivated for 20 h at 230 rpm in an Infors HR Multitron shaker (Infors, Bottmingen Switzerland) at 37 °C.

All cultivations were either performed in a stainless-steel Sartorius Biostat Cplus bioreactor (Sartorius, Göttingen, Germany) with 10 L working volume or in a DASGIP Mini bioreactor-4-parallel fermenter system (max. working volume: 2.5 L; Eppendorf, Hamburg, Germany). Cultivation offgas was analyzed by gas sensors - IR for CO_2 and ZrO_2 based for O_2 (Blue Sens Gas analytics, Herten, Germany).

Process control was established using the PIMS Lucullus and the DAS-GIP-control system, DASware-control, which logged the process parameters. During batch-phase and fedbatch phase pH was kept constant at 7.2 and controlled with base only (12.5% NH_4OH), while acid (5 % H_3PO_4) was added manually, when necessary. The pH was monitored using an EasyFerm Plus pH-sensor (Hamilton, Reno, NV, USA). The reactors were continuously stirred at 1400 rpm and aerated using a mixture of pressurized air and pure oxygen at 2 vvm. Dissolved oxygen (dO_2) was always kept higher than 30 % by increasing the ratio of oxygen in the ingas. The dissolved oxygen was monitored using a fluorescence dissolved oxygen electrode Visiferm DO (Hamilton, Reno, NV, USA) The fed-batch phase for biomass generation was followed by an induction phase using a feed medium with glucose as primary carbon source.

0.5 mM IPTG was added as an inducer once to start the induction of the cells. pH and temperature in the induction phase was adapted according to the design of experiments (DoE) given in **Figure 4** a). pH was altered between 6.7 and 7.7 and temperature between 30 °C and 40 °C. The center point at 35 °C and pH = 7.2 was cultivated in triplicate in order to assess statistical experimental error.

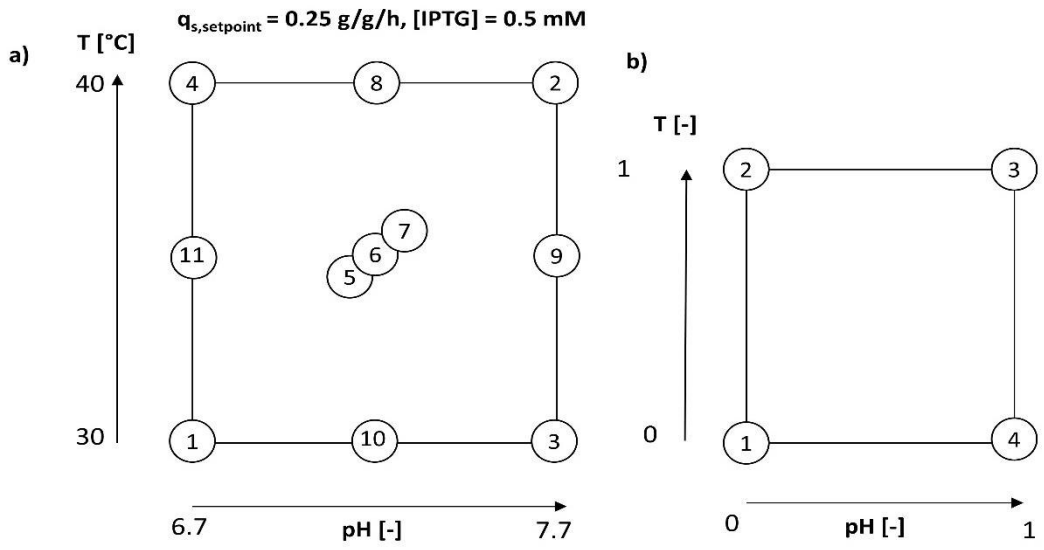

Figure 4: DoE for determination of the influence of classical process parameters on IB QAs. Starpoints (8,9,10,11) were performed in a DasGip parallel system, while the others were cultivated in a stainless-steel Sartorius Stedim reactor; b) reduced design space for *strain 2* based on optimal cultivation parameters.

Strain 2:

Strain 2 was cultivated at our industrial partner. The cultivation was similar to *strain 1* using chemically defined medium containing 15 g/L glucose in seed and 10 g/L glucose in main stage fermentations, respectively. Inoculum preparation and respective antibiotic selection were similar to *strain 1*, though during the main culture stage kanamycin was added. Seed and main culture cultivations were carried out in custom built 50 L stainless steel vessels with custom made fermentation software for process control. Throughout the seed and main fermentation stages the pH was adjusted to fit the parameters of the second DoE (**Figure 4** b) using 150 g/l sulphuric acid or 25 % ammonia. Temperature was adjusted to the corresponding values in main culture. Dissolved oxygen was adjusted to 30% using aeration with up to 2 vvm, 2 bar backpressure and stirring up to 500 rpm. Optical DO probes Visipro DO (Hamilton, Reno, NV, USA) and EasyFerm Plus pH probes (Mettler Toledo, Columbus, Ohio; USA) were used for monitoring and control. Off-gas analysis was conducted using a custom-built mass spectrometer facility. At OD_{600} > 8.5 in seed culture, main culture was inoculated using 8.6% (v/v). Upon glucose depletion a

glucose feed was initiated using a μ of 0.3 h^{-1} for 6 h and was kept constant at a final rate of exponential feed pattern until process termination. Expression was induced 2 hours after the end of exponential feeding for biomass production using 1 mM IPTG for 12 h in a reduced design space given in **Figure 4** b). As high temperatures and alkaline pH (fermentation conditions 2 in **Figure 4** a) showed pronounced lysis during the study, the design space for strain 2 was reduced to a more reasonable pH and temperature window which is commonly used for multiple *E. coli* cultivations. Absolute values for pH and T cannot be given due to confidential reasons by our industrial partner.

Cultivation Analytics

Biomass

For dry cell weight (DCW) measurements 1 mL of the cultivation broth was centrifuged at 9000 g, subsequently washed with 0.9 % NaCl solution and centrifuged again under the same conditions. After drying the cells at 105 °C for 48 h the pellet was evaluated gravimetrically. DCW measurements were performed in five replicates and the mean error for DCW was about 3 %. Offline OD_{600} measurements were performed in duplicates in a UV/VIS photometer Genisys 20 (Thermo Scientific, Waltham, MA, US).

Flow Cytometry

Flow cytometry (FCM) was carried out according to Langemann et al. [38]. We used a CyFlow® Cube 6 flow cytometer (Partec, Münster, Germany) with 488-nm blue solid-state lasers. Three fluorescence channels were available (FL1, 536/40 nm bandpass; FL2, 570/50 nm bandpass; FL3, 675 nm longpass) alongside forward scatter (trigger parameter) and side scatter detection. This device featured true absolute volumetric counting with a sample size of 50 to 100 μL. Data were collected using the software CyView 13 (Cube 6; Partec) and analyzed with the software FCS

Express V.4.07.0001 (DeNovo Software, Los Angeles, CA, USA). Membrane potential-sensitive dye $DiBAC_4(3)$ (abs./em. 493/516 nm) was used for the assessment of viability. Fluorescent dye RH414 (abs./em. 532/760 nm) was used for staining of plasma membranes yielding strong red fluorescent enhancement for the analysis of total cell number. Combining those two dyes it was possible to quantify the viable cell concentration. Stocks of 0.5 mM ($DiBAC_4(3)$) and 2 mM RH414 were prepared in dimethyl sulfoxide and stored at -20°C. Both dyes were purchased from AnaSpec (Fremont CA, USA). 1.5 µL of both stocks were added to 1 mL diluted sample resulting in final concentrations of 0.5 µM $DiBAC_4(3)$ and 2.0 µM RH414, respectively. Samples were measured directly after addition of the dyes, without further incubation.

Sugar analytics

Sugar concentrations in the filtered fermentation broth were determined using a Supelco C-610H HPLC column (Supelco, Bellefonte, PA, USA) on an Ultimate 300 HPLC system (Thermo Scientific, Waltham, MA, US) using 0.1 % H_3PO_4 as running buffer at 0.5 mL/min or an Aminex HPLC column (Biorad, Hercules; CA, USA) on an Agilent 1100 System (Agilent Systems, Santa Clara, CA, USA) with 4 mM H_2SO_4 as running buffer at 0.6 mL/min.

Product Analytics

IB Preparation

5 mL fermentation broth samples were centrifuged at 4800 rpm at 4 °C. The supernatant is discarded and the pellet is resuspended to a DCW of about 4 g/L in lysis buffer (100 mM Tris, 10 mM EDTA at pH = 7.4). Afterwards the sample was homogenized using a high-pressure homogenizer at 1500 bar for 10 passages (EmulsiflexC3; Avestin, Ottawa, Canada). After

centrifugation at 10000 rpm and 4 °C the supernatant was discarded and the resulting IB pellet was washed twice with ultrapure water and aliquoted into pellets à 2 mL broth, centrifuged (14000 rpm, 10 min 4 °C) and stored at -20 °C.

IB Size

Washed and aliquoted IB samples were resuspended in ultrapure water. 100 µL of appropriate dilution of the suspension were pipetted on a gold-sputtered (10 - 50 nm) polycarbonate filter (Millipore-Merck, Darmstadt, Germany) using reusable syringe filter holders with a diameter of 13 mm (Sartorius, Göttingen, Germany). 100 µL of ultrapure water were added and pressurized air was used for subsequent filtration. Additional 200 µL of ultrapure water were used for washing. The wet filters were fixed on a SEM sample holder using graphite adhesive tape and subsequently sputtered with gold to increase the contrast of the sample. SEM was performed using a QUANTA FEI SEM (Thermo Fisher, Waltham, MA, US) with a secondary electron detector (Dvorak, et al.). The acceleration voltage of the electron beam was set between 3 to 5 kV. To determine the diameter of the IBs, 50 IBs on SEM pictures were measured using the ImageJ plugin Fiji (Laboratory for Optical and Computational Instrumentation (LOCI), University of Wisconsin-Madison, US). SEM analytics of two different time points for both strains are given in **Figure 5.**

IB Titer for MPS1

For titer measurements IB pellets were solubilized using solubilization buffer (7.5 M guanidine hydrochloride, 62 mM Tris at pH = 8). The filtered samples are quantified by HPLC analysis (UltiMate 3000; Thermo Fisher, Waltham, MA, USA) using a reversed phase column (EC 150/4.6 Nucleosil 300-5 C8; Macherey-Nagel, Düren, Germany). The product was quantified with an UV detector (Thermo Fisher, Waltham, MA, USA) at 280 nm using Novartis BVS Ref. 02 as standard. Mobile phase was composed of acetonitrile and water both supplemented with

0.1% (v/v) trifluoride acetic acid. A linear gradient from 30% (v/v) acetonitrile to 100 % acetonitrile (ACN) was applied. A steep linear gradient from 10% ACN to 30 % ACN in 60 s was followed by a long linear gradient from 30 % to 55 % and by 3 regeneration steps.

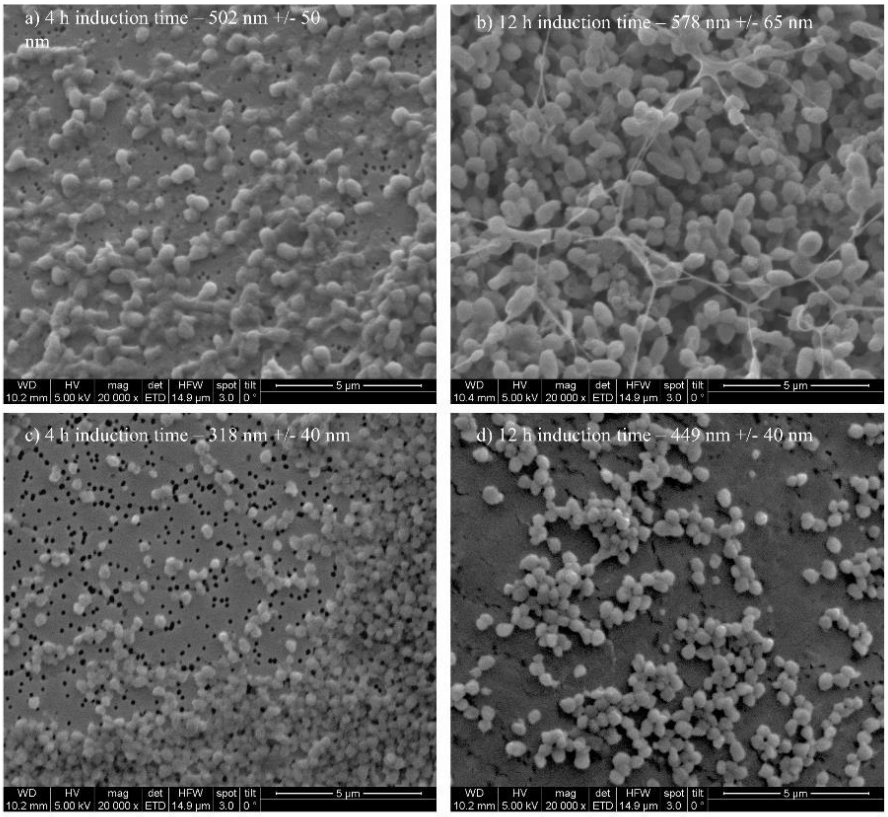

Figure 5: Extracted IBs filtered onto Au coated polycarbonate filter and analyzed using SEM for 4 h induction time and 12 h induction time. Strong difference in size can be spotted for the two-time points.

IB Titer for MPS2

IB titer was also determined by reversed phase HPLC at Sandoz GmbH (Process Analytics, Kundl, Tyrol, Austria). Pellets were defrosted at room temperature and solubilized by addition of dilution buffer (Strandberg and Enfors) (6 M guanidine hydrochloride, 50 mM Tris, pH 7.5) and sonication (Branson Ultrasonics, Danbury, Connecticut, USA). The filtered samples were analyzed by HPLC with a reversed phase column (Acquity UPLC BEH 300, C4, 1.7µm, 2.1 x 50 mm). Quantification was performed by UV detection at 214 nm wavelength and calibration with a

purified product standard. Mobile phases were composed of (A) water and (B) acetonitrile/pentanol (95/5, v/v) both supplemented with 0.1% (v/v) tetrafluoride acetic acid. The elution of the product was achieved with a linear gradient of both solvents.

IB Purity

Purity measurements were performed using chip-based protein assays with 2100 Bioanalyzer (Agilent Technologies, Santa Clara, CA, USA. The chip-based assay is based on SDS-PAGE and therefore separates molecules according to their size. Washed and homogenized IBs were dissolved in 3 M urea, 25 mM Tris at pH 7 and measured subsequently. The electropherogram was afterwards analyzed using OriginPro 2016 (Northampton, MA, USA) integrating the peak area of the protein of interest and normalizing the area in respect to the total area of the electropherogram.

IB conformational analysis by IR spectroscopy

Infrared (IR) spectra were recorded by an external-cavity quantum cascade laser-based IR transmission setup described in detail by Schwaighofer et al. (Schwaighofer, et al., 2018). A water-cooled external-cavity quantum cascade laser (Hedgehog, Daylight Solutions Inc., San Diego, USA) was used operating at a repetition rate of 100 kHz and a pulse width of 5000 ns. All spectra were recorded in the spectral tuning range between 1730–1470 cm^{-1}, covering the amide I and amide II region of proteins, at a scan speed of 1200 $cm^{-1}s^{-1}$. The MIR light was focused on the detector element by a gold plated off-axis parabolic mirror with a focal length of 43 mm. A thermoelectrically-cooled MCT detector operating at -78 °C (PCI-10.6, Vigo Systems S.A., Poland) was used as IR detector. To reduce the influence of water vapor, the setup was placed in a housing of polyethylene foil and constantly flushed with dry air. The measured signal was processed by a lock-in amplifier (Stanford Research Systems, CA, USA) and digitized by a NI DAQ 9239 24-bit ADC (National Instruments Corp., Austin, USA). Each single beam spectrum

consisting of 6000 data points was recorded during the tuning time for one scan of approx. 250 µs. A total of 100 scans were recorded for background and sample single beam spectra at a total acquisition time of 53 s. All measurements were carried out using a custom-built, temperature-controlled flow cell equipped with two MIR transparent CaF_2 windows and 31 µm-thick spacer, at 20 °C.

The laser was controlled by Daylight Solution driver software; data acquisition and temperature control were performed using a custom-made LabView-based GUI (National Instruments Corp., Austin, USA). Two IB samples with distinct size of 400 nm and 600 nm were compared with the finished formulated protein standard of *strain 1* (without N-Pro Taq).

2.3.Results and Discussion

The goal of this study was to investigate and to understand if and how IB attributes can be changed and tuned by upstream bioprocess (USP) technological methods. We tested the classical process parameters pH and temperature and the physiological parameter specific substrate uptake rate. The impact of specific USP parameters can be investigated using IB QAs as response for data evaluation. With knowledge about the tunability of IB QAs in the upstream, it is possible to simplify the subsequent downstream steps. Therefore, we tested two different proteins, with completely different structure including N-Pro fusion taq for *strain 1* and no fusion taq for *strain 2.* Both products have a high toxicity for the cell in common and are only expressed as IBs. The results constitute the key to custom made IBs and may be used as platform technology for the development of the USP for new products.

Impact of classical process parameters on IB QAs using strain 1 (N-Pro fused protein)

As IPTG based induction imposes a metabolic stress to the host organism, time dependent analysis of IB QAs is of utmost importance to identify critical process time points (e.g. cell death, product degradation) within individual cultivation runs. Therefore, IB QAs were analyzed every two hours within a maximum of 12 hours induction time. pH and T were altered based on the experimental plan, while specific substrate uptake rate ($q_{s,Glu}$) and inducer concentration were kept constant in all experiments. In **Table 2** the applied parameters for T, pH and $q_{s,Glu}$ for all performed cultivations in the DoE are displayed. **Figure 6** exemplarily shows IB QAs of one single cultivation run as a function of time. The received QAs purity, titer and size are used to build a data driven model using MODDE 10 (Umetrics, Sweden).

Table 2: Analysis of applied process parameters compared to set points in all DoE runs during induction phase.

DoE	pH_{set} [-]	T_{set}[°C]	pH_{real} [-]	T_{real} [°C]	$q_{s,Glu\ set}$ [g/g/h]	$q_{s,Glu\ real}$ [g/g/h]
1	*6.7*	*30.00*	*6.69*	*30.00*	*0.25*	*0.24*
10	*7.2*	*30.00*	*7.16*	*30.02*	*0.25*	*0.26*
3	*7.7*	*30.00*	*7,69*	*30.00*	*0.25*	*0.26*
11	*6.7*	*35.00*	*6.64*	*35.02*	*0.25*	*0.29*
5	*7.2*	*35.00*	*7.18*	*35.00*	*0.25*	*0.24*
6	*7.2*	*35.00*	*7.18*	*35.00*	*0.25*	*0.32*
9	*7.7*	*35.00*	*7.64*	*35.03*	*0.25*	*0.27*
4	*6.7*	*40.00*	*6.68*	*40.00*	*0.25*	*0.29*
8	*7.2*	*40.00*	*7.15*	*40.01*	*0.25*	*0.29*
2	*7.7*	*40.00*	*7.69*	*40.00*	*0.25*	*0.24*
7	*7.2*	*35.00*	*7.17*	*35.00*	*0.25*	*0.25*

A partial least square fit was used for all models. Model terms (linear, quadratic and interaction terms) were evaluated according to their validity (p-values) and to the overall model quality. A clear dependence for the applied variations in pH and T were found and visualized against

induction time giving a time dependent analysis of the QAs. The evaluation of the specific titer (based on titer (g/L) divided by the biomass at the given timepoint (gX/L, resulting in g/g)) against the induction time and pH and T showed a clear dependence.

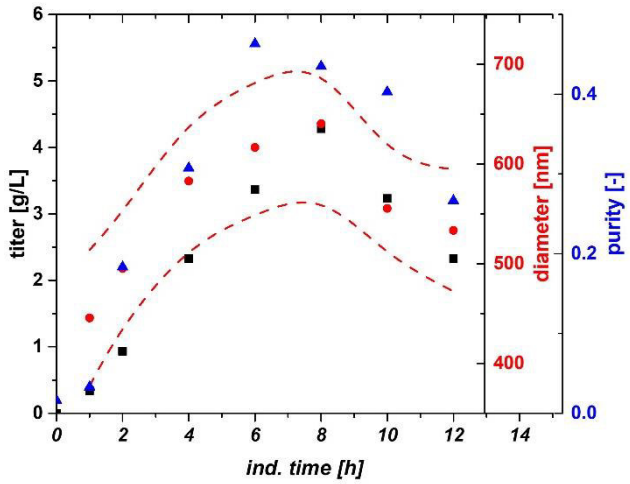

Figure 6: IB QAs as a function of induction time for the third centerpoint cultivation. Size is given with standard deviation (spline). Drop of titer/size and purity after 8 h is generally a result of increased cell lysis at elevated times.

The specific titer was used in order to compensate for deviations in the biomass after the non-induced fed batch, which yielded 25-30 g/L DCW. The maximum of spec. titer (not necessarily the spec. productivity at certain time point) was found at low T and low pH, shown in Figure 4 a). pH dependence got significant after 6 h of induction time and impacted (**Figure 7** b) the spec. titer. The maximum of recombinant protein was produced between 8 and 10 hours. This fact is well reflected by the const. parameter in **Figure 7** b). After 10 hours cell death leads to a degradation and reduction of the produced protein, also clearly deducible from the constant term, visible in FCM measurements and in pronounced glucose accumulation (data not shown). Within single cultivation runs titer and IB bead size showed a very linear relationship in the mean diameter and the standard deviation until the onset of cell death. Process parameters pH and T affected the growth of IB beads significantly. Generally, the largest IB bead size could be found close to the center point of the DoE in the beginning of induction. The shift to lower T and pH can be spotted after 6 h of induction time (compare to **Figure 7** c). Effects of cell death and product

degradation in titer could also be spotted in the IB bead size especially at 12 h. General trends of the fitting parameters are visualized in **Figure 7** d). The constant model parameter is increased over time which also indicates the growth of IB beads over induction time. Linear terms pH and T and quadratic pH term showed increased impact on the model with elevated time, while interaction term and quadratic T-term stayed rather constant.

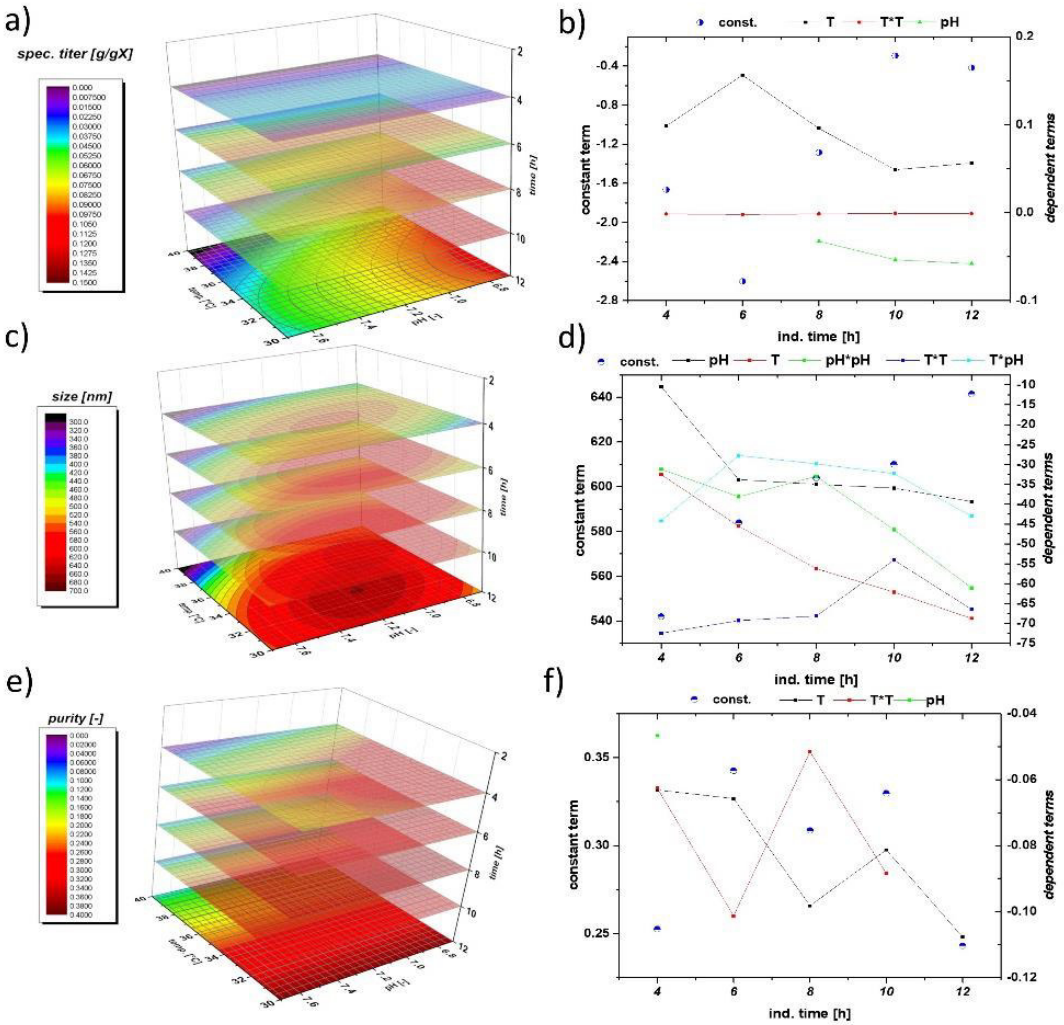

Figure 7: a) data driven model for time dependent analysis of IB specific titer; b) model fit parameter for titer. While in the beginning only temperature dependence is visible, a strong pH correlation can be found at t = 8 h; c) data driven model for time dependent analysis of IB bead size; d) model fit parameter for IB bead size. Due to standard deviation of 10 % in the analysis model parameters are rather complex.; e) Data driven model for time dependent analysis of IB purity; f) model fit parameter for purity. A sole temperature dependence is found beyond 4 h of induction

A Similar behavior for IB bead growth had already been obtained for a recombinant produced green fluorescent protein (GFP) in our group by Wurm et. al. (Wurm, et al., 2017). Instead of

altering pH and T like in this study, the induction strength using mixed feed systems with lactose as inducer was varied. Induction time and strength had a high impact on the IB bead size during these cultivations. In our model a certain deregulation of size compared to titer could be dedicated from the given data driven models. This fact is beneficial for regulation of individual parameters to increase the performance in the DSP process chain in a further aspect since size and titer can be varied separately to a certain extend. As third QA IB purity, as important factor for quality in the DSP, was analyzed.

The three-dimensional plot for purity determination is presented in **Figure 7** e). At times, up to four hours of induction pH influenced the purity of the IB samples. After four hours, a sole dependence on temperature was found indicating that low temperatures (30 °C in the design) favor cleaner IBs. Since titer and size maximum could be found at low temperatures and pH, purity after homogenization may be highly correlated to the degree of lysis during the fermentation run. Lower temperatures did not lead to significant cell death (when regarding up to 10 h of induction), impurities may be reduced by applying low temperatures compared to temperatures with increased cell death yields. So, **Figure 7** f) summarizes the model fit parameters as a function of time. pH did not contribute to the model fit beyond 4 h (only one point given). Temperature has a major influence on the duration of the induction time, which can already be detected in early stages of induction time. As purity is affected by the washing steps after homogenization different washing procedures may impact the value of absolute purity and the kind of impurity. Generally, porin structures and phospholipids from the outer membrane are the major part of impurities in the IB after homogenization (Rinas and Bailey, 1992, Rinas, et al., 1993). In literature IB beads had already been analyzed by SEM and AFM in order to get insight into morphology (García-Fruitós, et al., 2009) and into washing procedures and dependence of pH and T within (Rodríguez-Carmona, et al., 2010). Different washing procedure had also been analyzed in this work. Buffer based washing tends to show little influence in shape and morphology of IBs but has an effect on the analyzed purity value (**Supplementary 1**). This may be attributed to phospholipid content, resulting from homogenization of the cells, as buffer

treatment successfully increases purity. Effects of washing on phospholipid content is also reported in (Valax and Georgiou, 1993). Generally, SDS-PAGE techniques are used to separate different protein sizes. A few impurity peaks are found near the respective fusion protein size of 28.8 kDa and about 60 kDa (**Supplementary 3** an IB purity for 4 h and 12 h of the validation run)). These impurities correlating well to the size-range of a magnitude of outer membrane (e.g. ompA with 35.1 kDA (Molloy, et al., 2000)). To determine the extent of DNA in IB as impurities, we treated solubilized IB samples prior to an SDS-PAGE with DNAse 30 min at 37°C (DNAse 1, Thermo Scientific, Waltham, MA, US). No differences in the gel could be spotted between untreated and treated samples (**Supplementary 3** b). Therefore, we suppose little content of residual DNA within the IB samples, which was also described in (Valax and Georgiou, 1993). A higher IB purity is based on our model generally attributed to larger IB sizes. Since volume/surface ratio differs drastically compared to small beads less host cell structures can attach to the surface after homogenization. Buffer washing successfully removes a higher content of theses impurities.

To evaluate the three data driven model approaches, we performed a verification run was, aiming to achieve a maximum in titer of the recombinant protein including prediction of the respective attributes size and purity. Since the maximum of the titer could be found after 10 h of induction time, optimization is performed for this time stage. The process parameters received from the optimization algorithm for the induction phase were pH = 6.7, T = 31.5 °C. **Table 3** shows the comparison of the model prediction vs. the real measured values received after 10 h of induction. Standard cultivation reproducibility based on center point cultivations of *strain 1* are strongly time dependent, especially for titer and purity assessment.

Table 3: Prediction vs. measured QA of IBs for model validation run.

Val. run	**model**	**measured**	**assessment**
purity	*0.34522*	*0.397*	*Correct within 20% error for purity at 10 h*
Spez. titer (optimized)	*0.1131*	*0.140*	*higher than predicted*
size	*570.536*	*571.63*	*prediction correct*

Differences in the real $q_{s,Glu}$ during these three runs may affect the reproducibility, especially in the beginning of the cultivations as will be shown in the forthcoming chapter. Mean values and deviations for the center point runs of *strain 1* are given in **Supplementary 3**.The standard deviation for size is below 10% until 10 h of induction, heading to about 15 % at 12 h. Purity shows an error of about 30 % for until 8 hours reducing to values below 20 % afterwards. Low titer values are generally highly defective at early time stages of the induction phase as a result of the onset of production. These high errors of about 30% reduce to about 10 % after 8 h of induction. Using these assumptions for evaluation of the model clearly shown that model assumptions for size and purity QAs are correct within the given standard deviations. The IB bead size range after 10 h is predicted correctly, despite the general uncertainty of about 10 % in the measurement statistics. Purity was correct within the 20 % deviation at this time stage. Even slightly better results could be obtained for titer but are off the 10 % deviation. This may be based on the slightly higher $q_{s, Glu}$ of 0.3 g/g/h applied in this cultivation (overestimation of biomass after the fed-batch phase). Production of the protein of interest and the expression rate seems to be strongly correlated to the induction stress level of the cell. Lower temperatures seem to be favorable for the survival of the *E. coli* cells and positively influenced all three analyzed quality attributes. pH shifts to low pH increased the titer to a high degree at later induction stages and may be a result of a higher transmembrane potential, boosting the TCA and the energy metabolism (Stancik, et al., 2002). As *E. coli* can grow on a pH between 6.0 to 8.0, with an internal pH of 7.6 (Padan, et al., 1981), the rather acid pH-optimum is surprising at a first glance,

but when investigated it is likely that the pH of 6.7 could be causing less precipitate of diverse trace elements, which are added in the DeLisa media (DeLisa, et al., 1999). Having access to more co-factors could positively influence the IB-formation. pH shifts from 7.2 to 6.7 may also effect different enzymes in the cell, e.g. phosphofructokinase in glycolysis (Padan, et al., 1981).

Secondary structure analysis of IBs exhibiting different size

In order to understand the impact of different IB size produced in USP on the secondary structure, IR measurements in the MIR range were performed and compared to the correctly folded protein standard of *strain 1* for two distinct sizes exemplarily. **Figure 8** shows the IR spectra of the reference sample and IB beads with 400 and 600 nm in size from the same cultivation run.

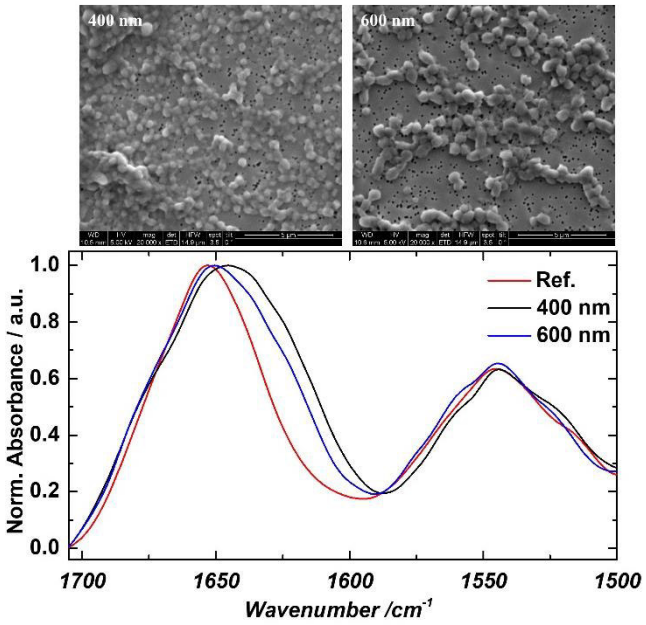

Figure 8: IR spectra of the two distinct bead sizes of 400 and 600 nm, compared to the correctly folded reference sample. SEM analytics of both samples are given above.

The IB samples were resuspended in MQ water and subsequently measured. The reference standard was measured in the formulated buffer. The IR spectrum of the reference shows a band

maximum at 1645 cm^{-1} in the amide I region as well as a narrow band at 1545 cm^{-1} in the amide II region that are characteristic for α-helical structures. In the reference sample, the native secondary structure of the protein is fully formed. Throughout the fermentation process, 400 nm size sample was taken after 4 h and the 600 nm sample was taken after 8 h. These samples also predominately feature α-helical secondary structure indicated by the amide I band maximum close to 1650 cm^{-1} (Barth, 2007). However, these samples also contain different, non-native secondary structure as denoted by the band shoulders at approx. 1625 and 1680 cm^{-1} that suggest β-sheet secondary structures. The IR spectra show that the extent of these non-native secondary structure components is different for the two samples taken from the cultivation and that the amount is lower in the sample that was taken at a later point in time. This is in accordance with the purity measurements and indicates that later cultivation times and larger IB sizes do not affect the secondary structure of the IBs negatively. These results can be compared to the work of Wurm et. al. (Wurm, et al., 2017) and corresponds to the data, that impurity content drastically decreases with IB size in solubilization and refolding.

Validation of the impact of classical process parameters on IB QAs using strain 2

For application of the proposed QA dependence used for *strain 1*, a reduced design space (compare to **Figure 4** b) for *strain 2* was applied and quality attributes were analyzed as described for *strain 1*. *Strain 2* also produces a toxic protein for the cells and is consequently expressed only as IBs but lacking the N-Pro fusion taq. As only four cultivations were performed, no statistical evaluation is used and fits were performed in order to have a reasonable model description and to reveal general trends during those cultivations. Estimation on standard deviations for the given QAs are already given in the previous section. In comparison to *strain 1* higher titers could be achieved during the cultivation. (**Figure 9** a) – normalized to the highest achieved titer in these cultivations, given in 1 [-]). Time dependent analysis of the IB bead size is shown in **Figure 9** b) and reveals the same trend as already valid for titer and purity. Low pH and low temperatures lead

to increased IB bead size in those cultivations (**Figure 9 c**). However, IB bead size is generally smaller in *strain 2*, when compared to *strain 1* respectively (N-Pro based protein, clearly visible by comparing Figures 2 b and 2 d). The dimensionless value of purity is generally very high as well, exceeding values of 0.5 even after 4 h of induction, compare to Figure 6 c). In accordance to *strain 1* the highest titers and purities are found at a low pH and low temperatures.

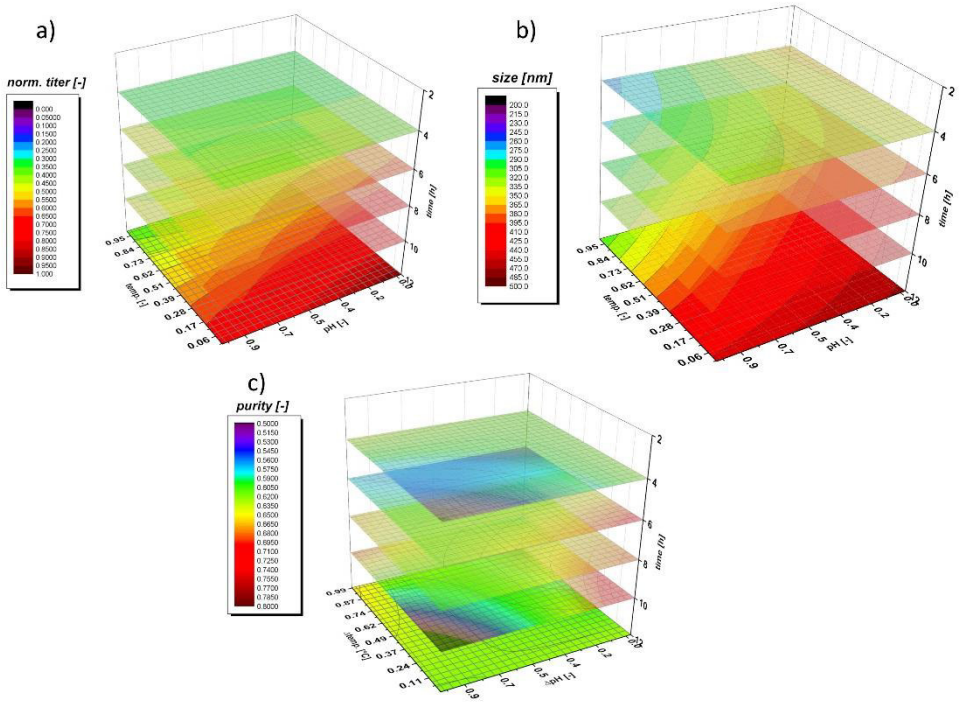

Figure 9: Data driven model for time dependent analysis of IB a) titer, b) size and c) purity of *strain 2* using a reduced DoE design (Figure 4 b). Trends are given with differences of the lowest process value. Very similar behavior to *strain 1* can be found, showing highest purity, size and titer at values for low T and pH. Higher titers are produced using this strain resulting in boosted purities compared to *strain 1*. The analyzed size similar to *strain 1*.

Different IB bead size for a broad number of proteins was already presented in literature: A GFP model protein, expressing IBs as well as soluble protein (Wurm, et al., 2017) showed IB bead size of a maximum of 600 nm at extended induction times using mixed feed systems with glucose and lactose. Since, GFP also is expressed as soluble protein, only the ratio between IB and soluble protein is altered based on the feeding strategies. Producing a maximum size of 600 nm, the GFP-model protein forms an intermediate between the measured maximum of *strain 1* (N-Pro) and *strain 2* in this work. Other works report IB sizes between 502 nm for DnaK- IBs and 580 nm for

ClpA-IBs (Díez-Gil, et al., 2010) and approximately 600 nm for G-CSF IBs (Peternel, et al., 2008) and are in a reasonable range compared with our products in this work. IB bead size is strongly dependent on the produced product, on the polypeptide sequence and on hydrophobicity of the protein structure. IB QAs can accordingly be altered with the used classical process parameter T and pH, but morphological considerations have generally to be taken into account and can be product-based very different. Since IPTG concentration of 0.5 mM is high enough to induce all present cells, the secondary structure of the expressed proteins of *strain 2* has to inhere in higher density in their structure regarding the titers. Denser structures are much easier to be separated in centrifugation processes in the downstream, since the difference of the density compared to the host cell debris is far higher. This fact may also affect the purity and results in those high purity values for *strain 2.* Computer tomographic analysis of transmission electron microscopy (not shown) of *strain 1* reveal cavities within single inclusion bodies in the cell and may be the result for density variations of different IB products. Based on the findings for both strains in this study, time-resolved analytics of the IB QAs can be used to optimize the USP. Knowledge of titer as key performance indicator is important for determination of the harvest time point. The resulting IB bead size (and purity) is beneficial for planning of further necessary steps in the downstream for a given product.

Impact of the physiological process parameter $q_{s,Glu}$ on IB quality attributes of strain 1 (N-Pro fused protein)

Classical process parameters showed a high impact on IB properties during induction phase. The knowledge for optimized parameters for *strain 1* –was used for altering the physiological parameter $q_{s,Glu}$. Temperature was decreased to 31.5 °C and pH was adapted to 6.7, while different setpoints for $q_{s,Glu}$ were established during induction phase. Setpoints and real values for the $q_{s,Glu}$ are given in **Table 4**.

Table 4: Applied $q_{s,Glu}$ vs. real $q_{s,Glu}$ values after reverse analysis of the cultivation data. Sugar accumulation and cell death at higher applied values result in higher standard deviations.

Run	**$q_{s,Glu\ set}$ [g/g/h]**	**$q_{s,Glu\ real}$ [g/g/h]**
1	*0.1*	*0.1 +/- 0.01*
2	*0.25*	*0.3 +/- 0.02*
3	*0.4*	*0.39 +/- 0.05*
4	*0.5*	*0.41 +/- 0.063*

The induction characteristic of the four performed runs are given in **Figure 10** a) showing glucose accumulation and percentage of dead cells for the four performed cultivations. It was already investigated in literature that the correlation of growth rate and the production of recombinant protein resulted in a decrease in μ the more recombinant protein is produced (Scott, et al., 2010). This correlation could be clearly monitored in our study during induction phase when high titers of recombinant protein were produced. As consequence the growth rate (not shown) decreased, leading to sugar accumulations as the feed-rate over the whole induction phase was applied constantly (Scott, et al., 2010). Higher applied $q_{s,Glu}$ resulted in early sugar accumulation and in increased number of dead cells in the cultivation and decreased the real $q_{s,Glu}$ extensively even

after some hours. After 12 hours of induction 50 % of the culture died at applied $q_{s,Glu}$ of 0.4 and 0.5 g/g/h, while very low $q_{s,Glu}$ showed neither cell death nor sugar accumulation.

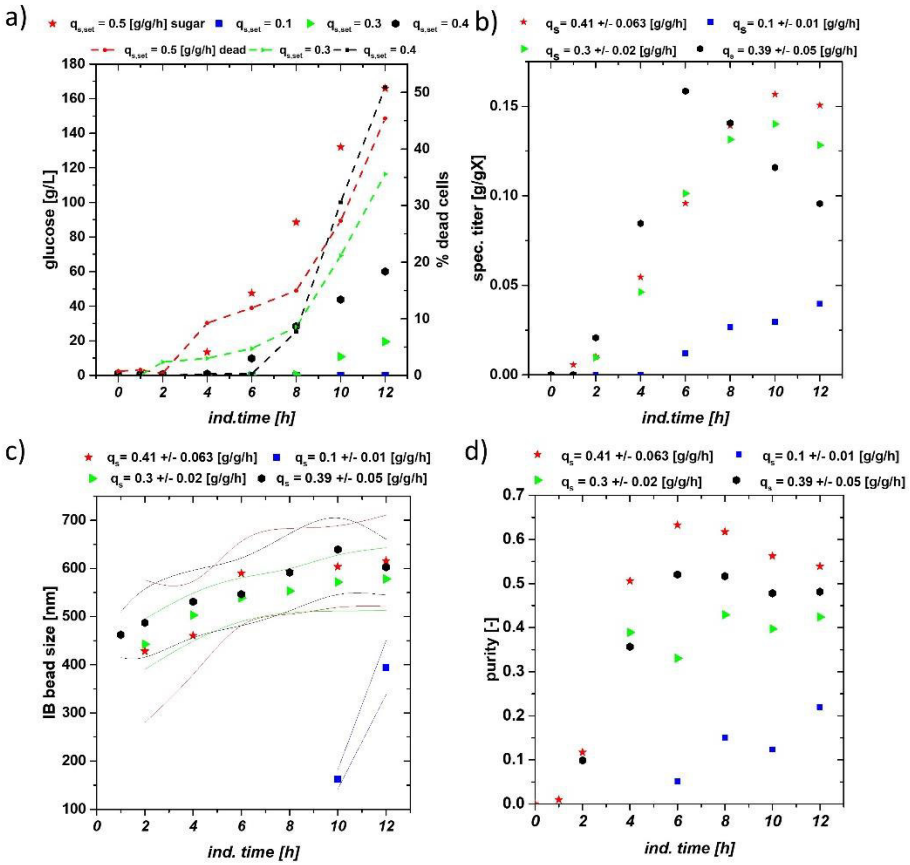

Figure 10: a) Sugar-accumulation and cell death measured by FCM for three cultivations at different $q_{s,Glu}$. Lowest $q_{s,Glu}$ shows no cell lysis and accumulation; b) specific titer of the recombinant protein fused to N-pro. Very high expression can be seen for the high $q_{s,Glu}$ until 6 h with decreasing $q_{s,Glu}$ also decreases product titer; c) size of the IB beads. $q_{s,Glu}$ = 0.41 g/g/h and $q_{s,Glu}$ = 0.39 g/g/h are very similar. A very steep increase is followed by a steady state; $q_{s,Glu}$ = 0.30 g/g/h shows increase over time, while size for $q_{s,Glu}$ = 0.10 g/g/h is only detectable at 10 and 12 h of induction; d) purity depicts clear dependence of all different $q_{s,Glu}$ setpoints, increasing the IB purity with higher $q_{s,Glu}$.

The time resolved titer measurements are given in **Figure 10** b). Very high specific titers could be found at $q_{s,Glu\text{-}set}$ = 0.5 g/g/h at 6 h of induction with highest volumetric productivities exceeding 1 g/L/h. However, the increased cell stress resulted in cell death and degradation of the product as could be seen in the decease of the titers at later time stages, respectively. After 12 h titers were almost identical irrespective of applied $q_{s,Glu}$ for high setpoints (0.3 – 0.5 g/g/h). That indicated, time dependent analysis of QAs is therefore of utmost importance, especially at physiological

process control. The peak value of the volumetric productivities (before degradation) showed a rising trend based on the mean $q_{s,Glu}$ values which were applied (**Supplementary 4**) and clearly indicated that the increased feeding rate is really beneficial for high productivity. The IB bead size given in **Figure 10** c) was generally very similar at $q_{s,Glu}$ = 0.3 – 0.5 g/g/h applied values, with $q_{s,Glu}$ = 0.3 g/g/h showing smaller diameters at later time stages. IB beads at $q_{s,Glu}$ = 0.1 g/g/h were not detectable with SEM until 10 h of induction time. Low $q_{s,Glu}$ yielded very small IB sizes and low titers in **Figure 10** b) as only low energy is available for production of the recombinant protein. A steep increase in the beginning of the induction time was generally accompanied by leveling off in diameter at later stages. Trends for IB purity are given in **Figure 10** d). Higher $q_{s,Glu}$ values were beneficial for protein purity, which were in reasonable accordance with trends for titer and size already seen in the previous chapter.

Based on these findings improved control strategies for IB production could be established in further development steps using the optimized process parameters for the two used strains in combination with physiological process control (time dependent adaption of the specific substrate uptake rate) during the induction phase.

2.4. Conclusions

IB quality attributes were analyzed in respect of changes in classical process parameters pH and T in the induction phase. Pronounced changes in QAs could be found in the analysis of IB titer, IB bead size and IB purity. Optimized process conditions for *strain 1* were found to be at pH = 6.7 and 31.5 °C during induction in respect of the produced maximum IB titer. These findings were checked using a second industrial relevant strain, revealing that low temperatures and low pH is highly beneficial for production of IBs. Therefore, we would like to hypothesize that yields of exclusively IB based products can be improved by applying low temperatures and a relatively low pH value during the induction phase as analyzed in this study for two very different products.

Despite of this platform knowledge, absolute values for size, titer and purity were strongly product dependent and exhibit very different values for every produced product.

The sweet spot conditions (pH = 6.7, T = 31.5 °C) for *strain 1* were used to show the impact of physiological control onto IB quality attributes. The four performed cultivations exhibited different specific substrate uptake rates ($q_{s,Glu}$) and revealed high impact on analyzed IB QAs. High constantly applied $q_{s,Glu}$ boosted titer, bead size and purity very early in the induction phase, but resulted generally in high glucose accumulation and cell death, while low $q_{s,Glu}$ did not stress the cells, but lead to very low production of IBs. Physiological control based on these findings may be highly industrially relevant in order to find IB parameters with high productivity, but also low contamination of host cell proteins and DNA.

We would also like to highlight that time dependent monitoring of the here defined IB-QAs can be used as a tool to optimize process parameters such as pH, temperature and ($q_{s,Glu}$). By improving the upstream conditions, we aim to trigger robust downstream procedures, increasing the overall time/space yield of IB-processes.

2. Impact of glycerol as carbon source onto specific sugar and inducer uptake rates and inclusion body productivity in *E. coli* BL21(DE3)

Based on the work in chapter 2 and recent studies by Wurm et al. (Wurm, et al., 2016, Wurm, et al., 2017) we analyzed the concomitant uptake of lactose as inducer based on applied substrate uptake rate of glycerol and glucose. Furthermore, a comparison of a product lacking plasmid is performed in comparison to the production strain. This work was performed with Julian Kopp and is published in **Bioengineering Journal** (Kopp, et al., 2017).

3.1. Introduction

The Gram-negative bacterium *E. coli* is the expression host of choice for the production of 30% to 40% of recombinant drugs in industry (Walsh, 2010, Gupta and Shukla, 2017). As *E. coli* shows very fast replication rates (Meuris, et al., 2014, Wurm, et al., 2016) on comparatively cheap media (DeLisa, et al., 1999), the benefits often outweigh the numerous purification steps (Berlec and Strukelj, 2013, Gupta and Shukla, 2017) and the missing glycosylation pattern (Spadiut, et al., 2014, Baeshen, et al., 2015, Gupta and Shukla, 2017). Recombinant protein production in *E. coli* gained more interest again as the demand in single chain antibody-fragments increased, which can be properly expressed in *E. coli* (Spadiut, et al., 2014, Gupta and Shukla, 2017). The strain BL21(DE3*)* created by F. Studier and B. Moffatt back in 1986 (Studier and Moffatt, 1986) is often used in an industrial scale, because of very low acetate formation, high replication rates as an effect of the integrated T7-polymerase (Steen, et al., 1986, Studier and Moffatt, 1986, Studier, et al., 1990, Dubendorff and Studier, 1991, Neubauer and Hofmann, 1994, Lyakhov, et al., 1998), as well as the possibility of protein secretion into the fermentation broth due to a type 2 secretion protein (Jeong, et al., 2009, Tseng, et al., 2009, Jeong, et al., 2015). As the lac operon is still one of the most favored promotors in pET-expression-systems (Dubendorff and Studier, 1991,

Marbach and Bettenbrock, 2012, Wurm, et al., 2016), it is generally used for insertion of the gene of interest. The repressor protein can only be blocked by allolactose or a structural analogue (Keiler, 2008), e.g.. the well-known inducer isopropyl β-D-1 thiogalactopyranoside (IPTG) (Neubauer and Hofmann, 1994, Wurm, et al., 2016). However, induction with IPTG stresses the cells, as IPTG in higher concentrations is referred to be toxic at elevated induction times (Neubauer and Hofmann, 1994, Viitanen, et al., 2003, Marbach and Bettenbrock, 2012). As tunable protein production is commonly applied in industry nowadays, mixed feed systems using either IPTG (Marisch, et al., 2013) or lactose (Neubauer, et al., 1992, Neubauer and Hofmann, 1994, Ukkonen, et al., 2013) as inducer did result in higher product yields, when compared to other inducer supplies (Marschall, et al., 2016). Soft Induction performed with lactose shows promising results (Neubauer, et al., 1992, Neubauer and Hofmann, 1994, Blommel, et al., 2007). As lactose can be metabolized in *E. coli*, it does not stress the cells as much as IPTG (Dvorak, et al., 2015). For the production of soluble proteins, induction with lactose usually is preferred (Wurm, et al., 2016), but it has also been shown that lactose shows promising results for Inclusion Bodies (IBs) and products located in the periplasm (Wurm, et al., 2016, Wurm, et al., 2017).

IBs have originally been believed to be waste products by bacteria (García-Fruitós, et al., 2012), until it was realized that IBs tend to form as a stress reaction by the cells resulting in a biologically inactive protein (Palmer and Wingfield, 2012, Ramón, et al., 2014, Villaverde, et al., 2015). Stress reactions of the cells can be caused by high temperatures, pH-shifts or due to high feeding rates. Higher feeding rates result in higher yields of product (Gupta and Shukla, 2017), which of course is advantageous combined with the possibility of expressing toxic proteins (Berlec and Strukelj, 2013). Still the downstream process (DSP) and especially the refolding unit operation is the time-consuming step in gaining the correctly folded product from *E. coli* cultivations (García-Fruitós, et al., 2012, Palmer and Wingfield, 2012, Ramón, et al., 2014, Villaverde, et al., 2015), which requires significantly more technology and time in purifying IBs (Palmer and Wingfield, 2012, Wingfield, 2014, Wingfield, et al., 2014). Though IBs can be produced in such excess, the amount of generated product often outweighs the DSP efforts and

makes the time/space yield more preferable for IBs (García-Fruitós, et al., 2012, Berlec and Strukelj, 2013, Baeshen, et al., 2015, Gupta and Shukla, 2017).

One of the most favored carbon sources in *E. coli* cultivations has always been glucose, as glucose has a very high affinity to the phosphotransferase system (Postma, et al., 1993, Deutscher, et al., 2006). Glucose provides a lot of energy for the cells, as it is directly induced into glycolysis as glucose 6-phosphate and consumed through the tricarboxylic acid cycle (TCA) (Ronimus and Morgan, 2003, Deutscher, et al., 2006). Usage of such, in combination with lactose may result in diauxic growth and catabolite repression, which are caused by the regulatory network that is induced by glucose (Stülke and Hillen, 1999, Kremling, et al., 2001, Bettenbrock, et al., 2006). Catabolite repression results in decreased lactose uptake rates when glucose is present in excess (Stülke and Hillen, 1999, Wurm, et al., 2017, Wurm, et al., 2017). Glycerol, first noticed in biotechnology as a by-product in the biodiesel production (Martínez-Gómez, et al., 2012), has shown quite promising results in terms of biomass/substrate yield in *E. coli* cultivations (Blommel, et al., 2007, Ukkonen, et al., 2013). To our knowledge, up to this point no catabolic repression has been reported, when glycerol was used as main carbon source (C-source) in combination with lactose (Lin, 1976). In addition, mixtures of glucose, glycerol and lactose have shown promising results for diverse products gained via autoinduction systems (Viitanen, et al., 2003, Blommel, et al., 2007). Recent studies (Wurm, et al., 2016, Wurm, et al., 2017) showed that the dependence of the inducer lactose influences the maximum IB production even on a quite low level of the specific glucose uptake rate. Low feeding rates of glucose would therefore result in the maximum inducer uptake rate, as cyclic adenosine monophosphate (cAMP)-levels increase at higher glucose addition and therefore decrease the affinity for the RNA-polymerase, decreasing the expression of the genes coding for the lac operon (Deutscher, et al., 2006). It is believed that cultivations with glycerol are able to overcome the problem of carbon catabolite repression and pave the way for usage of much higher specific C-source uptake rates, in order to increase time-space yields.

In this study, we performed cultivations with a BL21(DE3) strain, producing a recombinant protein coupled to a N-pro-fusion protein (Achmüller, et al., 2007), expressed as IB with the goal to yield in maximum recombinant protein production. It is believed that glycerol causes positive results for the mixed feed optimization when using lactose as an inducer, as glycerol - introduced into glycolysis but also into gluconeogenesis – yields high amount of energy supplied to the cultivation system (Zwaig, et al., 1970, Lin, 1976, Voegele, et al., 1993). Couple that with increased cAMP levels throughout the whole cultivation, (Deutscher, et al., 2006) glycerol is believed to be beneficial over a glucose cultivation system. It is shown, that the recombinant protein production is increased compared to glucose, as a result of more available energy.

3.2. Material and Methods

Bioreactor cultivations

All cultivations were carried out with the strain *E. coli* BL21(DE3) consisting of the pet[30a] plasmid system. The eukaryotic target protein was linked to a N-pro fusion tag (size of 28.8 kDA for the fusion protein) (Achmüller, et al., 2007). As the given protein is currently under patenting procedure at the industrial partner no detailed information can be given on the used protein.

All bioreactor and preculture cultivations were carried out using a defined minimal medium referred to DeLisa et al. (2015) (DeLisa, et al., 1999). Batch media and the preculture media had the same composition with different amounts of sugars respectively. The sugar concentrations for the phases were:

Table 5: respective sugar concentrations in media composition

	Amount of glucose	**Amount of glycerol**
Preculture	8.0 g/L	8.0 g/L
Batch-Media	20 g/L	20 g/L
Feed	either 250g/L or 300 g/L	

As pet 30a has a Kanamycin resistance gene, antibiotic was added throughout all fermentations, resulting in a final concentration of 0.02 g/L. All precultures were performed using 500 mL high yield flasks (containing the sugar concentrations given in **Table 5**. They were inoculated with 1.5 mL of bacteria solution stored in cryos at -80°C and subsequently cultivated for 20 h at 230 rpm in an Infors HR Multitron shaker (Infors, Bottmingen Switzerland) at 37°C.

All cultivations were either performed in a DASGIP Mini bioreactor-4-parallel fermenter system (max. working volume: 2.5 L; Eppendorf, Hamburg, Germany) or in a DASbox Mini Bioreactor 4-parallel fermenter system (max. working V.: 250 mL; Eppendorf, Hamburg, Germany). For measuring the CO_2 and O_2 flows a DASGIP-GA gas analyser was used (Eppendorf, Hamburg, Germany). The cultivations were controlled using the provided DAS-GIP-control system, DASware-control, which logged the process parameters. During cultivation pH was kept constant at 7.2 and controlled with base only (12.5% NH_4OH), while acid (10% H_3PO_4) was added manually, if necessary. The pH was monitored using a pH-sensor EasyFerm Plus (Hamilton, Reno, NV, USA). Base addition was monitored observing the flowrates of a DASbox MP8 Multipumpmodul. The reactors were continuously stirred at 1400 rpm.

Aeration was absolved using mixture of pressurized air and pure oxygen at 2 vvm, mixing the ratios of the airflow, that the dissolved oxygen (dO_2) was always higher than 40 %. The dissolved oxygen was monitored using a fluorescence dissolved oxygen electrode Visiferm DO 120 (Hamilton, Reno, NV, USA).

Cultivation scheme and q_s screening procedure

The batch media in the DASGIP reactors always contained 1 L DeLisa medium, while the DASbox Mini bioreactors contained a volume of 100 mL.

Only static q_s-controls were performed for these experiments, as the $q_{s,C}$ was not altered during induction phase (Wurm, et al., 2016, Wurm, et al., 2017). The procedure was always as follows: Preculture, Batch, non-induced fed-batch and induced fed batch with an adapted $q_{s,C}$.

Inoculation was always done with one tenth of the batch media volume, resulting in 100 mL of preculture. Preculture showed an OD_{600} of approximately 7 after cultivation (described above). The batch process, performed at 37 °C took around 6-7 hours, depending on the C-source used, and was finished, visible by a drop in the CO_2-signal. The 22 g/L of either glucose or glycerol usually resulted in a biomass of 9-10 g/L. After the batch was finished a non-induced fed-batch was started over night, at 35 °C and adapting the $q_{s,C}$ value to gain a biomass of approximately 30 g/L. After the non-induced fed-batch the volume was always decreased to 1 L, in order to keep induction conditions, the same. Afterwards $q_{s,C}$ was adapted to a certain point of interest, temperature was decreased to 30 °C and stabilized for 30 min before the inducer was added. Induction was always performed with a lactose pulse of 100 mL of a 300 g/L sterile lactose solution - resulting in a lactose concentration in the fermentation broth of approximately 30 g/L. Induction period always lasted 7 hours. The q_s control used here was performed using **equation 1** according to an exponential feed forward approach to keep q_s constant (Slouka, et al., 2016, Wurm, et al., 2016, Wurm, et al., 2017, Wurm, et al., 2017):

$$F(t) = \frac{q_{s,C} * X(t) * \rho_f}{c_f} \qquad \text{Equation 2}$$

With F being the feedrate [g/h], $q_{s,C}$ the specific Glucose or Glycerol uptake rate [g/g/h], X the absolute biomass [g], ρ_f the feed density [g/L] and c_f the feed concentration [g/L] respectively.

Process analytics

Samples are always taken after inoculation, upon end of the batch-phase and after the non-induced-fed batch was finished. During the induction period samples were either taken in 20- or

30-min intervals. Generally, biomass was measured using OD_{600} and dry cell weight (DCW), while flow cytometry analysis (=FCM) was used for determination of cell-death, especially in the induction phase. Optical density (OD_{600}) was measured using a Genesys 20 photometer (Thermo Scientific, Waltham, MA, USA). Since the linear range of the used photometer is between 0.2 and 0.8 [AU], samples were diluted with dH_2O to stay within that range. The dry cell weight was determined by vortexing the sample, pipetting 1 mL of sample solution in a pre-tared 2 mL Eppendorf-Safe-Lock Tube (Eppendorf, Hamburg, Germany) and centrifuged for 10 min at 11000 rpm at 4 °C. After centrifugation, the supernatant was used immediately for at-line high-pressure liquid chromatography (HPLC) measurement (see beneath), while the pellet was re-suspended with 1 mL of 0.9% NaCl solution and centrifuged at the same conditions. Afterwards the pellet was dried for at least 72 hours at 105 °C. Samples for FCM were diluted 1:100 with 0.9% NaCl solution, stored at 4 °C and measured after the process was finished. The measurement was performed using the software Cube 8 (Sysmex, Partec, Görlitz, Germany) according to Langemann et al. (Langemann, et al., 2016) using DiBAC4 (bis-(1,3-dibutylbarbituricacid) trimethineoxonol) and Rh414 dye. Rh414 binds to the plasma membrane and visualizes all cells, while DiBAC is sensitive to plasma membrane potential and therefore distinction between viable and non-viable cells can be achieved.

Product samples were taken for [P]-strain, after 2, 5 and 7 hours of induction phase. They were always treated as follows: 5 mL pipetted in a 50 mL Falcon tube, centrifuged for 10 min at 4800 rpm at 4 °C. The supernatant was discarded while the pellet was frozen at -20°C. Samples for homogenisation were disrupted as follows: The pellets were re-suspended in a Lysis buffer (0.1 M TRIS, 10 mM EDTA, pH = 7.4) according to its dry cell weight:

$$Volume\ Lysis\ Puffer = DCW * \frac{5}{4} \qquad \text{Equation 3}$$

After suspending the cells, they were treated with an EmusiflexC3 Homogenizer (Avestin, Ottowa, ON, USA) at 1500 bar. The duration of homogenisation was always calculated to achieve ten passages through the homogenizer. After washing the pellets twice with dH_2O, the samples

were measured using a HPLC method. The N-pro-fusion protein IB was measured via RP-HPLC (Thermo Scientific, Waltham, MA, USA) using a Nucleosil-column after solving in 7.5 M Guanidine Hydrochloride based buffer. The eluent was a gradient mixture of water with 0.1% TFA (tri-fluoric-acid) and Acetonitrile mixed with 0.1% TFA with a flow of 3 mL/min. Standard concentrations were 50, 140, 225, 320 and 500 mg/mL of an industrial supplied reference.

Sugar and glycerol concentrations were measured via HPLC-method (Thermo Scientific, Waltham, MA, USA) using a Supelcogel-column; Eluent: 0.1% H_3PO_4; Flow: 0.5 mL/min. Using this method glucose or glycerol accumulation as well as the lactose decrease and the galactose accumulation could be detected. Standards had a concentration of 0.5, 1, 5, 10 and 20 g/L of every sugar used throughout all fermentations. The HPLC run lasted always for 25 mins and chromatograms were analyzed using a Chromeleon Software (Dionex, Sunnyvale, CA, USA).

3.3. Results and Discussion

Mechanistic correlations of glycerol onto specific lactose uptake rate

The basic feeding rate for the induction phase for production of the recombined protein is a constant $q_{s,C}$ – given by a fed-batch carried out on glucose or glycerol depending on the experiment – and by a pulse of 10 vol% high concentrated lactose feed.

In order to get comparable datasets for all experiments a mechanistic model approach is performed. As shown in previous studies, the maximum possible specific lactose uptake rates depend on the specific glucose uptake rates which can be described by a mechanistic equation (see Eq. 3) (Wurm, et al., 2016, Wurm, et al., 2017). The maximum $q_{s,lac}$ rates depend Monod-like on $q_{s,glu}$ until a certain maximum is reached at a respectively low feeding rate of glucose, before $q_{s,lac}$ decreases at high $q_{s,glu}$ which performs analogue to substrate inhibition (Wurm, et al., 2016). Values for y = 0 correspond to the uptake rates on sole glucose/glycerol, respectively.

$$q_{s,lac} = q_{s,lac,max} \cdot \max\left(\left(\left(1 - \frac{q_{s,glu}}{q_{s,glu,crit}}\right)^{n}, 0\right) \cdot \left(\frac{q_{s,glu}}{q_{s,glu} + K_A} + \frac{q_{s,lac,noglu}}{q_{s,lac,max}}\right)\right) \qquad \text{Equation 4}$$

with $q_{s,lac}$ being the specific lactose uptake rate [g/g/h], $q_{s,lac,max}$ the maximum specific lactose uptake rate [g/g/h], $q_{s,glu}$ the specific glucose uptake rate [g/g/h], $q_{s,glu,crit}$ the critical specific glucose uptake rate up to which lactose is consumed [g/g/h], $q_{s,lac,noglu}$ the specific lactose uptake rate at $q_{s,glu}$ = 0 [g/g/h] and K_A the affinity constant for the specific lactose uptake rate [g/g/h]. n describes the type of inhibition (non-competitive, uncompetitive, competitive).

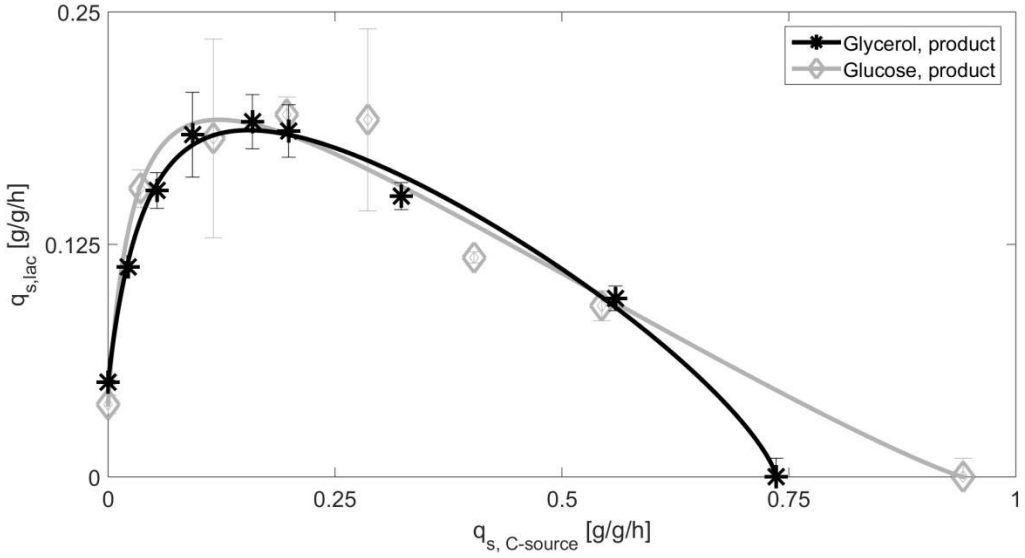

Figure 11: Extracted datapoints for q_s values including standard deviations for cultivations with glucose and glycerol in the production strain (glycerol product, glucose product). Solid lines represent the model-based approach for inducer uptake rates vs feeding rates models of glucose and glycerol.

As the model has already been established for four different products in glucose-lactose systems (Wurm, et al., 2017), it had to be shown if the same function fits for the given product. We fitted the model parameters as described in Wurm et al., where also detailed description of the model derivation can be found (Wurm, et al., 2016). As shown in **Figure 11** and **Table 6**, parameters can be found to describe the experimental data for glucose and glycerol as C-source. In absence of glucose, lactose cannot be taken up, since there is not enough adenosine triphosphate (ATP) produced. Once a certain threshold of glucose is passed, enough ATP is created to metabolize the inducer (Wurm, et al., 2016, Wurm, et al., 2017). The trend seen in the cultivations performed on glucose are explained by the well-known phenomenon of catabolite repression (CCR) (Stülke and Hillen, 1999, Bettenbrock, et al., 2006), as the lactose uptake rates decrease significantly with increasing the feeding rate. As *E. coli* BL21(DE3) is not able to metabolize galactose due to absence of a [gal] gene, which can be referred to a deletion of the genes gal M, K ,T ,E (Studier, et al., 2009, Xu, et al., 2012), galactose should accumulate in the fermentation broth (Bettenbrock, et al., 2006, Daegelen, et al., 2009). Hence, the galactose accumulation rate in the fermentation broth could generally be correlated to the lactose depletion rate during the cultivation (not shown).

However, the curves for glucose and glycerol are almost identical. Generally, a higher affinity for glucose is reported in literature (Deutscher, et al., 2006), resulting in a higher μ for those cultivations, as glycerol has less affinity to the phosphotransferase-system (=PTS), respectively (Bettenbrock, et al., 2006). This trend is in accordance with our data given in the value $q_{s,C,crit}$ in Tab. 2. Furthermore, biomass to substrate yields ($Y_{X/S}$) for glucose decrease in the induction phase from about 0.5 in the batch phase to about 0.336 +/- 0.05 after the one-point lactose addition. On the contrast $Y_{X/S}$ of glycerol are generally about 0.44 +/- 0.1 during the induction phase (Korz, et al., 1995).

Table 6: Model parameters and normalized-root-mean-square-error (NRMSE) for the different analysed cultivation

Cultivation System	$q_{s,lac,max}$*	K_A	$q_{s,C,crit}$	**n**	$q_{s,lac,noglu}$	**NRMSE**
	[g/g/h]	[g/g/h]	[g/g/h]	[-]	[g/g/h]	[%]
Glucose	0.23	0.032	0.94	1.14	0.039	6.5
Glycerol	0.23	0.053	0.74	0.74	0.051	2.6

This does not explain the very similar lactose uptake values at high $q_{s,C}$, since it is believed that carbon catabolite repression should not be present using glycerol as primary carbon source (Inada, et al., 1996). The production of the recombinant protein seems to induce stress resulting in the maximum possible activity inside the cell, which is represented by the similarity of the two curves. Therefore, the decrease of the $q_{s,lac}$ rate in the model based approach, actually referred to the CCR for glucose based systems so far ($\left(1-\frac{q_{s,glu}}{q_{s,glu,crit}}\right)^{n}$), may have to be reconsidered when glycerol is fed. In turn, our results would indicate that the decline cannot be attributed to carbon catabolite repression, also not for glucose. Glycerol does not interfere with the PTS transport system and no resulting change of the cAMP levels during uptake of lactose are to be believed on a first glance. Glycerol enters glycolysis as di-hydroxy-acetone-phosphate and is processed in glycolysis producing pyruvate, but also there are gluconeogenetic genes active providing the formation of glucose-6-phosphate (Larson, et al., 1987, Iuchi, et al., 1990, Martínez-Gómez, et al., 2012). As glycolysis seems to be running at maximum capacity, a bottleneck in trycarboxylic acid

cycle (TCA) may also be likely. Overload of the TCA-cycle has already been described by Heyland et al. (2011) (Heyland, et al., 2011), saying that TCA-cycle cannot metabolize all the pyruvate produced in glycolysis. It has also been referred that the cells try to gain energy in alternative ways such as using acetate as a terminal electron acceptor, or the usage of oxidative phosphorylation (Glick, 1995, Heyland, et al., 2011). However, as *E. coli* BL21(DE3) produces relatively low levels of acetate in general, the acetate formation is always beneath the threshold of the HPLC and may therefore not the predominant electron acceptor in this strain.

To test the observed effects, we tried a process technological method approach, rather than performing expensive and time consuming "omics" analysis. The pet[30a] plasmid was transformed into the used strain *E. coli* BL21(DE3) without the sequence for the recombinant protein, further referred as non-producer (Chan, et al.) strain. The strain was tested in the same analytical way as the used strain for recombinant protein production. HPLC raw data for lactose decrease are compared with an almost identical $q_{s,C}$ (~0,1 g/g/h) in **Figure 12.**

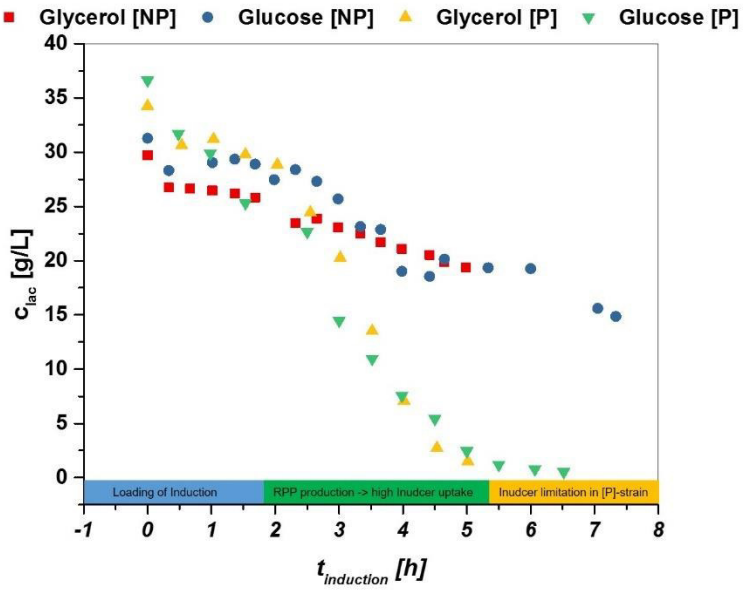

Figure 12: HPLC based data for decrease of lactose in fermentation broth exhibiting very similar $q_{s,C}$ values in [g/L]. A significant decrease over the time of induction is visible in producing [P] strains, while the decrease is way slower in non-producing [NP]-strain-cultivations.

Hereby three phases can be seen for the product producing strain in the induction phase, while only two phases can be seen in the [NP]-strain:

- Adaption phase: lactose gets transferred to alloactose and loads the induction (0 h - 2 h in induction phase).
- linear decrease of lactose as the system needs inducer for recombinant protein expression (2 h - 5 h).
- limitation of lactose in [P]-strain-> not sufficient inducer present, need for mixed feed system (5 h - 7 h), no inducer limitation seen in [NP]-strain, further decrease of inducer analogue to phase 2.

Results on the model-based approach for the glucose system are given in **Figure 13**.

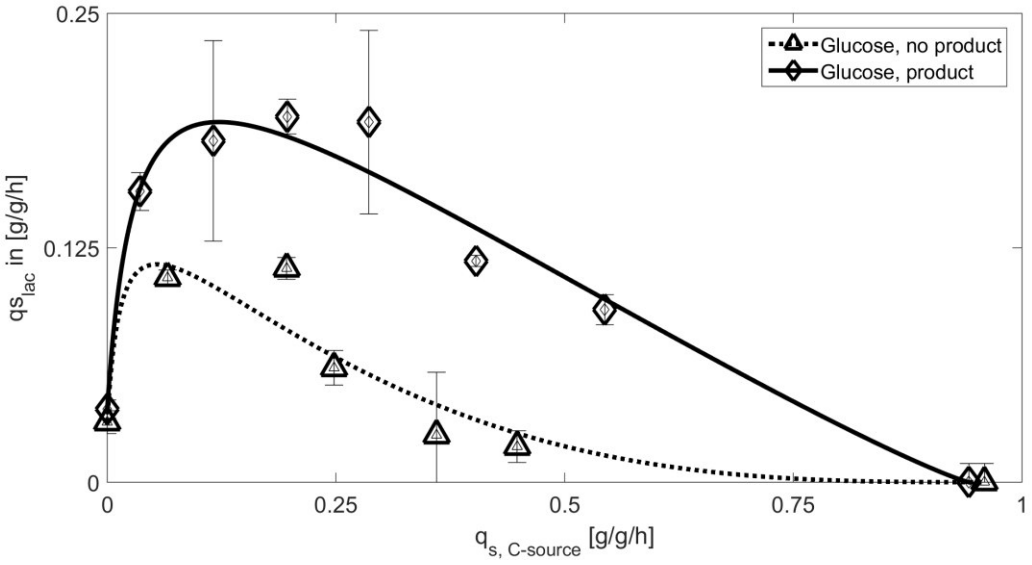

Figure 13: Extracted datapoints for $q_{s,C}$ values including standard deviations for cultivations with glucose using the product producing (glucose product) and the NP strain (glucose, no product). Solid lines represent the model-based approach for inducer uptake rates vs. feeding rates models of glucose. A clearly visible difference can be observed during these cultivations

The fermentations performed with the NP-strain showed lactose uptake rates resemble the expected carbon catabolite repression for glucose including high affinity of the PTS system at low $q_{s,glu}$ which can also be seen in **Table 6**. Despite the identical behavior of protein producing and NP strain, a clear difference in maximum $q_{s,lac}$ is obviously present. Higher consumption of glucose has impact on the cAMP level and decreases the specific uptake of lactose in the product producing strain. $Y_{X/S}$ stays very similar in both cases 0.37 +/- 0.05 for the protein producing strain vs. 0.383 +/- 0.053 for the NP strain. Given yields are a mean value over all $q_{s,C}$ values except for [lac] = 0 and [glu] = 0. So these general deviations in $q_{s,lac,max}$ can be attributed to the

increased energy demand during recombinant product production, as also the biomass yields stay the same. Lactose uptake rates on glycerol for the product producing and the NP strain are given in Fig. 3. Despite the quite straight forwards mechanistic explanation for glucose, glycerol biomass to substrate yields differ fundamentally for both experiments: $Y_{X/S}$ = 0.55 +/- 0.11 for the NP strain, while the producing strain has a $Y_{X/S}$ of 0.44 +/- 0.1. This fact may explain the much shallower uptake at low $q_{s,C}$ for the NP strain, but cannot explain the difference in the CCR term.

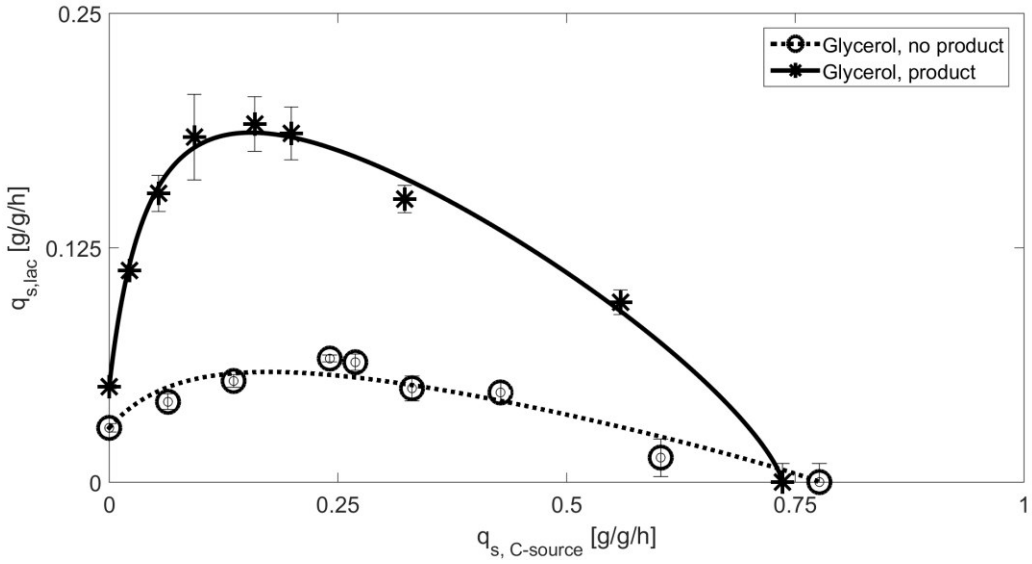

Figure 14: Extracted datapoints for $q_{s,C}$ values including standard deviations for cultivations with glycerol using the product producing (glycerol, product) and the NP strain (glycerol, no product). Solid lines represent the model-based approach for inducer uptake rates vs feeding rates models of glucose.

As a far higher biomass yield is present in the NP strain, only a reduced amount of lactose is taken up, which explains the decreased $q_{s,lac,max}$. However, the NP strain shows no pronounced substrate inhibition. The carbon catabolite repression term of the model on glycerol has only low impact (see **Table 6,** as the upregulation of cAMP using glycerol would also be beneficial for the lactose uptake mechanism in the PTS system (Deutscher, et al., 2006). Since the lactose facilitator is not considered to be the rate determining step in the glycerol metabolism, glycerol kinase closely regulated to the PTS system may cause the CCR-like effects (Zwaig, et al., 1970, Voegele, et al., 1993). As the feeding rate increases, the possibility of short-term local glucose and glycerol accumulation increases, eventually leading to diauxic growth and therefore decreased lactose rates

as glucose and glycerol have higher affinity than disaccharides for *E. coli* (Weissenborn, et al., 1992, Inada, et al., 1996, Hogema, et al., 1999, Deutscher, et al., 2006). The product producing strain shows a high regulated lactose uptake at low $q_{s,C}$ values, as a result of lower biomass yield and higher energy demand in production of the recombinant protein. Higher lactose uptake results in high intracellular glucose level, which show the similar feedback mechanism like in the glucose fed cultivations.

Table 7: Model parameters and normalized-root-mean-square-error (NRMSE) for the analyzed cultivation without recombinant product production

Cultivation System	**$q_{s,lac,max}$***	**K_A**	**$q_{s,glu,crit}$**	**n**	**$q_{s,lac,noglu}$**	**NRMSE**
	[g/g/h]	[g/g/h]	[g/g/h]	[-]	[g/g/h]	[%]
Glucose [NP]	0.14	0.016	0.96	2.92	0.032	12.7
Glycerol [NP]	0.10	0.13	0.78	0.90	0.029	9.7

As a result, both curves given in **Figure 11** have a very similar appearance, but are expected to have a very different regulation within. To get insight into respiratory activity, qCO_2 values are compared for all four fermentations, respectively. Evaluation is given in **Table 8** based on the applied $q_{s,C}$ values.

Table 8: specific substrate uptake rate vs. specific carbon evolution rate. Product producing strains have in general increased respiratory activity. NP strains show reduced respiratory activity. Standard deviation of qCO_2 increases at higher feeding rates

glucose		**glucose NP**		**glycerol**		**glycerol NP**	
$q_{s,C}$ [g/g/h]	qCO_2 [g/g/h]	$q_{s,C}$ [g/g/h]	qCO_2 [g/g/h]	$q_{s,C}$ [g/g/h]	qCO_2 [g/g/h]	$q_{s,C}$ [g/g/h]	qCO_2 [g/g/h]
0.036	2.15+/-0.33	0.066	1.69+/-0.25	0.022	2.91+/- 0.46	0.064	0.82+/-0.09
0.116	3.12+/-0.46	0.196	3.75+/-0.44	0.054	4.41+/- 0.78	0.136	1.85+/-0.21
0.197	3.98+/-0.55	0.224	3.35+/-0.42	0.093	3.88+/- 0.64	0.225	2.86+/-0.31
0.286	5.72+/-0.41	0.36	5.96+/-0.26	0.159	3.12+/-0.43	0.331	3.31+/-0.22
0.403	6.42+/-1.48	0.448	5.64+/-0.47	0.199	4.14+/-0.64	0.428	4.07+/-0.51
0.544	7.30+/-1.64			0.323	5.13+/-0.48	0.603	1.75+/-1.58
				0.559	7.18+/-2.10		

Highly similar respiratory activity is received for the product producing strain, almost linear increasing with $q_{s,C}$. For the NP strain, a general lower respiratory activity is seen for the glycerol fed strain. These results support the fact that lower energy demand is needed in this strain based on the general higher biomass yield and the fact that no recombinant protein is produced. In TCA first steps of amino acid synthesis are performed, therefore the production of non-essential AA would result in the accumulation of NADH (Jeremy M Berg 2002). As approximately two NADH molecules can be formed to one molecule of CO_2 the enhanced respiratory activity in the product producing strain is most likely coding for the enhanced production of non-essential AA, which are essential for the recombinant product. However, further analysis on stress induced changes in the gene expression may give valuable new insights into regulation mechanism in *E. coli.*

Productivity and physiology using glycerol as primary carbon source

As the overall goal is an increased production rate of recombinant protein, we compare titers of the produced IBs as a function of carbon source and uptake rate. In **Figure 15** a) the increase in IB titer over time is presented for two cultivations. The loading of the induction, which takes about 2 hours, can be clearly dedicated in these results, with no titer of the recombinant protein to be found within the first 2 hours (also compare to **Figure 12**). **Figure 15** b) shows product IB titers after 7 h induction time, which are plotted against the corresponding $q_{s,C}$. Only the feed-rate of glucose/glycerol which adapted for the static experiment in the induced fed-batch phase is used in this plot -as cultivations are induced with one lactose pulse, the $q_{s,C}$ is non-cumulative. Generally, an increase in the feeding rate is beneficial for product formation. Cultivations carried out on glycerol tend to produce more recombinant protein with a product optimum at a $q_{s,}$-glycerol-level seen around 0.3-0.35 g/g/h. It may be possible that even higher product titers can be found within the range of 0.3 to 0.55 g/g/h. Cultivations carried out on glucose also tend to produce more product when the feeding rate is shifted to rather high rates, as well. Very similar IB titers can be obtained at high $q_{s,C}$ levels, but are far away from the observed maximum.

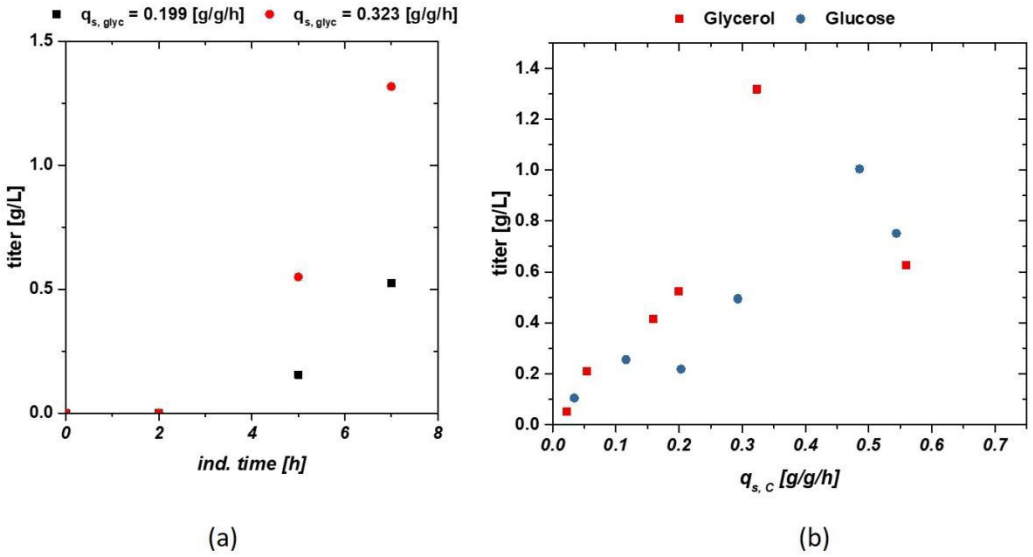

Figure 15: a) Time dependence for two IB titers starting from lactose addition to 7 h of induction; b) Titers of the recombinant produced protein, after homogenization of the inclusion bodies and a two-time washing plotted vs. the q_s of glucose and glycerol; a trend can be seen in gaining more product when cultivations are carried out on glycerol compared to glucose, respectively

The high increase in titer as a function of $q_{s,C}$ in glycerol may be a result of the higher biomass (higher $Y_{X/S}$ during induction) usually present in glycerol fed induction phases. The phenomenon of high product formation rates at high feeding levels, was much to our surprise, as we expected to see enhanced stress reactions by the cells due to overfeeding – especially at later time stages - usually present in IPTG induced cultures. Though we see only very little levels of glucose or glycerol accumulation in our HPLC-measurements (data not shown). This could be, as the fermentation conditions in the induction phase are respectively mild. Temperature is decreased to 30 °C and induction with lactose is regarded to be a softer induction, than IPTG, as lactose can be metabolized by *E. coli* (Neubauer, et al., 1992, Ukkonen, et al., 2013). In literature it has been reported that the catabolic repression increases with higher temperatures (Marr, et al., 1964). Altering the temperature in the induction phase, would have probably led to very different results in lactose uptake rates as well as different product data. Also, we want to highlight that every induction here was only performed with a one-time lactose pulse, which is most likely an insufficient induction, as there may be too little inducer in the media, which can be seen in **Figure 12**. In the following development steps, mixed feeds using glycerol in combination with lactose

must be established and measured as this would lead to a constant and complete induction of the system. However, the product data supports the results, that most probably very different regulation mechanism in *E. coli* lead to the same visible uptake rates in **Figure 11**, but have severe effects on the productivity on the different carbon sources.

Physiological analysis using flow cytometry (FCM) is presented in **Figure 16** a) and b). The NP strain given in **Figure 16** a) has very similar appearance for glucose and glycerol, respectively, increasing number of dead cells by increasing the feeding rate beyond a certain threshold, imposing stress to the cell. Throughout the whole experimental design, producing cells grown on glycerol exhibit a smaller cell size compared to cells grown on glucose (not shown). Since cell debris and residual particles are seen at similar cell sizes like glycerol grown cells a general higher abundance is present during those cultivations. To cope with this problem, FCM data after the non-induced fed-batch is subtracted from the subsequent measurements.

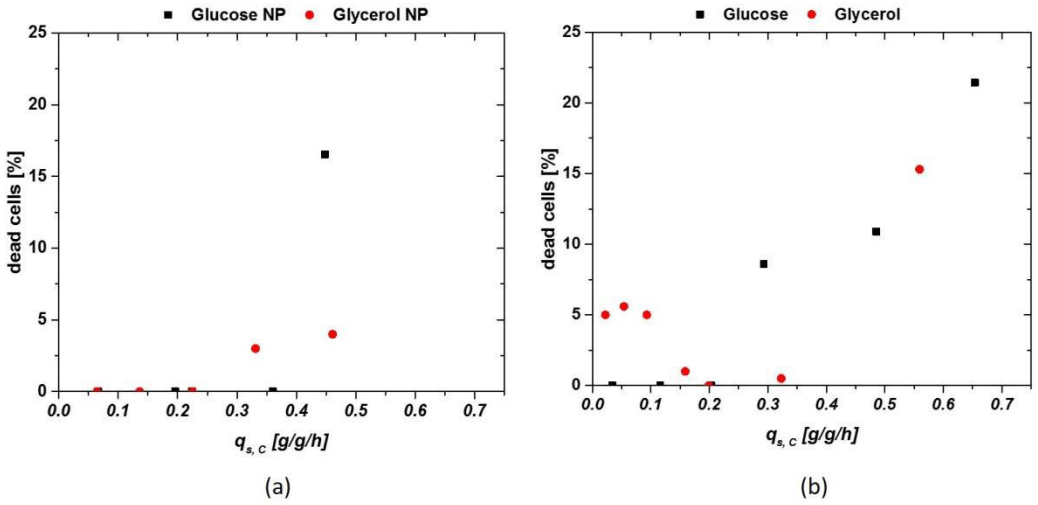

Figure 16: a) FCM analysis of NP strain 5 h after lactose pulse. As no protein data are received from these cultivations, the induction time was limited to 5 hours; b) FCM analysis of the product producing strain. Glycerol imposes stress at low feeding rates, while glucose shows increase in cell stress beginning at about 0.25 g/g/h.

The viability of both cultivation strategies for an induction time of 6 hours – often used for IB production at industrial scale - is given in **Figure 16** b), with a strong contrast between glucose and glycerol. While cells fed with glucose show no cell lysis at low $q_{s,C}$ levels and are very similar to NP strain in 5 a), glycerol shows certain stress reaction resulting in about 5 % dead cells until a

0.2 g/g/h. Afterwards stable conditions for glycerol can be found, while stress is induced at glucose fed systems starting at about 0.25 g/g/h. As the overnight fed-batch phase generally exhibited a q_s of 0.25 g/g/h, the switch to very low $q_{s,C}$ in the induction phase, combined with the lactose pulse, may impose the cell stress seen in 5% dead cells in **Figure 16** b). This corresponds well to the product data in Fig. 5 with similar or even higher productivity of glucose at low $q_{s,C}$ levels, but higher productivity for glycerol at moderate to high levels. Including the fact that glycerol shows higher biomass yields during induction with lactose, glycerol may be well used as an alternative main carbon source in *E. coli* cultivations, even though glucose has high affinity to the phosphotransferase system (PTS). It has already been reported that addition of glycerol to a glucose-lactose induction system increases product formation (Viitanen, et al., 2003, Mayer, et al., 2014). As glycerol needs increased cAMP-levels, which are also needed for lactose uptake (Bettenbrock, et al., 2006), this might be a key function in regulating higher lactose uptake and subsequently increasing productivity and product titer.

Furthermore, as glycerol is a cheap media compared to glucose, an application of glycerol in mixed-feed system with lactose may be highly beneficial for recombinant protein production performed in industry.

3.4. Conclusions

In this work, it was investigated, the effects of glycerol or glucose on lactose uptake rates for an IB based process using *E. coli* BL21(DE3). Feeding and uptake rates are compared and evaluated in terms of productivity and physiology using FCM.

It is shown that both C-sources show identical lactose uptake rates as a function of $q_{s,C}$. The used model based approach already performed for different products in Wurm et al (Wurm, et al., 2017) can be used for description of both curves. It has been detected that glycerol is beneficial

over the usage of glucose for maximizing the recombinant protein production of a lactose induced system.

Glycerol and glucose most probably exhibit different regulation of the carbon catabolite repression - the reduction of lactose uptake at higher $q_{s,C}$ levels. This hypothesis is supported by cultivation and evaluation of a non-producer strain exhibiting the expected behavior for both C sources, respectively. As this behavior was not seen in the producing strain, it seems like the expression hosts are performing at maximum capacity in recombinant protein production. Additionally, glycerol is referred to different metabolic pathways (Lin, 1976), eventually increasing the metabolic flux (Heyland, et al., 2011) towards recombinant protein production.

Physiology and productivity support the hypothesis that glycerol is promising C-source for cultivations using mixed feed systems with moderate to high $q_{s,C}$ values in order to boost time-space yields. As scale-up in *E. coli* systems can be performed relatively easily (Gupta and Shukla, 2017), the much lower costs of glycerol, when compared to glucose respectively, might provide interesting options for industrial and other large scale applications.

4. Control Strategies for Production of Recombinant Proteins based on the Cumulative Sugar Uptake and the Oxygen Uptake rate

In the previous chapters the impact of CPPs on the product QAs was analyzed and quantified. It was shown that long induction times and high specific substrate feeding rates result in high cell stress and degradation of the IB during cultivation since the viable cell concentration decreases when using IPTG as inducer However, high specific substrate feeding rates are very beneficial for early product formation. In this chapter, several control approaches are described to increase product formation without loss of viability during the cultivation. These two papers are submitted to **Microorganisms (Special Issue: Recombinant Protein Production)** and **Applied Microbiology and Biotechnology.**

4.1. Introduction for Titer as Key Performance Indicator

The gram-negative bacterium *E. coli* is the expression host of choice for the production of 30% to 40% of recombinant drugs in industry (Walsh, 2010, Gupta and Shukla, 2017). As E. coli shows very fast replication rates (Meuris, et al., 2014, Wurm, et al., 2016) on comparatively cheap media (DeLisa, et al., 1999), the benefits often outweigh the numerous purification steps (Berlec and Strukelj, 2013, Gupta and Shukla, 2017) and the missing glycosylation pattern on the recombinant product (Spadiut, et al., 2014, Baeshen, et al., 2015, Gupta and Shukla, 2017). Recombinant protein production in E. coli gained more interest again as the demand in single chain antibody-fragments increased, which can be properly expressed in E. coli (Spadiut, et al., 2014, Gupta and Shukla, 2017). The strain BL21(DE3) created by F. Studier and B. Moffatt back in 1986 (Studier and Moffatt, 1986) is often used in industrial scale, because of very low acetate formation, high replication rates as an effect of the integrated T7-polymerase (Steen, et al., 1986, Studier and Moffatt, 1986, Studier, et al., 1990, Dubendorff and Studier, 1991, Neubauer and Hofmann, 1994,

Lyakhov, et al., 1998), as well as the possibility of protein secretion into the fermentation broth due to a type 2 secretion protein (Jeong, et al., 2009, Tseng, et al., 2009, Jeong, et al., 2015). As the lac operon is still one of the most favoured promotors in pET-expression-systems (Dubendorff and Studier, 1991, Marbach and Bettenbrock, 2012, Wurm, et al., 2016), it is generally used for insertion of the gene of interest. The repressor protein can only be blocked by allolactose or a structural analogue (Keiler, 2008), e.g. the well-known inducer isopropyl β-D-1 thiogalactopyranoside (IPTG) (Neubauer and Hofmann, 1994, Wurm, et al., 2016).

Inclusion bodies (IBs) have been believed to be waste products by bacteria originally (García-Fruitós, et al., 2012), until it was realized that IBs tend to form as a stress reaction by the cells resulting in a biologically inactive protein (Palmer and Wingfield, 2012, Ramón, et al., 2014, Villaverde, et al., 2015). Stress reactions of the cells can be caused by high temperatures, pH-shifts or due to high feeding rates (Dvorak, et al., 2015). Exacerbation of substrate toxicity by IPTG in *Escherichia coli* BL21(DE3) carrying a synthetic metabolic pathway. These factors tend to result in higher yields of product (Gupta and Shukla, 2017), which of course is advantageous combined with the possibility of expressing toxic proteins (Berlec and Strukelj, 2013). Still the DSP and especially the refolding unit operation is the time-consuming step in gaining the correctly folded product from E. coli cultivations (García-Fruitós, et al., 2012, Palmer and Wingfield, 2012, Ramón, et al., 2014, Villaverde, et al., 2015), which requires significantly more technology and time, when purifying IBs (Palmer and Wingfield, 2012, Wingfield, 2014, Wingfield, et al., 2014). However, IBs can be produced in such excess, that the amount of generated product often outweighs the DSP efforts and makes the time/space yield more preferable for IBs (García-Fruitós, et al., 2012, Berlec and Strukelj, 2013, Baeshen, et al., 2015, Gupta and Shukla, 2017).

One of the most favoured carbon sources in E. coli cultivations has always been glucose, as it has a very high affinity to the phosphotransferase system (Postma, et al., 1993, Deutscher, et al., 2006). Glucose provides a lot of energy for the cells, as it is directly induced into glycolysis as glucose 6-phosphate and consumed through the TCA-cycle (Ronimus and Morgan, 2003,

Deutscher, et al., 2006). However, as glucose is quite expensive compared to other C-sources, cultivation is preferable performed with waste products, like glycerol, which was first noticed in biotechnology as a by-product in the biodiesel production (Martínez-Gómez, et al., 2012). It has shown quite promising results in terms of biomass/substrate yield in E. coli cultivations (Blommel, et al., 2007, Ukkonen, et al., 2013). In addition, mixtures of glucose, glycerol and lactose have shown good results for diverse products gained via autoinduction systems (Viitanen, et al., 2003, Blommel, et al., 2007). In a previous study, we presented that glycerol used as primary C-source for E. coli cultivations shows the same performance during biomass production as glucose, but even increased the specific titer of the product (Kopp, et al., 2017).

In this study, we performed cultivations with an *E. coli* BL21(DE3) strain, producing a recombinant model protein coupled to a N-pro-fusion protein (Achmüller, et al., 2007), thus expressed as an IB, with the goal to yield maximum recombinant protein production with volumetric IB titer as key performance indicator (KPI). Optimized process parameters for temperature and pH were used throughout the whole work and the controlled specific substrate feeding rate (qs,C) was adapted and responses for the IB product were analysed. High feeding rates yielded high productivity in the beginning of induction but also a high number of dead cells in later process state. Therefore, we developed different strategies and a model-based approach for determination of the optimal expression of the recombinant model protein using a new process value, which is based on cumulated glycerol uptake per dry cell weight of the cells (dSn).

4.2. Material and Methods for Titer Determination

Bioreactor cultivations

All cultivations were carried out with the strain *E. coli* BL21(DE3) carrying a pet30a plasmid system with a proprietary industrial relevant model protein. The target protein strain was linked to a N-pro fusion protein (Achmüller, et al., 2007). All bioreactor and preculture cultivations were carried out using a defined minimal medium referred to DeLisa et al. (DeLisa, et al., 1999). Batch media and the preculture media had the same composition with different amounts of glycerol, respectively. The glycerol concentrations for the phases were:

Table 9: respective sugar concentrations in media composition

Phase	**Amount of Glycerol**
Preculture	8 g/L
Batch-Media	20 g/L
Feed	either 300 g/L or 600 g/L

As pet 30a has a Kanamycin resistance gene, antibiotic was added throughout all fermentations in a final concentration of 0.02 g/L. Precultures were performed using 500 mL high yield flasks (containing the glycerol concentrations given in Tab. 1) or 100 ml Erlenmeyer shake flasks for DasGIP systems. They were inoculated with 1.5 mL of bacteria solution stored in cryo stocks at -80°C and subsequently cultivated for 20 h at 230 rpm in an Infors HR Multitron shaker (Infors, Bottmingen Switzerland) at 37°C.

All cultivations were either performed in a Sartorius Biostat Cplus bioreactor (Sartorius, Göttingen, Germany) with 10 L working volume or in a DASGIP Bioreactor 4-parallel fermenter system (max. working V.: 1.7 L; Eppendorf, Hamburg, Germany). Cultivation offgas was

analyzed by gas sensors -IR for CO_2 and ZrO_2 based for O_2 (Blue Sens Gas analytics, Herten, Germany). The cultivations were controlled using Lucullus process control system (SecureCell, Schlieren, Switzerland) or the provided DAS-GIP-control system, DASware-control, which logged process parameters. The reactors were continuously stirred at 1400 rpm.

During cultivation pH was kept constant at 6.7 and temperature at 31.5°C and controlled with base only (12.5% NH_4OH), while acid (10% H_3PO_4) was added manually, if necessary. The pH was monitored using a pH-sensor EasyFerm Plus (Hamilton, Reno, NV, USA). Aeration was carried out using mixture of pressurized air and pure oxygen at 2 vvm. Oxygen was added accordingly to keep dissolved oxygen (dO_2) was always higher than 30 %. The dissolved oxygen was monitored using a fluorescence dissolved oxygen electrode Visiferm DO (Hamilton, Reno, NV, USA).

Cultivation scheme and q_s adaption

Inoculation was always done with one tenth of the batch media volume. Preculture showed an OD_{600} of approximately 7 after cultivation for approximately 20h. The batch process, performed at 37°C took around 6-7 hours and was finished, visible by a drop in the CO_2-signal. The 20 g/L of glycerol usually resulted in a biomass of 9-10 g/L. After the batch was finished a non-induced fed-batch was started over night, at 35°C and adapting the $q_{s,C}$ value to gain a biomass of approximately 30 g/L. Afterwards $q_{s,C}$ was adapted to a certain point of interest, temperature was decreased to 31.5 °C and pH 6.7 and stabilized for 30 min before the inducer was added. Induction was always performed with a 0.5 mM IPTG and lasted for highest of 12 hours.

For screening of glycerol accumulation and cell death, only static feed forward q_s-controls were performed during induction phase (Wurm, et al., 2016, Wurm, et al., 2017). Exponential feed was established according to **equation 5**, an exponential feed forward approach to keep $q_{s,C}$ constant (Slouka, et al., 2016, Wurm, et al., 2016, Wurm, et al., 2017, Wurm, et al., 2017):

$$F(t) = \frac{q_{s,C} * X(t) * \rho_f}{c_f}$$ Equation 5

With F being the feedrate [g/h], $q_{s,C}$ the specific glycerol uptake rate [g/g/h], X(t) the absolute biomass [g], ρ_F the feed density [g/L] and c_F the feed concentration [g/L] respectively. For applied control strategies adaption of the $q_{s,C}$ during the induction time is performed based on **equation 5**.

Process analytics

Samples were always taken after inoculation, upon end of the batch-phase and after the non-induced-fed batch was finished. During the induction period samples were either taken in 60 or 120 min intervals. Generally, biomass was measured using OD_{600} and DCW (dry cell weight), while flow cytometry analysis (FCM) was used for determination of cell-death, especially in the induction phase. Optical density (OD_{600}) was measured using a Genesys 20 photometer (Thermo Scientific, Waltham, MA, USA). Since the linear range of the used photometer is between 0.1 and 0.8, samples were diluted with dH_2O to stay within that range. The dry cell weight was determined by vortexing the sample, pipetting 1 mL of sample solution in a pre-tared 2 mL Eppendorf-Safe-Lock Tube (Eppendorf, Hamburg, Germany) and centrifuged for 10 min at 10000 rpm at 4°C. After centrifugation, the supernatant was used immediately for at-line HPLC measurement (see beneath), while the pellet was re-suspended with 1 mL of 0.9% NaCl solution and centrifuged at the same conditions. Afterwards the pellet was dried for at least 72 hours at 105 °C. Samples for viable cell concentration (VCC) were measured using flow cytometry (FCM). Samples were diluted 1:100 with 0.9% NaCl solution, stored at 4°C and measured after the process was finished. The measurement was performed using the software Cube 8 (Sysmex, Partec, Görlitz, Germany) according to Langemann et al. (2016) (Langemann, et al., 2016) using DiBAC4 (bis-(1,3-dibutylbarbituricacid) trimethineoxonol) and Rh414 dye. Rh414 binds to the

plasma membrane and visualizes all cells, while DiBAC is sensitive to plasma membrane potential and therefore distinction between viable and non-viable cells can be achieved.

Glycerol concentrations were measured via HPLC-method (Thermo Scientific, Waltham, MA, USA) using a Supelcogel-column; Eluent: 0.1% H_3PO_4; Flow: 0.5 mL/min or an Aminex HPLC column (Biorad, Hercules; CA, USA) on an Agilent 1100 System (Agilent Systems, Santa Clara, CA, USA) with 4 mM H2SO4 as running buffer at 0.6 mL/min. Using this method glycerol accumulation could be detected. Prepared standards had concentrations covering the range from 1 to 50 g/L of glycerol. The HPLC run lasted always for 30 mins and Chromatograms were analyzed using a Chromeleon Software (Dionex, Sunnyvale, CA, USA).

Product Analytics

IB Preparation

5 mL fermentation broth samples were centrifuged at 4800 rpm at 4 °C. The supernatant is discarded and the pellet was resuspended to a DCW of about 4 g/L in lysis buffer (100 mM Tris, 10 mM EDTA at pH = 7.4). Afterwards the sample was homogenized using a high-pressure homogenizer at 1500 bar for 10 passages (EmulsiflexC3; Avestin, Ottawa, Canada). After centrifugation at 10000 rpm and 4 °C the supernatant was discarded and the resulting IB pellet was washed twice with ultrapure water and aliquoted into pellets à 2 mL broth, centrifuged (14000 rpm, 10 min 4 °C) and stored at -20 °C.

IB Titer

For titer measurements IB pellets were solubilized using solubilization buffer (7.5 M Guanidine Hydrochloride, 62 mM Tris at pH = 8). The filtered samples are quantified by HPLC analysis

(UltiMate 3000; Thermo Fisher, Waltham, MA, USA) using a reversed phase column (EC 150/4.6 Nucleosil 300-5 C8; Macherey-Nagel, Düren, Germany). The product was quantified with an UV detector (Thermo Fisher, Waltham, MA, USA) at 214 nm using Novartis BVS Ref. 02 as standard. Mobile phase was composed of acetonitrile and water both supplemented with 0.1% (v/v) tetrafluoride acetic acid. A linear gradient from 30% (v/v) acetonitrile to 100 % acetonitrile (ACN) was applied. A steep linear gradient from 10% ACN to 30 % ACN in 60 s was followed by a long linear gradient from 30 % to 55 % and by 3 regeneration steps.

Modelling of process parameters and KPIs

For the development of our model, mechanistic links were established using the software Matlab 2017. Within this model only time of the induced fed batch was simulated, as no alteration of viable cell concentration nor product formation occurred within batch & non-induced-fed batch (FB)-cultivation. Static inputs for the model consisted of volume [L], substrate in fermentation broth [g/L] and biomass [g/L] at timepoint $t_{induction}$ = 0 h. Further feed concentration [g/L], $Y_{X/S}$ [g/L] and $q_{S,max}$ [g/g/h] were needed for modelling the behavior of the induction phase. Defining basic mass equations on FB process behavior, prediction of classic process parameters like volume, substrate metabolization, biomass formation was established via differential terms given beneath. Due to simplification, volume increase during fermentation was calculated via feed addition only:

$$x.S.dxdt = '(EQ.F_{in} / x(1) * p.c_{glu}.Value - x(2)) - EQ.qs * x(3)'$$

$$x.CDW.dxdt = 'x(3) * \left(EQ.qx - EQ.F_{in} * x(1) \right)$$

$$y.V.eq = 'x(1)'$$

$$y.V.Unit = 'L'$$

$$y.S.eq = 'x(2)'$$

$y.S.Unit = 'g/L'$

$y.CDW.eq = 'x(3)'$

$y.CDW.Unit = ' g/L'$

With S being the substrate [g], F_{in} the feed [mL/h], c_{Glu} the feed concentration [g/L], CDW the dry cell weight [g/L], q_s the specific substrate feeding rate [g/g/h] – simulated in the model - and q_x the specific biomass generation rate [g/g/h] based on q_s. Several additional functions were established as so called "helper equations" in the model to predict further mechanistic correlations.

4.3. Results and Discussion for Titer as KPI

IB Titer as key performance indicator (KPI) is of utmost importance for determination of the harvest time point - generally based on empirical knowledge of the process - to receive optimal conditions in the downstream. We present a methodology for not only optimizing the process performance irrespective of strain and C-source, but also give a blueprint for establishing a model-based approach for estimation of viable cell concentration and titer with the need of only performing a few experiments for a specific product.

Static $q_{s,C}$ feeding strategies

The aim of this screening approach was to find optimal feeding parameter for IB production in *E. coli* processes, altering IB titer as KPI using different setpoints for the specific glycerol uptake rate $q_{s,C}$. Classical and physiological process parameters using glucose as carbon source have already been analyzed in recent work (Slouka Christoph, 2018). These findings resulted in the pH and temperature parameters used in this study (T = 31.5 °C, pH = 6.7 for the induction phase).

Glycerol based cultivations exhibit different benefits: the media is comparably cheap as glycerol is regarded as waste product; the degree of reduction is slightly higher compared to glucose; productivity seems to be positively influenced using glycerol as primary carbon source (Kopp, et al., 2017). We tested four different setpoints for $q_{s,C}$ during the induction phase and analyzed general performance and IB productivity (**Figure 17**). At high $q_{s,C}$ early glycerol accumulation was observed, exceeding 100 g/L at a $q_{s,C}$ – set of 0.5 g/g/h. Additionally, product degradation was present (**Figure 17** b after reaching a threshold of about 10 g/L glycerol in the fermentation broth). However, high $q_{s,C}$ favored product formation especially in the beginning compared to mediate/low $q_{s,c}$ (**Figure 17** b).

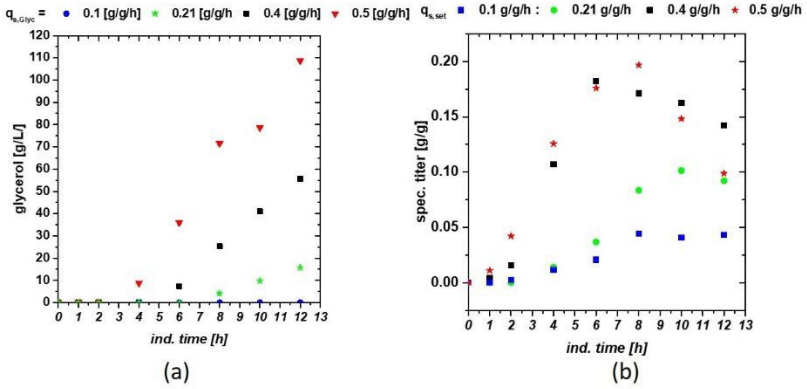

Figure 17: (a) Sugar accumulation measured in the supernatant during the course of induction with different static qs,C set-values.;(b) Specific titers of the recombinantly produced protein. High qs;C values are beneficial for the production – especially in the beginning of the induction phase -, but lead to pronounced protein degradation over time.

Glycerol accumulation in the broth can be a result of overfeeding in the exponential feed forward, overestimating the active biomass X(t) at the given timepoint. Hence, it was also shown that cells producing high amount of recombinant protein suffer from a so called "µ-decrease" over time of induction, eventually leading to non-C-limited feeding. Interdependence of cell growth and gene expression: origins and consequences. Offline biomass measurement methods, like OD_{600} and CDW, just reflect the total biomass inside the reactor and give no information on metabolic activity nor on the physiological state. To overcome this limitation, flow cytometry measurements are routinely performed during cultivations (using dyes as markers for all cells and dead intact

cells). Detection of onset of cell death can also be checked using HPLC fingerprinting methods in addition to FCM measurements (Rajamanickam, et al., 2017). At $q_{s,C}$ values above 0.4 g/g/h a strong increase in dead cells after 5 hours of induction was visible (**Figure 18** a). This time point was in good correlation to the onset of sugar accumulation (**Figure 17** a). As high production of a recombinant protein affects the protein synthesis chain of the cell a decrease in growth rate leads to cell death at later induction time (Scott, et al., 2010). The reduction of viable biomass in comparison to the total biomass is exemplarily given for the highest applied $q_{s,C}$. Regarding these results, the host cells require a high feeding rate at the beginning of induction in order to produce high levels of IBs. Hence, after 5 hours after induction, drops in viable cell concentration (VCC) correlating with higher glycerol accumulation indicate that the metabolism of cells shifts to a different state, most likely caused by the stress in producing the recombinant protein. Physiological feeding rate should therefore be adapted to the different metabolism of the cells in order to still provide high levels of viability and prevent cell death.

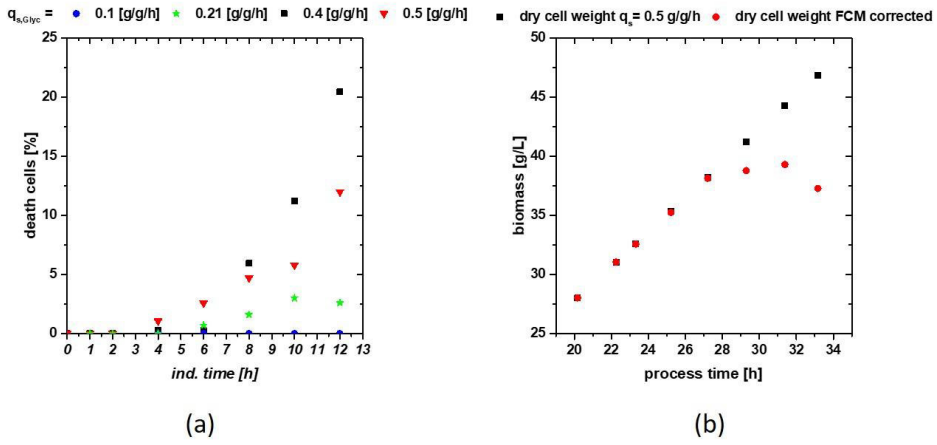

Figure 18: (a) Cell death during induction time affected by the applied qs,C; b) Exemplarily reduction of the active biomass (circles) in the reactor compared to the absolute biomass in the reactor (rectangles = dry cell weight).

For easy comparison between different physiological feeding strategies, the cumulated specific sugar uptake rate dSn [g/g] value (**equation 6**) was established in our group, which can be used for making a normalization on the fed C-source in respect to the total biomass at the induction time (Reichelt, et al., 2016):

$$dSn = \frac{\int_0^t m_C dt}{X(t=0)}$$ Equation 6

with m_C [g] being the fed mass of carbon source, dt [h] the respective time interval and X(t) [g] the non-corrected biomass at the sampling timepoint t in dry cell weight. The induction time scale can now be exchanged for the dSn value during the induction phase. Low $q_{s,C}$ values result in a low dSn value, while high $q_{s,C}$ increases the values since a high amount of glycerol is fed based on the biomass. The interaction between the IB titer and dSn is presented in **Figure 19**. The titer maximum of all fermentations (except for $q_{s,C}$ = 0.1 g/g/h, which only resulted in a low dSn after 12 hours of induction) was found in a range from 3.5 to 6 g/g. The highest specific titer was found irrespective of dSn at the highest $q_{s,C}$ value of 0.5 g/g/h. However, feeding beyond a dSn value of 6 g/g did not show any beneficial effect, but did decrease the product titer leading to high exceptional glycerol accumulation and triggered the release of host cell proteins, since cell death set in (Rajamanickam, et al., 2017).

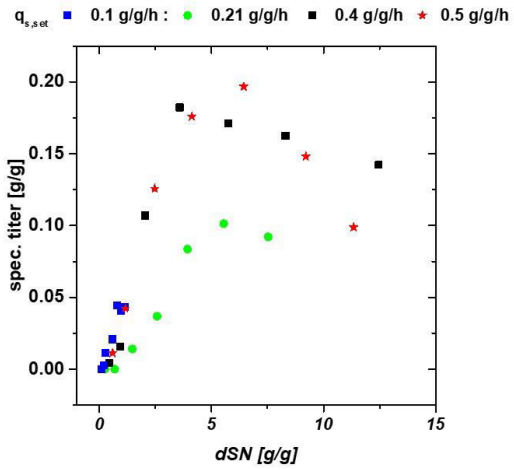

Figure 19: dSn-based analysis for specific titers. The amount of fed glycerol results in highest titers between a dSn of about 3.5 to 6 g/g.

Summarizing, titer is strongly affected by the fed glycerol during the cultivation. In order to reduce product degradation, cell death has to be prevented during the induction phase.

Offline dSn controlled feeding strategies

We demonstrated that physiological feeding has to be adapted in order to prevent a drop in the viable cell concentration at later induction times. However, high applied $q_{s,C}$ boosts the product formation, especially in the first hours of induction and should therefore be applied for high space time yields. As dSn analysis in Figure 3 a revealed, values between 3.5 and 6 g/g resulted in the highest specific IB titers. Therefore, an adaption of the applied $q_{s,C}$ after this stage was necessary to prevent cell death and inefficient sugar feeding. We adapted **equation 6** for online calculation in the process control system of the dSn value given in **equation 7**:

$$dSn_{control} = \frac{weight_{feed}(t) - weight_{feed}(0)}{X(t=0)} * \left(\frac{1000}{\rho_{Feed}}\right) \qquad \text{Equation 7}$$

with $weight_{feed}$ for actual timepoint and in the beginning of the induction phase (t=0), the total biomass in the beginning of the induction X(t=0) and the feed density ρ_{feed}. Based on this control, two different cultivation strategies were examined: The first had an instant drop of the $q_{s,C}$ to 0.1 g/g/h after reaching a dSn value of 3.5 g/g (blue squares in Figure 4); in the second one $q_{s,C}$ was subsequently reduced to 0.4 and 0.3 g/g/h after dSn of 3.5 g/g was reached (green diamonds in Figure 4). Reduction of the $q_{s,C}$ was performed using **equation 5**, estimating the total biomass X(t) by the measured OD_{600} value at this timepoint.

The feeding strategy is shown in **Figure 20** a Red circles show the constant $q_{s,C}$ feeding control with very pronounced sugar accumulation as already seen in **Figure 17** a. The lowest sugar was consumed when dropping the $q_{s,C}$ instantly to 0.1 g/g/h.

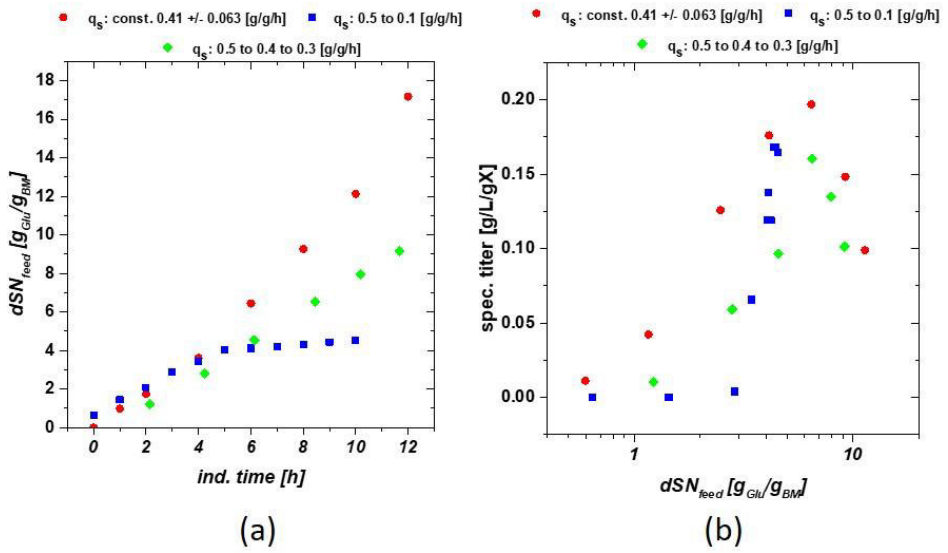

Figure 20: (a) Feeding strategy of three representative cultivations. The change in exponential feeding was triggered at a dSn of 3.5 g/g; (b) Specific titer for constant $q_{s,C}$, instant drop and stepwise drop. Highest titers could be found at instant drop strategy.

This strategy was also very beneficial regarding the IB specific titer given in **Figure 20** b. The instant drop allowed high specific titer compared to the constant $q_{s,C}$ control but without high degradation of the product. This fact gets clear in visualization of the specific productivity q_p (**Table 10**).

Table 10**:** Comparison of the measured q_p and the measured cell viability.

Ind. time [h]	***Static $q_{s,C}$ = 0.5 g/g/h (Baeshen, et al.)***	***Drop to 0.1 g/g/h (blue)***	***Stepwise drop (green)***
	q_p [mg/g/h] / dead cells [%]		
1	7 / <1 %	0 / <1 %	0 / <1 %
2	27 / <1 %	4 / <1 %	4 / <1 %
4	38 / <1 %	34 / <1 %	26 / <1 %
6	23 / 1.1 %	19 / <1 %	23 / 10.5 %
8	10 / 4.7 %	35 / <1 %	23 / 24.8 %
10	-14 / 5.8 %	-9 / <1 %	-5 / 39 %

Peak productivity can be found at the instant drop cultivation without pronounced degradation. Decrease in specific productivity and negative productivity reflect degradation of the product, based on the reduction of the VCC. The offline dSn control is therefore highly favorable for fed-batch based cultivations. Only a quarter of the C-source is needed compared to the static $q_{s,C}$ experiment, reducing the costs of the media drastically (even with glycerol regarded as waste resource). Furthermore, the highest specific productivity is found with this strategy combined with a long-time stability of the produced product - for about 5 hours in the fermentation broth – prolonging the harvest time range. The reduction to 0.1 g/g/h was chosen empirically based on the stability of the cells at low feeding rates and resulted in well-chosen process performance, eventually achieving high VCC. However, the absolute optimum for reduction of the feed cannot be dedicated by the offline dSn control strategies. According to our results, fed-batch based cultivations induced with IPTG producing a recombinant protein exclusively in IB, seem to be limited in productivity based on the product (Slouka Christoph, 2018) but process performance and stability can be optimized using this improved control strategy.

Oxygen Uptake Rate as online trigger for determination of transition for dSn controlled cultures

dSn based screening and control can be easily adapted for a known, reproducible process, but are nevertheless dependent of knowledge on biomass after the fed-batch and on the transition to cell death to start the control strategy. Generally, process control is performed by applying mechanistics of empirical models for prediction of the performed process or for several key performance indicators (KPI) (Sagmeister, et al., 2013, Ehgartner, et al., 2015, Kroll, et al., 2017). Regularly, the prediction of biomass and inhibiting metabolites are the quantities of interest and are tried to be simulated for predictive control of the bioprocess. Prediction of product attributes or KPIs within the cultivation is – especially in high dynamic microbial processes – challenging. No direct control is given over the process, allowing to react upon unexpected perturbations using the dSn based control strategy. Therefore, we adapted strategies for determination of oxidative metabolism in E. coli by Schaepe et. al. (Schaepe, et al., 2014). The authors reported high acetate production after limitation on the oxidative metabolism, visible by leveling of the oxygen uptake rate (Seras-Franzoso, et al.). This limitation in the metabolism is also visible in linear increasing the $q_{s,C}$ given in **Figure 21** a. However, we did not see acetate production with our strain (at least below the limit of detection of the HPLC method during fed batch cultivations), but strong sugar accumulation starting at this timepoint. A leveling off in the OUR indicated that no more glycerol was consumed by the cell and feeding should be stopped or decreased at this timepoint. Upon this point the feeding was stopped and the cells were able to consume glycerol present in the broth. Total consumption of glycerol was again visible as drop in the OUR.

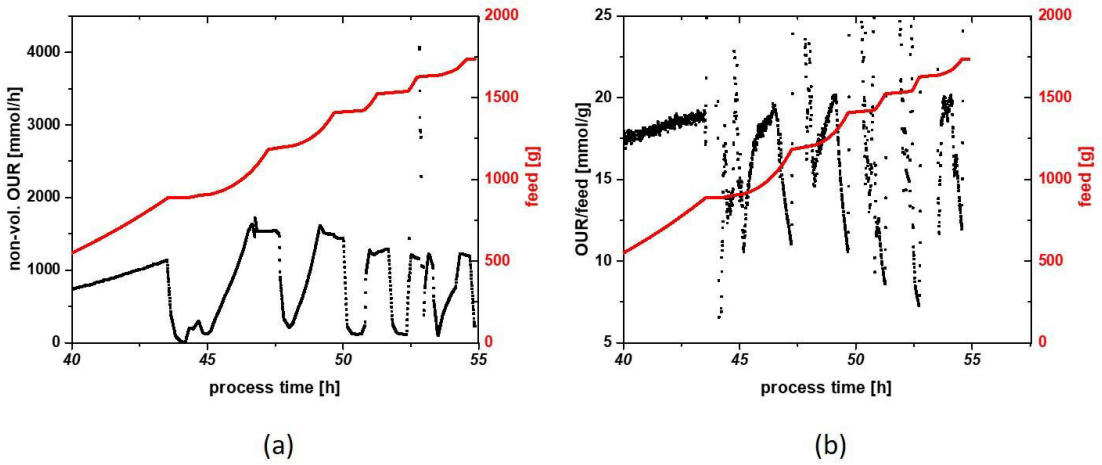

Figure 21: (**a**) Non volumetric OUR as a function of linear increasing $q_{s,C}$ values during induction phase (exponential increase in mass feed – red). Sugar accumulation in the broth leads to flattening of the OUR signal; (**b**) OUR normalized to fed mass of glycerol. A drop in the signal indicates sugar accumulation and can be used as trigger for the dSn based control. Sugar digestion capacity is constantly decreasing over time.

Upon drop, the feed was started again and glycerol was consumed by the cells until a plateau was reached again. This procedure was repeated several times during the experimental run. The capacity of sugar metabolism was decreasing over induction time as already reported before (Scott, et al., 2010, Schaepe, et al., 2014, Reichelt, et al., 2016). This fact may be used for determination of cell death during induction but was not performed within this study. Using the OUR directly leaves with three distinct states of metabolism: complete oxidative while the OUR rises, overwhelming of the metabolism visible in the plateau and complete glycerol consumption triggered by the OUR drop. In order to make detection of the trigger point between complete oxidative metabolism and overwhelming easier to control we established a derived value, with normalization of the non-volumetric OUR to the glycerol feed (**Figure 21** b). A steady increase of the derived quantity reflects oxidative metabolism, while a drop after a maximum indicates overwhelming of the oxidative metabolism at the given $q_{s,C}$ value. State of the art measurements use photometric assays or HPLC methods for measurement of the C-source but have the disadvantage that sampling is necessary and analysis might take up to 30 min. However, this signal can be used to detect glycerol accumulation directly online during the process and adapt the feeding rate accordingly to prevent cell lysis during the induction period even if no knowledge

about the produced protein is given. However, it has to be kept in mind, that the limiting factor of the OUR-signal is the gas analyzer device, which has to cope with all occurring O_2 concentrations in the given induction phase to calculate reasonable OUR values. Hence, addition of pure oxygen to the aeration gas-flow could be causing deviation in the measurement signals of the gas analyzer, affecting the OUR. Using this method, feeding strategies could be adapted to receive the optimized process conditions, which could not be dedicated by the dSn offline control given in the previous chapter.

Model based approach for prediction of IB titer as KPI

Model based controls with the aim to optimize the titer of the recombinantly produced protein are often based on soft-sensor approaches combining offgas and metabolite measurements (metabolic flux analysis) (Gustavsson and Mandenius, 2013). The presented offgas based OUR determination is limited in use for trigging the feeding rate to levels suitable in the current metabolism of the cells. However, no direct observability of VCC and IB titer as KPI is given within this method. Currently there is a high need for process understanding and quality by design (QbD) criteria for pharmaceutical products, which also demanded by regulatory instructions like the FDA (Food and Administration, 2004). New physiological and model-based control strategies for production of recombinant proteins in microbials are presented in different works (Looser, et al., 2015, Luchner, et al., 2015, Wurm, et al., 2017, Chan, et al., 2018). Based on that, we applied a model-based approach to directly predict our product's IB titer and the VCC concentration during the induction phase. Based on the static $q_{s,C}$ experiments, we deviated empirical relations for specific titer and death rate during our cultivation (compare to **Figure 18**) These relations are the basis for the model workflow given in Figure 6.

The model workflow established by the static $q_{s,C}$ experiments was taken to predict VCC and IB titer of the dSn run with the best performance (**Figure 22**). VCC was approximated using a linear

relationship of dSn to percentage dead cells. The data set for $q_{s,C}$ = 0.4 g/g/h was not used for this fit since dead yields were unexpectedly high in this cultivation run (**Figure 17** a). Using empiric fits from several fermentation runs made it possible to predict the viable cell concentration. Therefore a "death rate" was simulated, being highly dependent on feeding rate and process time.

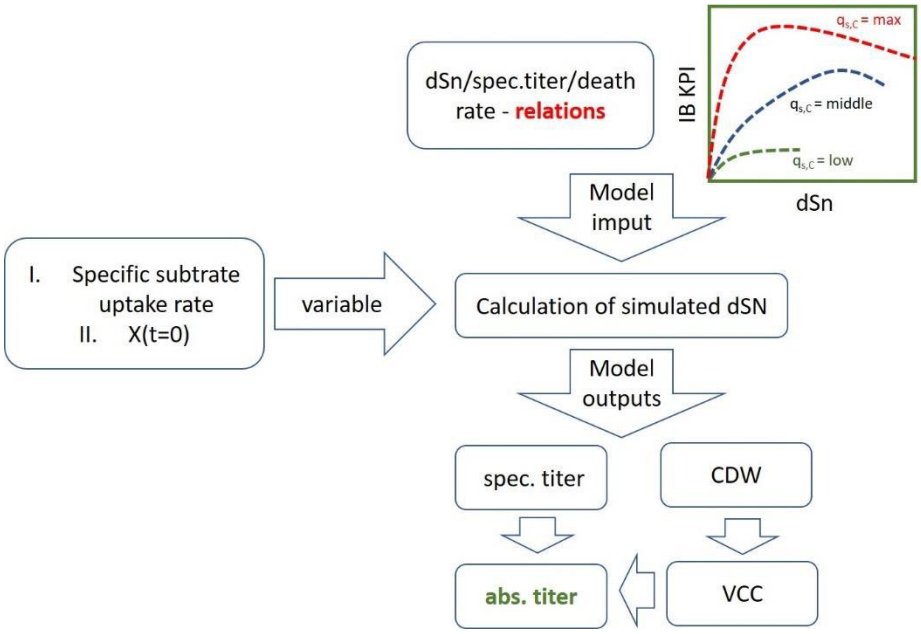

Figure 22:Empirical relations derived from static $q_{s,C}$ experiments. Induction phase variables are the applied $q_{s,C}$ during for the cultivation and the biomass before induction phase. Calculation of absolute titers are performed using the VCC approximation during induction.

Titer approximation during the cultivation was challenging based on incorporation of the titer degradation at high dSn values into a mechanistic description, given in **Figure 23**. a. We logarithmized the specific titer and applied the bilinear fit to the region of titer increase and the region of titer degradation. Red regions reflect the 95% confidence interval of the fitting routine. Specific titer, calculated from cell dry weight showed a dependence onto feeding rate. For dSn values lower than 2.90181 g/g EQ1 was used for fitting and once feeding rates exceeded dSn= 2.90181 g/g, EQ2 was used (**Equations 8 and 9**):

$$EQ1: specTit = -2.08028 + (0.4552 * dsn) \qquad \text{Equation 8}$$

$$EQ2: specTit = z + (-0.01948 * (dsn - 2.90181)$$ Equation 9

$$with\ z = -2.08028 + (0.4552 * 2.90181)$$ Equation 10

Results showed that product titer was highly coupled to the viable cell concentration. Any decrease monitored in VCC, was always observed in a product decrease. A correlation between specific titer and VCC was established, calculating overall titer. The calculated dSn of transition was calculated with 2.9 g/g, which is in reasonable accordance to our experimental data. VCC is accepted with an error of 5% of the given model value, since biomass values are beyond 25 to 30 g/L after the biomass generation phase (**Figure 23** b). VCC was well described by the model, and no cell lysis could be monitored during this specific run (which is in accordance with the FCM derived data). The simulated VCC data was used to calculate the titer for the given process (compare to **Figure 22).** The titer (given in **Figure 23** c) was the most difficult quantity to capture. We based a 20 % error on titer-based model as the overall error estimation to specially access the variations in the beginning. During early stages of induction time, titer measurements were below limit of quantification (LoQ) and further HPLC based titer measurement regularly showed a rather small error of about 7 % in the measurement. Estimation of early titer up to 4 hours of induction time reflected an approximation rather than an absolute value.

However, product titer is used often as KPI for harvesting time point an accurate approximation of late titer values is of high importance. Values after six hours of induction were already within the 20 % accuracy and late values are well described by the model approximation and were very close to the mean modelled value (straight line in **Figure 23** c. During the cultivation almost, no degradation of titer was observed in the later phase, which is in accordance with the model.

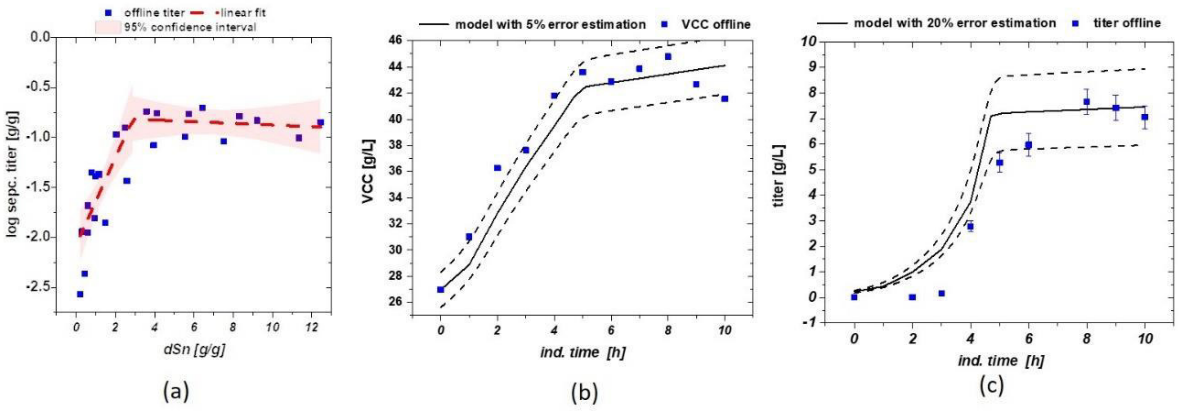

Figure 23: **(a)** Data driven model for specific titer of the N-Pro fused model protein, including 95% confidence interval. A bilinear fit is used for description of the log(specific titer); **(b)** VCC model with 5% error estimation including data from FCM measurement, **(c)** titer calculated via VCC. Late model values fit well to offline measured titers.

Model based approaches for estimation of different feeding strategies can be easily used for adaption of control for new IB producing products. Using two to three fed-batch cultivations with different static $q_{s,C}$ values are necessary for establishing a model for the optimized feeding strategy in combination with overfeeding monitoring using the derived OUR/feed presented in the previous chapter. As cell lysis is notorious for protease release into fermentation broth, high VCC at harvest time point should provide positive effects on further ongoing downstream applications. We are currently investigating our model with further additional strains, but we already want to highlight the straight forward methodology given by this model-based approach as a beneficial tool for process development in the pharmaceutical industry.

4.4. Conclusion

In this work, we aimed for optimization of the key performance indicator IB titer of a given process by varying the specific substrate feeding rate for the analyzed strain and identifying clear indicators for process harvest / substrate accumulation to avoid product degradation. Different cultivations could be easily compared using the dSn value, which has a production maximum of about 3 g/g. The relations for VCC and titer based on this dSn approach could be used for process design but also for modelling of given product dependences. These approaches can afterwards be

easily adapted for direct process control using the OUR value as online signal for onset of glycerol accumulation during the process. With a direct control over the IB titer during the measurements, batch to batch variations could be minimized increasing the performance during the subsequent down streaming steps.

4.5. Introduction Size as QA

The gram-negative bacterium *E. coli* might be one of the best characterized organisms and has found its place in many different industrial applications (Walsh, 2010, Gupta and Shukla, 2017), because *E. coli* shows very fast replication rates (Meuris, et al., 2014, Wurm, et al., 2016) on comparatively cheap media (DeLisa, et al., 1999). However, the missing glycosylation pattern (Spadiut, et al., 2014, Baeshen, et al., 2015, Gupta and Shukla, 2017) as well as intracellular protein production implies major drawbacks when compared to mammalian cells and yeasts as hosts (Cass, et al., 2005). Still, proteins which do not need major posttranslational modifications can be produced in bacteria at low costs in short process times (Spadiut, et al., 2013). The strain BL21(DE3) created by F. Studier and B. Moffatt back in 1986 (Studier and Moffatt, 1986) is often used in an industrial scale, because of very low acetate formation, high replication rates as an effect of the integrated T7-polymerase (Steen, et al., 1986, Studier and Moffatt, 1986, Studier, et al., 1990, Dubendorff and Studier, 1991, Neubauer and Hofmann, 1994, Lyakhov, et al., 1998). Repressing the lac operon with isopropyl β-D-1 thiogalactopyranoside (IPTG) is still state of the art in most industrial applications (Marbach and Bettenbrock, 2012, Dvorak, et al., 2015), as the pET-expression-system is known of high replication rates, leading to high amounts of the desired protein (Dubendorff and Studier, 1991, Marbach and Bettenbrock, 2012, Wurm, et al., 2016).

Inclusion bodies (Inada, et al.) have emerged from their role as waste products (García-Fruitós, et al., 2012) and even are purposely produced in many processes nowadays (Ramón, et al., 2014). IBs have been believed to be a result of diverse stress reactions, resulting in biologically inactive protein (Palmer and Wingfield, 2012, Ramón, et al., 2014, Villaverde, et al., 2015). Their formation is hard to prevent but on the other hand side IBs open up the door for the production of toxic proteins (Berlec and Strukelj, 2013). Intracellular stress can be caused by high temperatures, pH-shifts or due to high feeding rates (Slouka Christoph, 2018). However, some of these stress reactions tend to impact in higher yields of product (Gupta and Shukla, 2017). Still down-stream

processing (DSP) and especially the refolding unit operation is the most time-consuming step in gaining the correctly folded product from *E. coli* cultivations (García-Fruitós, et al., 2012, Palmer and Wingfield, 2012, Ramón, et al., 2014, Villaverde, et al., 2015), which requires significantly more technology and time, when purifying protein aggregates (Palmer and Wingfield, 2012, Wingfield, 2014, Wingfield, et al., 2014). In recent years IBs were found to exhibit not only inactive protein structures, but also parts which show enzyme activity (Hrabárová, et al., 2015). These IBs are nowadays called non-classical Inclusion Bodies (ncIBs) and show highly active protein, directly without time consuming refolding steps (García-Fruitós, et al., 2005, Jevševar, et al., 2005, Peternel and Komel, 2010). Active parts of the IB may also be directly used as biocatalysts in different reactions, combining the well mechanical properties with enzymatic reactivity. It has also been shown, that the size has an influence onto the biological activity of the protein (García-Fruitós, et al., 2007, García-Fruitós, et al., 2009). Beside their enzymatic usage IBs may also be used based on their mechanical properties as they generally inhibit a distinct bead size combined with high mechanical stability. Therefore, application as nanoparticulate material and as material for tissue engineering is considered (Díez-Gil, et al., 2010, García-Fruitós, et al., 2012). IB bead size is known to be based on the harvest time during the cultivation. In a recent study, we analyzed detailed effects of classical process parameters pH and temperature on the IB bead size as a function of the induction time (Slouka Christoph, 2018). Therefore, control of IB size during the cultivation is an important issue as size is a critical quality attribute (CQA) during these processes. Process performance needs to be directed towards optimal size needed in DSP for pharmaceutical relevant components. For IBs used as biocatalysts or nanomaterials knowledge about the distinct bead size during cultivation is required to have improved performance (García-Fruitós, et al., 2009).

Effects of feeding strategies onto product have been already investigated by Spadiut et al. (Spadiut, et al., 2014) as alterations of the specific growth rate are known to have major influences onto product formation. As high recombinant protein production does implement changes in cell physiology, it is known that there is decrease of growth rate over the duration of

induction time (Scott, et al., 2010). Also biomass formation does suffer from protein induction as it has been referred that biomass yields decrease over induction time, especially when compared to mock strains (Rozkov, et al., 2004). Helping to optimize feeding strategies, the term q_s has been introduced, determining specific sugar uptake rates, per gram biomass in certain time intervals (Spadiut, et al., 2014). Quantitative comparison of dynamic physiological feeding profiles for recombinant protein production with Pichia pastoris}. Within this study it was also shown that a stepwise increase, such as a q_s-ramp, is superior to a constant feeding profile in *Pichia pastoris* protein production. The influence of q_s ramps onto inclusion body formation was performed by Reichelt et al. (Reichelt, et al., 2016). Within this study also the term "$q_{s,crit}$" was determined, describing the maximum physiological substrate uptake rate. It was shown within this study, that the physiological feeding rate in *E. coli* is highly dependent onto process parameters and consists of a rather "dynamic nature" Reichelt, 2017, Physiological capacities decline during induced bioprocesses leading to substrate accumulation (Reichelt, et al., 2017).

In this study, we followed that hypothesis that the specific substrate uptake rate may be a suitable process parameter to steer IB CQA, such as IB size. We performed cultivations with a *E. coli* BL21(DE3) strain, producing a recombinant protein coupled to a N-pro-fusion protein (Achmüller, et al., 2007), expressed exclusively as an IB with the goal to control inclusion body size within the cells based on physiological feeding. Optimized process parameters for T and pH were used throughout the whole work, derived in from a different previous study. The specific substrate feeding rate ($q_{s,C}$) was adapted using glycerol and glucose and responses onto IB bead size were analyzed**.** Usage of glycerol as media is comparable cheap and since glycerol is regarded as a waste product (Martínez-Gómez, et al., 2012) it might find further applications in future manufacturing. The degree of reduction on glycerol is slightly higher when compared to glucose and titer based productivity seemed to be positively influenced using glycerol as primary carbon source (Kopp, et al., 2017). We show that IB bead size can be adjusted via the amount of fed carbon source, when keeping T and pH during induction constant. Size variations could be

detected throughout the cultivations using scanning electron microscopy. The knowledge generated by these cultivations is used to model IB size based on the glycerol consumption and predict IB size of a cultivation in real time. Using this model-based approach, a defined IB-size at the time point of harvest can be simulated, which should enhance performance as biomaterials or lead to optimized DSP for pharmaceutical products.

4.6. Material and Methods Size as QA

For cultivation process and analytics see **chapter 4.2.**

IB Bead Size

Washed and aliquoted IB samples were resuspended in ultrapure water. 100 µL of appropriate dilution of the suspension were pipetted on a gold-sputtered (10 - 50 nm) polycarbonate filter (Millipore-Merck, Darmstadt, Germany) using reusable syringe filter holders with a diameter of 13 mm (Sartorius, Göttingen, Germany). 100 µL of ultrapure water were added and pressurized air was used for subsequent filtration. Additional 200 µL of ultrapure water were used for washing. The wet filters were fixed on a SEM sample holder using graphite adhesive tape and subsequently sputtered with gold to increase the contrast of the sample. SEM was performed using a QUANTA FEI SEM (Thermo Fisher, Waltham, MA, US) with a secondary electron detector (Dvorak, et al.). The acceleration voltage of the electron beam was set between 3 to 5 kV. To determine the diameter of the IBs, 50 IBs on SEM pictures were measured using the ImageJ plugin Fiji (Laboratory for Optical and Computational Instrumentation (LOCI), University of Wisconsin-Madison, US).

4.7. Results and Discussion for Size as QA

Within this study, we investigated size dependence based on physiological feeding in *E. coli*. The harvested and washed IBs were analyzed via SEM and diameter was measured subsequently. A correlation of the IB size based on the fed substrate could clearly be indicated. A hyperbolic relation of the size could be used to establish model-based approach to predict IB size for our model protein during cultivation.

Static $q_{s,C}$ feed forwards feeding for size determination

Within a screening approach we tried to trigger the optimal feeding parameter for IB production in *E. coli* processes. Set-point alteration for the specific glycerol or glucose uptake rate $q_{s,C}$, did influence the IB bead size respectively. Classical and physiological process parameters using glucose as carbon source had already been analyzed in recent work (Slouka Christoph, 2018). These findings resulted in the optimized pH and temperature parameters used in this study (T = 31.5 °C, pH = 6.7 for the induction phase). In **Figure 24** an exemplary SEM picture of IBs including measurement of the size is given. These pictures were used to define IB size dependence of an individual cultivation **Figure 24** b). At later induction times, decrease in size and increase in standard deviation indicated ongoing cell death measured via flow cytometry and sugar accumulation (not shown).

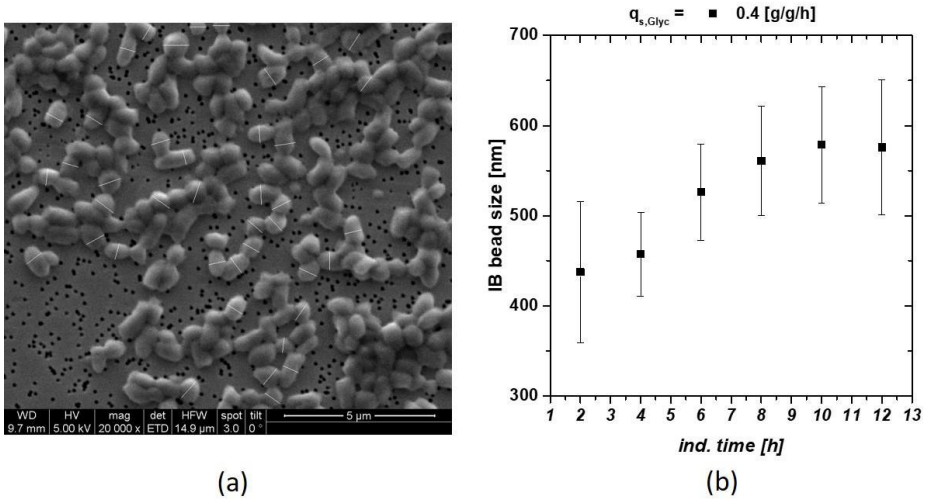

Figure 24: **a**) IB beads at time point of harvest (12h of induction) after homogenization and subsequent washing with ultrapure water; **b)** IB bead size at qs,C of 0.4 g/g/h using glycerol as C-source. Late degradation is based on reduction in the viable cell concentration.

We tested four different setpoints for $q_{s,C}$ during the induction phase for both carbon sources and analyzed the resulting IB sizes. At high $q_{s,C}$ early C-source accumulation could be observed with present product degradation. For easy comparison between different physiological feeding strategies and different used C-sources, the cumulative sugar uptake value, dSn [g/g], (**equation 6**) could be used making a normalization on the fed mass C-source in respect to the total biomass at the induction time (Reichelt, et al., 2016):

The induction time scale can now be exchanged for the dSn value during the induction phase. Low $q_{s,C}$ values result in a low dSn value, while high $q_{s,C}$ increases the values, as a high amount of C-source is fed throughout the process. The interaction between the IB bead size and dSn is presented in Figure 2 a, comparing four runs with glycerol as C-source. Single bead size was strongly affected by the fed substrate starting with about 350 nm (threshold of the measurement principle) to a size over 600 nm in mean. A modified hyperbolic kinetic term could be used to describe this behavior of the mean diameters of the IBs in **equation 11**:

$$IB_{size} = IB_{size,max} * \frac{dSn}{K_m + dSn}$$ Equation 11

replacing the maximum reaction speed term with the maximum IB size ($IB_{size,max}$) and the substrate dependence through the respective dSn value. K_m defines the trigger point where half of the possible size is reached and may therefore be used as transition value for change of low sizes towards large IB-size interesting for further downstream applications. High feeding rates might help to reach this trigger point earlier, hence physiological limitations such as µ-decrease over induction time have to be considered, in order to prevent cell death (Scott, et al., 2010). The results of the fit are given in **Figure 25** b for both C-sources.

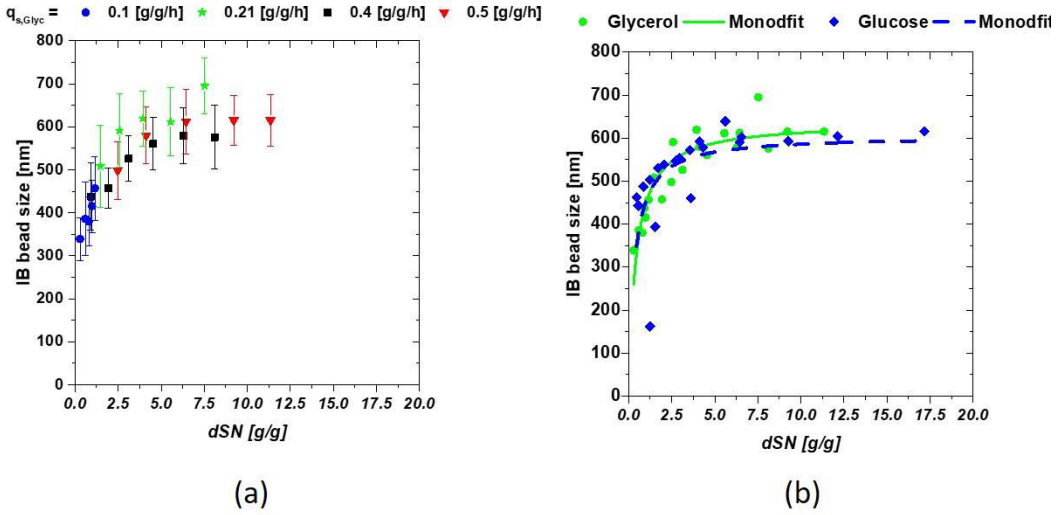

Figure 25: (**a**) IB-bead size dependencies on the amount of fed glycerol shown calculated as dSn value **b**) dependence of the IB bead diameter when compared between glucose and glycerol.

The previously mentioned hyperbolic fit can be seen by observing **Figure 25** b as IB-size is highly dependent on the amount of fed C-source. The performed fit yielded following constants for all cultivations at the constant parameters T and pH are given in **Table 11.** K_M represents the mass glycerol needed for 1 g of biomass to reach $\mathbf{IB_{size,max/2.}}$

Table 11: Fitting results for hyperbolic-fit Eq. 3 for IB bead size dependence

	glucose	**glycerol**
K_m [g/g]	0.33 +/- 0.14	0.42 +/- 0.06
$IB_{size,max}$ [nm]	605.4 +/- 37	638 +/- 17

Both C-sources showed very similar results using the fit given in Eq. 3. Very small sizes were not easily accessible using SEM based techniques. Therefore, the highest error was to be expected in the approximation of the early induction times, as filter porosity was above the threshold. Maximum IB size was observed at approximately 620 nm for our model protein. IB bead size could not be influenced by the C-source, as differences seen here were within the standard deviation, but only by the respective amount of fed C-source (provided that T and pH are not altered during the induction phase). K_m and $IB_{size,\ max}$ are highly product and induction dependent. For receiving IBs with defined size, low $q_{s,C}$ values can be recommended, as protein aggregation is a very fast process, and therefore size alterations might be difficult to trigger. Very small defined sizes could be produced in the beginning and sizes are longer stable at these feeding rates. Altering induction strength with lactose showed similar dependence by using green fluorescent protein as model protein for mixed feed development (Wurm, et al., 2018). Within this study it was shown that IB-size is tunable by adjusting the lactose concentration as inducer. It was shown that low levels of lactose resulted in sizes only as big as 400 nm but using higher concentrations of lactose for induction, IB-bead sizes move up to 600 nm. However, this variation in size seems to be a result from insufficient induction, resulting from eventually given low lactose feeding rates. Within this study we want to highlight that inclusion body size is highly dependent onto the amount of the fed C-source, given that the system is fully induced with IPTG. Based on these results, glycerol-fed cultivations resulted in identical size for IB beads compared to glucose, although glycerol does open up major advantages on a cultivation side (Slouka Christoph, 2018). The derived straight forward dependence of the IB bead size based on hyperbolic saturation kinetics could be easily used in a model-based approach. Online application of the model during the process would help to reduce or even replace complex offline analytics.

Model based approach for prediction of IB bead size

Based on the $q_{s,C}$ experiments with feed forward approach, we derived empirical relation for IB size during our cultivation (compare to **Figure 25** b). These relations were the basis for the model workflow used for determination of size in real time during a process based on the applied feeding strategy. We applied the dSn principle for a cultivation in order to keep viable cell concentration high and receive a high product titer. The exact feeding strategy using the dSn value over induction time is given in **Figure 26** a (blue rectangles). A high $q_{s,C}$ of glycerol was varied from 0.5 g/g/h to 0.1 g/g/h at a dSn value of 4 g/g. Corresponding size measurements are given in **Figure 26** a (red circles). As size and titer do show a linear correlation, the shift from a high to a $q_{s,C}$ should result in optimal size at the time-point of harvest.

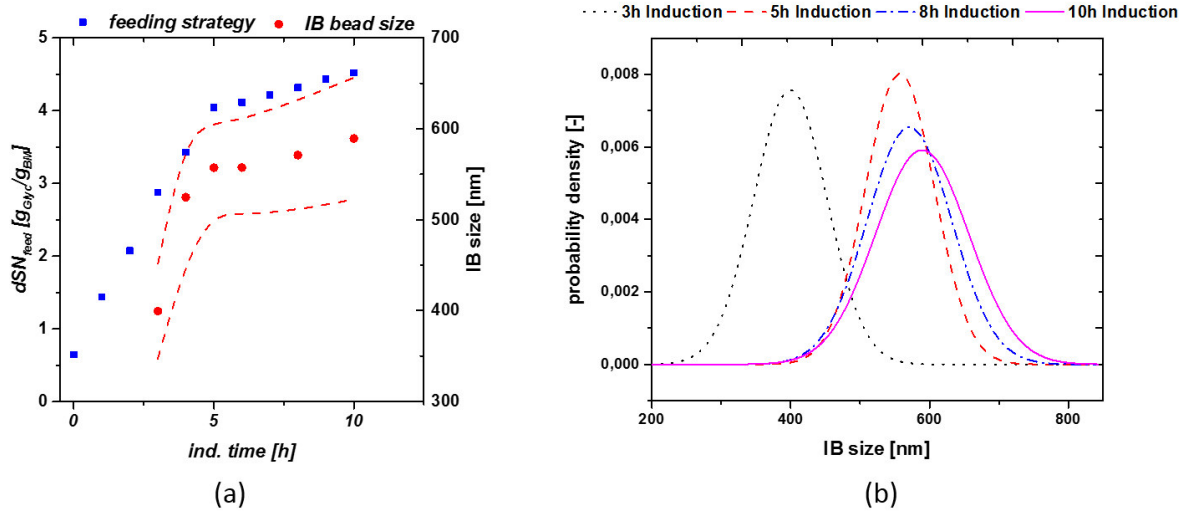

Figure 26: **(a)** Model cultivation with change in the $q_{s,C}$ from 0.5 g/g/h to 0.1 g/g/h at a dSn value of about 4 g/g. The lower $q_{s,C}$ value results in a high viable cell concentration at late induction times; **(b)** probability density plot of cultivations as a function of induction time

Exchanging a static feeding strategy with the feeding control shown in **Figure 26** a, does implement a size growth even at late induction times and is triggering maximum size towards the time-point of harvest. Optimized feeding strategies, varying μ over induction time, seem to boost the overall product titer (Reichelt, et al., 2016). As size and titer show a linear correlation (compare to **Figure 27** b) overall product formation can be increased, applying the $q_{s,C}$ shift from

0.5 to 0.1 g/g/h. Standard deviation of IB-bead size (plotted in **Figure 26** a also increases over time, which is in correlation with literature (Wurm, et al., 2018). The probability density plot (shown in **Figure 26** b) as a function of induction time based on a normal distribution of our IBs confirmed, that IB-bead size distribution increased over induction time. Within this cultivation only little deviation could be monitored towards end of induction time as $q_{s,C}$ was adapted to 20% of the previous feeding rate.

Process control can generally be performed by applying mechanistic of empirical models for prediction of the performed process or for at least several key performance indicators (KPI) (Sagmeister, et al., 2013, Ehgartner, et al., 2015, Kroll, et al., 2017). Regularly, the prediction of biomass and inhibiting metabolites are the quantities of interest and are tried to be simulated for predictive control of the bioprocess. Prediction of product attributes within the cultivation is challenging – especially in high dynamic microbial processes.

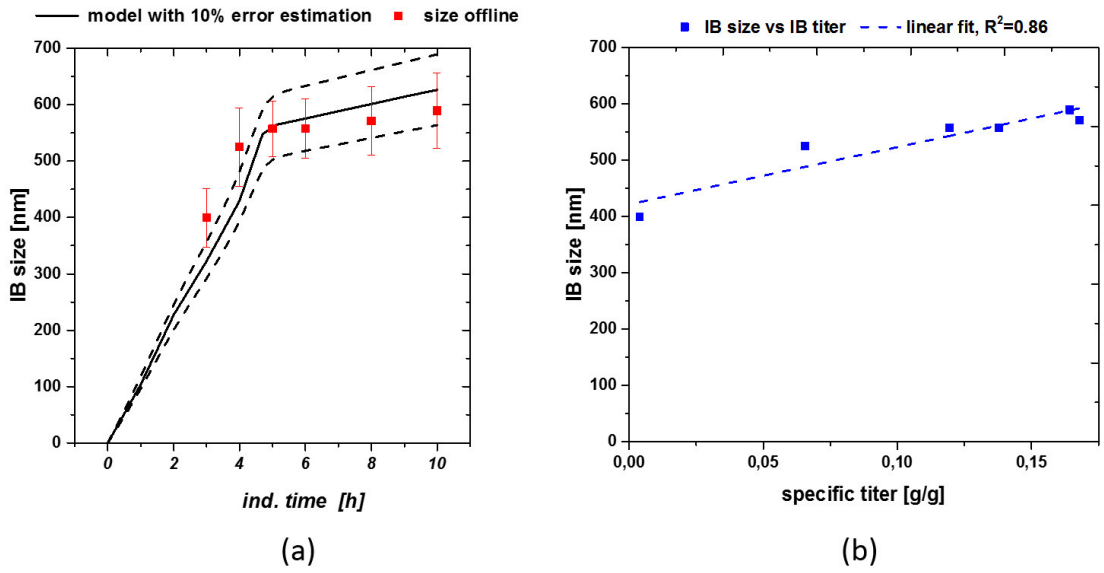

Figure 27**: (a)** Size modeling including real measured data with standard deviations. Especially early sizes could only be described using the model-based approach**; (b)** Size-titer correlation for fermentation with feeding strategy implied in Figure 3 a.

For the development of our model, mechanistic links were established using the software Matlab 2017. Within this model only time of the induced fed batch was simulated, as no inclusion bodies were formed within batch and non-induced-fed batch (FB)-cultivation. Static inputs for the model consisted of volume [L], substrate in fermentation broth [g/L] and biomass [g/L] at timepoint $t_{induction}$ = 0 h. Further feed concentration [g/L], $Y_{X/S}$ [g/L] and $q_{s,max}$ [g/g/h] were needed for modelling the behavior of the induction phase. Defining basic mass equations on fed-batch process behavior, prediction of classic process parameters like volume, substrate metabolization, biomass formation was established via the differential terms given beneath. Due to simplification, volume increase during fermentation was calculated via feed addition only:

$$x.S.dxdt = '(EQ.F_{in} / x(1) * p.c_{glu}.Value - x(2)) - EQ.qs * x(3)'$$

$$x.CDW.dxdt = 'x(3) * \left(EQ.qx - EQ.F_{in} * x(1)\right)$$

$$Volume: x(1) = [L]$$

$$Substrate: x(2) = [g]$$

$$CDW: x(3) = \left[\frac{g}{L}\right]$$

With S being the substrate [g], F_{in} the feed [mL/h], c_{Glu} the feed concentration [g/L], CDW the dry cell weight [g/L], q_s the specific substrate feeding rate [g/g/h] – simulated in the model - and q_x the specific biomass generation rate [g/g/h] based on q_s. This enabled us to simulate the process based on the inputs received from the static $q_{s,C}$ experiments. Size could be easily modeled using the already presented hyperbolic saturation terms as helper equation in the model. **Figure 27** a shows the modeled size estimation based on the previously established kinetics in **equation 11**. As acceptance criteria for product-based attributes we used 10 % error of the model for size. Size was well described by the model, resulting in only small variations, still lying within the standard deviation. Using the given model size estimation up to the beginning of the induction phase can be made, even if no analytical method is available for direct determination (e.g. SEM threshold).

If the product is used for a biocatalyst or nano-biomaterial with defined size, harvesting time point can easily be determined within the cultivation (García-Fruitós, et al., 2012).

Model based approaches for estimation of different feeding strategies can be easily used for adaption of control for new IB producing products. Deriving data from two to three fed-batch cultivations with different static $q_{s,C}$ values is necessary to establish this very model. Afterwards the optimized feeding strategy for the desired protein can be simulated and experimentally confirmed. These straight forward methodology triggers this model-based approach a high beneficial tool for process development in the pharmaceutical industry.

4.8. Conclusions

In this work we aimed for analyzing the effect of varying the specific substrate feeding rate on IB CQA, such as IB size. Different cultivations could be easily compared using the previously established dSn value, as cumulated sugar uptake rate can be presented neatly arranged. Performing cultivations with altered feeding rates, showed that maximum size was achieved at a dSn value of approximately 4 g/g. Feeding beneath a dSn value of 4 g/g resulted in highly time resolved results, which might be useful for model development. As low feeding rates did not reach exceed the trigger-point in IB-formation (defined here as K_m-value) these feeding strategies may not find an application in production scale, as IB titer is too low for further ongoing DSP applications. Applying a q_s-shift during induction phase boosted IB-formation even after dSn = 4 g /g was exceeded. Application of this feeding strategy kept cells in a viable state and further will help to achieve maximum size within shorter induction times. The relations for size based dSn approach could be used for process design but also for modelling of given product dependences.

We are currently investigating our model with other additional strains, trying to establish product-independent robust Upstream Processing. Triggering optimal IB-bead-size at the time-point of harvest will help to improve the cost-and time-intensive downstream processing.

5. Determination of Viable Cell Concentrations (VCC) using Electrochemical Sensors in the Low Frequency Regime

For development of suitable process analytical tools, knowledge about key quantities in the performed cultivations is very important. We analyzed different cultivations with constant classical process parameters (pH, T) using principal component analysis in order to see coupled quantities for development of PAT tools. We introduced different time independent values of ten cultivations given in **Table 12.** Several of those values are clarified in **Figure 28** a), especially mean slopes for product increase and degradation.

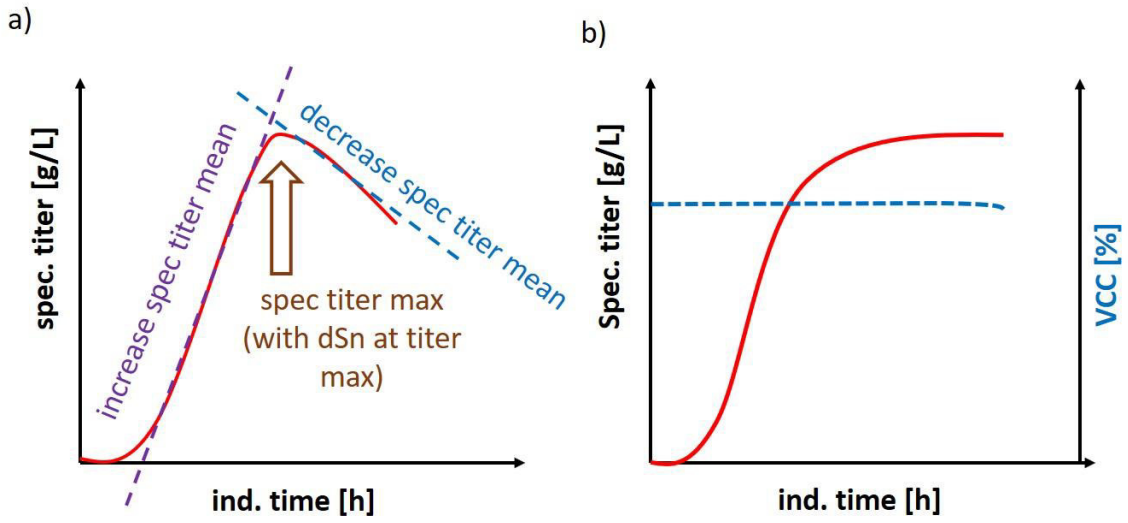

Figure 28: a) sketch of the important time dependent parameters of the KPI spec. titer. All other values are maxima (like size) or at induction time of 12 hours; b) Desired fed-batch behavior, with no visible degradation of spec. titer and high VCC concentration during the whole induction time.

The desired fed-batch based on the specific titer is given in **Figure 28** b). The final aim is to receive a time stable KPI with no product degradation in order to have a large harvest interval instead of a given time point including a high product quality.

Table 12: Feature matrix of ten cultivations (presented in the previous chapters) with characteristic time independent quantities

process	Size max	spec. titer max	Incease in spec titer mean	degradation titer mean	dSn at titer max	dead cell at t= 12 h	sugar t = 12 h
	[nm]	[g/g]	[g/g/h]	[g/g/h]	[g/g]	[%]	[g/L]
static glycerol qs_mid	695.03	0.10131	0.01361	-0.00461	5.57	3	15.8
static glycerol qs_low	456.64	0.04307	0.00448	0	1.16	0	0
static glycerol qs_high	578.83	0.18221	0.03742	-0.00639	3.59	20.4	55.7
static glycerol qs_high	615.19	0.1968	0.02778	-0.02451	6.44	11.9	108.7
qs ramp down glycerol qs_mid	678.18	0.1602	0.02336	-0.01834	4.69	69.6	8.50
qs drop to 0.1 glycerol qs_mid	639.29	0.17386	0.0038	-0.0041	3.65	4.8	5.78
static glucose qs_mid	578.01	0.14008	0.01725	-0.0059	3.56	35.6	19.4
static glucose qs_low	394.05	0.03959	0.00483	0	1.54	0	0
static glucose qs_high	532.03	0.15672	0.01736	-0.00308	12.13	45.4	166.0
static glucose qs_high	639.29	0.15847	0.02779	-0.01066	2.74	50.9	60

The PCA revealed that three components already cover 83 % of the difference in all cultivations. The biplot for the performed PCA is given in **Figure 29.** PCA analysis biplot for component three is given in the supplementary material (**Supplementary 6**). For better comparison of the given cultivations, information about physiological feeding and C-source were not included into the feature matrix. Three distinct groupings are visible for: The green grouping represents cultivations with low $q_{s,C}$ where low titer, size is visible. No degradation effects can be seen in these cultivations which is reasonable, since the 12 h induction time is not enough for full production. The blue grouping shows cultivations with $q_{s,mean}$ of about 0.3 g/g/h (static and dSn controlled). Mean specific titer are reasonable in those cultivations and only a few dead cells are present in those runs. These cultivations are stable concerning degradation of the product and only use a decent amount of sugar (dSn max value). Switching the physiological feeding to high $q_{s,C}$ rates – red group – very high spec. titer and high IB bead sizes can be observed including high productivities. However, also a high amount of dead cell (reduction in VCC) and increased

product degradation is found within these cultivations. Furthermore, high sugar need (accumulation) increases the costs of these cultivations drastically.

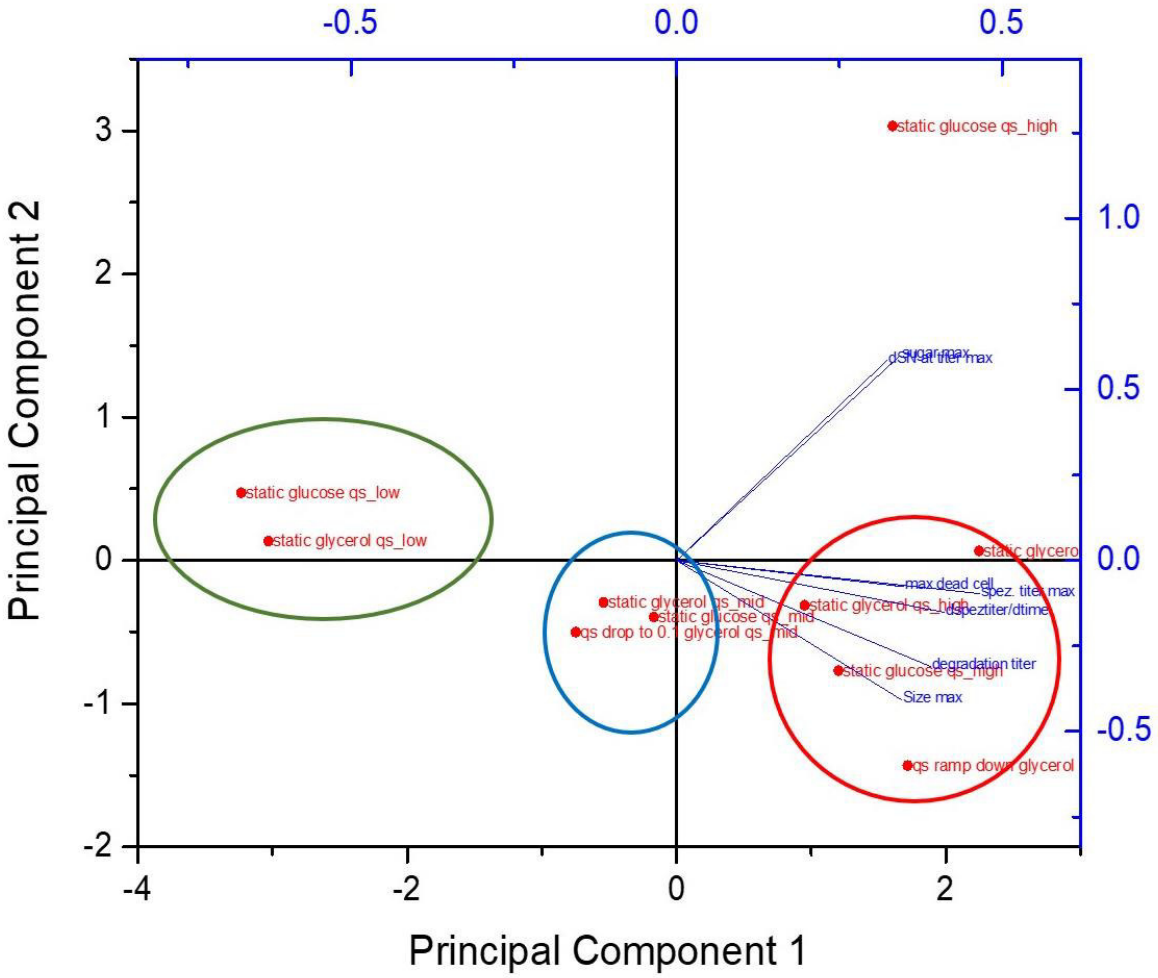

Figure 29: PC 1 and 2 in a biplot with the analyzed quantities and the respective grouping of the cultivations.

As VCC and product dependent quantities are highly correlated in principal component 1 – compare to **Table 13** – measurement of the VCC during the process is a very promising tool for process analytics especially at high feeding rates ($q_{s,C}$ of 0.4 to 0.5 g/g/h) during induction phase. Furthermore, a high VCC during induction time is expected to lead to a high product quality with large harvest interval as given in **Figure 28** b). Based on these considerations, VCC measurements as PAT tool during induction time (or even the whole process) would lead to a stable reproducible process for *E. coli*-based cultivations.

Table 13: Extracted Eigenvectors for the three analyzed principal components.

	Coefficients of PC1	Coefficients of PC2	Coefficients of PC3
Size max	0.34505	-0.4067	0.57693
spez. titer max	0.46473	-0.09641	0.21808
dspeztiter/dtime	0.41119	-0.15148	-0.44287
degradation titer	0.38959	-0.30922	0.00246
dSN at titer max	0.3232	0.58482	0.30803
max dead cell	0.34887	-0.07691	-0.57027
sugar max	0.34342	0.59901	-0.05787

As state-of-the-art determination of VCC is based on offline methods, we tried a different approach during this thesis. Chapter 3 and 4 already indicated the importance for knowledge of the cell physiology during cultivation and especially during protein production. Keeping the viable cell concentration (VVC) high is therefore of utmost importance and direct measurement of VCC is a perfect tool to react upon process perturbations. We already presented a novel sensor development for *E. coli* cultivations in **Sensor Journal** (Slouka, et al., 2016). This sensor was further developed and applied for a different usage in food producing industry. We tested the setup with bakers' yeast with the final goal for establishment in the brewing industry. This work was published in **Chemosensors Journal** (Slouka, et al., 2017) with the title "**Low Frequency Electrochemical Impedance Spectroscopy as Monitoring Tool for Yeast Growth in Industrial Brewing Processes".**

5.1. Introduction

Microbial cultivations play a key role in many different fields like food, drug and bulk chemical production as well as in waste to value concepts (Gavrilescu and Chisti, 2005). Process monitoring like pH, dO_2 and offgas analysis are state of the art in today's industrial cultivations to guarantee product quality and safety. However, the most important parameter in bioprocesses, the biomass, can be only determined using offline methods or complex soft sensor applications

(Sagmeister, et al., 2013). These control systems are often dependent on inline/online/atline detection systems like e.g. high-performance liquid chromatography for metabolites, offgas balance and/or dielectric spectroscopy measurements. The use of accurate and reliable biomass measurement systems (Clarke, et al., 1986, Kiviharju, et al., 2008), especially of viable cell concentrations (VCC) enable proper process control tools, which lead subsequently to more robust and reliable bioprocesses. VCC is measured using offline measurement principles including marker proteins or fluorescence probes, like flow cytometry or confocal microscopy (Davey and Kell, 1996, Veal, et al., 2000). Since those control and analytical tools are cost intensive, classical bulk food products – like yeast and beer – are produced in rather uncontrolled environment. Not only the complex raw material, but especially growth conditions of the yeast (propagation and fermentation) are of high importance for the quality of the final product. The implementation of online vitality measurements in brewing industry has historically be hindered by affordable, simple, robust and reproducible test (Lodolo, et al., 2008).

In general, online and inline biomass measurement approaches are rather scarce and are based on physical measurement principles. One principle generally applied is high frequency alternating current (AC) impedance spectroscopy with high field amplitudes used on the basis of the so called ß-dispersion (Schwan and Foster, 1980, Schwan, 1984). Cells with an integer cell membrane affect the relative permittivity between two electrodes and therefore this signal is used for estimation of VCC. Detailed description on the measurement principles can be found in Refs. (Yardley, et al., 2000, Soley, et al., 2005, Carvell and Dowd, 2006, Dabros, et al., 2009).

The model organism for application of AC measurements in the ß-dispersion range are yeasts being a very important expression host for recombinant proteins (Buckholz and Gleeson, 1991, Cereghino and Cregg, 1999, Gerngross, 2004). Also, approaches towards more complex expression systems, like filamentous fungi and CHO cells are already performed (Ferreira, et al., 2005, Ehgartner, et al., 2015, Konakovsky, et al., 2015). These measurements show a strong dependence upon physical process parameters (like aeration and stirring – causing gas bubbles,

temperature shifts and pH gradients) and are furthermore highly affected by changes in the media composition during cultivation.

However, not only high frequency impedance spectroscopy in the ß-range can be used for determination of biomass, but also changes of the electrical double layer by adsorption/desorption of cells at the electrode surface (detectable at low frequencies in the mHz range, α-dispersion) provide valuable information. Beside the cell type itself (cell wall/membrane compositions, size and shape), many physical parameters especially in the media (pH, ion concentrations) can influence the potential distribution in the double layer (Poortinga, et al., 2002, Bot and Prodan, 2009). Furthermore, the given method via α-dispersion detection is capable of detecting even very small numbers of bacteria in soil, food and feces polluted water using interdigitated microelectrode designs (Gonzalez, et al., 1998, Yang, et al., 2003, Radke and Alocilja, 2004, Yang, et al., 2004, Liu, et al., 2011, Lei, 2014). These studies were only performed in very small scale with a low cell concentration. In general, a threshold in the measurement is present at low cell concentration. Exceeding this limitation, very stable signals over time were achieved in these measurements. Beside direct measurements in the broth, a modified electrode system in an interdigitated design can be used (K'Owino and Sadik, 2005, Wu, et al., 2005, Bayoudh, et al., 2008). First approaches towards process monitoring were shown by Kim et al. (Kim, et al., 2009), who worked with an inline sensor used in the lower frequency range between 40 Hz and 10 kHz for real time monitoring of biomass. Kim et al. showed the feasibility for measuring changes in the double layer capacitance, but no analysis of the double layer capacitance (C_{DL}) itself was performed, only discrete extracted values for distinct frequency values were used. Recent studies on *E. coli* showed reasonable results for VCC determination not only in batch phase, but also in fedbatch approaches leading to far higher cell densities (Slouka, et al., 2016).

In this study impedance measurements in the α-dispersion range are performed during batch-based cultivation of *S. cerevisiae* aimed for usage in brewing applications. Different state-of-the-art methods are applied for determination of the corresponding total biomass – dry cell weight (DCW), and OD_{610} offline. Flow cytometry (FCM) in combination with fluorescence dye DiBAC

is used for cell physiology evaluation to account for changes in the viability during cultivation. With this knowledge, we are able to correlate total biomass to the extracted double layer capacitance.

A prototype inline probe was designed and built for easy plug in measurement of the biomass. Online and new inline probes are tested using defined media with glucose and maltose in different concentrations and malt extract as complex base material in brewing.

5.2. Materials and Methods

Expression host and Cultivation

All cultivations were performed using *S. Cerevisiae* strain supplied by Brauerei GUSSWERK (Salzburg, Austria). For the preculture 500 mL sterile Delft medium was inoculated from frozen stocks (1.5 mL, -80°C) and incubated in a 2500 mL High-Yield shake flask for 20 h (230 rpm, 28°C). Batch and cultivations were performed in a stainless-steel Sartorius Biostat Cplus bioreactor (Sartorius, Göttingen, Germany) with 10 L working volume and Infors Techfors-S bioreactor (Infors HT; Bottmingen, Switzerland) with 20 L working volume. Aerobic batches were performed using 1000 to 1400 rpm stirrer speed with aeration of 2 vvm. Anaerobic batches were performed using 600 rpm and 2 to 4 l/min N_2 – flow. Composition of the used defined Delft medium was: 7.5 g/L $(NH_4)_2SO_4$, 14.4 g/L KH_2PO_4, 0.5 g/L $MgSO_4 \cdot 7\ H_2O$; 2 mL of Trace metal stock, 1 mL of vitamins, 50 µL PPG as Antifoam and maltose and glucose in different concentration as carbon source. For malt extract-based fermentation, a preculture with Delft media was performed and afterwards inoculated into malt extract solution (150 g/L malt extract in deionized water) (Weyermann, Bavarian Pilsner, Bamberg, Germany).

Analytical procedures

For DCW measurements 1 mL of the cultivation broth was centrifuged at about 9000 g, subsequently washed with 0.9 % NaCl solution and centrifuged again. After drying the cells at 105 °C for 48 h the pellet was evaluated gravimetrically. DCW measurements were performed in five replicates and the mean error for DCW was about 3 %. Offline OD_{610} measurements were performed in duplicates in a UV/VIS photometer Genisys 20 (Thermo Scientific, Waltham, MA, US).

Verification of cell viability in defined media samples was done by flow cytometric (FCM) measurements. After addition of DiBAC (bis-(1,3-dibutylbarbituricacid)trimethineoxonol) diluted cultivation broth was measured using a CyFlow Cube 8 flow cytometer (Sysmex-Partec, Bornbach, Germany). DiBAC is sensitive to plasma membrane potential and therefore distinction between viable and non-viable cells can be achieved. Detailed information on the viability assay can be found elsewhere. Overall errors with this method were in the range of 0.5 to 1 %.

Sugar concentrations in the fermentation broth were determined using a Supelco C-610H HPLC column (Supelco, Bellefonte, PA, USA) on an Ultimate 300 HPLC system (Thermo Scientific, Waltham, MA, US) using 0.1 % H_3PO_4 as running buffer at 0.5 mL/min. Ethanol concentrations were determined using an Aminex HPLC column (Biorad, Hercules; CA, USA) on an Agilent 1100 System (Agilent Systems, Santa Clara, CA, USA) with 40 mM H_2SO_4 as running buffer at 0.6 mL/min. Cultivation offgas was analyzed by gas sensors -IR for CO_2 and ZrO_2 based for O_2 (Blue Sens Gas analytics, Herten, Germany).

Impedance Measurements

Physical analysis of VCC in state-of-the-art capacitance probes, which rely on β-dispersion (10^7 Hz- 10^4 Hz), show high dependence on process parameters (e.g. stirring, temperature, pH, salt and

substrate concentration etc.) and cultivation phase (exponential growth phase, starvation phase, etc.) (Mishima, et al., 1991, Soley, et al., 2005). We focused the measurement on a different physical phenomenon (α-dispersion), which yields valuable information mainly about biomass concentration. The so called α-dispersion effect, at frequencies below 10 kHz, which is most probably a result of deformation of ionic species around the cell membranes, is used for these measurements. Dielectric response is therefore proportional to the ionic charge gathered around the membrane of adsorbed cells on the electrode (Poortinga, et al., 2002, Bot and Prodan, 2009). Impedance measurements were recorded in the range of 10^6 to 10^{-1} Hz with amplitudes of 100 to 250 mV using an Alpha-A High Resolution Dielectric Analyzer (Novocontrol, Montabaur, Germany). Since measurements in this frequency range are largely determined by the double layer region between electrode and media, rather minor interferences with process parameters (aeration, stirring) were to be expected. Online flow cells show the benefit of laminar flow through the cell and minor turbulence, but have generally the problem of differences in the process state (side stream) and performing sterilization procedures. Inline probes should overcome these problems but may be strongly affected by the process parameters. Details on the fitting procedure and data evaluation are given in (Slouka, et al., 2016).

Inline probe construction

As online probes are not directly situated inside the reactor, but often supplied by a side stream of the fermentation broth, changes in the metabolism in this time interval may be highly possible, but also less disruption of the signal is observed by stirrer and aeration of the system. Furthermore, online probes always impose the danger of contamination to the process, since the sterile barrier is not kept inside the fermenter. Therefore, for sterile processes without constant streams of broth, the assembly of an inline probe prototype using a commonly used 25 mm B. Braun safety port with O – ring (Ingold connector) is done. Materials have been chosen to be

permanent stable at 130 °C, and can easily sustain in situ autoclavation procedures. Physical analysis of VCC is monitored and investigated by the inline probe sketched in **Figure 30**.

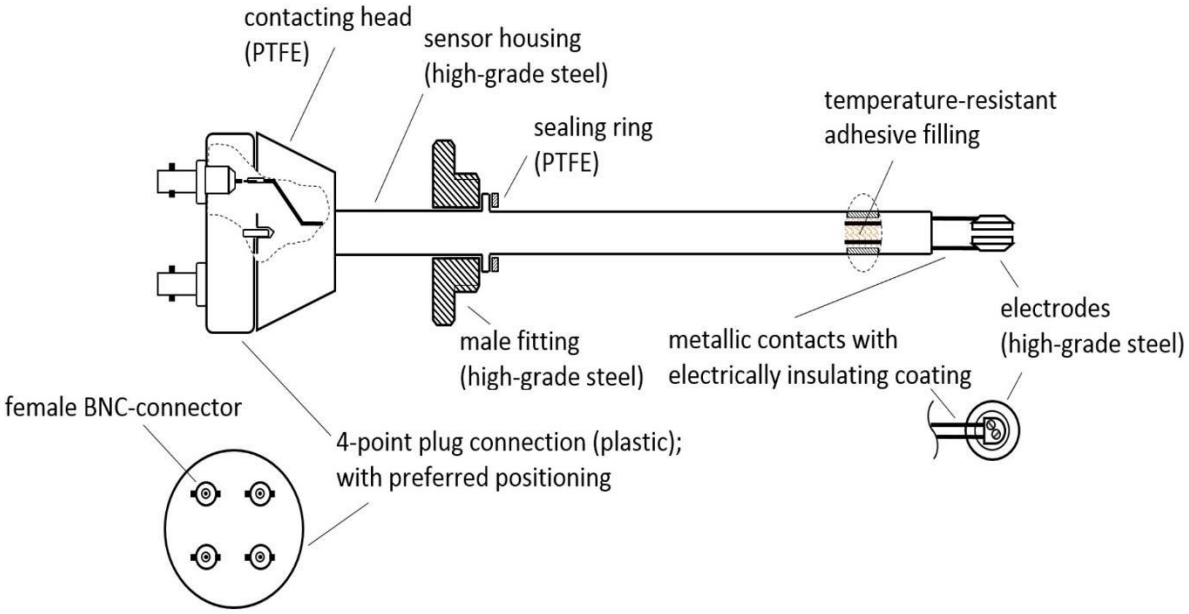

Figure 30: Sketch of the inline probe prototype indicating used materials and wiring. Connection to the impedance analyzer was performed using 4-point BNC "Bayonet Neill Concelman" connection.

The body as well as the electrodes of the inline probe consist of high-grade steel, i.e. austenitic stainless steel, which is approx. 140 mm in length and at least 12 mm in diameter. Each electrode has a diameter of 10 mm. The gap between the electrodes is approx. 2 mm.

5.3. Results and Discussion

Aerobic and anaerobic batch cultivations in defined media monitored in online mode

Cultivation of yeast, as a well-known host for diauxic growth, is cultivated aerobically and anaerobically using different carbon sources, preliminary present in malted barley and wheat grain. A batch-based design is used in both cultivations. Growth rates of corresponding cultivations in **Figure 30**. are given in **Table 14**. The specific growth rate describes the increase

of biomass in a given time interval normalized to the biomass inside the reactor (dx/dt*1/x(t), with x being the biomass).

Table 14: Specific growth rate μ of batch phases determined by offline DCW measurements (given in Fig 1 a).

Cultivation	**μ [1/h]**
Aerobically	0.345 +/- 0.04
Anaerobically	0.150 +/- 0.02

Raw data and general considerations

The measured impedance raw data were analyzed by a resistance R_{DL} in parallel to a non-ideal capacitance CPE_{DL} (parameter Q, n). These elements most probably originate from the double layer region close to the electrode and can be expressed by Equation 12:

$$Z_{DL} = 1/(R_{DL}^{-1}+(i\omega)^{n}*Q_{DL}) \qquad \text{Equation 13}$$

ω is the arc frequency and i is the imaginary number. n and Q are obtained from a fit to experimental data. In principle, these parameters can be used to calculate the double layer capacitance (C_{DL}) according to $C_{DL} = (R_{DL}^{1-n}*Q_{DL})^{1/n}$.

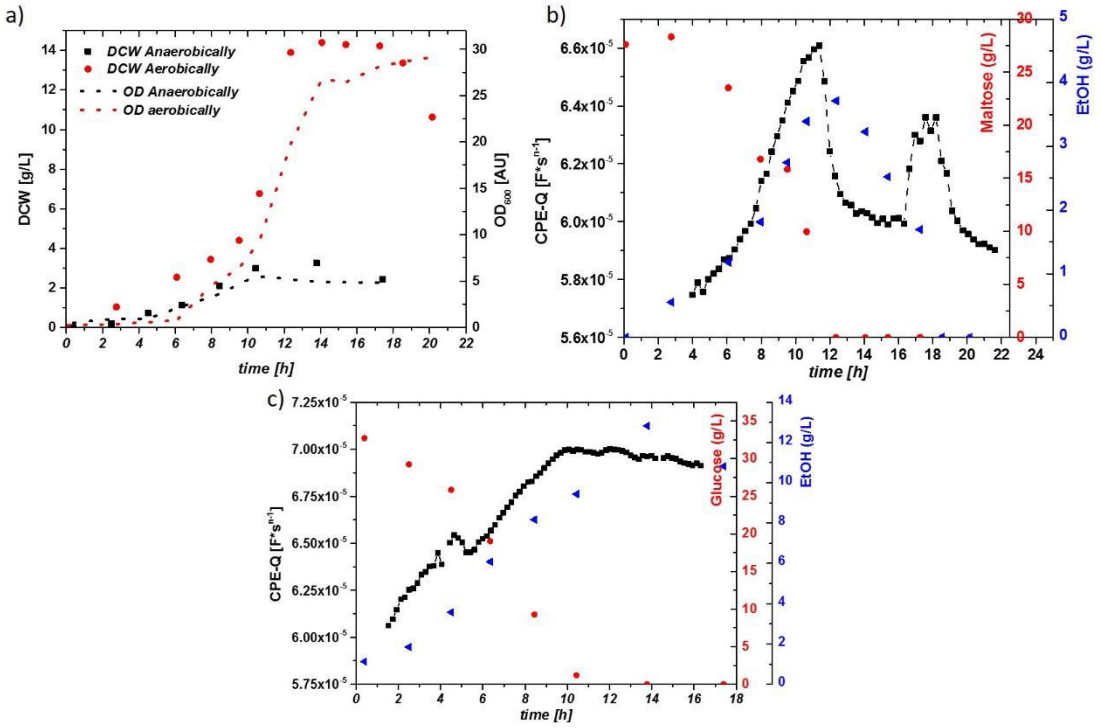

Figure 31: a) Time courses of the DCW [g/L] and OD [AU] for the aerobically and anaerobically cultivated *S. cerevisiae*. Corresponding µ values are given in Tab. 1; **b)** Impedance signal – CPE-Q – and maltose/ethanol concentrations over time during the aerobic cultivation. A drop in the impedance signal is visible after depletion of maltose (change in metabolism). A further small increase upon ethanol uptake can be observed, until the second carbon source is depleted; **c)** Impedance Signal – here CPE-Q – and glucose/ethanol concentrations during the anaerobic cultivation. No sudden decrease of impedance signal is spotted after depletion of glucose in the media. Rather a constant decrease in the signal can be observed.

Aerobic growth of yeast results in partial aerobic metabolism and partial fermentation, well known as Crabtree effect. During anaerobic growth sugars are solely fermented to ethanol. Corresponding DCW and OD of two cultivations are given in **Figure 31** a. During growth on high concentration on glucose the respiratory capacity is generally too low and ethanol is produced simultaneously. Sugar decreases and ethanol production are given in **Figure 31** b including the Q value of the online impedance probe. Upon sugar depletion in the fermentation broth at t = 12 h, a strong decrease in the impedance signal is observed, which corresponds to the growth on ethanol. Anaerobic growth on glucose yields much higher ethanol concentrations (about 1.5 vol% in this run), **Figure 31** c. The impedance signal increases over time with maximum upon complete glucose depletion. Since ethanol cannot be metabolized anaerobically and accumulates in the

supernatant, no change in cell metabolism is expected, but rather a shift from exponential growth into stationary phase. Therefore, no steep drop in the impedance signal is observed, but a smooth decrease over several hours.

Aerobic cultivations

However, the double layer resistance (Yardley, et al.) cannot be fitted accurately [32] (especially for the inline probe) as a result of the high overall fitting error, as already observed for cultivations with *E. coli.* Furthermore, n values, received from fittings with CPE elements, show deviations dependent on the cultivation state (aerobically/anaerobically) and especially on the type of probe (inline/online). These changes in n value make a comparison of runs difficult. For better description of the different metabolic states the fitting procedure is modified. For easier comparability of the performed runs, n is fixed to 1 in the following data analysis, reflecting the idealized capacitance (C_{ideal}) of the sample.

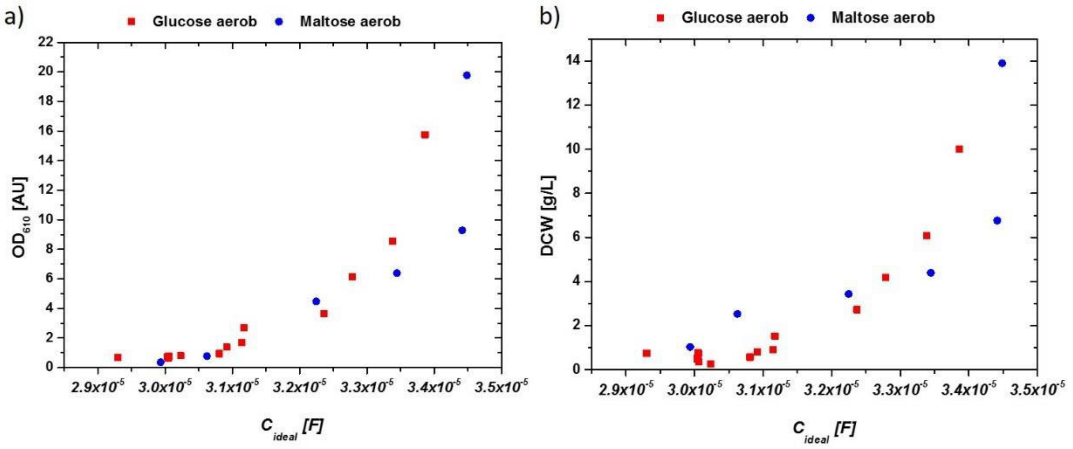

Figure 32: a) OD_{610} vs. extracted capacitance of impedance signal in aerobic cultivations with glucose and maltose.; b) DCW vs. extracted capacitance of impedance signal in aerobic cultivation. Very similar responses are obtained for both cultivations irrespective of the used C-source.

Measured values for biomass determination (OD_{610} and DCW) are correlated to the received idealized impedance signal referred as C_{ideal}. The corresponding data for aerobic cultivations on

glucose as well as on maltose are given in **Figure 32** a for OD and **Figure 32** b for DCW measurement.

The late time during end of batch shows deviations in the impedance signal, as a result of metabolic changes in the system (compare to **Figure 31** b). Deviations between glucose and maltose may be a result of different sugar transport through the membrane. Since maltose uptake is mediated by a proton mediated symporter, a change in the counterion-cloud and therefore changes in the overall impedance are very likely (Weusthuis, et al., 1994). Furthermore, changes in the overall membrane structure, producing maltose transporting proteins (maltose permease), not present in only glucose grown cells, may change the magnitude of the impedance signal in those cultivations. However, the impedance signal especially in the end of the aerobic batch phase hold valuable information on the present metabolism of *S. cerevisiae*.

Anaerobic cultivations

Ethanol production may have further effect on the impedance signal holding information about the physiological state of the system. Sugar concentrations up to 200 g/L showed no effect on the magnitude of the impedance signal (Slouka, et al., 2016). However, growth conditions of *S. cerevisiae* may have impact on the impedance signal. To test the impact of growth conditions, different anaerobic cultivations were performed, according to **Table 15**. Oxygen from air was eliminated with a flow of 4 L/min nitrogen through the fermenter. Gas analysis of the off gas confirmed the absence of oxygen throughout the entire batch.

Table 15: Starting sugar concentrations in different anaerobic batch runs extracted by HPLC measurement.

Cultivation	Maltose [g/L]	Glucose [g/L]
ANA1	-	32.7
ANA2	44.4	54.2
ANA3	-	22.5

Raw data of a cultivation with different sugar concentration (compare to Fig. 2 c) including maltose and glucose grown anaerobically showed high ethanol concentrations, which reached a maximum of about 3 vol% in these cultivation (ANA2).

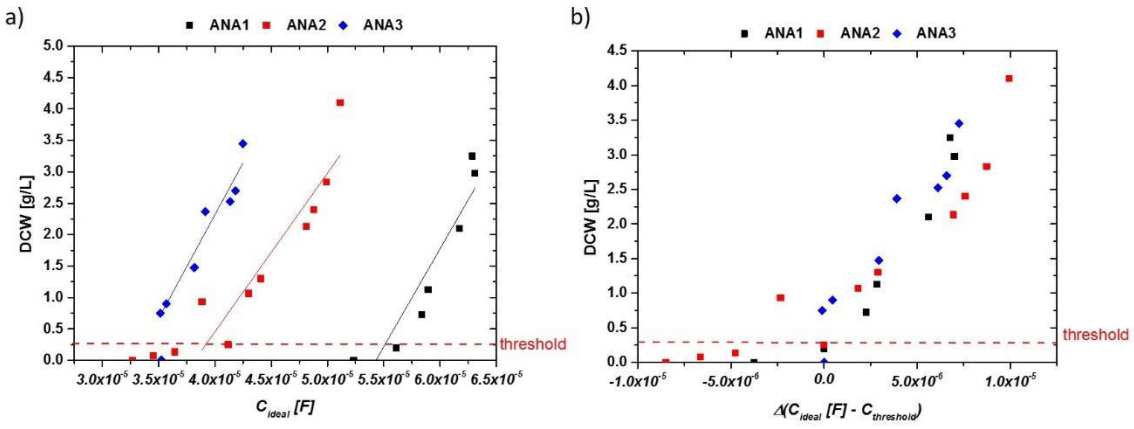

Figure 33: a) Idealized capacitances of anaerobic runs exhibiting up to 100 g/L sugar in the fermentation broth (mixture of maltose and glucose). Ethanol concentrations reached 3 vol%. Different absolute values can be found in these cultivations, but the increase of the impedance signal with DCW is very similar; b) DCW vs. delta of impedance signal (ideal capacity) in the anaerobic runs. Normalization to the threshold value of about 0.3 g/L result in very reproducible signals for very different fermentation runs.

Anaerobic growth can be well described, except for very early time points, where cell densities are below the thresholds of about 0.3 g/L. For inline OD measurements, very similar results can be obtained (not shown). Generally, the fits for aerobic and anaerobic cultivations are used to estimate biomass in real-time for the aerobic and anaerobic runs. As a very good linear description can be obtained in anaerobic runs, real time estimation of biomass is straight forward,

as shown in **Figure 33** a and **Figure 33** b after normalization to the threshold of the impedance signal.

Using these results, DCW (half-filled circles) values are well described by the impedance signal over process time (**Figure 34** a). A general quality of the fit is given in **Figure 34** b. The calculated DCW vs. the measured DCW is situated close to the 1st median. Values not situated along the first median indicate for the overall error in the fitting routine, compared to a residual analysis. As cell densities are very low during these cultivations, errors during the DCW measurement are about 10 % of the actual mean value (highlighted for ANA2 in **Figure 34** b. When comparing accuracy and threshold to *E. coli* cultivations, *S. cerevisiae* cultivations have a very good reproducibility in aerobic and anaerobic growth using the online impedance probe even in the low biomass concentration regime. A threshold of about 0.3 g/L DCW is also a strong benefit for monitoring high dynamic systems.

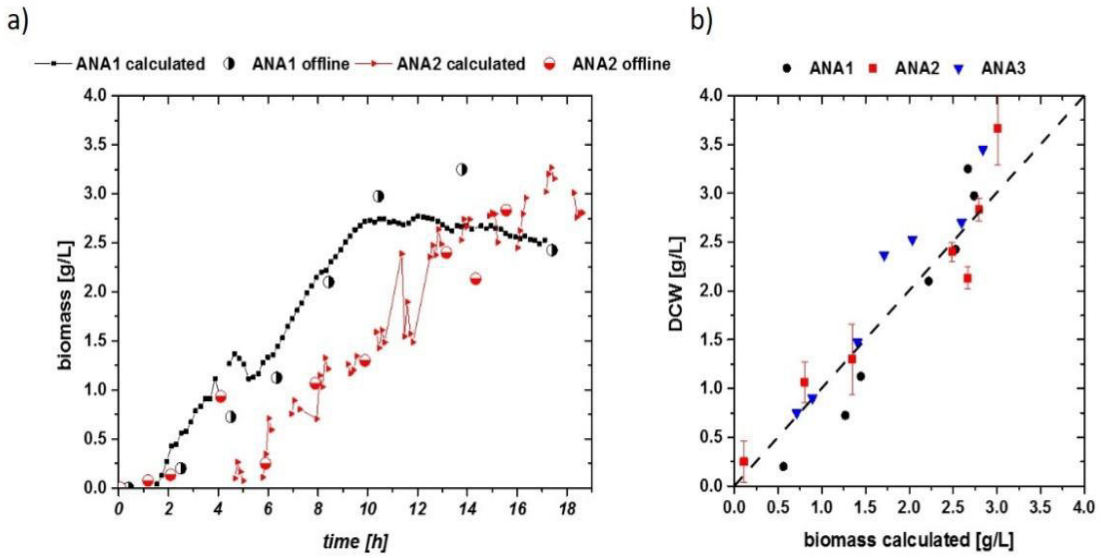

Figure 34: a) biomass calculated of the impedance signal fit extracted in Fig. 4 a) including offline measured DCW values as circles. Flow cytometric measurements confirmed that no dead population is visible, so DCW can be compared to the viable cell concentration in these runs; b) residual analysis of the three anaerobic runs. Despite the low cell densities, a very accurate correlation can be found in all cultivations. Error bars are exemplarily plotted for ANA2 cultivation.

Aerobic and anaerobic cultivations in defined media using the new inline probe

Impedance signal in the online mode could be used to estimate the viable cell concentrations in aerobic and anaerobic cultivations. The newly built inline probe prototype is measured alternating to the online probe in two cultivation runs (one aerobic and one anaerobic). Impedance raw data of the aerobic run are given in **Figure 35** a. Two very distinct features are visible. At higher frequencies, a shift to negative differential resistances is visible. Similar phenomena have already been observed in *E. coli* fermentations even before inoculation of the system (Slouka, et al., 2016). Further, a reduction of the capacity by an order of magnitude is observed between online probe and inline probe, compare to **Figure 35** a.

The capacitance of our almost ideal plate capacitor design as built in the inline and online probe is proportional to

$$C = \varepsilon * d/A \qquad \text{Equation 14}$$

with C being the capacity [F], d the distance between the plates; ε is the dielectric constant ($\varepsilon_R * \varepsilon_0$) and A is the area of the electrode. For an electrode with half the diameter, the capacitance signal should decrease by a factor of four. Stirring and aeration of the system may have effects on the used electrode area and reduce the measured capacitance even more.

The extracted idealized capacitance of an aerobic run measured using the inline probe is given in **Figure 35** b, including process values of glucose consumption and ethanol production. Gaps in the time scale are caused by alternating measurement of inline and online probe during the cultivation. After one hour, an increasing signal in capacitance is found in accordance with measurements using the online probe. However, higher fluctuations in the signal are visible, making a smoothing of the raw capacitance signal beneficial. Smoothing was done in the aerobic fermentation using OriginPro 9 [Northampton, MA, USA] 5-point FFT smoothing procedure.

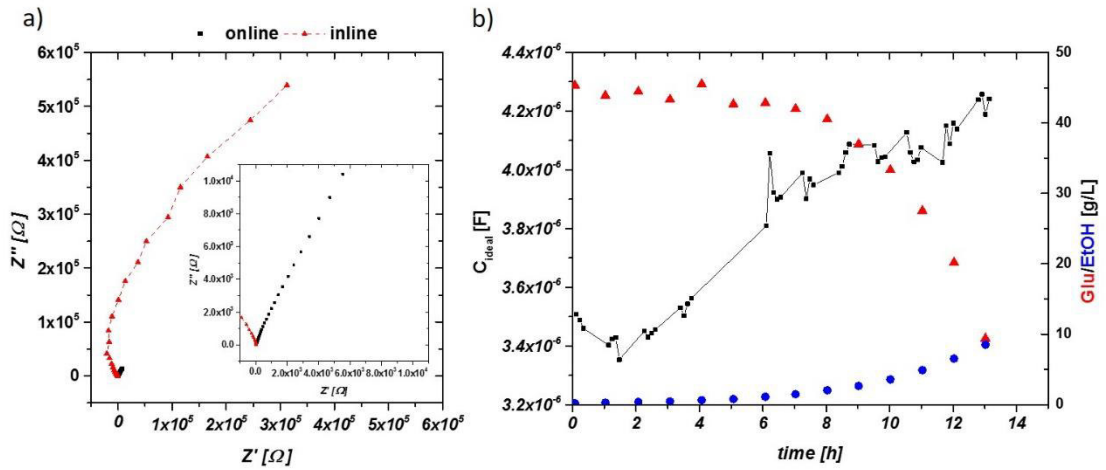

Figure 35: a) Impedance raw-data in Nyquist plot for an aerobic cultivation. Black squares represent signal from the online probe – enlarged in the inlay -, red triangles the inline probe at similar time stages. Capacitance of the inline probe is one order of magnitude lower (as a result of smaller electrode areas).; b) the dependence of impedance signal (not smoothed), glucose consumption and ethanol production in an aerobic cultivation using the inline probe.

The smoothed signals – especially for the aerobic run - are now used for fitting the biomass data. The corresponding results are given in **Figure 36** a. Obviously, a higher threshold for accurate data acquisition is found in the inline probe having the lower limit of 1 g/L DCW biomass (compared to about 0.3 g/L for the inline probe). Exceeding the threshold, a good linear trend can generally be seen in aerobic and anaerobic fermentation in both samples.

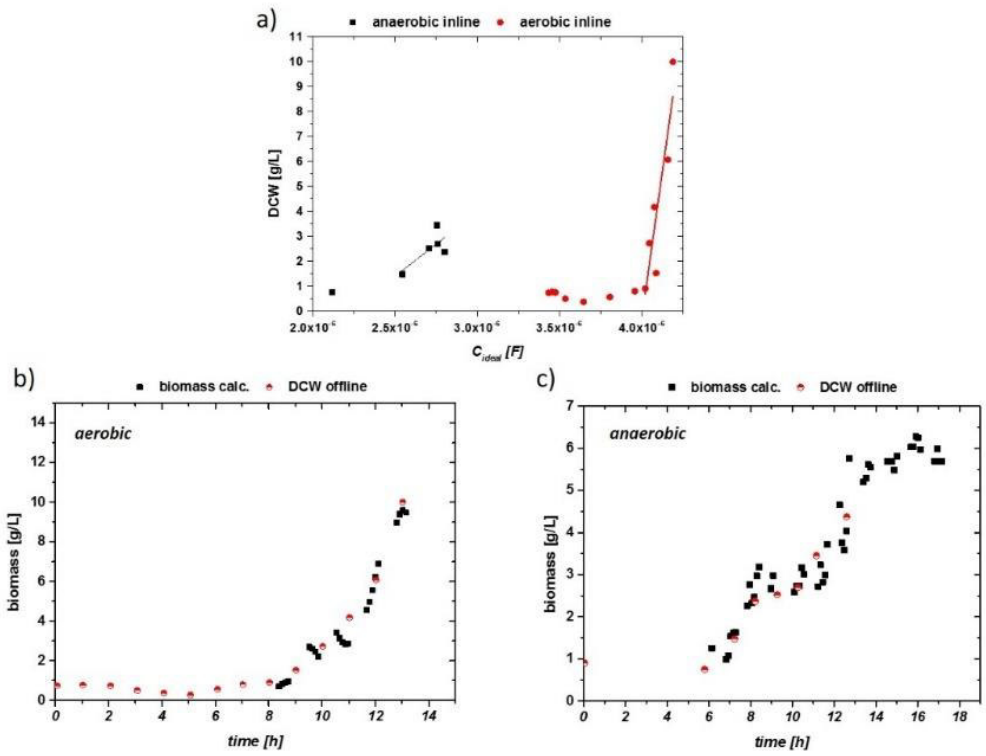

Figure 36: a) Impedance signal vs. offline DCW for aerobic (circles) and anaerobic (squares) cultivation with linear fits beyond a threshold of 1 g/l DCW; b) Impedance signal of aerobic run (smoothed) and calculated via linear fit into a viable biomass. This is correlated to the offline DCW; **c)** impedance signal vs. DCW of the anaerobic run

The correlations of calculated biomass compared to offline biomass are given in **Figure 36** b and c). Early stages without pronounced growth cannot be monitored during the cultivation. The exponential growth can be described accurately with the inline probe despite high aeration and stirring rates. Promising results are also obtained for the anaerobic cultivation, despite higher fluctuations in the signal. For defined minimal media the measurement with the inline probe show reproducible, stable results in the used systems (Sartorius and Techfors with 10 to 20 L maximum volume of the fermenter).

Larger systems in brewing industry, including longer residual times in the side stream may affect the online signal and change absolute impedance signal and slopes of the DCW vs. capacitance curves. Furthermore, larger tank reactors may include inhomogeneities within the system, which have effects on the signal and have to be taken into account. As residual times in the different

bypasses may result in high variations, online probes therefore should be calibrated within the measurement system. Signals of the assembled inline probe are affected by process conditions like stirring and aeration, which result in higher fluctuations of the signal in general. Increase in electrode area may have beneficial impact on the stability of the signal, since absolute capacitance values are one order of magnitude lower compared to the online probe.

Aerobic growth of yeast on complex malt extract medium

Defined media have the advantage of good reproducibility and easy analytics like OD for biomass determination and HPLC for sugar/ethanol analytics, and are therefore perfectly suited for the first development steps. However, since defined media are scarce used in industrial process for yeast production, malt extract for production of pilsner beer was used for this cultivation run. Complex media like malt extract and molasses often have the drawback that OD measurement generally show a very high blank adsorption (especially in the IR range) and cannot easily be used online in those cultivations for determination of the total biomass.

The performed cultivation was analyzed by HPLC and offgas analytics to determine the end of the batch phase. HPLC data for sugar and ethanol are given in **Supplementary 5**. A mixture of different mono- and polysaccharides is consumed during fermentation. This leads to 10.6 g/L DCW and 3.2 vol% ethanol after the batch phase at about t = 16 h. Online and inline impedance measurements were performed in alternating mode in one cultivation. Raw data for the online impedance signal is given in **Figure 37** a including information on the ethanol concentration during the cultivation. A steep increase is followed by a shoulder at about 13 hours of cultivation time, which may indicate a change in sugar metabolism at the end of the batch phase. At process time t = 16 h, a decrease of the impedance signal is visible, generally observed at growth on ethanol. However, the decrease in the signal is rather smooth, compared to the distinct drop in defined media (compare to **Figure 31** b). Interpolation of the signal and 5 point FFT smoothing

was performed to reduce the noise in the signal. The same procedure was done for the inline impedance signal, given in **Figure 37** b. In the inline signal a distinct decrease of capacitance can be spotted after the end of the batch phase, accompanied by an increase on ethanol growth at later process time.

The obtained smoothed and interpolated data are compared to the DCW taken and plotted in **Figure 37** c for the online probe and in d for the inline probe. The slopes of the signals are very similar to extracted values for defined media samples (red/blue dots). However, an obvious shift in the signal intensity can be observed for both probes.

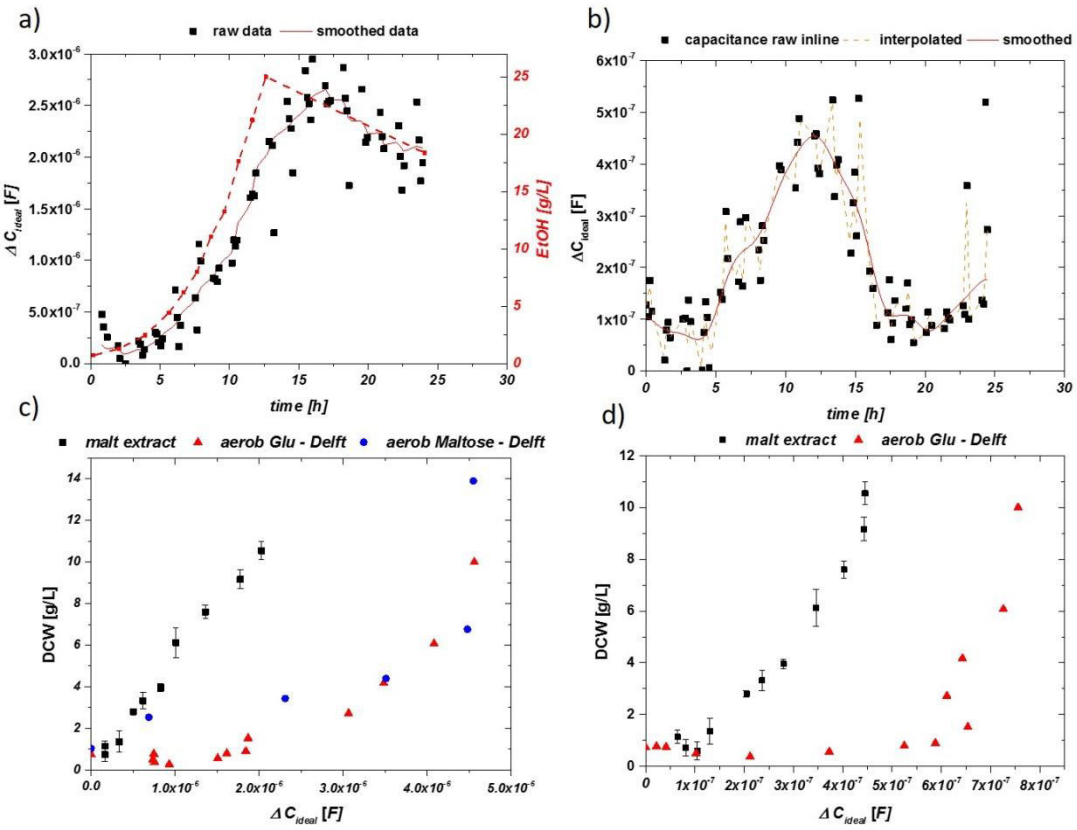

Figure 37: a) Impedance signal over cultivation time for the online probe using only malt extract as growth media. The line (orange) shows the interpolation procedure. As in related aerobic cultivation a drop in the impedance is observed after consumption of sugars; b) Impedance signal raw data and interpolated and smoothed of the inline probe; **c)** normalized impedance signal vs. DCW for the online probe using malt extract compared to defined media; **d)** normalized impedance signal vs. DCW for the inline probe using malt extract and defined media with glucose.

A linear fitting is applied to the impedance vs DCW plot in **Figure 37** c and DCW is calculated through the impedance signal and compared to the offline measured signal in **Figure 38**. Beyond

the given threshold of 1 g/L a good description of the process can be achieved in usage of the inline probe.

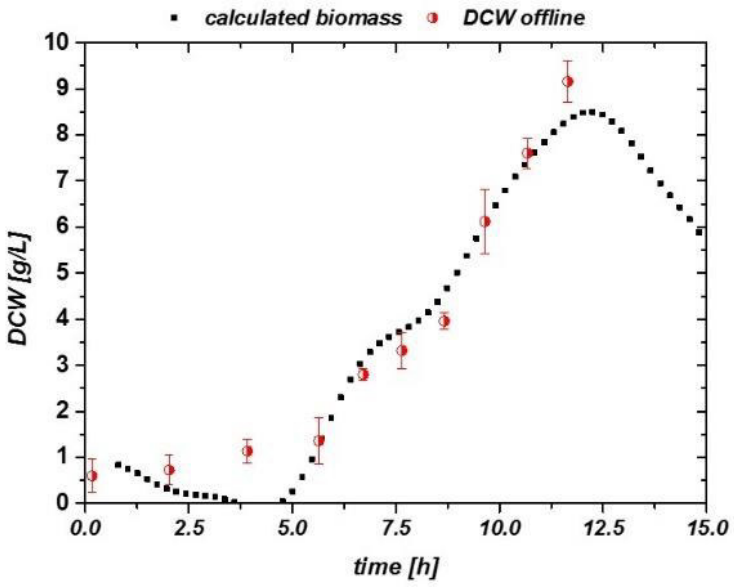

Figure 38: impedance signal vs. DCW of the inline probe in complex media malt extract. A good description is found beyond 1 g/L DCW in this experiment.

Based on these first measurements in complex media, impedance spectroscopy at frequencies in the kHz to mHz range seems to be a promising tool for online process monitoring in yeast production processes and maybe even in anaerobic refining processes in brewing applications. The present decrease in signal upon complete sugar consumption is a powerful feature as a stop criterion in those cultivations. An optimization in the signal to noise ratio, especially for the inline probe, would be beneficial for increasing accuracy of the biomass estimation. However, tower type reactors are generally used in brewing application, rather than stirred tank reactors due to aroma compound reasons (Okabe, et al., 1992). Hence, the used stirring and aeration rates for the development are much harsher compared to industry, and therefore a much more stable signal is to be expected. Calibration of the probe may be done once within the used system and used growth media and can should be stable for forthcoming measurements.

5.4.Conclusions

New online and inline probes based on electrochemical impedance spectroscopy at low frequencies for measurement of viable cell concentration for *S. cerevisiae* were tested. First cultivations were monitored using a former developed online probe for pharmaceutical *E. coli* fed batch cultivations. Batch cultivations on defined media for aerobic and anaerobic growth showed stable results irrespective of carbon source and concentrations. A newly assembled inline probe was tested in aerobic and anaerobic cultivations in defined media and compared to the online probe. A good description of the biomass growth during the process is achieved. Beside the determination of the biomass during the cultivation, physiological states could be determined depending on the respire condition of the cells. This measurement setup for biomass is high beneficial especially in complex media like malt extract or molasses, since optical online methods cannot be used in this optical dense media. The developed system shows therefore high potential for monitoring cell growth and harvest time points for yeast and beer producing industry.

6. Conclusion and Outlook

6.1. Scientific questions

Following scientific questions and aims were addressed during this thesis:

I. **Are we able to detect variances in inclusion body quality attributes (size, purity) by means of analytical techniques? Can these quality attributes be changed based on the two classical process parameters pH and temperature in the induction phase?**

We tested the dependence for pH, temperature and physiological feeding control for two industrial relevant proteins. We successfully established analytical techniques for determination of the quality attribute size (scanning electron microscopy, atomic force microscopy and high fluorescence microscopy) and purity (Bioanalyzer based assays). A clear dependence for titer as key performance indicator and the given quality attributes could be dedicated generally dependent on the physiological state of the cells. Low pH and temperature are favorable during production of IB based products.

II. **Can product formation be boosted by usage of glycerol instead of glucose, overcoming the limitation of carbon catabolite repression (CCR) when using lactose as inducer? Can cell stress be reduced by usage of lactose as inducer instead of IPTG?**

As glucose is rather expensive as raw material for industry, we used the waste product glycerol for the entire cultivation. Glycerol based runs generally performed equally good to glucose in terms of biomass growth in batch and fed-batch and productivity during induction. Lactose as inducer can reduce cell stress during cultivation and gives additional energy in terms of cleaved glucose usage. However, CCR cannot be overcome by usage of glycerol with lactose as inducer as cell intern glucose concentrations show the same effect during cultivation.

III. As cell stress leads to reduction of viable cell concentration and subsequent product degradation, control strategies need to be applied to overcome these issues. Are there trigger parameters for determination of cell stress, and can control strategies be applied based on these?

As IPTG based induction imposes a high cell stress, physiological feeding has to be adapted to keep viable cell concentration high. We established different control strategies based on the cumulative sugar uptake value (dSn) and tested first approaches using the Oxygen Uptake Rate (Seras-Franzoso, et al.) as online trigger parameter. With according design of dSn cultivation we could established high titers without cell lysis. Furthermore, the C-source usage could be reduced drastically compared to feed-forward strategies. First model-based approaches for titer as KPI and size as QA make prediction in real time possible.

IV. Viable cell concentration is the most important parameter during cultivations with microorganism as they are the catalysator or producer of the value product? Is it possible to determine viable cell concentration and/or the physiological state of the cell using hard sensor methods?

Viable cell concentration (VCC) can generally be measured using different methods, e.g. as colony forming units, with usage of counting cells, with usage of flow cytometry or with soft sensor approaches. However, no direct measurement in the reactor is possible using these methods. We tried to develop an electrochemical measurement principle based on low frequency impedance spectroscopy to determine VCC and physiological state of the cells inside the reactor. Proof of principle for *E. coli* were already established in an earlier project (Slouka, et al., 2016). The work was continued for *S. cerevisiae* used in food industry and showed the high feasibility of the method. It can be used to monitor VCC in real-time and distinguish between different physiological state of the cells.

6.2. Outlook: Triggers to enable continuous upstream processing

Today's state of the art of microbial processes in the pharmaceutical industry are fed-batch based cultivations, which generally consist of a biomass production phase followed by an induction phase for producing the desired recombinant product. It was shown in this thesis, that these approaches lead to highly time-dependent changes in productivity and product quality, which are expressed in product QA like IB size and purity and as KPI like titer. Consequently, this approach requests a very large amount of empirical knowledge for every single product in the upstream processing. Gaining detailed knowledge of critical process parameters (CPP) like pH and temperature, viable cell concentration, physiological feeding and limiting media components and/or precursors helped us to get out of the 'empirical' black box and to gain a fundamental process understanding, which can be used as a platform knowledge. This enables prediction of product quality attributes for given process parameters and to control the process in real time, combined with a high variety of process analytical tools (PAT), like the recent developed impedance probe.

The given platform knowledge presented in this thesis is tested on an industrial based *E. coli* inclusion body process in continuous mode. The aim is to increase performance in production of a pharmaceutical relevant high value product to eliminate time-dependency of product quality attributes. The CPPs for the product were identified based on a DoE design altering pH, T and physiological feeding control in this thesis. Furthermore, knowledge created in our group on a mild induction approach, using lactose instead of IPTG improved the process performance in terms of high viable cell concentrations during the cultivation, as viability of cells is especially important in long-term cultivations. These optimized process conditions are used for enabling continuous cultivations for the given product. Further developing steps including splitting of biomass production and induction in a two-compartment system are ongoing and show high potential for further increased process performance.

Supplementary Material

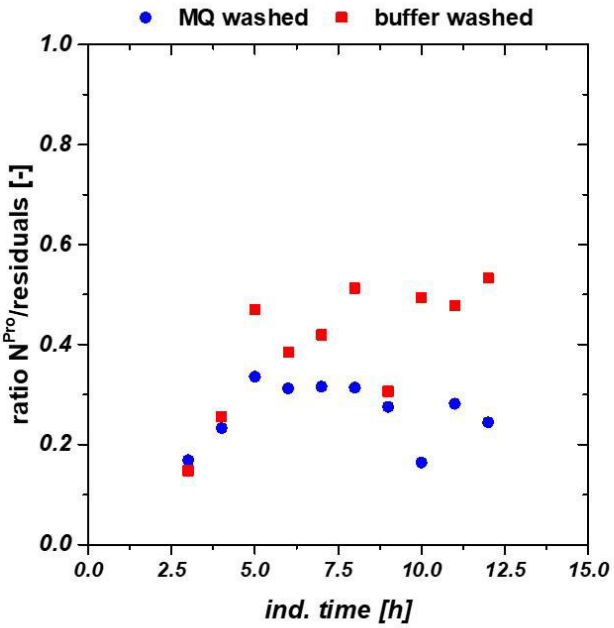

Supplementary 1: Analysis of the first center point run representing IB purity. Buffer washed samples showed generally higher purity. Differences in size and titer are within the given standard deviation.

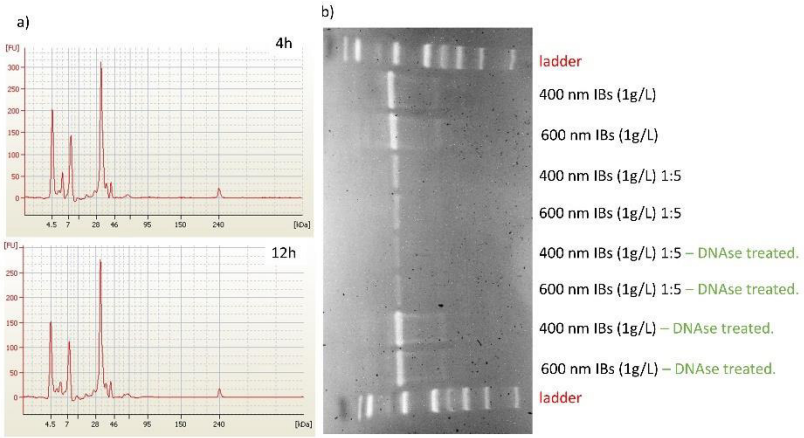

Supplementary 2: a) Electropherogram for two different timepoints during a cultivation (4 h and 12 h). A clear visibility of impurity pattern near the protein of interest (high peak after 28 kDa) is given; b) SDS-Page for visualization of DNA related impurities. No distinct differentiation can be made between DNase treatment and virgin sample.

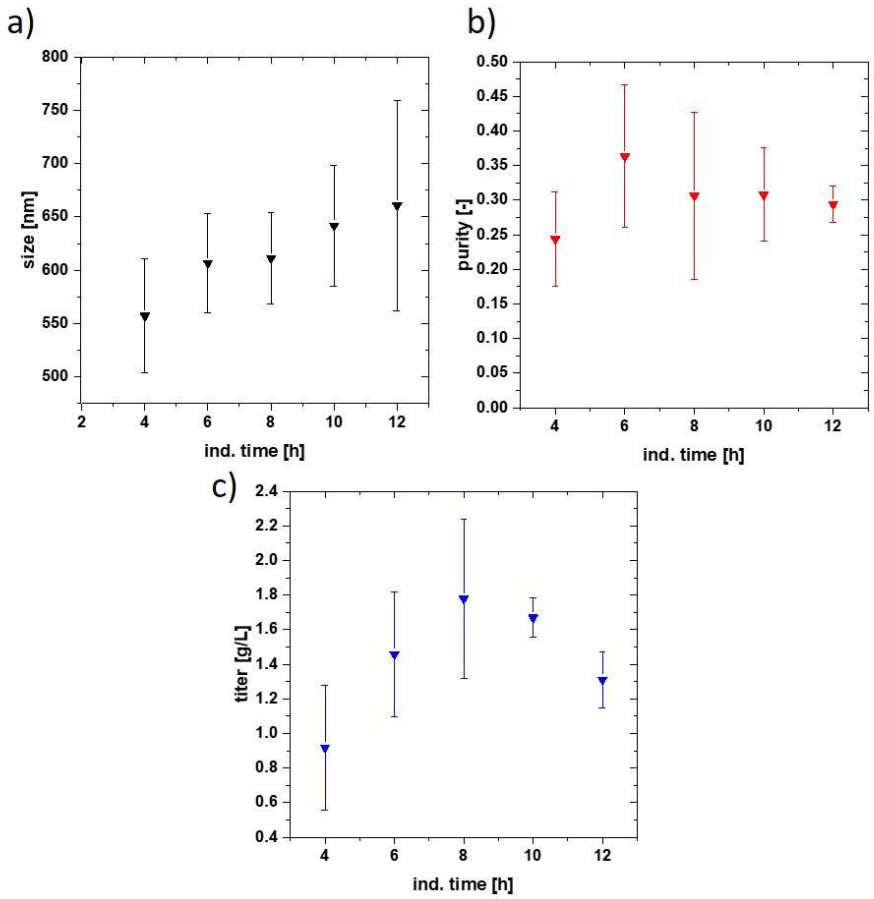

Supplementary 3: a) Mean value for size and deviations of the three individual center point runs. Error stays constant; b) purity-based analysis, with decreasing error over time; c) titer-based analysis. Error decreases drastically in later time stages (range of constant titer or even proteolytic degradation).

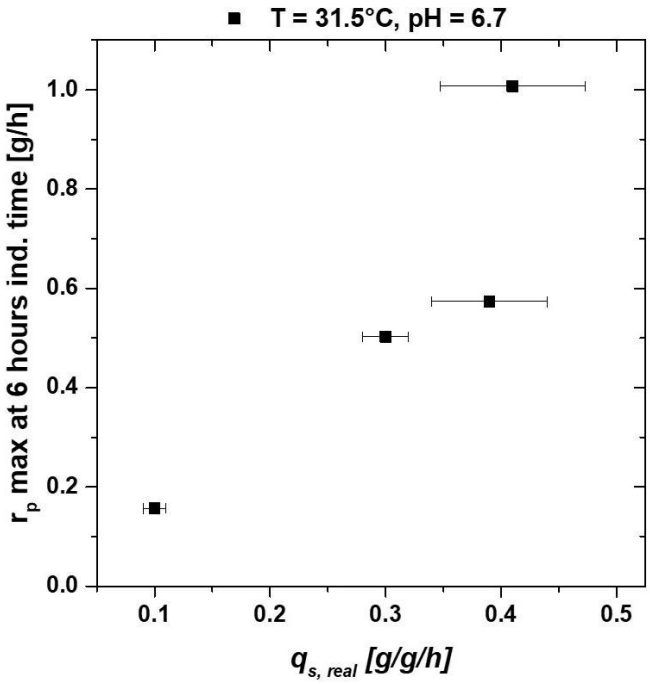

Supplementary 4: $q_{s,real}$ with standard deviation based on the reverse analysis. The higher the q_s the higher is the error, due to onset of degradation and sugar accumulation in the broth. A rising trend can be dedicated from these measurements.

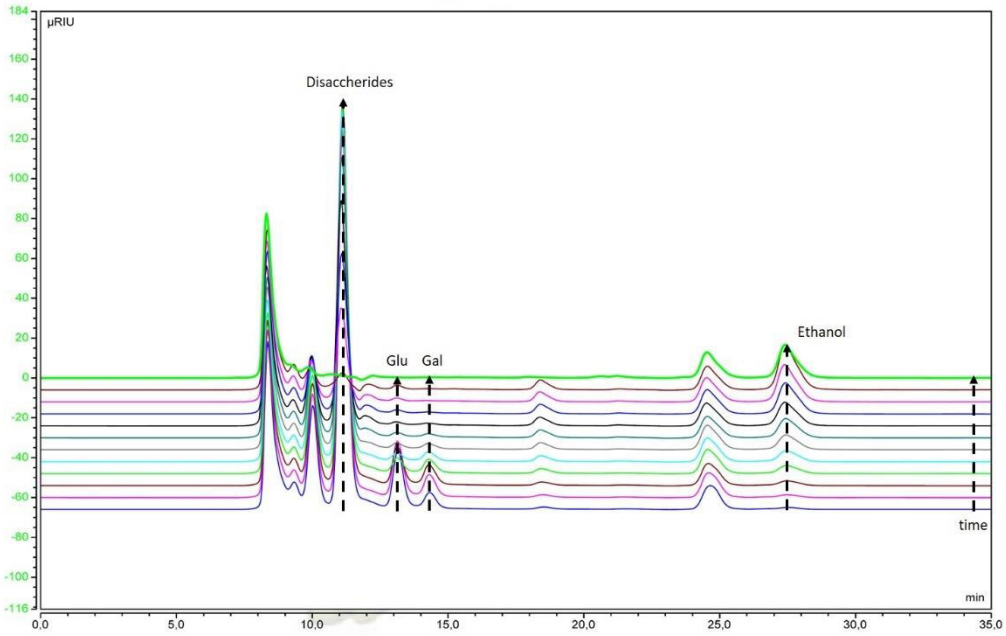

Supplementary 5: HPLC data for malt extract analysis used in sensor development.

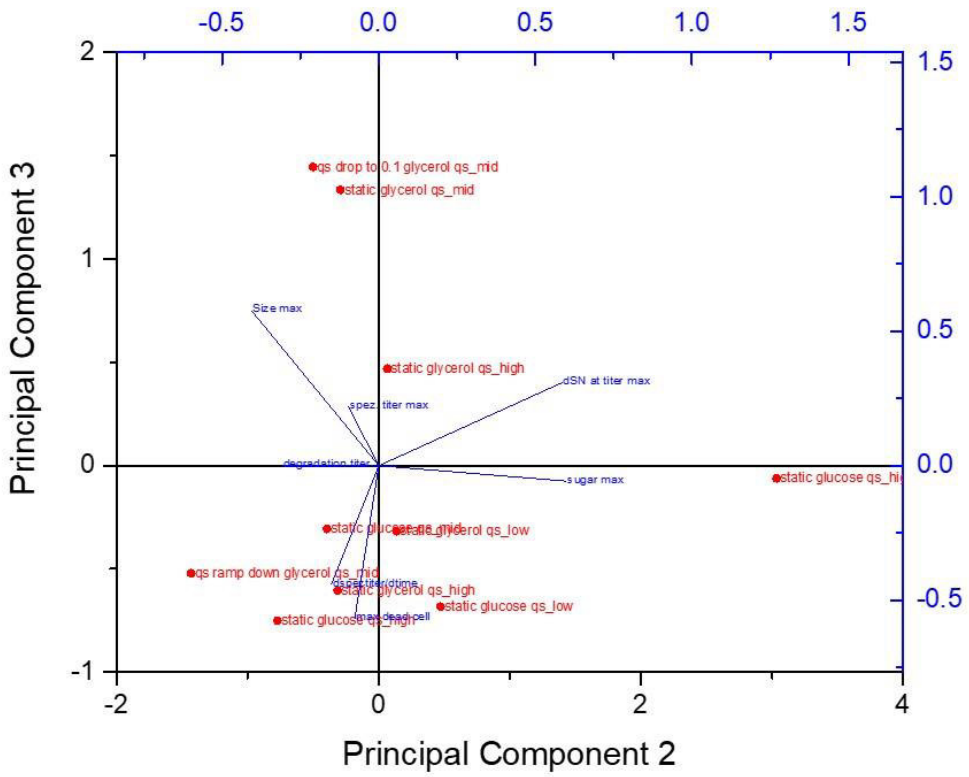

Supplementary 6: Biplot of PCA analysis for component 2 and component 3.

Abbreviations

AC	alternating current
ACN	Acetonitrile
AFM	Atomic Force Microscopy
BNC	Bayonet Neill Concelman
C_{DL}	double layer capacitance
CHO	Chinese hamster ovary (cells)
CPE	constant phase element
DCW	dry cell weight
DiBAC	(bis-(1,3-dibutylbarbituricacid)trimethineoxonol)
dO_2	dissolved oxygen
DoE	Design of Experiments
DSP	Downstream Processing
EIS	electrochemical impedance spectroscopy
FCM	Flow cytometry
GFP	green fluorescent protein
HPLC	high-pressure liquid chromatography
IB	Inclusion body
IPTG	isopropyl β-D-1 thiogalactopyranoside
IR	Infrared
MQ	Ultrapure water
OD	optical density
QA	Quality attribute
$q_{s,Glu}$ [g/g/h]	specific substrate uptake rate (glucose)
R	resistance
r_p [g/L/h]	volumetric productivity
SEM	Scanning electron microscopy
TCA	Tricarboxylic acid (cycle)
TEM	Transmission Electron Microscopy
USP	Upstream Processing
UV	Ultraviolet
VCC	viable cell concentration
Z	general impedance
ε	dielectric constant
ω	arc frequency

Captions

Figure 1: Workflow of IB production with link to different further used process steps during upstream and downstream. 9

Figure 2: Product development chain for (IB) products and it's iterative optimization process. .. 20

Figure 3: Workflow of this thesis to acquire process understanding during the given product development. Part I and II are presented in the following chapters. For part III first approaches will be presented for viable cell concentration as an important factor for PAT analytics. 24

Figure 4: DoE for determination of the influence of classical process parameters on IB QAs. Starpoints (8,9,10,11) were performed in a DasGip parallel system, while the others were cultivated in a stainless-steel Sartorius Stedim reactor; b) reduced design space for *strain 2* based on optimal cultivation parameters. 31

Figure 5: Extracted IBs filtered onto Au coated polycarbonate filter and analyzed using SEM for 4 h induction time and 12 h induction time. Strong difference in size can be spotted for the two-time points. 35

Figure 6: IB QAs as a function of induction time for the third centerpoint cultivation. Size is given with standard deviation (spline). Drop of titer/size and purity after 8 h is generally a result of increased cell lysis at elevated times. 39

Figure 7: a) data driven model for time dependent analysis of IB specific titer; b) model fit parameter for titer. While in the beginning only temperature dependence is visible, a strong pH correlation can be found at t = 8 h; c) data driven model for time dependent analysis of IB bead size; d) model fit parameter for IB bead size. Due to standard deviation of 10 % in the analysis model parameters are rather complex.; e) Data driven model for time dependent analysis of IB purity; f) model fit parameter for purity. A sole temperature dependence is found beyond 4 h of induction 40

Figure 8: IR spectra of the two distinct bead sizes of 400 and 600 nm, compared to the correctly folded reference sample. SEM analytics of both samples are given above. 44

Figure 9: Data driven model for time dependent analysis of IB a) titer, b) size and c) purity of *strain 2* using a reduced DoE design (Figure 4 b). Trends are given with differences of the lowest process value. Very similar behavior to *strain 1* can be found, showing highest purity, size and titer at values for low T and pH. Higher titers are produced using this strain resulting in boosted purities compared to *strain 1*. The analyzed size similar to *strain 1*. 46

Figure 10: a) Sugar-accumulation and cell death measured by FCM for three cultivations at different $q_{s,Glu}$. Lowest $q_{s,Glu}$ shows no cell lysis and accumulation; b) specific titer of the recombinant protein fused to N-pro. Very high expression can be seen for the high $q_{s,Glu}$ until 6 h with decreasing $q_{s,Glu}$ also decreases product titer; c) size of the IB beads. $q_{s,Glu}$ = 0.41 g/g/h and $q_{s,Glu}$ = 0.39 g/g/h are very similar. A very steep increase is followed by a steady state; $q_{s,Glu}$ = 0.30 g/g/h shows increase over time, while size for $q_{s,Glu}$ = 0.10 g/g/h is only detectable at 10 and 12 h of induction; d) purity depicts clear dependence of all different $q_{s,Glu}$ setpoints, increasing the IB purity with higher $q_{s,Glu}$. 49

Figure 11: Extracted datapoints for q_s values including standard deviations for cultivations with glucose and glycerol in the production strain (glycerol product, glucose product). Solid lines represent the model-based approach for inducer uptake rates vs feeding rates models of glucose and glycerol. 61

Figure 12: HPLC based data for decrease of lactose in fermentation broth exhibiting very similar $q_{s,C}$ values in [g/L]. A significant decrease over the time of induction is visible in producing [P] strains, while the decrease is way slower in non-producing [NP]-strain-cultivations. 63

Figure 13: Extracted datapoints for $q_{s,C}$ values including standard deviations for cultivations with glucose using the product producing (glucose product) and the NP strain (glucose, no product). Solid lines represent the model-based approach for inducer uptake rates vs. feeding rates models of glucose. A clearly visible difference can be observed during these cultivations 64

Figure 14: Extracted datapoints for $q_{s,C}$ values including standard deviations for cultivations with glycerol using the product producing (glycerol, product) and the NP strain (glycerol, no product). Solid lines represent the model-based approach for inducer uptake rates vs feeding rates models of glucose. 65

Figure 15: a) Time dependence for two IB titers starting from lactose addition to 7 h of induction; b) Titers of the recombinant produced protein, after homogenization of the inclusion bodies and a two-time washing plotted vs. the q_s of glucose and glycerol; a trend can be seen in gaining more product when cultivations are carried out on glycerol compared to glucose, respectively..... 68

Figure 16: a) FCM analysis of NP strain 5 h after lactose pulse. As no protein data are received from these cultivations, the induction time was limited to 5 hours; b) FCM analysis of the product producing strain. Glycerol imposes stress at low feeding rates, while glucose shows increase in cell stress beginning at about 0.25 g/g/h. 69

Figure 17: (a) Sugar accumulation measured in the supernatant during the course of induction with different static qs,C set-values.;(b) Specific titers of the recombinantly produced protein. High qs;C values are beneficial for the production – especially in the beginning of the induction phase -, but lead to pronounced protein degradation over time. 81

Figure 18: (a) Cell death during induction time affected by the applied qs,C; b) Exemplarily reduction of the active biomass (circles) in the reactor compared to the absolute biomass in the reactor (rectangles = dry cell weight). 82

Figure 19: dSn-based analysis for specific titers. The amount of fed glycerol results in highest titers between a dSn of about 3.5 to 6 g/g. 83

Figure 20: (a) Feeding strategy of three representative cultivations. The change in exponential feeding was triggered at a dSn of 3.5 g/g; (b) Specific titer for constant $q_{s,C}$, instant drop and stepwise drop. Highest titers could be found at instant drop strategy. 85

Figure 21: (**a**) Non volumetric OUR as a function of linear increasing $q_{s,C}$ values during induction phase (exponential increase in mass feed – red). Sugar accumulation in the broth leads to flattening of the OUR signal; (**b**) OUR normalized to fed mass of glycerol. A drop in the signal indicates sugar accumulation and can be used as trigger for the dSn based control. Sugar digestion capacity is constantly decreasing over time. 88

Figure 22:Empirical relations derived from static $q_{s,C}$ experiments. Induction phase variables are the applied $q_{s,C}$ during for the cultivation and the biomass before induction phase. Calculation of absolute titers are performed using the VCC approximation during induction. 90

Figure 23: **(a)** Data driven model for specific titer of the N-Pro fused model protein, including 95% confidence interval. A bilinear fit is used for description of the log(specific titer); **(b)** VCC model with 5% error estimation including data from FCM measurement, **(c)** titer calculated via VCC. Late model values fit well to offline measured titers. 92

Figure 24: **a**) IB beads at time point of harvest (12h of induction) after homogenization and subsequent washing with ultrapure water; **b)** IB bead size at qs,C of 0.4 g/g/h using glycerol as C-source. Late degradation is based on reduction in the viable cell concentration..... 99

Figure 25: (**a**) IB-bead size dependencies on the amount of fed glycerol shown calculated as dSn value **b**) dependence of the IB bead diameter when compared between glucose and glycerol.... 100

Figure 26: **(a)** Model cultivation with change in the $q_{s,C}$ from 0.5 g/g/h to 0.1 g/g/h at a dSn value of about 4 g/g. The lower $q_{s,C}$ value results in a high viable cell concentration at late induction times; **(b)** probability density plot of cultivations as a function of induction time 102

Figure 27**: (a)** Size modeling including real measured data with standard deviations. Especially early sizes could only be described using the model-based approach**; (b)** Size-titer correlation for fermentation with feeding strategy implied in Figure 3 a. 103

Figure 28: a) sketch of the important time dependent parameters of the KPI spec. titer. All other values are maxima (like size) or at induction time of 12 hours; b) Desired fed-batch behavior, with no visible degradation of spec. titer and high VCC concentration during the whole induction time. 107

Figure 29: PC 1 and 2 in a biplot with the analyzed quantities and the respective grouping of the cultivations. 109

Figure 30: Sketch of the inline probe prototype indicating used materials and wiring. Connection to the impedance analyzer was performed using 4-point BNC “Bayonet Neill Concelman” connection. 116

Figure 31: a) Time courses of the DCW [g/L] and OD [AU] for the aerobically and anaerobically cultivated *S. cerevisiae*. Corresponding μ values are given in Tab. 1; **b)** Impedance signal – CPE-Q – and maltose/ethanol concentrations over time during the aerobic cultivation. A drop in the impedance signal is visible after depletion of maltose (change in metabolism). A further small

increase upon ethanol uptake can be observed, until the second carbon source is depleted; **c)** Impedance Signal – here CPE-Q – and glucose/ethanol concentrations during the anaerobic cultivation. No sudden decrease of impedance signal is spotted after depletion of glucose in the media. Rather a constant decrease in the signal can be observed. 118

Figure 32: a) OD_{610} vs. extracted capacitance of impedance signal in aerobic cultivations with glucose and maltose.; b) DCW vs. extracted capacitance of impedance signal in aerobic cultivation. Very similar responses are obtained for both cultivations irrespective of the used C-source. 119

Figure 33: a) Idealized capacitances of anaerobic runs exhibiting up to 100 g/L sugar in the fermentation broth (mixture of maltose and glucose). Ethanol concentrations reached 3 vol%. Different absolute values can be found in these cultivations, but the increase of the impedance signal with DCW is very similar; b) DCW vs. delta of impedance signal (ideal capacity) in the anaerobic runs. Normalization to the threshold value of about 0.3 g/L result in very reproducible signals for very different fermentation runs. 121

Figure 34: a) biomass calculated of the impedance signal fit extracted in Fig. 4 a) including offline measured DCW values as circles. Flow cytometric measurements confirmed that no dead population is visible, so DCW can be compared to the viable cell concentration in these runs; b) residual analysis of the three anaerobic runs. Despite the low cell densities, a very accurate correlation can be found in all cultivations. Error bars are exemplarily plotted for ANA2 cultivation. 122

Figure 35: a) Impedance raw-data in Nyquist plot for an aerobic cultivation. Black squares represent signal from the online probe – enlarged in the inlay -, red triangles the inline probe at similar time stages. Capacitance of the inline probe is one order of magnitude lower (as a result of smaller electrode areas).; b) the dependence of impedance signal (not smoothed), glucose consumption and ethanol production in an aerobic cultivation using the inline probe. 124

Figure 36: a) Impedance signal vs. offline DCW for aerobic (circles) and anaerobic (squares) cultivation with linear fits beyond a threshold of 1 g/l DCW; b) Impedance signal of aerobic run

(smoothed) and calculated via linear fit into a viable biomass. This is correlated to the offline DCW; **c)** impedance signal vs. DCW of the anaerobic run 125

Figure 37: a) Impedance signal over cultivation time for the online probe using only malt extract as growth media. The line (orange) shows the interpolation procedure. As in related aerobic cultivation a drop in the impedance is observed after consumption of sugars; b) Impedance signal raw data and interpolated and smoothed of the inline probe; **c)** normalized impedance signal vs. DCW for the online probe using malt extract compared to defined media; **d)** normalized impedance signal vs. DCW for the inline probe using malt extract and defined media with glucose. 127

Figure 38: impedance signal vs. DCW of the inline probe in complex media malt extract. A good description is found beyond 1 g/L DCW in this experiment. 128

Table 1**:** Differences in QA, and performance indicators for different IB based products. QAs can be influenced by process parameters in the USP. 21

Table 2: Analysis of applied process parameters compared to set points in all DoE runs during induction phase. 38

Table 3: Prediction vs. measured QA of IBs for model validation run. 43

Table 4: Applied $q_{s,Glu}$ vs. real $q_{s,Glu}$ values after reverse analysis of the cultivation data. Sugar accumulation and cell death at higher applied values result in higher standard deviations. 48

Table 5: respective sugar concentrations in media composition 55

Table 6: Model parameters and normalized-root-mean-square-error (NRMSE) for the different analysed cultivation 62

Table 7: Model parameters and normalized-root-mean-square-error (NRMSE) for the analyzed cultivation without recombinant product production 66

Table 8: specific substrate uptake rate vs. specific carbon evolution rate. Product producing strains have in general increased respiratory activity. NP strains show reduced respiratory activity. Standard deviation of qCO_2 increases at higher feeding rates 66

Table 9: respective sugar concentrations in media composition 75

Table 10**:** Comparison of the measured q_p and the measured cell viability. 86

Table 11: Fitting results for hyperbolic-fit Eq. 3 for IB bead size dependence 100

Table 12: Feature matrix of ten cultivations (presented in the previous chapters) with characteristic time independent quantities 108

Table 13: Extracted Eigenvectors for the three analyzed principal components. 110

Table 14: Specific growth rate μ of batch phases determined by offline DCW measurements (given in Fig 1 a). 117

Table 15: Starting sugar concentrations in different anaerobic batch runs extracted by HPLC measurement. 121

Literature

Achmüller, C.; Kaar, W.; Ahrer, K.; Wechner, P.; Hahn, R.; Werther, F.; Schmidinger, H.; Cserjan-Puschmann, M.; Clementschitsch, F.; Striedner, G.; Bayer, K.; Jungbauer, A.; Auer, B., N(pro) fusion technology to produce proteins with authentic N termini in E. coli. *Nat Methods* 2007, *4* (12), 1037-43.

Akbari, V.; Sadeghi, H. M. M.; Jafarian-Dehkordi, A.; Chou, C. P.; Abedi, D., Optimization of a single-chain antibody fragment overexpression in Escherichia coli using response surface methodology. *Research in Pharmaceutical Sciences* 2015, *10* (1), 75-83.

Altamirano, M. M.; Golbik, R.; Zahn, R.; Buckle, A. M.; Fersht, A. R., Refolding chromatography with immobilized mini-chaperones. *Proceedings of the National Academy of Sciences* 1997, *94* (8), 3576-3578.

Baeshen, M. N.; Al-Hejin, A. M.; Bora, R. S.; Ahmed, M. M.; Ramadan, H. A.; Saini, K. S.; Baeshen, N. A.; Redwan, E. M., Production of Biopharmaceuticals in E. coli: Current Scenario and Future Perspectives. *J Microbiol Biotechnol* 2015, *25* (7), 953-62.

Baeshen, N. A.; Baeshen, M. N.; Sheikh, A.; Bora, R. S.; Ahmed, M. M.; Ramadan, H. A.; Saini, K. S.; Redwan, E. M., Cell factories for insulin production. *Microb Cell Fact* 2014, *13*, 141.

Barth, A., Infrared spectroscopy of proteins. *Biochimica et Biophysica Acta (BBA)-Bioenergetics* 2007, *1767* (9), 1073-1101.

Bayoudh, S.; Othmane, A.; Ponsonnet, L.; Ouada, H. B., Electrical detection and characterization of bacterial adhesion using electrochemical impedance spectroscopy-based flow chamber. *Colloids and Surfaces A: physicochemical and engineering aspects* 2008, *318* (1), 291-300.

Berlec, A.; Strukelj, B., Current state and recent advances in biopharmaceutical production in Escherichia coli, yeasts and mammalian cells. *J Ind Microbiol Biotechnol* 2013, *40* (3-4), 257-74.

Bettenbrock, K.; Fischer, S.; Kremling, A.; Jahreis, K.; Sauter, T.; Gilles, E. D., A quantitative approach to catabolite repression in Escherichia coli. *J Biol Chem* 2006, *281* (5), 2578-84.

Blommel, P. G.; Becker, K. J.; Duvnjak, P.; Fox, B. G., Enhanced bacterial protein expression during auto-induction obtained by alteration of lac repressor dosage and medium composition. *Biotechnol Prog* 2007, *23* (3), 585-98.

Bot, C.; Prodan, C., Probing the membrane potential of living cells by dielectric spectroscopy. *European Biophysics Journal* 2009, *38* (8), 1049-1059.

Buckholz, R. G.; Gleeson, M. A. G., Yeast Systems for the Commercial Production of Heterologous Proteins. *Nat Biotech* 1991, *9* (11), 1067-1072.
Carvell, J. P.; Dowd, J. E., On-line measurements and control of viable cell density in cell culture manufacturing processes using radio-frequency impedance. *Cytotechnology* 2006, *50* (1-3), 35-48.
Cass, B.; Pham, P. L.; Kamen, A.; Durocher, Y., Purification of recombinant proteins from mammalian cell culture using a generic double-affinity chromatography scheme. *Protein expression and purification* 2005, *40* (1), 77-85.
Castellanos-Mendoza, A.; Castro-Acosta, R. M.; Olvera, A.; Zavala, G.; Mendoza-Vera, M.; García-Hernández, E.; Alagón, A.; Trujillo-Roldán, M. A.; Valdez-Cruz, N. A., Influence of pH control in the formation of inclusion bodies during production of recombinant sphingomyelinase-D in Escherichia coli. *Microb Cell Fact* 2014, *13*, 137.
Cereghino, G. P. L.; Cregg, J. M., Applications of yeast in biotechnology: protein production and genetic analysis. *Current opinion in biotechnology* 1999, *10* (5), 422-427.
Chan, Z.; Chen, X.; Hou, Y.; Gao, B.; Zhao, C.; Yang, S.; Zeng, R., Enhanced a novel β-agarase production in recombinant Escherichia coli BL21 (DE3) through induction mode optimization and glycerol feeding strategy. *Acta Oceanologica Sinica* 2018, *37* (2), 110-118.
Clark, E. D. B., Protein refolding for industrial processes. *Current opinion in biotechnology* 2001, *12* (2), 202-207.
Clarke, D.; Blake-Coleman, B.; Carr, R.; Calder, M.; Atkinson, T., Monitoring reactor biomass. *Trends in biotechnology* 1986, *4* (7), 173-178.
Cohen, S. N.; Chang, A. C.; Boyer, H. W.; Helling, R. B., Construction of biologically functional bacterial plasmids in vitro. *Proc Natl Acad Sci U S A* 1973, *70* (11), 3240-4.
Dabros, M.; Dennewald, D.; Currie, D. J.; Lee, M. H.; Todd, R. W.; Marison, I. W.; von Stockar, U., Cole–Cole, linear and multivariate modeling of capacitance data for on-line monitoring of biomass. *Bioprocess and biosystems engineering* 2009, *32* (2), 161-173.
Daegelen, P.; Studier, F. W.; Lenski, R. E.; Cure, S.; Kim, J. F., Tracing ancestors and relatives of Escherichia coli B, and the derivation of B strains REL606 and BL21(DE3). *J Mol Biol* 2009, *394* (4), 634-43.
Davey, H. M.; Kell, D. B., Flow cytometry and cell sorting of heterogeneous microbial populations: the importance of single-cell analyses. *Microbiological Reviews* 1996, *60* (4), 641-696.
DeLisa, M. P.; Li, J.; Rao, G.; Weigand, W. A.; Bentley, W. E., Monitoring GFP-operon fusion protein expression during high cell density cultivation of Escherichia coli using an on-line optical sensor. *Biotechnol Bioeng* 1999, *65* (1), 54-64.
Deutscher, J.; Francke, C.; Postma, P. W., How phosphotransferase system-related protein phosphorylation regulates carbohydrate metabolism in bacteria. *Microbiol Mol Biol Rev* 2006, *70* (4), 939-1031.
Díez-Gil, C.; Krabbenborg, S.; García-Fruitós, E.; Vazquez, E.; Rodríguez-Carmona, E.; Ratera, I.; Ventosa, N.; Seras-Franzoso, J.; Cano-Garrido, O.; Ferrer-Miralles, N., The nanoscale properties of bacterial inclusion bodies and their effect on mammalian cell proliferation. *Biomaterials* 2010, *31* (22), 5805-5812.
Dubendorff, J. W.; Studier, F. W., Controlling basal expression in an inducible T7 expression system by blocking the target T7 promoter with lac repressor. *J Mol Biol* 1991, *219* (1), 45-59.
Dvorak, P.; Chrast, L.; Nikel, P. I.; Fedr, R.; Soucek, K.; Sedlackova, M.; Chaloupkova, R.; de Lorenzo, V.; Prokop, Z.; Damborsky, J., Exacerbation of substrate toxicity by IPTG in Escherichia coli BL21(DE3) carrying a synthetic metabolic pathway. *Microb Cell Fact* 2015, *14*, 201.
Dvorak, P.; Chrast, L.; Nikel, P. I.; Fedr, R.; Soucek, K.; Sedlackova, M.; Chaloupkova, R.; Lorenzo, V.; Prokop, Z.; Damborsky, J., Exacerbation of substrate toxicity by IPTG in Escherichia coli BL21 (DE3) carrying a synthetic metabolic pathway. *Microbial cell factories* 2015, *14* (1), 201.
Eggenreich, B.; Willim, M.; Wurm, D. J.; Herwig, C.; Spadiut, O., Production strategies for active heme-containing peroxidases from E. coli inclusion bodies–a review. *Biotechnology Reports* 2016, *10*, 75-83.
Ehgartner, D.; Sagmeister, P.; Herwig, C.; Wechselberger, P., A novel real-time method to estimate volumetric mass biodensity based on the combination of dielectric spectroscopy and soft-sensors. *J. Chem. Technol. Biotechnol.* 2015, *90* (2), 262-272.

Ehgartner, D.; Sagmeister, P.; Langemann, T.; Meitz, A.; Lubitz, W.; Herwig, C., A novel method to recover inclusion body protein from recombinant E. coli fed-batch processes based on phage ΦX174-derived lysis protein E. *Applied microbiology and biotechnology* 2017, *101* (14), 5603-5614.
Fahnert, B.; Lilie, H.; Neubauer, P., Inclusion bodies: formation and utilisation. In *Physiological Stress Responses in Bioprocesses*, Springer: 2004; pp 93-142.
Ferreira, A. P.; Vieira, L. M.; Cardoso, J. P.; Menezes, J. C., Evaluation of a new annular capacitance probe for biomass monitoring in industrial pilot-scale fermentations. *Journal of biotechnology* 2005, *116* (4), 403-409.
Food; Administration, D., Guidance for industry, PAT-A Framework for Innovative Pharmaceutical Development, Manufacturing and Quality Assurance. *http://www. fda. gov/cder/guidance/published. html* 2004.
Gabrielczyk, J.; Kluitmann, J.; Dammeyer, T.; Jördening, H.-J., Effects of ionic strength on inclusion body refolding at high concentration. *Protein expression and purification* 2017, *130*, 100-106.
García-Fruitós, E., Inclusion bodies: a new concept. *Microbial cell factories* 2010, *9* (1), 80.
García-Fruitós, E.; Arís, A.; Villaverde, A., Localization of functional polypeptides in bacterial inclusion bodies. *Applied and environmental microbiology* 2007, *73* (1), 289-294.
García-Fruitós, E.; González-Montalbán, N.; Morell, M.; Vera, A.; Ferraz, R. M.; Arís, A.; Ventura, S.; Villaverde, A., Aggregation as bacterial inclusion bodies does not imply inactivation of enzymes and fluorescent proteins. *Microbial cell factories* 2005, *4* (1), 27.
García-Fruitós, E.; Vázquez, E.; Díez-Gil, C.; Corchero, J. L.; Seras-Franzoso, J.; Ratera, I.; Veciana, J.; Villaverde, A., Bacterial inclusion bodies: making gold from waste. *Trends in biotechnology* 2012, *30* (2), 65-70.
García-Fruitós, E.; Rodríguez-Carmona, E.; Díez-Gil, C.; Ferraz, R. M.; Vázquez, E.; Corchero, J. L.; Cano-Sarabia, M.; Ratera, I.; Ventosa, N.; Veciana, J., Surface cell growth engineering assisted by a novel bacterial nanomaterial. *Advanced Materials* 2009, *21* (42), 4249-4253.
García-Fruitós, E.; Sabate, R.; de Groot, N. S.; Villaverde, A.; Ventura, S., Biological role of bacterial inclusion bodies: a model for amyloid aggregation. *The FEBS journal* 2011, *278* (14), 2419-2427.
Gavrilescu, M.; Chisti, Y., Biotechnology—a sustainable alternative for chemical industry. *Biotechnology advances* 2005, *23* (7), 471-499.
Gerngross, T. U., Advances in the production of human therapeutic proteins in yeasts and filamentous fungi. *Nat Biotech* 2004, *22* (11), 1409-1414.
Giacalone, M. J.; Gentile, A. M.; Lovitt, B. T.; Berkley, N. L.; Gunderson, C. W.; Surber, M. W., Toxic protein expression in Escherichia coli using a rhamnose-based tightly regulated and tunable promoter system. *Biotechniques* 2006, *40* (3), 355-367.
Glick, B. R., Metabolic load and heterologous gene expression. *Biotechnol Adv* 1995, *13* (2), 247-61.
Gonzalez, J.; Santana, a. F.; Mirza-Rosca, J., Effect of bacterial biofilm on 316 SS corrosion in natural seawater by EIS. *Corrosion science* 1998, *40* (12), 2141-2154.
Govers, S. K.; Dutré, P.; Aertsen, A., In vivo disassembly and reassembly of protein aggregates in Escherichia coli. *Journal of bacteriology* 2014, JB. 01549-14.
Gundinger, T.; Spadiut, O., A comparative approach to recombinantly produce the plant enzyme horseradish peroxidase in Escherichia coli. *Journal of biotechnology* 2017, *248*, 15-24.
Gupta, S. K.; Shukla, P., Microbial platform technology for recombinant antibody fragment production: A review. *Crit Rev Microbiol* 2016, *43* (1), 31-42.
Gustavsson, R.; Mandenius, C.-F., Soft sensor control of metabolic fluxes in a recombinant Escherichia coli fed-batch cultivation producing green fluorescence protein. *Biopro. and biosyst. eng.* 2013, *36* (10), 1375-1384.
Han, G. H.; Seong, W.; Fu, Y.; Yoon, P. K.; Kim, S. K.; Yeom, S.-J.; Lee, D.-H.; Lee, S.-G., Leucine zipper-mediated targeting of multi-enzyme cascade reactions to inclusion bodies in Escherichia coli for enhanced production of 1-butanol. *Metabolic engineering* 2017, *40*, 41-49.
Heyland, J.; Blank, L. M.; Schmid, A., Quantification of metabolic limitations during recombinant protein production in Escherichia coli. *J Biotechnol* 2011, *155* (2), 178-84.

Hogema, B. M.; Arents, J. C.; Bader, R.; Postma, P. W., Autoregulation of lactose uptake through the LacY permease by enzyme IIAGlc of the PTS in Escherichia coli K-12. *Mol Microbiol* 1999, *31* (6), 1825-33.
Hrabárová, E.; Achbergerová, L.; Nahálka, J., Insoluble protein applications: the use of bacterial inclusion bodies as biocatalysts. In *Insoluble Proteins*, Springer: 2015; pp 411-422.
Huang, C.-J.; Lin, H.; Yang, X., Industrial production of recombinant therapeutics in Escherichia coli and its recent advancements. *Journal of industrial microbiology & biotechnology* 2012, *39* (3), 383-399.
Inada, T.; Kimata, K.; Aiba, H., Mechanism responsible for glucose-lactose diauxie in Escherichia coli: challenge to the cAMP model. *Genes Cells* 1996, *1* (3), 293-301.
Iuchi, S.; Cole, S. T.; Lin, E. C., Multiple regulatory elements for the glpA operon encoding anaerobic glycerol-3-phosphate dehydrogenase and the glpD operon encoding aerobic glycerol-3-phosphate dehydrogenase in Escherichia coli: further characterization of respiratory control. *J Bacteriol* 1990, *172* (1), 179-84.
Jeong, H.; Barbe, V.; Lee, C. H.; Vallenet, D.; Yu, D. S.; Choi, S. H.; Couloux, A.; Lee, S. W.; Yoon, S. H.; Cattolico, L.; Hur, C. G.; Park, H. S.; Ségurens, B.; Kim, S. C.; Oh, T. K.; Lenski, R. E.; Studier, F. W.; Daegelen, P.; Kim, J. F., Genome sequences of Escherichia coli B strains REL606 and BL21(DE3). *J Mol Biol* 2009, *394* (4), 644-52.
Jeong, H.; Kim, H. J.; Lee, S. J., Complete Genome Sequence of Escherichia coli Strain BL21. *Genome Announc* 2015, *3* (2).
Jeremy M Berg , J. L. T., and Lubert Stryer . Biochemistry, 5th edition. 5th ed.; New York, 2002.
Jevševar, S.; Gaberc-Porekar, V.; Fonda, I.; Podobnik, B.; Grdadolnik, J.; Menart, V., Production of nonclassical inclusion bodies from which correctly folded protein can be extracted. *Biotechnology progress* 2005, *21* (2), 632-639.
Jong, W. S.; Vikström, D.; Houben, D.; van Saparoea, H. B. B.; Gier, J.-W.; Luirink, J., Application of an E. coli signal sequence as a versatile inclusion body tag. *Microbial cell factories* 2017, *16* (1), 50.
K'Owino, I. O.; Sadik, O. A., Impedance spectroscopy: a powerful tool for rapid biomolecular screening and cell culture monitoring. *Electroanalysis* 2005, *17* (23), 2101-2113.
Keiler, K. C., Biology of trans-translation. *Annu Rev Microbiol* 2008, *62*, 133-51.
Khlebnikov, A.; Skaug, T.; Keasling, J. D., Modulation of gene expression from the arabinose-inducible araBAD promoter. *Journal of Industrial Microbiology and Biotechnology* 2002, *29* (1), 34-37.
Kim, Y.-H.; Park, J.-S.; Jung, H.-I., An impedimetric biosensor for real-time monitoring of bacterial growth in a microbial fermentor. *Sensors and Actuators B: Chemical* 2009, *138* (1), 270-277.
Kischnick, S.; Weber, B.; Verdino, P.; Keller, W.; Sanders, E. A.; Anspach, F. B.; Fiebig, H.; Cromwell, O.; Suck, R., Bacterial fermentation of recombinant major wasp allergen Antigen 5 using oxygen limiting growth conditions improves yield and quality of inclusion bodies. *Protein expression and purification* 2006, *47* (2), 621-628.
Kiviharju, K.; Salonen, K.; Moilanen, U.; Eerikäinen, T., Biomass measurement online: the performance of in situ measurements and software sensors. *Journal of industrial microbiology & biotechnology* 2008, *35* (7), 657-665.
Konakovsky, V.; Yagtu, A. C.; Clemens, C.; Müller, M. M.; Berger, M.; Schlatter, S.; Herwig, C., Universal Capacitance Model for Real-Time Biomass in Cell Culture. *Sensors* 2015, *15* (9), 22128-22150.
Kopp, J.; Slouka, C.; Ulonska, S.; Kager, J.; Fricke, J.; Spadiut, O.; Herwig, C., Impact of Glycerol as Carbon Source onto Specific Sugar and Inducer Uptake Rates and Inclusion Body Productivity in E. coli BL21 (DE3). *Bioeng* 2017, *5* (1), 1.
Korz, D. J.; Rinas, U.; Hellmuth, K.; Sanders, E. A.; Deckwer, W. D., Simple fed-batch technique for high cell density cultivation of Escherichia coli. *J Biotechnol* 1995, *39* (1), 59-65.
Kremling, A.; Bettenbrock, K.; Laube, B.; Jahreis, K.; Lengeler, J. W.; Gilles, E. D., The organization of metabolic reaction networks. III. Application for diauxic growth on glucose and lactose. *Metab Eng* 2001, *3* (4), 362-79.
Kroll, P.; Hofer, A.; Stelzer, I. V.; Herwig, C., Workflow to set up substantial target-oriented mechanistic process models in bioprocess engineering. *Process Biochemistry* 2017, *62*, 24-36.

Langemann, T.; Mayr, U. B.; Meitz, A.; Lubitz, W.; Herwig, C., Multi-parameter flow cytometry as a process analytical technology (PAT) approach for the assessment of bacterial ghost production. *Appl Microbiol Biotechnol* 2016, *100* (1), 409-18.
Larson, T. J.; Ye, S. Z.; Weissenborn, D. L.; Hoffmann, H. J.; Schweizer, H., Purification and characterization of the repressor for the sn-glycerol 3-phosphate regulon of Escherichia coli K12. *J Biol Chem* 1987, *262* (33), 15869-74.
Lei, K. F., Review on impedance detection of cellular responses in micro/nano environment. *Micromachines* 2014, *5* (1), 1-12.
Lin, E. C., Glycerol dissimilation and its regulation in bacteria. *Annu Rev Microbiol* 1976, *30*, 535-78.
Ling, C.; Zhang, J.; Lin, D.; Tao, A., Approaches for the generation of active papain-like cysteine proteases from inclusion bodies of Escherichia coli. *World Journal of Microbiology and Biotechnology* 2015, *31* (5), 681-690.
Liu, J.; Li, H.; Zhang, F.; Li, X.; Wang, L.; Chen, Y., Online impedance monitoring of yeast cell culture behaviors. *Microelectronic Engineering* 2011, *88* (8), 1711-1713.
Liu, W.; Cellmer, T.; Keerl, D.; Prausnitz, J. M.; Blanch, H. W., Interactions of lysozyme in guanidinium chloride solutions from static and dynamic light-scattering measurements. *Biotechnology and bioengineering* 2005, *90* (4), 482-490.
Lodolo, E. J.; Kock, J. L.; Axcell, B. C.; Brooks, M., The yeast Saccharomyces cerevisiae–the main character in beer brewing. *FEMS yeast research* 2008, *8* (7), 1018-1036.
Looser, V.; Bruhlmann, B.; Bumbak, F.; Stenger, C.; Costa, M.; Camattari, A.; Fotiadis, D.; Kovar, K., Cultivation strategies to enhance productivity of Pichia pastoris: a review. *Biotechnol. Adv.* 2015, *33* (6), 1177-1193.
Luchner, M.; Striedner, G.; Cserjan-Puschmann, M.; Strobl, F.; Bayer, K., Online prediction of product titer and solubility of recombinant proteins in Escherichia coli fed-batch cultivations. *J. Chem. Technol. Biotechnol.* 2015, *90* (2), 283-290.
Lyakhov, D. L.; He, B.; Zhang, X.; Studier, F. W.; Dunn, J. J.; McAllister, W. T., Pausing and termination by bacteriophage T7 RNA polymerase. *J Mol Biol* 1998, *280* (2), 201-13.
Marbach, A.; Bettenbrock, K., lac operon induction in Escherichia coli: Systematic comparison of IPTG and TMG induction and influence of the transacetylase LacA. *Journal of biotechnology* 2012, *157* (1), 82-88.
Marisch, K.; Bayer, K.; Cserjan-Puschmann, M.; Luchner, M.; Striedner, G., Evaluation of three industrial Escherichia coli strains in fed-batch cultivations during high-level SOD protein production. *Microb Cell Fact* 2013, *12*, 58.
Marr, A. G.; Ingraham, J. L.; Squires, C. L., EFFECT OF THE TEMPERATURE OF GROWTH OF ESCHERICHIA COLI ON THE FORMATION OF BETA-GALACTOSIDASE. *J Bacteriol* 1964, *87*, 356-62.
Marschall, L.; Sagmeister, P.; Herwig, C., Tunable recombinant protein expression in E. coli: enabler for continuous processing? *Appl Microbiol Biotechnol* 2016, *100* (13), 5719-28.
Martínez-Gómez, K.; Flores, N.; Castañeda, H. M.; Martínez-Batallar, G.; Hernández-Chávez, G.; Ramírez, O. T.; Gosset, G.; Encarnación, S.; Bolivar, F., New insights into Escherichia coli metabolism: carbon scavenging, acetate metabolism and carbon recycling responses during growth on glycerol. *Microb Cell Fact* 2012, *11*, 46.
Martínez-Gómez, K.; Flores, N.; Castañeda, H. M.; Martínez-Batallar, G.; Hernández-Chávez, G.; Ramírez, O. T.; Gosset, G.; Encarnación, S.; Bolivar, F., New insights into Escherichia coli metabolism: carbon scavenging, acetate metabolism and carbon recycling responses during growth on glycerol. *Microbial cell factories* 2012, *11* (1), 46.
Mayer, S.; Junne, S.; Ukkonen, K.; Glazyrina, J.; Glauche, F.; Neubauer, P.; Vasala, A., Lactose autoinduction with enzymatic glucose release: characterization of the cultivation system in bioreactor. *Protein Expr Purif* 2014, *94*, 67-72.
Meuris, L.; Santens, F.; Elson, G.; Festjens, N.; Boone, M.; Dos Santos, A.; Devos, S.; Rousseau, F.; Plets, E.; Houthuys, E.; Malinge, P.; Magistrelli, G.; Cons, L.; Chatel, L.; Devreese, B.; Callewaert, N.,

GlycoDelete engineering of mammalian cells simplifies N-glycosylation of recombinant proteins. *Nat Biotechnol* 2014, *32* (5), 485-9.
Mishima, K.; Mimura, A.; Takahara, Y.; Asami, K.; Hanai, T., On-line monitoring of cell concentrations by dielectric measurements. *Journal of fermentation and bioengineering* 1991, *72* (4), 291-295.
Mollania, N.; Khajeh, K.; Ranjbar, B.; Rashno, F.; Akbari, N.; Fathi-Roudsari, M., An efficient in vitro refolding of recombinant bacterial laccase in Escherichia coli. *Enzyme and microbial technology* 2013, *52* (6-7), 325-330.
Molloy, M. P.; Herbert, B. R.; Slade, M. B.; Rabilloud, T.; Nouwens, A. S.; Williams, K. L.; Gooley, A. A., Proteomic analysis of the Escherichia coli outer membrane. *European journal of biochemistry* 2000, *267* (10), 2871-2881.
Murarka, A.; Dharmadi, Y.; Yazdani, S. S.; Gonzalez, R., Fermentative utilization of glycerol by Escherichia coli and its implications for the production of fuels and chemicals. *Appl Environ Microbiol* 2007, *74* (4), 1124-35.
Nahálka, J.; Vikartovská, A.; Hrabárová, E., A crosslinked inclusion body process for sialic acid synthesis. *Journal of biotechnology* 2008, *134* (1-2), 146-153.
Neubauer, P.; Hofmann, K., Efficient use of lactose for the lac promoter-controlled overexpression of the main antigenic protein of the foot and mouth disease virus in Escherichia coli under fed-batch fermentation conditions. *FEMS Microbiol Rev* 1994, *14* (1), 99-102.
Neubauer, P.; Hofmann, K.; Holst, O.; Mattiasson, B.; Kruschke, P., Maximizing the expression of a recombinant gene in Escherichia coli by manipulation of induction time using lactose as inducer. *Appl Microbiol Biotechnol* 1992, *36* (6), 739-44.
Okabe, M.; Katoh, M.; Furugoori, F.; Yoshida, M.; Mitsui, S., Growth and fermentation characteristics of bottom brewer's yeast under mechanical stirring. *Journal of fermentation and bioengineering* 1992, *73* (2), 148-152.
Padan, E.; Zilberstein, D.; Schuldiner, S., pH homesstasis in bacteria. *Biochimica et Biophysica Acta (BBA)-Reviews on Biomembranes* 1981, *650* (2-3), 151-166.
Palmer, I.; Wingfield, P. T., Preparation and extraction of insoluble (inclusion-body) proteins from Escherichia coli. *Curr Protoc Protein Sci* 2012, *Chapter 6*, Unit6.3.
Peternel, S.; Gaberc-Porekar, V.; Komel, R., Bacterial growth conditions affect quality of GFP expressed inside inclusion bodies. *Acta Chim Slov* 2009, *56* (4), 860-7.
Peternel, Š.; Grdadolnik, J.; Gaberc-Porekar, V.; Komel, R., Engineering inclusion bodies for non denaturing extraction of functional proteins. *Microbial Cell Factories* 2008, *7* (1), 34.
Peternel, Š.; Jevševar, S.; Bele, M.; Gaberc-Porekar, V.; Menart, V., New properties of inclusion bodies with implications for biotechnology. *Biotechnology and applied biochemistry* 2008, *49* (4), 239-246.
Peternel, Š.; Komel, R., Isolation of biologically active nanomaterial (inclusion bodies) from bacterial cells. *Microbial cell factories* 2010, *9* (1), 66.
Poortinga, A. T.; Bos, R.; Norde, W.; Busscher, H. J., Electric double layer interactions in bacterial adhesion to surfaces. *Surface science reports* 2002, *47* (1), 1-32.
Postma, P. W.; Lengeler, J. W.; Jacobson, G. R., Phosphoenolpyruvate:carbohydrate phosphotransferase systems of bacteria. *Microbiol Rev* 1993, *57* (3), 543-94.
Qi, X.; Sun, Y.; Xiong, S., A single freeze-thawing cycle for highly efficient solubilization of inclusion body proteins and its refolding into bioactive form. *Microbial cell factories* 2015, *14* (1), 24.
Radke, S. M.; Alocilja, E. C., Design and fabrication of a microimpedance biosensor for bacterial detection. *Sensors Journal, IEEE* 2004, *4* (4), 434-440.
Rajamanickam, V.; Wurm, D.; Slouka, C.; Herwig, C.; Spadiut, O., A novel toolbox for E. coli lysis monitoring. *Anal. Bioanal. Chem.* 2017, *409* (3), 667-671.
Rajamanickam, V.; Wurm, D.; Slouka, C.; Herwig, C.; Spadiut, O., A novel toolbox for E. coli lysis monitoring. *Analytical and bioanalytical chemistry* 2017, *409* (3), 667-671.
Ramón, A.; Señorale-Pose, M.; Marín, M., Inclusion bodies: not that bad…. *Front Microbiol* 2014, *5*, 56.
Reichelt, W. N.; Brillmann, M.; Thurrold, P.; Keil, P.; Fricke, J.; Herwig, C., Physiological capacities decline during induced bioprocesses leading to substrate accumulation. *Biotechnol J* 2017, *12* (7).

Reichelt, W. N.; Brillmann, M.; Thurrold, P.; Keil, P.; Fricke, J.; Herwig, C., Physiological capacities decline during induced bioprocesses leading to substrate accumulation. *Biotechnol. J.* 2017, *12* (7), 1600547.
Reichelt, W. N.; Brillmann, M.; Thurrold, P.; Keil, P.; Fricke, J.; Herwig, C., Physiological capacities decline during induced bioprocesses leading to substrate accumulation. *Biotechnology Journal* 2017, *12* (7), 1600547-n/a.
Reichelt, W. N.; Kaineder, A.; Brillmann, M.; Neutsch, L.; Taschauer, A.; Lohninger, H.; Herwig, C., High throughput inclusion body sizing: Nano particle tracking analysis. *Biotechnol J* 2017, *12* (6).
Reichelt, W. N.; Kaineder, A.; Brillmann, M.; Neutsch, L.; Taschauer, A.; Lohninger, H.; Herwig, C., High throughput inclusion body sizing: Nano particle tracking analysis. *Biotechnology Journal* 2017, *12* (6).
Reichelt, W. N.; Thurrold, P.; Brillmann, M.; Kager, J.; Fricke, J.; Herwig, C., Generic biomass estimation methods targeting physiologic process control in induced bacterial cultures. *Eng Life Sci* 2016, *16* (8), 720-730.
Reichelt, W. N.; Thurrold, P.; Brillmann, M.; Kager, J.; Fricke, J.; Herwig, C., Generic biomass estimation methods targeting physiologic process control in induced bacterial cultures. *Engineering in Life Sciences* 2016, *16* (8), 720-730.
Rinas, U.; Bailey, J. E., Protein compositional analysis of inclusion bodies produced in recombinant Escherichia coli. *Applied Microbiology and Biotechnology* 1992, *37* (5), 609-614.
Rinas, U.; Boone, T. C.; Bailey, J. E., Characterization of inclusion bodies in recombinant Escherichia coli producing high levels of porcine somatotropin. *Journal of Biotechnology* 1993, *28* (2), 313-320.
Rinas, U.; Garcia-Fruitós, E.; Corchero, J. L.; Vázquez, E.; Seras-Franzoso, J.; Villaverde, A., Bacterial inclusion bodies: discovering their better half. *Trends in biochemical sciences* 2017, *42* (9), 726-737.
Rodríguez-Carmona, E.; Cano-Garrido, O.; Seras-Franzoso, J.; Villaverde, A.; García-Fruitós, E., Isolation of cell-free bacterial inclusion bodies. *Microbial cell factories* 2010, *9* (1), 1.
Rodríguez-Carmona, E.; Cano-Garrido, O.; Seras-Franzoso, J.; Villaverde, A.; García-Fruitós, E., Isolation of cell-free bacterial inclusion bodies. *Microbial cell factories* 2010, *9* (1), 71.
Rodríguez-Carmona, E.; Villaverde, A., Nanostructured bacterial materials for innovative medicines. *Trends in microbiology* 2010, *18* (9), 423-430.
Ronimus, R. S.; Morgan, H. W., Distribution and phylogenies of enzymes of the Embden-Meyerhof-Parnas pathway from archaea and hyperthermophilic bacteria support a gluconeogenic origin of metabolism. *Archaea* 2003, *1* (3), 199-221.
Rozkov, A.; Avignone-Rossa, C.; Ertl, P.; Jones, P.; O'Kennedy, R.; Smith, J.; Dale, J.; Bushell, M., Characterization of the metabolic burden on Escherichia coli DH1 cells imposed by the presence of a plasmid containing a gene therapy sequence. *Biotechnology and bioengineering* 2004, *88* (7), 909-915.
Sagmeister, P.; Wechselberger, P.; Jazini, M.; Meitz, A.; Langemann, T.; Herwig, C., Soft sensor assisted dynamic bioprocess control: Efficient tools for bioprocess development. *Chem. Eng. Sci.* 2013, *96*, 190-198.
Sahdev, S.; Khattar, S. K.; Saini, K. S., Production of active eukaryotic proteins through bacterial expression systems: a review of the existing biotechnology strategies. *Mol Cell Biochem* 2007, *307* (1-2), 249-64.
Sans, C.; García-Fruitós, E.; Ferraz, R. M.; González-Montalbán, N.; Rinas, U.; López-Santín, J.; Villaverde, A.; Álvaro, G., Inclusion bodies of fuculose-1-phosphate aldolase as stable and reusable biocatalysts. *Biotechnology progress* 2012, *28* (2), 421-427.
Schaepe, S.; Kuprijanov, A.; Simutis, R.; Lübbert, A., Avoiding overfeeding in high cell density fed-batch cultures of E. coli during the production of heterologous proteins. *J. Biotechnol.* 2014, *192*, 146-153.
Schwaighofer, A.; Montemurro, M.; Freitag, S.; Kristament, C.; Culzoni, M. J.; Lendl, B., Beyond FT-IR Spectroscopy: EC-QCL based mid-IR Transmission Spectroscopy of Proteins in the Amide I and Amide II Region. *Analytical Chemistry* 2018.
Schwan, H. P., Electrical and acoustic properties of biological materials and biomedical applications. *Biomedical Engineering, IEEE Transactions on* 1984, (12), 872-878.
Schwan, H. P.; Foster, K. R., RF-field interactions with biological systems: electrical properties and biophysical mechanisms. *Proceedings of the IEEE* 1980, *68* (1), 104-113.

Scott, M.; Gunderson, C. W.; Mateescu, E. M.; Zhang, Z.; Hwa, T., Interdependence of cell growth and gene expression: origins and consequences. *Science* 2010, *330* (6007), 1099-102.
Seras-Franzoso, J.; Peebo, K.; Luis Corchero, J.; Tsimbouri, P. M.; Unzueta, U.; Rinas, U.; Dalby, M. J.; Vazquez, E.; García-Fruitós, E.; Villaverde, A., A nanostructured bacterial bioscaffold for the sustained bottom-up delivery of protein drugs. *Nanomedicine* 2013, *8* (10), 1587-1599.
Singh, A.; Upadhyay, V.; Upadhyay, A. K.; Singh, S. M.; Panda, A. K., Protein recovery from inclusion bodies of Escherichia coli using mild solubilization process. *Microbial cell factories* 2015, *14* (1), 41.
Singh, S. M.; Panda, A. K., Solubilization and refolding of bacterial inclusion body proteins. *Journal of bioscience and bioengineering* 2005, *99* (4), 303-310.
Slouka, C.; Brunauer, G.; Kopp, J.; Strahammer, M.; Fricke, J.; Fleig, J.; Herwig, C., Low-Frequency Electrochemical Impedance Spectroscopy as a Monitoring Tool for Yeast Growth in Industrial Brewing Processes. *Chemosensors* 2017, *5* (3), 24.
Slouka, C.; Wurm, D. J.; Brunauer, G.; Welzl-Wachter, A.; Spadiut, O.; Fleig, J.; Herwig, C., A Novel Application for Low Frequency Electrochemical Impedance Spectroscopy as an Online Process Monitoring Tool for Viable Cell Concentrations. *Sensors (Basel)* 2016, *16* (11).
Slouka Christoph, K. J., Hutwimmer Stefan ,Strahammer Michael ,Strohmer Daniel, Eitenberger Elisabeth, Schwaighofer Andreas, Herwig Christoph, Custom Made Inclusion Bodies: Impact of classical process parameters and physiological parameters on Inclusion Body quality attributes. *Microb. Cell Fact.* 2018, *17* (1), 148.
Slouka Christoph, K. J., Hutwimmer Stefan ,Strahammer Michael ,Strohmer Daniel, Eitenberger Elisabeth, Schwaighofer Andreas, Herwig Christoph, Custom Made Inclusion Bodies: Impact of classical process parameters and physiological parameters on Inclusion Body quality attributes. *Microbial cell factories* 2018, *17* (1), 148.
Soley, A.; Lecina, M.; Gámez, X.; Cairo, J.; Riu, P.; Rosell, X.; Bragos, R.; Godia, F., On-line monitoring of yeast cell growth by impedance spectroscopy. *Journal of Biotechnology* 2005, *118* (4), 398-405.
Spadiut, O.; Capone, S.; Krainer, F.; Glieder, A.; Herwig, C., Microbials for the production of monoclonal antibodies and antibody fragments. *Trends Biotechnol* 2013, *32* (1), 54-60.
Spadiut, O.; Zalai, D.; Dietzsch, C.; Herwig, C., Quantitative comparison of dynamic physiological feeding profiles for recombinant protein production with Pichia pastoris. *Bioprocess and biosystems engineering* 2014, *37* (6), 1163-1172.
Stancik, L. M.; Stancik, D. M.; Schmidt, B.; Barnhart, D. M.; Yoncheva, Y. N.; Slonczewski, J. L., pH-dependent expression of periplasmic proteins and amino acid catabolism in Escherichia coli. *Journal of bacteriology* 2002, *184* (15), 4246-4258.
Steen, R.; Dahlberg, A. E.; Lade, B. N.; Studier, F. W.; Dunn, J. J., T7 RNA polymerase directed expression of the Escherichia coli rrnB operon. *EMBO J* 1986, *5* (5), 1099-103.
Strandberg, L.; Enfors, S. O., Factors influencing inclusion body formation in the production of a fused protein in Escherichia coli. *Appl Environ Microbiol* 1991, *57* (6), 1669-74.
Studier, F. W.; Daegelen, P.; Lenski, R. E.; Maslov, S.; Kim, J. F., Understanding the differences between genome sequences of Escherichia coli B strains REL606 and BL21(DE3) and comparison of the E. coli B and K-12 genomes. *J Mol Biol* 2009, *394* (4), 653-80.
Studier, F. W.; Moffatt, B. A., Use of bacteriophage T7 RNA polymerase to direct selective high-level expression of cloned genes. *J Mol Biol* 1986, *189* (1), 113-30.
Studier, F. W.; Rosenberg, A. H.; Dunn, J. J.; Dubendorff, J. W., Use of T7 RNA polymerase to direct expression of cloned genes. *Methods Enzymol* 1990, *185*, 60-89.
Stülke, J.; Hillen, W., Carbon catabolite repression in bacteria. *Curr Opin Microbiol* 1999, *2* (2), 195-201.
Thomas, J. G.; Baneyx, F., Protein misfolding and inclusion body formation in recombinant Escherichia coli cells overexpressing heat-shock proteins. *Journal of Biological Chemistry* 1996, *271* (19), 11141-11147.
Tokatlidis, K.; Dhurjati, P.; Millet, J.; Béguin, P.; Aubert, J.-P., High activity of inclusion bodies formed in Escherichia coli overproducing Clostridium thermocellum endoglucanase D. *FEBS letters* 1991, *282* (1), 205-208.

Tseng, T. T.; Tyler, B. M.; Setubal, J. C., Protein secretion systems in bacterial-host associations, and their description in the Gene Ontology. *BMC Microbiol* 2009, *9 Suppl 1*, S2.
Ukkonen, K.; Mayer, S.; Vasala, A.; Neubauer, P., Use of slow glucose feeding as supporting carbon source in lactose autoinduction medium improves the robustness of protein expression at different aeration conditions. *Protein Expr Purif* 2013, *91* (2), 147-54.
Valax, P.; Georgiou, G., Molecular Characterization of β-Lactamase Inclusion Bodies Produced in Escherichia coli. 1. Composition. *Biotechnology progress* 1993, *9* (5), 539-547.
Veal, D.; Deere, D.; Ferrari, B.; Piper, J.; Attfield, P., Fluorescence staining and flow cytometry for monitoring microbial cells. *Journal of immunological methods* 2000, *243* (1-2), 191-210.
Viitanen, M. I.; Vasala, A.; Neubauer, P.; Alatossava, T., Cheese whey-induced high-cell-density production of recombinant proteins in Escherichia coli. *Microb Cell Fact* 2003, *2* (1), 2.
Villaverde, A.; Corchero, J. L.; Seras-Franzoso, J.; Garcia-Fruitós, E., Functional protein aggregates: just the tip of the iceberg. *Nanomedicine (Lond)* 2015, *10* (18), 2881-91.
Voegele, R. T.; Sweet, G. D.; Boos, W., Glycerol kinase of Escherichia coli is activated by interaction with the glycerol facilitator. *J Bacteriol* 1993, *175* (4), 1087-94.
Walsh, G., Therapeutic insulins and their large-scale manufacture. *Appl Microbiol Biotechnol* 2004, *67* (2), 151-9.
Walsh, G., Biopharmaceutical benchmarks 2010. *Nat Biotechnol* 2010, *28* (9), 917-24.
Walsh, G., Biopharmaceutical benchmarks 2014. *Nat Biotechnol* 2014, *32* (10), 992-1000.
Wang, X.; Zhou, B.; Hu, W.; Zhao, Q.; Lin, Z., Formation of active inclusion bodies induced by hydrophobic self-assembling peptide GFIL8. *Microbial cell factories* 2015, *14* (1), 88.
Wegerer, A.; Sun, T.; Altenbuchner, J., Optimization of an E. coli L-rhamnose-inducible expression vector: test of various genetic module combinations. *BMC biotechnology* 2008, *8* (1), 2.
Weissenborn, D. L.; Wittekindt, N.; Larson, T. J., Structure and regulation of the glpFK operon encoding glycerol diffusion facilitator and glycerol kinase of Escherichia coli K-12. *J Biol Chem* 1992, *267* (9), 6122-31.
Weusthuis, R. A.; Pronk, J. T.; Van Den Broek, P.; Van Dijken, J., Chemostat cultivation as a tool for studies on sugar transport in yeasts. *Microbiological reviews* 1994, *58* (4), 616-630.
Wingfield, P. T., Preparation of Soluble Proteins from Escherichia coli. *Curr Protoc Protein Sci* 2014, *78*, 6.2.1-22.
Wingfield, P. T.; Palmer, I.; Liang, S. M., Folding and Purification of Insoluble (Inclusion Body) Proteins from Escherichia coli. *Curr Protoc Protein Sci* 2014, *78*, 6.5.1-30.
Worrall, D.; Goss, N., The formation of biologically active beta-galactosidase inclusion bodies in Escherichia coli. *Australian journal of biotechnology* 1989, *3* (1), 28-32.
Wu, J.; Ben, Y.; Chang, H.-C., Particle detection by electrical impedance spectroscopy with asymmetric-polarization AC electroosmotic trapping. *Microfluidics and Nanofluidics* 2005, *1* (2), 161-167.
Wurm, D. J.; Hausjell, J.; Ulonska, S.; Herwig, C.; Spadiut, O., Mechanistic platform knowledge of concomitant sugar uptake in Escherichia coli BL21 (DE3) strains. *Scientific Reports* 2017, *7*, 45072.
Wurm, D. J.; Herwig, C.; Spadiut, O., How to Determine Interdependencies of Glucose and Lactose Uptake Rates for Heterologous Protein Production with E. coli. *Methods Mol Biol* 2017, *1586*, 397-408.
Wurm, D. J.; Quehenberger, J.; Mildner, J.; Eggenreich, B.; Slouka, C.; Schwaighofer, A.; Wieland, K.; Lendl, B.; Rajamanickam, V.; Herwig, C., Teaching an old pET new tricks: tuning of inclusion body formation and properties by a mixed feed system in E. coli. *Applied microbiology and biotechnology* 2018, *102* (2), 667-676.
Wurm, D. J.; Quehenberger, J.; Mildner, J.; Eggenreich, B.; Slouka, C.; Schwaighofer, A.; Wieland, K.; Lendl, B.; Rajamanickam, V.; Herwig, C.; Spadiut, O., Teaching an old pET new tricks: tuning of inclusion body formation and properties by a mixed feed system in E. coli. *Appl Microbiol Biotechnol* 2017.
Wurm, D. J.; Veiter, L.; Ulonska, S.; Eggenreich, B.; Herwig, C.; Spadiut, O., The E. coli pET expression system revisited-mechanistic correlation between glucose and lactose uptake. *Appl Microbiol Biotechnol* 2016, *100* (20), 8721-9.
Xu, J.; Banerjee, A.; Pan, S. H.; Li, Z. J., Galactose can be an inducer for production of therapeutic proteins by auto-induction using E. coli BL21 strains. *Protein Expr Purif* 2012, *83* (1), 30-6.

Yamaguchi, H.; Miyazaki, M., Refolding techniques for recovering biologically active recombinant proteins from inclusion bodies. *Biomolecules* 2014, *4* (1), 235-251.
Yamamoto, E.; Yamaguchi, S.; Sasaki, N.; Kim, H.-B.; Kitamori, T.; Nagamune, T., Artificial chaperone-assisted refolding in a microchannel. *Bioprocess and biosystems engineering* 2010, *33* (1), 171.
Yang, L.; Li, Y.; Griffis, C. L.; Johnson, M. G., Interdigitated microelectrode (IME) impedance sensor for the detection of viable Salmonella typhimurium. *Biosensors and bioelectronics* 2004, *19* (10), 1139-1147.
Yang, L.; Ruan, C.; Li, Y., Detection of viable Salmonella typhimurium by impedance measurement of electrode capacitance and medium resistance. *Biosensors and Bioelectronics* 2003, *19* (5), 495-502.
Yardley, J. E.; Kell, D. B.; Barrett, J.; Davey, C. L., On-line, real-time measurements of cellular biomass using dielectric spectroscopy. *Biotechnology and Genetic Engineering Reviews* 2000, *17* (1), 3-36.
Zwaig, N.; Kistler, W. S.; Lin, E. C., Glycerol kinase, the pacemaker for the dissimilation of glycerol in Escherichia coli. *J Bacteriol* 1970, *102* (3), 753-9.

Appendix: Original Manuscripts

Slouka *et al. Microb Cell Fact (2018) 17:148*
https://doi.org/10.1186/s12934-018-0997-5

Microbial Cell Factories

RESEARCH

Open Access

Custom made inclusion bodies: impact of classical process parameters and physiological parameters on inclusion body quality attributes

Christoph Slouka[1], Julian Kopp[1], Stefan Hutwimmer[2], Michael Strahammer[1], Daniel Strohmer[1], Elisabeth Eitenberger[3], Andreas Schwaighofer[3] and Christoph Herwig[1,4*]

Abstract

Background: The bacterium *E. coli* is a major host for recombinant protein production of non-glycosylated products. Depending on the expression strategy, the recombinant protein can be located intracellularly. In many cases the formation of inclusion bodies (IBs), protein aggregates inside of the cytoplasm of the cell, is favored in order to achieve high productivities and to cope with toxic products. However, subsequent downstream processing, including homogenization of the cells, centrifugation or solubilization of the IBs, is prone to variable process performance or can be characterized by low extraction yields as published elsewhere. It is hypothesized that variations in IB quality attributes (QA) are responsible for those effects and that such attributes can be controlled by upstream process conditions. This contribution is aimed at analyzing how standard process parameters, such as pH and temperature (T) as well as different controlled levels of physiological parameters, such as specific substrate uptake rates, can vary IB quality attributes.

Results: Classical process parameters like pH and T influence the expression of analyzed IB. The effect on the three QAs titer, size and purity could be successfully revealed. The developed data driven model showed that low temperatures and low pH are favorable for the expression of the two tested industrially relevant proteins. Based on this knowledge, physiological control using specific substrate feeding rate (of glucose) $q_{s,Glu}$ is altered and the impact is tested for one protein.

Conclusions: Time dependent monitoring of IB QA—titer, purity, IB bead size—showed a dependence on classical process parameters pH and temperature. These findings are confirmed using a second industrially relevant strain. Optimized process conditions for pH and temperature were used to determine dependence on the physiological parameters, the specific substrate uptake rate ($q_{s,Glu}$). Higher $q_{s,Glu}$ were shown to have a strong influence on the analyzed IB QAs and drastically increase the titer and purity in early time stages. We therefore present a novel approach to modulate—time dependently—quality attributes in upstream processing to enable robust downstream processing.

Keywords: *Escherichia coli*, Inclusion body quality attributes, Recombinant protein production, Upstream development

*Correspondence: christoph.herwig@tuwien.ac.at
[4] Institute of Chemical, Environmental and Bioscience Engineering, Research Area Biochemical Engineering, Vienna University of Technology, Gumpendorfer Strasse 1a, 1060 Vienna, Austria
Full list of author information is available at the end of the article

Background

The gram-negative bacterium *E. coli* is the expression host of choice for the production of 30–40% of recombinant drugs in industry [1, 2]. As *E. coli* shows very fast replication rates [3, 4] on comparatively inexpensive media [5], the benefits often outweigh the numerous purification steps [1, 6] and the missing glycosylation pattern [1, 7, 8]. Recombinant protein production in *E. coli* regained more interest as the demand in single chain antibody-fragments increased, which can be properly expressed in *E. coli* [1, 8]. The strain BL21(DE3) created by F. Studier and B. Moffatt back in 1986 [9] is often used in an industrial scale, because of very low acetate formation, high replication rates [9–14], as well as the possibility of protein secretion into the fermentation broth due to a type 2 secretion protein [15–17]. For expression of the recombinant protein, the lac operon is still one of the most favored promotors in pET-expression-systems using integrated T7-polymerase for high transcriptional rates [3, 12, 18]. The repressor protein can only be blocked by allolactose or a structural analogue [19], e.g. the well-known expensive inducer isopropyl β-D-1 thiogalactopyranoside (IPTG) [3, 13]. However, induction with IPTG stresses the cells, as IPTG in higher concentrations is known to be toxic [13, 18, 20].

Recombinant proteins are often expressed as inclusion bodies (IB). IBs have originally been believed to be waste products by bacteria [21], until it was realized that they are formed as a stress reaction by the cells resulting in a biologically inactive precipitated protein [22–24]. Such stress reactions can be caused by high temperatures, pH-shifts or occur due to high feeding rates. These factors tend to result in higher yields of product [1], which of course are advantageous combined with the possibility of expressing toxic proteins [6]. Still, the DSP and especially the refolding unit operation suffers in robustness and is the most time-consuming step in gaining the correctly folded product from *E. coli* cultivations [21–24], which requires significantly more technology and time, when purifying IBs [22, 25, 26].

Quality attributes (or key performance indicator) of IBs, such as titer and morphology changes during extraction procedures have already been studied and show that IBs are dynamic structures depending on the cultivation and extraction conditions [27–29]. First approaches towards IB sizing in the upstream process have already been made within our group by Reichelt et al. [30] using transmission electron microscopy [31] in combination with nanoparticle tracking analysis (NTA) revealing general trends of IB growth during cultivation. Further studies show that IBs consist of up to 50% correctly folded protein in contrast to the general perception of IBs as inactive structures [29, 32]. Combined with the fact that IBs can be produced in high concentration (so that the amount of generated product often outweighs the additional downstream steps), IB based processes are believed to fundamentally boost time/space yields for recombinant protein production [1, 6, 7, 21]. Knowledge about the state of IB QAs during a cultivation process is therefore of utmost importance. Three IB QAs are generally of importance: bead size, titer and purity, as those three quality attributes were already defined elsewhere [21, 30, 33, 34]. It has been reported that inclusion body sizes can be measured with different methods, e.g. AFM (atomic force microscopy), TEM and NTA [21, 30, 33]. SDS-pages and ELISA-methods have been often reported as tool to determine impurities and titer in the IB product samples [35]. The impact of single process parameters like pH on IB QAs has already been investigated in literature [36, 37]. Reichelt et al. [34] showed that alterations of ($q_{s,glu}$) influence the behavior of common IB-processes, using IPTG as an inducer. The impact of the feeding rate onto product formation in *E. coli* BL21(DE3) has been investigated recently, though lactose was used as inducer instead of IPTG [38]. However, no monitoring of all IB-QAs over induction time has been performed in any of the previous studies.

In this study we performed cultivations with a BL21(DE3) strain, producing a recombinant protein coupled to a N-pro-fusion protein [39]—*strain 1*—and a non N-Pro fused protein—*strain 2*-, both exclusively expressing IBs, as the products are highly toxic for the cell. Classical process parameters were monitored as a function of induction time. The impact of process parameters on IB bead size in combination with purity and titer as a function of time has not been investigated in depth. Secondary structure of different IB sizes were analyzed using IR and showed no differences for IB beads of different size compared to the standard. Based on these results, the physiological parameter of the specific substrate uptake rate ($q_{s,glu}$) is altered at constant pH and T for *strain 1* and QAs are analyzed time-dependently. In this current study we collected time resolved results, which are used to optimize the USP. In conclusion, it is demonstrated that low T and low pH in combination with high $q_{s,glu}$ are beneficial for increasing the productivity and robustness of IB based processes for the two tested proteins.

Methods

Strains

Strain 1 was an *E. coli* BL21(DE3) with the pET[30a] plasmid system (kanamycin resistance) for recombinant protein production. The target protein was linked to a N-pro fusion protein used for purification [39]. *Strain 2*, *E. coli* BL21(DE3), (kanamycin resistance) was used for testing the results obtained with *strain 1.* Expression of the

protein occurs only as IB since the product is toxic to the cell. No N-Pro tag is fused to this product.

Bioreactor cultivations

Strain 1

All bioreactor and preculture cultivations for *strain 1* were carried out using a defined minimal medium referred to DeLisa et al. [5]. Batch media and the preculture media had the same composition with different amounts of glucose respectively. The glucose concentrations for the phases were: 8 g/L for the preculture, 20 g/L for the batch phase. The feed for fed-batch and induction had a concentration of 300 g/L glucose.

Antibiotic was added throughout all fermentations, resulting in a final concentration of 0.02 g/L of kanamycin. All precultures were performed using 500 mL high yield flasks. They were inoculated with 1.5 mL of bacteria solution stored in cryos at − 80 °C and subsequently cultivated for 20 h at 230 rpm in an Infors HR Multitron shaker (Infors, Bottmingen Switzerland) at 37 °C.

All cultivations were either performed in a stainless-steel Sartorius Biostat Cplus bioreactor (Sartorius, Göttingen, Germany) with 10 L working volume or in a DASGIP Mini bioreactor-4-parallel fermenter system (max. working volume: 2.5 L; Eppendorf, Hamburg, Germany). Cultivation off gas was analyzed by gas sensors—IR for CO_2 and ZrO_2 based for O_2 (Blue Sens Gas analytics, Herten, Germany).

Process control was established using the PIMS Lucullus and the DAS-GIP-control system, DASware-control, which logged the process parameters. During batch-phase and fedbatch phase pH was kept constant at 7.2 and controlled with base only (12.5% NH_4OH), while acid (5% H_3PO_4) was added manually, when necessary. The pH was monitored using an EasyFerm Plus pH-sensor (Hamilton, Reno, NV, USA). The reactors were continuously stirred at 1400 rpm and aerated using a mixture of pressurized air and pure oxygen at 2 vvm. Dissolved oxygen (dO_2) was always kept higher than 30% by increasing the ratio of oxygen in the ingas. The dissolved oxygen was monitored using a fluorescence dissolved oxygen electrode Visiferm DO (Hamilton, Reno, NV, USA). The fed-batch phase for biomass generation was followed by an induction phase using a feed medium with glucose as primary carbon source.

0.5 mM IPTG was added as an inducer once to start the induction of the cells. pH and temperature in the induction phase was adapted according to the design of experiments (DoE) given in Fig. 1a. pH was altered between 6.7 and 7.7 and temperature between 30 and 40 °C. The center point at 35 °C and pH 7.2 was cultivated in triplicate in order to assess statistical experimental error.

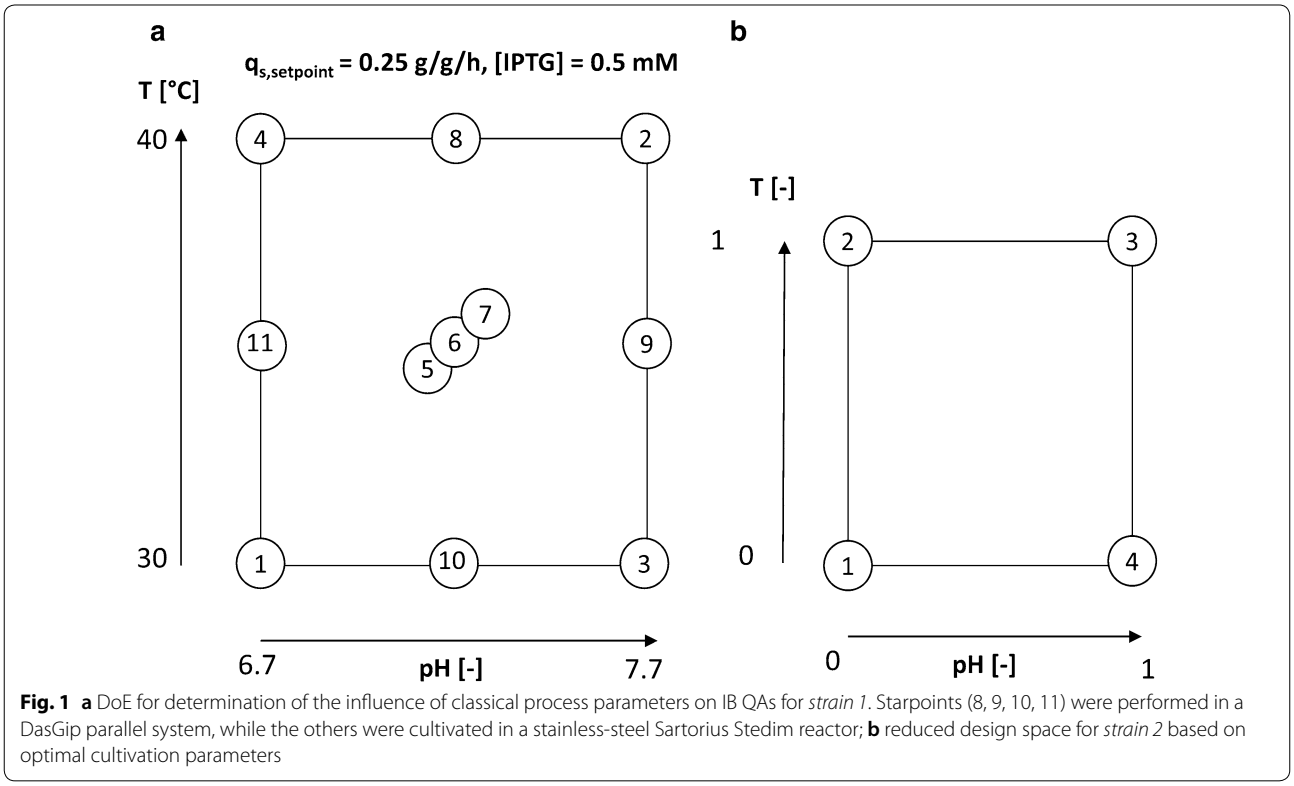

Fig. 1 **a** DoE for determination of the influence of classical process parameters on IB QAs for *strain 1*. Starpoints (8, 9, 10, 11) were performed in a DasGip parallel system, while the others were cultivated in a stainless-steel Sartorius Stedim reactor; **b** reduced design space for *strain 2* based on optimal cultivation parameters

Strain 2

Strain 2 was cultivated at our industrial partner. The cultivation was similar to *strain 1* using chemically defined medium containing 15 g/L glucose in seed and 10 g/L glucose in main stage fermentations, respectively. Inoculum preparation and respective antibiotic selection were similar to *strain 1*, though during the main culture stage kanamycin was added. Seed and main culture cultivations were carried out in custom built 50 L stainless steel vessels with custom made fermentation software for process control. Throughout the seed and main fermentation stages the pH was adjusted to fit the parameters of the second DoE (Fig. 1b) using 150 g/L sulphuric acid or 25% ammonia. Temperature was adjusted to the corresponding values in main culture. Dissolved oxygen was adjusted to 30% using aeration with up to 2 vvm, 2 bar backpressure and stirring up to 500 rpm. Optical DO probes Visipro DO (Hamilton, Reno, NV, USA) and EasyFerm Plus pH probes (Mettler Toledo, Columbus, Ohio; USA) were used for monitoring and control. Off-gas analysis was conducted using a custom-built mass spectrometer facility. At $OD_{600} > 8.5$ in seed culture, main culture was inoculated using 8.6% (v/v). Upon glucose depletion a glucose feed was initiated using a μ of 0.3 h^{-1} for 6 h and was kept constant at a final rate of exponential feed pattern until process termination. Expression was induced 2 h after the end of exponential feeding for biomass production using 1 mM IPTG for 12 h in a reduced design space given in Fig. 1b. As high temperatures and alkaline pH (fermentation conditions 2 in Fig. 1a) showed pronounced lysis during the study, the design space for strain 2 was reduced to a more reasonable pH and temperature window which is commonly used for multiple *E. coli* cultivations. Absolute values for pH and T cannot be given due to confidential reasons by our industrial partner.

Cultivation analytics

Biomass

For dry cell weight (DCW) measurements 1 mL of the cultivation broth was centrifuged at 9000 rpm, subsequently washed with 0.9% NaCl solution and centrifuged again under the same conditions. After drying the cells at 105 °C for 48 h the pellet was evaluated gravimetrically. DCW measurements were performed in five replicates and the mean error for DCW was about 3%. Offline OD_{600} measurements were performed in duplicates in a UV/VIS photometer Genisys 20 (Thermo Scientific, Waltham, MA, US).

Flow cytometry

Flow cytometry (FCM) was carried out according to Langemann et al. [36]. We used a CyFlow® Cube 6 flow cytometer (Partec, Münster, Germany) with 488-nm blue solid-state lasers. Three fluorescence channels were available (FL1, 536/40 nm bandpass; FL2, 570/50 nm bandpass; FL3, 675 nm longpass) alongside forward scatter (trigger parameter) and side scatter detection. This device featured true absolute volumetric counting with a sample size of 50–100 μL. Data were collected using the software CyView 13 (Cube 6; Partec) and analyzed with the software FCS Express V.4.07.0001 (DeNovo Software, Los Angeles, CA, USA). Membrane potential-sensitive dye $DiBAC_4(3)$ (abs./em. 493/516 nm) was used for the assessment of viability. Fluorescent dye RH414 (abs./em. 532/760 nm) was used for staining of plasma membranes yielding strong red fluorescent enhancement for the analysis of total cell number. Combining those two dyes it was possible to quantify the viable cell concentration. Stocks of 0.5 mM ($DiBAC_4(3)$) and 2 mM RH414 were prepared in dimethyl sulfoxide and stored at −20 °C. Both dyes were purchased from AnaSpec (Fremont CA, USA). 1.5 μL of both stocks were added to 1 mL diluted sample resulting in final concentrations of 0.5 μM $DiBAC_4(3)$ and 2.0 μM RH414, respectively. Samples were measured directly after addition of the dyes, without further incubation.

Sugar analytics

Sugar concentrations in the filtered fermentation broth were determined using a Supelco C-610H HPLC column (Supelco, Bellefonte, PA, USA) on an Ultimate 300 HPLC system (Thermo Scientific, Waltham, MA, US) using 0.1% H_3PO_4 as running buffer at 0.5 mL/min or an Aminex HPLC column (Biorad, Hercules; CA, USA) on an Agilent 1100 System (Agilent Systems, Santa Clara, CA, USA) with 4 mM H_2SO_4 as running buffer at 0.6 mL/min.

Product analytics

IB preparation

5 mL fermentation broth samples were centrifuged at 4800 rpm at 4 °C. The supernatant is discarded and the pellet is resuspended to a DCW of about 4 g/L in lysis buffer (100 mM Tris, 10 mM EDTA at pH 7.4). Afterwards the sample was homogenized using a high-pressure homogenizer at 1500 bar for 10 passages (Emulsiflex C3; Avestin, Ottawa, Canada). After centrifugation at 10,000 rpm and 4 °C the supernatant was discarded and the resulting IB pellet was washed twice with ultrapure water and aliquoted into pellets à 2 mL broth, centrifuged (14,000 rpm, 10 min 4 °C) and stored at −20 °C.

IB size

Washed and aliquoted IB samples were resuspended in ultrapure water. 100 μL of appropriate dilution of the suspension were pipetted on a gold-sputtered (10–50 nm)

polycarbonate filter (Millipore-Merck, Darmstadt, Germany) using reusable syringe filter holders with a diameter of 13 mm (Sartorius, Göttingen, Germany). 100 µL of ultrapure water were added and pressurized air was used for subsequent filtration. Additional 200 µL of ultrapure water were used for washing. The wet filters were fixed on a SEM sample holder using graphite adhesive tape and subsequently sputtered with gold to increase the contrast of the sample. SEM was performed using a QUANTA FEI SEM (Thermo Fisher, Waltham, MA, US) with a secondary electron detector [40]. The acceleration voltage of the electron beam was set between 3 and 5 kV. To determine the diameter of the IBs, 50 IBs on SEM pictures were measured using the ImageJ plugin Fiji [Laboratory for Optical and Computational Instrumentation (LOCI), University of Wisconsin-Madison, US]. SEM analytics of two different time points for both strains are given in Fig. 2.

IB titer for strain 1

For titer measurements IB pellets were solubilized using solubilization buffer (7.5 M guanidine hydrochloride, 62 mM Tris at pH 8). The filtered samples are quantified by HPLC analysis (UltiMate 3000; Thermo Fisher, Waltham, MA, USA) using a reversed phase column (EC 150/4.6 Nucleosil 300-5 C8; Macherey–Nagel, Düren, Germany). The product was quantified with an UV detector (Thermo Fisher, Waltham, MA, USA) at 214 nm using Novartis BVS Ref. 02 as standard. Mobile phase was composed of acetonitrile and water both supplemented with 0.1% (v/v) trifluoride acetic acid. A linear gradient from 30% (v/v) acetonitrile to 100% acetonitrile (ACN) was applied. A steep linear gradient from 10% ACN to 30% ACN in 60 s was followed by a long linear gradient from 30 to 55% and by three regeneration steps.

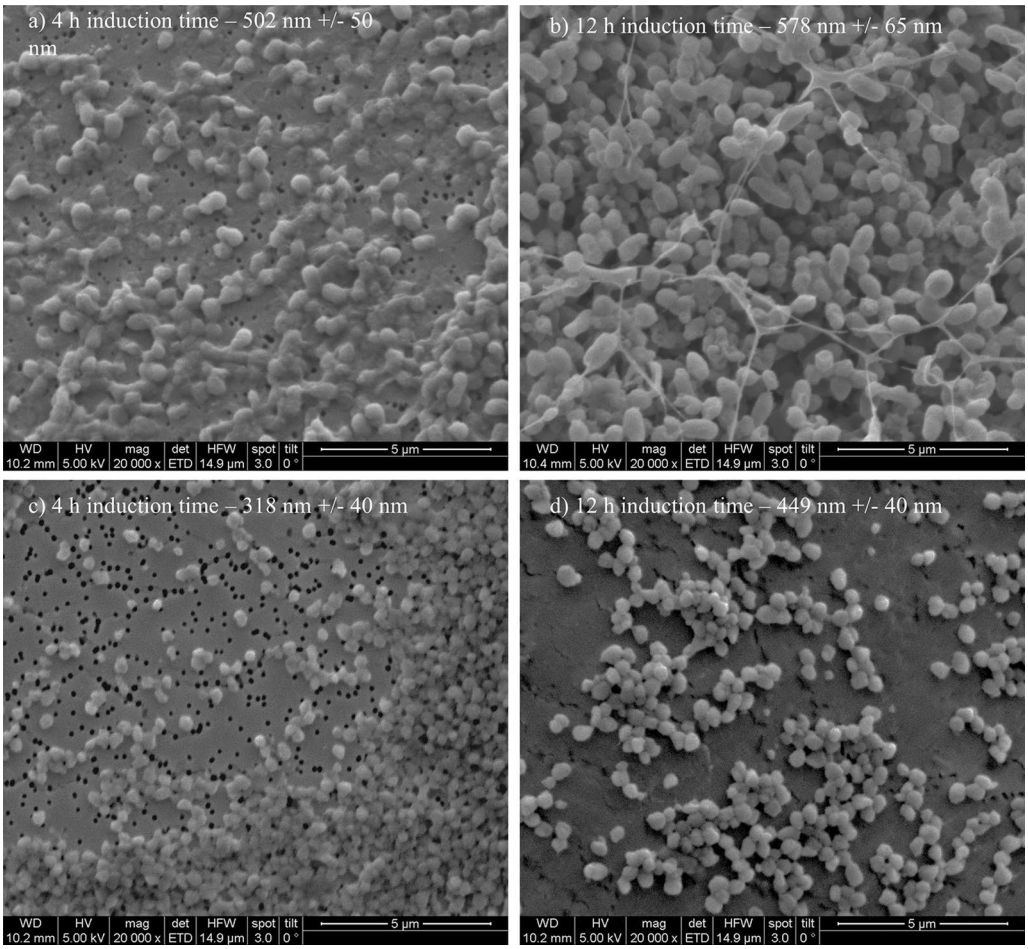

Fig. 2 Extracted IBs filtered onto Au coated polycarbonate filter and analyzed using SEM for 4 h induction time and 12 h induction time. Strong difference in size can be spotted for the two-time points

IB titer for strain 2

IB titer was also determined by reversed phase HPLC at Sandoz GmbH (Process Analytics, Kundl, Tirol, Austria). Pellets were defrosted at room temperature and solubilized by addition of dilution buffer [36] (6 M guanidine hydrochloride, 50 mM Tris, pH 7.5) and sonication (Branson Ultrasonics, Danbury, Connecticut, USA). The filtered samples were analyzed by HPLC with a reversed phase column (Acquity UPLC BEH 300, C4, 1.7 µm, 2.1 × 50 mm). Quantification was performed by UV detection at 214 nm wavelength and calibration with a purified product standard. Mobile phases were composed of (A) water and (B) acetonitrile/pentanol (95/5, v/v) both supplemented with 0.1% (v/v) tetrafluoride acetic acid. The elution of the product was achieved with a linear gradient of both solvents.

IB purity

Purity measurements were performed using chip-based protein assays with 2100 Bioanalyzer (Agilent Technologies, Santa Clara, CA, USA. The chip-based assay is based on SDS-PAGE and therefore separates molecules according to their size. Washed and homogenized IBs were dissolved in 3 M urea, 25 mM Tris at pH 7 and measured subsequently. The electropherogram was afterwards analyzed using OriginPro 2016 (Northampton, MA, USA) integrating the peak area of the protein of interest and normalizing the area in respect to the total area of the electropherogram.

IB conformational analysis by IR spectroscopy

Infrared (IR) spectra were recorded by an external-cavity quantum cascade laser-based IR transmission setup described in detail by Schwaighofer et al. [31]. A water-cooled external-cavity quantum cascade laser (Hedgehog, Daylight Solutions Inc., San Diego, USA) was used operating at a repetition rate of 100 kHz and a pulse width of 5000 ns. All spectra were recorded in the spectral tuning range between 1730 and 1470 cm^{-1}, covering the amide I and amide II region of proteins, at a scan speed of 1200 cm^{-1} s^{-1}. The MIR light was focused on the detector element by a gold plated off-axis parabolic mirror with a focal length of 43 mm. A thermoelectrically-cooled MCT detector operating at −78 °C (PCI-10.6, Vigo Systems S.A., Poland) was used as IR detector. To reduce the influence of water vapor, the setup was placed in a housing of polyethylene foil and constantly flushed with dry air. The measured signal was processed by a lock-in amplifier (Stanford Research Systems, CA, USA) and digitized by a NI DAQ 9239 24-bit ADC (National Instruments Corp., Austin, USA). Each single beam spectrum consisting of 6000 data points was recorded during the tuning time for one scan of approx. 250 µs. A total of 100 scans were recorded for background and sample single beam spectra at a total acquisition time of 53 s. All measurements were carried out using a custom-built, temperature-controlled flow cell equipped with two MIR transparent CaF_2 windows and 31 µm-thick spacer, at 20 °C.

The laser was controlled by Daylight Solution driver software; data acquisition and temperature control were performed using a custom-made LabView-based GUI (National Instruments Corp., Austin, USA). Two IB samples with distinct size of 400 nm and 600 nm were compared with the finished formulated protein standard of *strain 1* (without N-Pro Taq).

Results and discussion

The goal of this study was to investigate and to understand if and how IB attributes can be changed and tuned by upstream bioprocess (USP) technological methods. We tested the classical process parameters pH and temperature and the physiological parameter specific substrate uptake rate. The impact of specific USP parameters can be investigated using IB QAs as response for data evaluation. With knowledge about the tunability of IB QAs in the upstream, it is possible to simplify the subsequent downstream steps. Therefore, we tested two different proteins, with completely different structure including N-Pro fusion tag for *strain 1* and no fusion tag for *strain 2*. Both products have a high toxicity for the cell in common and are only expressed as IBs. The results constitute the key to custom made IBs and may be used as platform technology for the development of the USP for new products.

Impact of classical process parameters on IB QAs using *strain 1* (N-Pro fused protein)

As IPTG based induction imposes a metabolic stress to the host organism, time dependent analysis of IB QAs is of utmost importance to identify critical process time points (e.g. cell death, product degradation) within individual cultivation runs. Therefore, IB QAs were analyzed every 2 h within a maximum of 12 h induction time. pH and T were altered based on the experimental plan, while specific substrate uptake rate ($q_{s,Glu}$) and inducer concentration were kept constant in all experiments. In Table 1 the applied parameters for T, pH and $q_{s,Glu}$ for all performed cultivations in the DoE are displayed. Figure 3 exemplarily shows IB QAs of one single cultivation run as a function of time. The received QAs purity, titer and size are used to build a data driven model using MODDE 10 (Umetrics, Sweden). A partial least square fit was used for all models. Model terms (linear, quadratic and interaction terms) were evaluated according to their validity (p-values) and to the overall

Table 1 Analysis of applied process parameters compared to set points in all DoE runs during induction phase

DoE	pH_{set} (−)	T_{set} (°C)	pH_{real} (−)	T_{real} (°C)	$q_{s,Glu\ set}$ (g/g/h)	$q_{s,Glu\ real}$ (g/g/h)
1	6.7	30.00	6.69	30.00	0.25	0.24
10	7.2	30.00	7.16	30.02	0.25	0.26
3	7.7	30.00	7.69	30.00	0.25	0.26
11	6.7	35.00	6.64	35.02	0.25	0.29
5	7.2	35.00	7.18	35.00	0.25	0.24
6	7.2	35.00	7.18	35.00	0.25	0.32
9	7.7	35.00	7.64	35.03	0.25	0.27
4	6.7	40.00	6.68	40.00	0.25	0.29
8	7.2	40.00	7.15	40.01	0.25	0.29
2	7.7	40.00	7.69	40.00	0.25	0.24
7	7.2	35.00	7.17	35.00	0.25	0.25

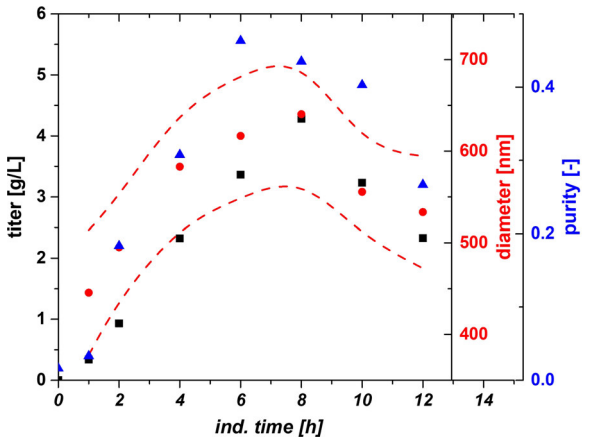

Fig. 3 IB QAs as a function of induction time for the third center point cultivation. Size is given with standard deviation (spline). Drop of titer/size and purity after 8 h is generally a result of increased cell lysis at elevated times

model quality. A clear dependence for the applied variations in pH and T were found and visualized against induction time giving a time dependent analysis of the QAs. The evaluation of the specific titer [based on titer (g/L) divided by the biomass at the given timepoint (gX/L, resulting in g/g)] against the induction time and pH and T showed a clear dependence. The specific titer was used in order to compensate for deviations in the biomass after the non-induced fed batch, which yielded 25–30 g/L DCW. The maximum of spec. titer (not necessarily the spec. productivity at certain time point) was found at low T and low pH, shown in Fig. 4a. pH dependence got significant after 6 h of induction time and impacted (Fig. 4b) the spec. titer. The maximum of recombinant protein was produced between 8 and 10 h. This fact is well reflected by the const. parameter in Fig. 4b. After 10 h cell death leads to a degradation and reduction of the produced protein, also clearly deducible from the constant term, visible in FCM measurements and in pronounced glucose accumulation (data not shown).

Within single cultivation runs titer and IB bead size showed a very linear relationship in the mean diameter and the standard deviation until the onset of cell death. Process parameters pH and T affected the growth of IB beads significantly. Generally, the largest IB bead size could be found close to the center point of the DoE in the beginning of induction. The shift to lower T and pH can be spotted after 6 h of induction time (compare to Fig. 4c). Effects of cell death and product degradation in titer could also be spotted in the IB bead size especially at 12 h. General trends of the fitting parameters are visualized in Fig. 4d. The constant model parameter is increased over time which also indicates the growth of IB beads over induction time. Linear terms pH and T and quadratic pH term showed increased impact on the model with elevated time, while interaction term and quadratic T-term stayed rather constant. A similar behavior for IB bead growth had already been obtained for a recombinant produced green fluorescent protein (GFP) in our group by Wurm et al. [33]. Instead of altering pH and T like in this study, the induction strength using mixed feed systems with lactose as inducer was varied. Induction time and strength had a high impact on the IB bead size during these cultivations. In our model a certain deregulation of size compared to titer could be dedicated from the given data driven models. This fact is beneficial for regulation of individual parameters to increase the performance in the DSP process chain in a further aspect since size and titer can be varied separately to a certain extend. As third QA IB purity, as important factor for quality in the DSP, was analyzed.

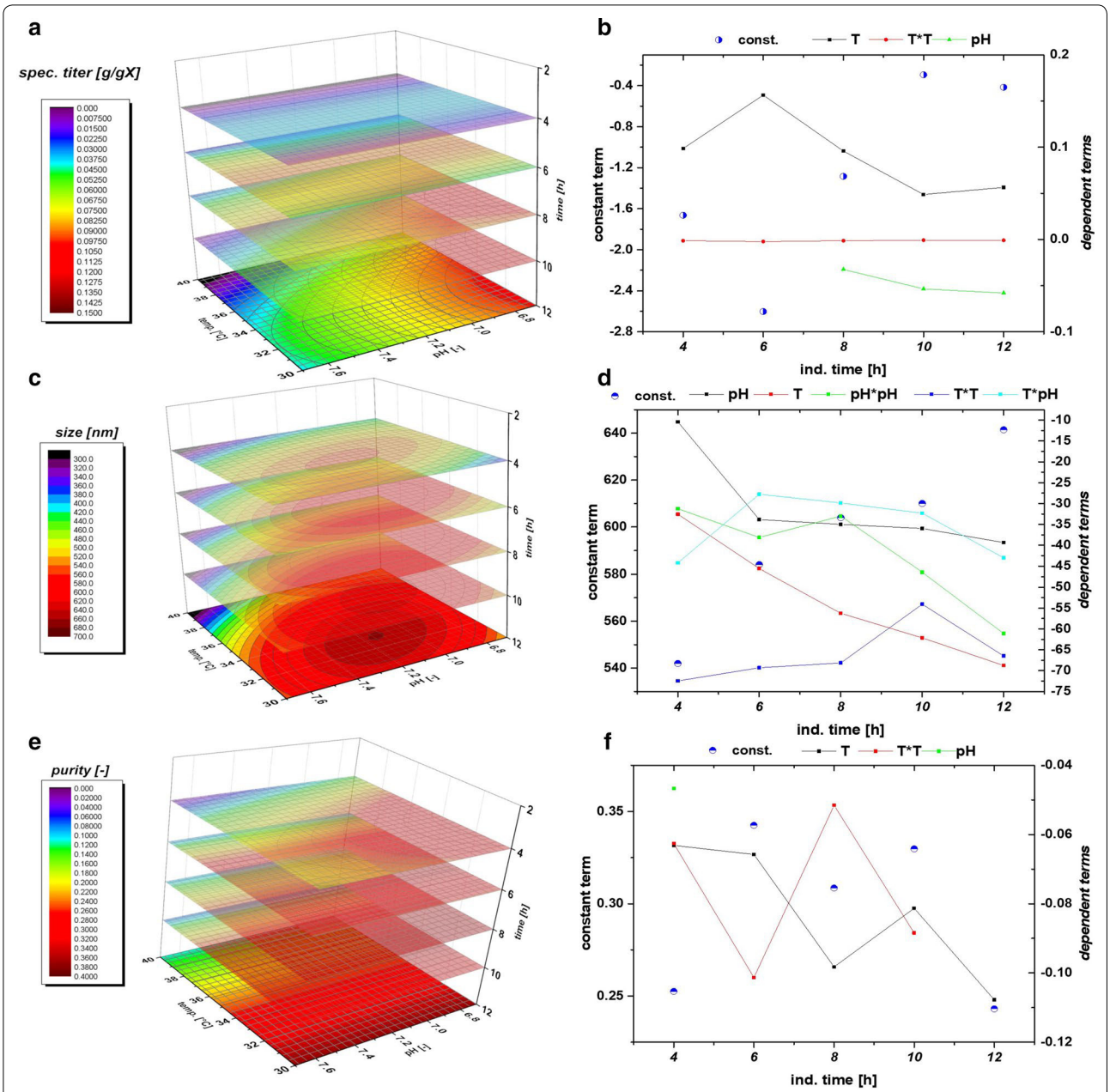

Fig. 4 **a** Data driven model for time dependent analysis of IB specific titer; **b** model fit parameter for titer. While in the beginning only temperature dependence is visible, a strong pH correlation can be found at t = 8 h; **c** data driven model for time dependent analysis of IB bead size; **d** model fit parameter for IB bead size. Due to standard deviation of 10% in the analysis model parameters are rather complex; **e** data driven model for time dependent analysis of IB purity; **f** model fit parameter for purity. A sole temperature dependence is found beyond 4 h of induction

The three-dimensional plot for purity determination is presented in Fig. 4e. At times, up to 4 h of induction pH influenced the purity of the IB samples. After 4 h, a sole dependence on temperature was found indicating that low temperatures (30 °C in the design) favor cleaner IBs. Since titer and size maximum could be found at low temperatures and pH, purity after homogenization may be highly correlated to the degree of lysis during the fermentation run. Lower temperatures did not lead to significant cell death (when regarding up to 10 h of induction), impurities may be reduced by applying low temperatures compared to temperatures with increased cell death yields. So, Fig. 4f summarizes the model fit parameters as a function of time. pH did not contribute to the

model fit beyond 4 h (only one point given). Temperature has a major influence on the duration of the induction time, which can already be detected in early stages of induction time. As purity is affected by the washing steps after homogenization different washing procedures may impact the value of absolute purity and the kind of impurity. Generally, porin structures and phospholipids from the outer membrane are the major part of impurities in the IB after homogenization [41, 42]. In literature IB beads had already been analyzed by SEM and AFM in order to get insight into morphology [43] and into washing procedures and dependence of pH and T within [44]. Different washing procedure had also been analyzed in this work. Buffer based washing tends to show little influence in shape and morphology of IBs but has an effect on the analyzed purity value (Additional file 1: Figure S1). This may be attributed to phospholipid content, resulting from homogenization of the cells, as buffer treatment successfully increases purity. Effects of washing on phospholipid content is also reported in [45]. Generally, SDS-PAGE techniques are used to separate different protein sizes. A few impurity peaks are found near the respective fusion protein size of 28.8 kDa and about 60 kDa (Additional file 2: Figure S2 an IB purity for 4 h and 12 h of the validation run). These impurities correlating well to the size-range of a magnitude of outer membrane (e.g. ompA with 35.1 kDA [46]). To determine the extent of DNA in IB as impurities, we treated solubilized IB samples prior to an SDS-PAGE with DNAse 30 min at 37 °C (DNAse 1, Thermo Scientific, Waltham, MA, US). No differences in the gel could be spotted between untreated and treated samples (Additional file 2: Figure S2b). Therefore, we suppose little content of residual DNA within the IB samples, which was also described in [45]. A higher IB purity is based on our model generally attributed to larger IB sizes. Since volume/surface ratio differs drastically compared to small beads less host cell structures can attach to the surface after homogenization. Buffer washing successfully removes a higher content of these impurities.

To evaluate the three data driven model approaches, we performed a verification run, aiming to achieve a maximum in titer of the recombinant protein including prediction of the respective attributes size and purity. Since the maximum of the titer could be found after 10 h of induction time, optimization is performed for this time stage. The process parameters received from the optimization algorithm for the induction phase were pH 6.7, T = 31.5 °C. Table 2 shows the comparison of the model prediction vs. the real measured values received after 10 h of induction. Standard cultivation reproducibility based on center point cultivations of *strain 1* are strongly time dependent, especially for titer and purity

Table 2 Prediction vs. measured QA of IBs for model validation run

Val. run	Model	Measured	Assessment
Purity	0.345	0.397	Correct within 20% error for purity at 10 h
Spez. titer (optimized)	0.113	0.140	Higher than predicted
Size	570.53	571.63	Prediction correct

assessment. Differences in the real $q_{s,Glu}$ during these three runs may affect the reproducibility, especially in the beginning of the cultivations as will be shown in the forthcoming chapter. Mean values and deviations for the center point runs of *strain 1* are given in Additional file 3: Figure S3. The standard deviation for size is below 10% until 10 h of induction, heading to about 15% at 12 h. Purity shows an error of about 30% for until 8 h reducing to values below 20% afterwards. Low titer values are generally highly defective at early time stages of the induction phase as a result of the onset of production. These high errors of about 30% reduce to about 10% after 8 h of induction. Using these assumptions for evaluation of the model clearly shown that model assumptions for size and purity QAs are correct within the given standard deviations. The IB bead size range after 10 h is predicted correctly, despite the general uncertainty of about 10% in the measurement statistics. Purity was correct within the 20% deviation at this time stage. Even slightly better results could be obtained for titer but are off the 10% deviation. This may be based on the slight higher $q_{s,Glu}$ of 0.3 g/g/h applied in this cultivation (overestimation of biomass after the fed-batch phase). Production of the protein of interest and the expression rate seems to be strongly correlated to the induction stress level of the cell. Lower temperatures seem to be favorable for the survival of the *E. coli* cells and positively influenced all three analyzed quality attributes. pH shifts to low pH increased the titer to a high degree at later induction stages and may be a result of a higher transmembrane potential, boosting the TCA and the energy metabolism [47]. As *E. coli* can grow on a pH between 6.0 and 8.0, with an internal pH of 7.6 [48], the rather acid pH-optimum is surprising at a first glance, but when investigated it is likely that the pH of 6.7 could be causing less precipitate of diverse trace elements, which are added in the DeLisa media [5]. Having access to more co-factors could positively influence the IB-formation. pH shifts from 7.2 to 6.7 may also effect different enzymes in the cell, e.g. phosphofructokinase in glycolysis [48].

Secondary structure analysis of IBs exhibiting different size

In order to understand the impact of different IB size (produced in USP) on the secondary structure, IR measurements in the MIR range were performed and compared to the correctly folded protein standard of *strain 1* for two distinct sizes exemplarily. Figure 5 shows the IR spectra of the reference sample and IB beads with 400 and 600 nm in size from the same cultivation run. The IB samples were resuspended in MQ water and subsequently measured. The reference standard was measured in the formulated buffer. The IR spectrum of the reference shows a band maximum at 1645 cm^{-1} in the amide I region as well as a narrow band at 1545 cm^{-1} in the amide II region that are characteristic for α-helical structures. In the reference sample, the native secondary structure of the protein is fully formed. Throughout the fermentation process, 400 nm size sample was taken after 4 h and the 600 nm sample was taken after 8 h. These samples also predominately feature α-helical secondary structure indicated by the amide I band maximum close to 1650 cm^{-1} [49]. However, these samples also contain different, non-native secondary structure as denoted by the band shoulders at approx. 1625 and 1680 cm^{-1} that suggest β-sheet secondary structures. The IR spectra show that the extent of these non-native secondary structure components is different for the two samples taken from the cultivation and that the amount is lower in the sample that was taken at a later point in time. This is in accordance with the purity measurements and indicates that later cultivation times and larger IB sizes do not affect the secondary structure of the IBs negatively. These results can be compared to the work of Wurm et al. [33] and corresponds to the data, that impurity content drastically decreases with IB size in solubilization and refolding.

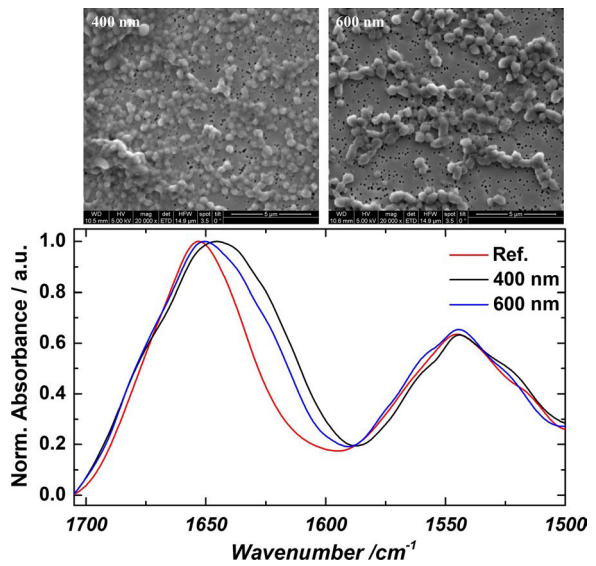

Fig. 5 IR spectra of the two distinct bead sizes of 400 and 600 nm, compared to the correctly folded reference sample. SEM analytics of both samples are given above

Validation of the impact of classical process parameters on IB QAs using *strain 2*

For application of the proposed QA dependence used for *strain 1*, a reduced design space (compare to Fig. 1b) for *strain 2* was applied and quality attributes were analyzed as described for *strain 1*. *Strain 2* also produces a toxic protein for the cells and is consequently expressed only as IBs but lacking the N-Pro fusion tag. As only four cultivations were performed, no statistical evaluation is used and fits were performed in order to have a reasonable model description and to reveal general trends during those cultivations. Estimation on standard deviations for the given QAs are already given in the previous section. In comparison to *strain 1* higher titers could be achieved during the cultivation. (Figure 6a—normalized to the highest achieved titer in these cultivations, given in 1 [−]). Time dependent analysis of the IB bead size is shown in Fig. 6b and reveals the same trend as already valid for titer and purity. Low pH and low temperatures lead to increased IB bead size in those cultivations. However, IB bead size is generally smaller in *strain 2*, when compared to *strain 1* respectively (N-Pro based protein, clearly visible by comparing Fig. 2b, d). The dimensionless value of purity is generally very high as well, exceeding values of 0.5 even after 4 h of induction, compare to Fig. 6c. In accordance to *strain 1* the highest titers and purities are found at a low pH and low temperatures.

Different IB bead size for a broad number of proteins was already presented in literature: A GFP model protein, expressing IBs as well as soluble protein [33] showed IB bead size of a maximum of 600 nm at extended induction times using mixed feed systems with glucose and lactose. Since, GFP also is expressed as soluble protein, only the ratio between IB and soluble protein is altered based on the feeding strategies. Producing a maximum size of 600 nm, the GFP-model protein forms an intermediate between the measured maximum of *strain 1* (N-Pro) and *strain 2* in this work. Other works report IB sizes between 502 nm for DnaK-IBs and 580 nm for ClpA-IBs [27] and approximately 600 nm for G-CSF IBs [28] and are in a reasonable range compared with our products in this work. IB bead size is strongly dependent on the produced product, on the polypeptide sequence and on hydrophobicity of the protein structure. IB QAs can accordingly be altered with the used classical process parameter T and pH, but morphological considerations have generally to be taken into account and can be product-based

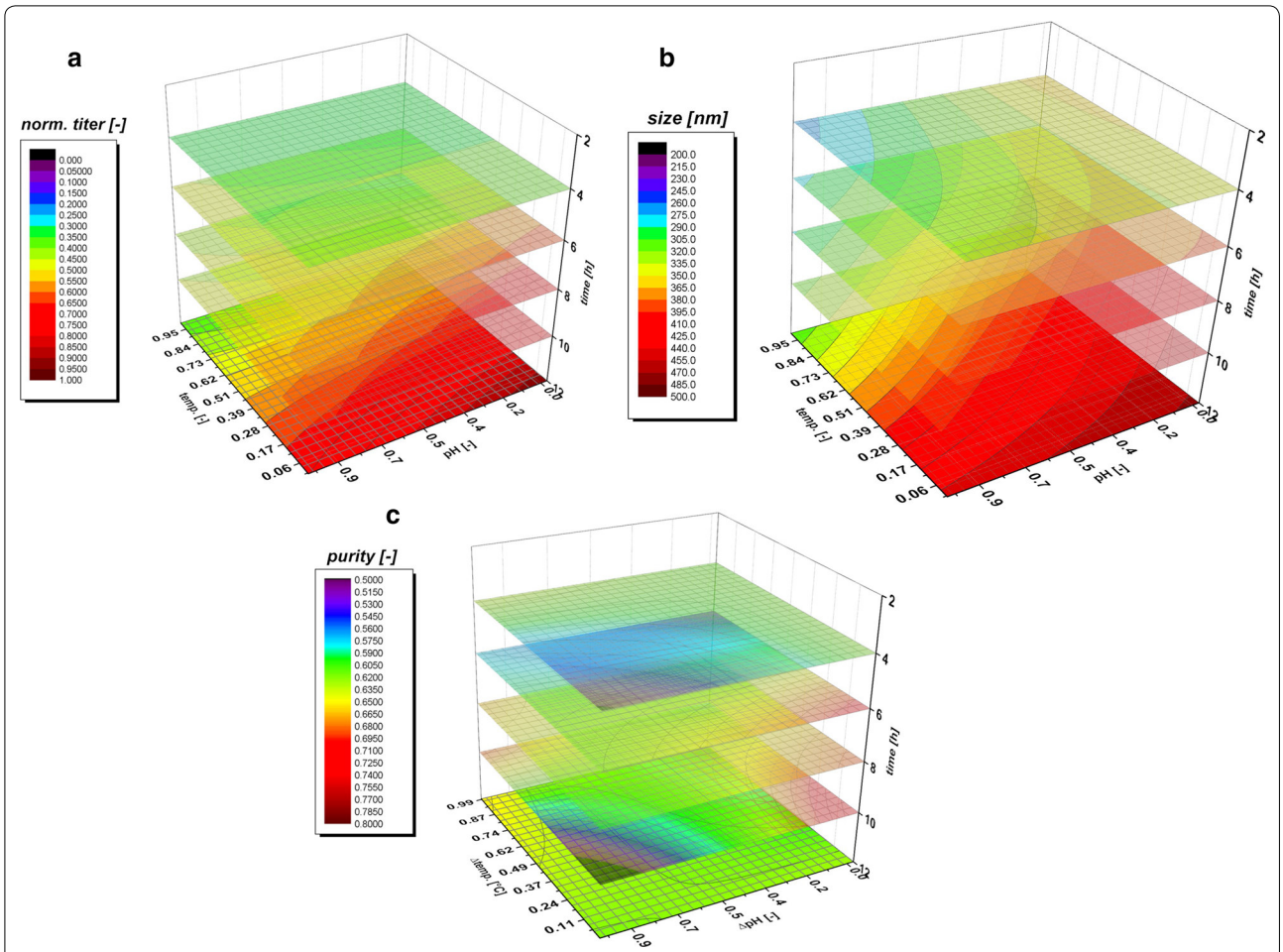

Fig. 6 Data driven model for time dependent analysis of IB **a** titer, **b** size and **c** purity of *strain 2* using a reduced DoE design (Fig. 1b). Trends are given with differences of the lowest process value. Very similar behavior to *strain 1* can be found, showing highest purity, size and titer at values for low T and pH. Higher titers are produced using this strain resulting in boosted purities compared to *strain 1*. The analyzed size similar to *strain 1*

very different. Since IPTG concentration of 0.5 mM is high enough to induce all present cells, the secondary structure of the expressed proteins of *strain 2* has to inhere in higher density in their structure regarding the titers. Denser structures are much easier to be separated in centrifugation processes in the downstream, since the difference of the density compared to the host cell debris is far higher. This fact may also affect the purity and results in those high purity values for *strain 2.* Computer tomographic analysis of transmission electron microscopy (not shown) of *strain 1* reveal cavities within single inclusion bodies in the cell and may be the result for density variations of different IB products. Based on the findings for both strains in this study, time-resolved analytics of the IB QAs can be used to optimize the USP. Knowledge of titer as key performance indicator is important for determination of the harvest time point. The resulting IB bead size (and purity) is beneficial for planning of further necessary steps in the downstream for a given product.

Impact of the physiological process parameter $q_{s,Glu}$ on IB quality attributes of *strain 1* (N-Pro fused protein)

Classical process parameters showed a high impact on IB properties during induction phase. The knowledge for optimized parameters for *strain 1*—was used for altering the physiological parameter $q_{s,Glu}$. Temperature was decreased to 31.5 °C and pH was adapted to 6.7, while different setpoints for $q_{s,Glu}$ were established during induction phase. Setpoints and real values for the $q_{s,Glu}$ are given in Table 3. The induction characteristic of the four performed runs are given in Fig. 7a showing glucose

Table 3 Applied $q_{s,Glu}$ vs. real $q_{s,Glu}$ values after reverse analysis of the cultivation data

Run	$q_{s,Glu\ set}$	$q_{s,Glu\ real}$
1	0.1	0.1 ± 0.01
2	0.25	0.3 ± 0.02
3	0.4	0.39 ± 0.05
4	0.5	0.41 ± 0.063

Sugar accumulation and cell death at higher applied values result in higher standard deviations

accumulation and percentage of dead cells for the four performed cultivations. It was already investigated in literature that the correlation of growth rate and the production of recombinant protein resulted in a decrease in μ the more recombinant protein is produced [50]. This correlation could be clearly monitored in our study during induction phase when high titers of recombinant protein were produced. As consequence the growth rate (not shown) decreased, leading to sugar accumulations as the feed-rate over the whole induction phase was applied constantly [50]. Higher applied $q_{s,Glu}$ resulted in early sugar accumulation and in increased number of dead cells in the cultivation and decreased the real $q_{s,Glu}$ extensively even after some hours. After 12 h of induction 50% of the culture died at applied $q_{s,Glu}$ of 0.4 and 0.5 g/g/h, while very low $q_{s,Glu}$ showed neither cell death nor sugar accumulation. The time resolved titer measurements are given in Fig. 7b. Very high specific titers could be found at $q_{s,Glu\text{-}set} = 0.5$ g/g/h at 6 h of induction with highest volumetric productivities exceeding 1 g/L/h. However, the increased cell stress resulted in cell death and degradation of the product as could be seen in the decease of the titers at later time stages, respectively. After 12 h titers were almost identical irrespective of applied $q_{s,Glu}$ for high setpoints (0.3–0.5 g/g/h). That indicated, time dependent analysis of QAs is therefore of utmost importance, especially at physiological process control. The peak value of the volumetric productivities (before degradation) showed a rising trend based on the mean $q_{s,Glu}$ values which were applied (Additional file 4: Figure S4) and clearly indicated that the increased feeding rate is really beneficial for high productivity. The IB bead size given in Fig. 7c was generally very similar at $q_{s,Glu} = 0.3$–0.5 g/g/h applied values, with $q_{s,Glu} = 0.3$ g/g/h showing smaller diameters at later time stages. IB beads at $q_{s,Glu} = 0.1$ g/g/h were not detectable with SEM until 10 h of induction time. Low $q_{s,Glu}$ yielded very small IB sizes and low titers in Fig. 7b as only low energy is available for production of the recombinant protein. A steep increase in the beginning of the induction time was generally accompanied by leveling off in diameter at later stages. Trends for IB purity are given in Fig. 7d. Higher $q_{s,Glu}$ values were beneficial for protein purity, which were in reasonable accordance with trends for titer and size already seen in the previous chapter.

Based on these findings improved control strategies for IB production could be established in further development steps using the optimized process parameters for the two used strains in combination with physiological process control (time dependent adaption of the specific substrate uptake rate) during the induction phase.

Conclusions

IB quality attributes were analyzed in respect of changes in classical process parameters pH and T in the induction phase. Pronounced changes in QAs could be found in the analysis of IB titer, IB bead size and IB purity. Optimized process conditions for *strain 1* were found to be at pH 6.7 and 31.5 °C during induction in respect of the produced maximum IB titer. These findings were checked using a second industrial relevant strain, revealing that low temperatures and low pH is highly beneficial for production of IBs. Therefore, we would like to hypothesize that yields of exclusively IB based products can be improved by applying low temperatures and a relatively low pH value during the induction phase as analyzed in this study for two very different products. Despite of this platform knowledge, absolute values for size, titer and purity were strongly product dependent and exhibit very different values for every produced product.

The sweet spot conditions (pH 6.7, T = 31.5 °C) for *strain 1* were used to show the impact of physiological control onto IB quality attributes. The four performed cultivations exhibited different specific substrate uptake rates ($q_{s,Glu}$) and revealed high impact on analyzed IB QAs. High constantly applied $q_{s,Glu}$ boosted titer, bead size and purity very early in the induction phase, but resulted generally in high glucose accumulation and cell death, while low $q_{s,Glu}$ did not stress the cells, but lead to very low production of IBs. Physiological control based on these findings may be highly industrially relevant in

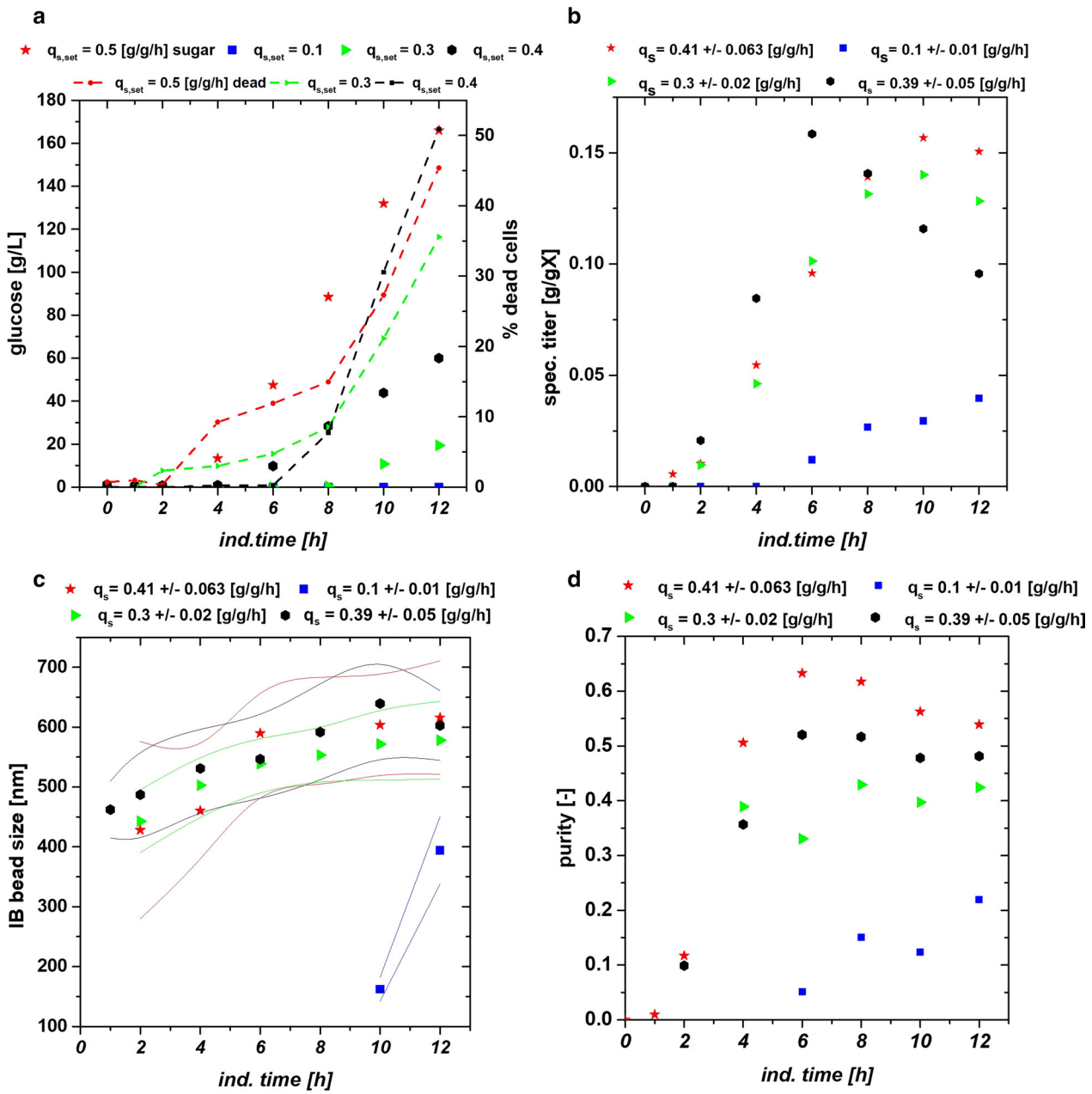

Fig. 7 **a** Sugar-accumulation and cell death measured by FCM for three cultivations at different $q_{s,Glu}$. Lowest $q_{s,Glu}$ shows no cell lysis and accumulation; **b** specific titer of the recombinant protein fused to N-pro. Very high expression can be seen for the high $q_{s,Glu}$ until 6 h with decreasing $q_{s,Glu}$ also decreases product titer; **c** size of the IB beads. $q_{s,Glu} = 0.41$ g/g/h and $q_{s,Glu} = 0.39$ g/g/h are very similar. A very steep increase is followed by a steady state; $q_{s,Glu} = 0.30$ g/g/h shows increase over time, while size for $q_{s,Glu} = 0.10$ g/g/h is only detectable at 10 and 12 h of induction; **d** purity depicts clear dependence of all different $q_{s,Glu}$ setpoints, increasing the IB purity with higher $q_{s,Glu}$

order to find IB parameters with high productivity, but also low contamination of host cell proteins and DNA.

We would also like to highlight that time dependent monitoring of the here defined IB-QAs can be used as a tool to optimize process parameters such as pH, temperature and ($q_{s,Glu}$). By improving the upstream conditions, we aim to trigger robust downstream procedures, increasing the overall time/space yield of IB-processes.

Additional files

Additional file 1: Figure S1. Analysis of the first center point run representing IB purity. Buffer washed samples showed generally higher purity. Differences in size and titer are within the given standard deviation.

Additional file 2: Figure S2. a) Electropherogram for two different timepoints during a cultivation (4 h and 12 h). A clear visibility of impurity pattern near the protein of interest (high peak after 28 kDa) is given; b) SDS-Page for visualization of DNA related impurities. No distinct differentiation can be made between DNase treatment and virgin sample.

Additional file 3: Figure S3. a) Mean value for size and deviations of the three individual center point runs. Error stays constant; b) purity-based analysis, with decreasing error over time; c) titer-based analysis. Error decreases drastically in later time stages (range of constant titer or even proteolytic degradation).

Additional file 4: Figure S4. $q_{s,real}$ with standard deviation based on the reverse analysis. The higher the q_s the higher is the error, due to onset of degradation and sugar accumulation in the broth. A rising trend can be dedicated from these measurements.

Abbreviations

ACN: acetonitrile; AFM: atomic force microscopy; DCW: dry cell weight; dO_2: dissolved oxygen; DoE: design of experiments; DSP: downstream processing; FCM: flow cytometry; GFP: green fluorescent protein; IB: inclusion body; IPTG: isopropyl β-D-1 thiogalactopyranoside; IR: infrared; MQ: ultrapure water; QA: quality attribute; $q_{s,Glu}$ (g/g/h): specific substrate uptake rate (glucose); r_p (g/L/h): volumetric productivity; SEM: scanning electron microscopy; TCA: tricarboxylic acid (cycle); TEM: transmission electron microscopy; USP: upstream processing; UV: ultraviolet.

Authors' contributions

CS, SH, and CH designed the study. CS, JK, MS and DS conducted the experiments and analyzed the data at TU Wien. SH supervised the cultivations at Sandoz GmbH for *strain 2*. EE conducted the SEM measurements. AS performed IR measurements and data analysis. CS, SH and CH drafted the manuscript. All authors read and approved the final manuscript.

Author details

[1] Christian Doppler Laboratory for Mechanistic and Physiological Methods for Improved Bioprocesses, Institute of Chemical Engineering, Vienna University of Technology, Vienna, Austria. [2] Sandoz GmbH, Biochemiestrasse 10, 6250 Kundl, Tirol, Austria. [3] Institute of Chemical Technology and Analytics, Getreidemarkt 9/164, 1060 Vienna, Austria. [4] Institute of Chemical, Environmental and Bioscience Engineering, Research Area Biochemical Engineering, Vienna University of Technology, Gumpendorfer Strasse 1a, 1060 Vienna, Austria.

Acknowledgements

The authors acknowledge the TU Wien University Library for financial support through its Open Access Funding Program. The authors want to thank the coworkers at Novartis GmbH, especially Mareike Jakobs, who helped with the analysis of the conducted experiments and did proofreading of the manuscript.

Competing interests

The authors declare that they have no competing interests.

Availability of data and materials

The datasets used analyzed during the current study are available from the corresponding author on reasonable request. Additional given information is added as three additional figures in this manuscript.

Consent for publication

Not applicable.

Ethics approval and consent to participate

Not applicable.

Funding

The authors acknowledge the Christian Doppler society for funding of this project.

Publisher's Note

Received: 14 May 2018 Accepted: 14 September 2018
Published online: 20 September 2018

References

1. Gupta SK, Shukla P. Microbial platform technology for recombinant antibody fragment production: a review. Crit Rev Microbiol. 2017;43:31–42.
2. Walsh G. Biopharmaceutical benchmarks 2010. Nat Biotechnol. 2010;28:917–24.
3. Wurm DJ, Veiter L, Ulonska S, Eggenreich B, Herwig C, Spadiut O. The *E. coli* pET expression system revisited-mechanistic correlation between glucose and lactose uptake. Appl Microbiol Biotechnol. 2016;100:8721–9.
4. Meuris L, Santens F, Elson G, Festjens N, Boone M, Dos Santos A, Devos S, Rousseau F, Plets E, Houthuys E, et al. GlycoDelete engineering of mammalian cells simplifies *N*-glycosylation of recombinant proteins. Nat Biotechnol. 2014;32:485–9.
5. DeLisa MP, Li J, Rao G, Weigand WA, Bentley WE. Monitoring GFP-operon fusion protein expression during high cell density cultivation of *Escherichia coli* using an on-line optical sensor. Biotechnol Bioeng. 1999;65:54–64.
6. Berlec A, Strukelj B. Current state and recent advances in biopharmaceutical production in *Escherichia coli*, yeasts and mammalian cells. J Ind Microbiol Biotechnol. 2013;40:257–74.
7. Baeshen MN, Al-Hejin AM, Bora RS, Ahmed MM, Ramadan HA, Saini KS, Baeshen NA, Redwan EM. Production of biopharmaceuticals in *E. coli*: current scenario and future perspectives. J Microbiol Biotechnol. 2015;25:953–62.
8. Spadiut O, Capone S, Krainer F, Glieder A, Herwig C. Microbials for the production of monoclonal antibodies and antibody fragments. Trends Biotechnol. 2014;32:54–60.
9. Studier FW, Moffatt BA. Use of bacteriophage T7 RNA polymerase to direct selective high-level expression of cloned genes. J Mol Biol. 1986;189:113–30.
10. Steen R, Dahlberg AE, Lade BN, Studier FW, Dunn JJ. T7 RNA polymerase directed expression of the *Escherichia coli* rrnB operon. EMBO J. 1986;5:1099–103.
11. Studier FW, Rosenberg AH, Dunn JJ, Dubendorff JW. Use of T7 RNA polymerase to direct expression of cloned genes. Methods Enzymol. 1990;185:60–89.
12. Dubendorff JW, Studier FW. Controlling basal expression in an inducible T7 expression system by blocking the target T7 promoter with lac repressor. J Mol Biol. 1991;219:45–59.
13. Neubauer P, Hofmann K. Efficient use of lactose for the lac promoter-controlled overexpression of the main antigenic protein of the foot and mouth disease virus in *Escherichia coli* under fed-batch fermentation conditions. FEMS Microbiol Rev. 1994;14:99–102.
14. Lyakhov DL, He B, Zhang X, Studier FW, Dunn JJ, McAllister WT. Pausing and termination by bacteriophage T7 RNA polymerase. J Mol Biol. 1998;280:201–13.
15. Jeong H, Barbe V, Lee CH, Vallenet D, Yu DS, Choi SH, Couloux A, Lee SW, Yoon SH, Cattolico L, et al. Genome sequences of *Escherichia coli* B strains REL606 and BL21 (DE3). J Mol Biol. 2009;394:644–52.
16. Jeong H, Kim HJ, Lee SJ. Complete genome sequence of *Escherichia coli* strain BL21. Genome Announc. 2015;3:e00134-15.
17. Tseng TT, Tyler BM, Setubal JC. Protein secretion systems in bacterial-host associations, and their description in the Gene Ontology. BMC Microbiol. 2009;9(Suppl 1):S2.

18. Marbach A, Bettenbrock K. lac operon induction in *Escherichia coli*: systematic comparison of IPTG and TMG induction and influence of the transacetylase LacA. J Biotechnol. 2012;157:82–8.
19. Keiler KC. Biology of trans-translation. Annu Rev Microbiol. 2008;62:133–51.
20. Viitanen MI, Vasala A, Neubauer P, Alatossava T. Cheese whey-induced high-cell-density production of recombinant proteins in *Escherichia coli*. Microb Cell Fact. 2003;2:2.
21. García-Fruitós E, Vázquez E, Díez-Gil C, Corchero JL, Seras-Franzoso J, Ratera I, Veciana J, Villaverde A. Bacterial inclusion bodies: making gold from waste. Trends Biotechnol. 2012;30:65–70.
22. Palmer I, Wingfield PT. Preparation and extraction of insoluble (inclusion-body) proteins from *Escherichia coli*. Curr Protoc Protein Sci. 2012;70:6.3.1.
23. Ramón A, Señorale-Pose M, Marín M. Inclusion bodies: not that bad…. Front Microbiol. 2014;5:56.
24. Villaverde A, Corchero JL, Seras-Franzoso J, Garcia-Fruitós E. Functional protein aggregates: just the tip of the iceberg. Nanomedicine (Lond). 2015;10:2881–91.
25. Wingfield PT, Palmer I, Liang SM. Folding and purification of insoluble (inclusion body) proteins from *Escherichia coli*. Curr Protoc Protein Sci. 2014;78:6.5.1–5.30.
26. Wingfield PT. Preparation of soluble proteins from *Escherichia coli*. Curr Protoc Protein Sci. 2014;78:6.2.1–2.22.
27. Díez-Gil C, Krabbenborg S, García-Fruitós E, Vazquez E, Rodríguez-Carmona E, Ratera I, Ventosa N, Seras-Franzoso J, Cano-Garrido O, Ferrer-Miralles N, et al. The nanoscale properties of bacterial inclusion bodies and their effect on mammalian cell proliferation. Biomaterials. 2010;31:5805–12.
28. Peternel Š, Jevševar S, Bele M, Gaberc-Porekar V, Menart V. New properties of inclusion bodies with implications for biotechnology. Biotechnol Appl Biochem. 2008;49:239–46.
29. Peternel Š, Grdadolnik J, Gaberc-Porekar V, Komel R. Engineering inclusion bodies for non denaturing extraction of functional proteins. Microb Cell Fact. 2008;7:34.
30. Reichelt WN, Kaineder A, Brillmann M, Neutsch L, Taschauer A, Lohninger H, Herwig C. High throughput inclusion body sizing: Nano particle tracking analysis. Biotechnol J. 2017;12:1600471.
31. Schwaighofer A, Montemurro M, Freitag S, Kristament C, Culzoni MJ, Lendl B. Beyond FT-IR spectroscopy: EC-QCL based mid-IR transmission spectroscopy of proteins in the amide I and amide II region. Anal Chem. 2018;90:7072–9.
32. Jevševar S, Gaberc-Porekar V, Fonda I, Podobnik B, Grdadolnik J, Menart V. Production of nonclassical inclusion bodies from which correctly folded protein can be extracted. Biotechnol Prog. 2005;21:632–9.
33. Wurm DJ, Quehenberger J, Mildner J, Eggenreich B, Slouka C, Schwaighofer A, Wieland K, Lendl B, Rajamanickam V, Herwig C, Spadiut O. Teaching an old pET new tricks: tuning of inclusion body formation and properties by a mixed feed system in *E. coli*. Appl Microbiol Biotechnol. 2017;102:667–76.
34. Reichelt WN, Brillmann M, Thurrold P, Keil P, Fricke J, Herwig C. Physiological capacities decline during induced bioprocesses leading to substrate accumulation. Biotechnol J. 2017;12:1600547.
35. Kischnick S, Weber B, Verdino P, Keller W, Sanders EA, Anspach FB, Fiebig H, Cromwell O, Suck R. Bacterial fermentation of recombinant major wasp allergen Antigen 5 using oxygen limiting growth conditions improves yield and quality of inclusion bodies. Protein Expr Purif. 2006;47:621–8.
36. Langemann T, Mayr UB, Meitz A, Lubitz W, Herwig C: Multi-parameter flow cytometry as a process analytical technology (PAT) approach for the assessment of bacterial ghost production. Appl Microbiol Biotechnol. 2016;100:409–18.
37. Castellanos-Mendoza A, Castro-Acosta RM, Olvera A, Zavala G, Mendoza-Vera M, García-Hernández E, Alagón A, Trujillo-Roldán MA, Valdez-Cruz NA. Influence of pH control in the formation of inclusion bodies during production of recombinant sphingomyelinase-D in *Escherichia coli*. Microb Cell Fact. 2014;13:137.
38. Kopp J, Slouka C, Ulonska S, Kager J, Fricke J, Spadiut O, Herwig C. Impact of glycerol as carbon source onto specific sugar and inducer uptake rates and inclusion body productivity in *E. coli* BL21 (DE3). Bioengineering (Basel). 2017;5:1.
39. Achmüller C, Kaar W, Ahrer K, Wechner P, Hahn R, Werther F, Schmidinger H, Cserjan-Puschmann M, Clementschitsch F, Striedner G, et al. N(pro) fusion technology to produce proteins with authentic N termini in *E. coli*. Nat Methods. 2007;4:1037–43.
40. Dvorak P, Chrast L, Nikel PI, Fedr R, Soucek K, Sedlackova M, Chaloupkova R, de Lorenzo V, Prokop Z, Damborsky J. Exacerbation of substrate toxicity by IPTG in *Escherichia coli* BL21 (DE3) carrying a synthetic metabolic pathway. Microb Cell Fact. 2015;14:201.
41. Rinas U, Boone TC, Bailey JE. Characterization of inclusion bodies in recombinant *Escherichia coli* producing high levels of porcine somatotropin. J Biotechnol. 1993;28:313–20.
42. Rinas U, Bailey JE. Protein compositional analysis of inclusion bodies produced in recombinant *Escherichia coli*. Appl Microbiol Biotechnol. 1992;37:609–14.
43. García-Fruitós E, Rodríguez-Carmona E, Díez-Gil C, Ferraz RM, Vázquez E, Corchero JL, Cano-Sarabia M, Ratera I, Ventosa N, Veciana J. Surface cell growth engineering assisted by a novel bacterial nanomaterial. Adv Mater. 2009;21:4249–53.
44. Rodríguez-Carmona E, Cano-Garrido O, Seras-Franzoso J, Villaverde A, García-Fruitós E. Isolation of cell-free bacterial inclusion bodies. Microb Cell Fact. 2010;9:1.
45. Valax P, Georgiou G. Molecular characterization of β-lactamase inclusion bodies produced in *Escherichia coli*. 1. Composition. Biotechnol Prog. 1993;9:539–47.
46. Molloy MP, Herbert BR, Slade MB, Rabilloud T, Nouwens AS, Williams KL, Gooley AA. Proteomic analysis of the *Escherichia coli* outer membrane. FEBS J. 2000;267:2871–81.
47. Stancik LM, Stancik DM, Schmidt B, Barnhart DM, Yoncheva YN, Slonczewski JL. pH-dependent expression of periplasmic proteins and amino acid catabolism in *Escherichia coli*. J Bacteriol. 2002;184:4246–58.
48. Padan E, Zilberstein D, Schuldiner S. pH homesstasis in bacteria. Biochim Biophys Acta (BBA) Rev Biomembr. 1981;650:151–66.
49. Barth A. Infrared spectroscopy of proteins. Biochim Biophys Acta (BBA) Bioenerg. 2007;1767:1073–101.
50. Scott M, Gunderson CW, Mateescu EM, Zhang Z, Hwa T. Interdependence of cell growth and gene expression: origins and consequences. Science. 2010;330:1099–102.

bioengineering

MDPI

Article

Impact of Glycerol as Carbon Source onto Specific Sugar and Inducer Uptake Rates and Inclusion Body Productivity in *E. coli BL21*(*DE3*)

Julian Kopp [1], Christoph Slouka [1], Sophia Ulonska [2], Julian Kager [2], Jens Fricke [1], Oliver Spadiut [2] and Christoph Herwig [1,2,*]

[1] Christian Doppler Laboratory for Mechanistic and Physiological Methods for Improved Bioprocesses, Institute of Chemical, Environmental and Biological Engineering, Vienna University of Technology, 1060 Vienna, Austria; julian.kopp@tuwien.ac.at (J.K.); christoph.slouka@tuwien.ac.at (C.S.); fricke_jens@gmx.de (J.F.)

[2] Research Division Biochemical Engineering, Institute of Chemical, Environmental and Biological Engineering, Vienna University of Technology, 1060 Vienna , Austria; sophia.ulonska@tuwien.ac.at (S.U.); julian.kager@tuwien.ac.at (J.K.); oliver.spadiut@tuwien.ac.at (O.S.)

* Correspondence: christoph.herwig@tuwien.ac.at; Tel.: +43-(1)-58801-166084

Academic Editor: Mark Blenner
Received: 24 October 2017; Accepted: 19 December 2017; Published: 21 December 2017

Abstract: The Gram-negative bacterium *E. coli* is the host of choice for a multitude of used recombinant proteins. Generally, cultivation is easy, media are cheap, and a high product titer can be obtained. However, harsh induction procedures using isopropyl β-D-1 thiogalactopyranoside as inducer are often referred to cause stress reactions, leading to a phenomenon known as "metabolic" or "product burden". These high expressions of recombinant proteins mainly result in decreased growth rates and cell lysis at elevated induction times. Therefore, approaches tend to use "soft" or "tunable" induction with lactose and reduce the stress level of the production host. The usage of glucose as energy source in combination with lactose as induction reagent causes catabolite repression effects on lactose uptake kinetics and as a consequence reduced product titer. Glycerol—as an alternative carbon source—is already known to have positive impact on product formation when coupled with glucose and lactose in auto-induction systems, and has been referred to show no signs of repression when cultivated with lactose concomitantly. In recent research activities, the impact of different products on the lactose uptake using glucose as carbon source was highlighted, and a mechanistic model for glucose-lactose induction systems showed correlations between specific substrate uptake rate for glucose or glycerol ($q_{s,C}$) and the maximum specific lactose uptake rate ($q_{s,lac,max}$). In this study, we investigated the mechanistic of glycerol uptake when using the inducer lactose. We were able to show that a product-producing strain has significantly higher inducer uptake rates when being compared to a non-producer strain. Additionally, it was shown that glycerol has beneficial effects on viability of cells and on productivity of the recombinant protein compared to glucose.

Keywords: *E. coli*; mixed feed system; glycerol; recombinant proteins; bioprocess engineering

1. Introduction

The Gram-negative bacterium *E. coli* is the expression host of choice for the production of 30% to 40% of recombinant drugs in industry [1,2]. As *E. coli* shows very fast replication rates [3,4] on comparatively cheap media [5], the benefits often outweigh the numerous purification steps [1,6] and the missing glycosylation pattern [1,7,8]. Recombinant protein production in *E. coli* gained more interest again as the demand in single-chain antibody fragments increased, which can be properly

expressed in *E. coli* [1,8]. The strain *BL21*(*DE3*), created by F. Studier and B. Moffatt back in 1986 [9], is often used in an industrial scale because of very low acetate formation, high replication rates as an effect of the integrated T7-polymerase [9–14], as well as the possibility of protein secretion into the fermentation broth due to a type 2 secretion protein [15–17]. As the lac operon is still one of the most favored promotors in pET-expression systems [3,12,18], it is generally used for insertion of the gene of interest. The repressor protein can only be blocked by allolactose or a structural analogue [19], e.g., the well-known inducer isopropyl β-D-1 thiogalactopyranoside (IPTG) [3,13]. However, induction with IPTG stresses the cells, as IPTG in higher concentrations is referred to be toxic at elevated induction times [13,18,20]. As tunable protein production is commonly applied in industry nowadays, mixed-feed systems using either IPTG [21] or lactose [13,22,23] as inducer did result in higher product yields when compared to other inducer supplies [24]. Soft induction performed with lactose shows promising results [13,23,25]. As lactose can be metabolized in *E. coli*, it does not stress the cells as much as IPTG [26]. For the production of soluble proteins, induction with lactose usually is preferred [3], but it has also been shown that lactose shows promising results for Inclusion Bodies (IBs) and products located in the periplasm [3,27].

IBs have originally been believed to be waste products by bacteria [28], until it was realized that IBs tend to form as a stress reaction by the cells resulting in a biologically inactive protein [29–31]. Stress reactions of the cells can be caused by high temperatures, pH-shifts, or due to high feeding rates. Higher feeding rates result in higher yields of product [1], which of course is advantageous when combined with the possibility of expressing toxic proteins [6]. Still, the downstream process (DSP), and especially the refolding unit operation, is the time-consuming step in gaining the correctly folded product from *E. coli* cultivations [28–31], which requires significantly more technology and time in purifying IBs [29,32,33]. Though IBs can be produced in such excess, the amount of generated product often outweighs the DSP efforts and makes the time-space yield more preferable for IBs [1,6,7,28].

One of the most favoured carbon sources in *E. coli* cultivations has always been glucose, as glucose has a very high affinity to the phosphotransferase system [34,35]. Glucose provides a lot of energy for the cells, as it is directly induced into glycolysis as glucose 6-phosphate and consumed through the tricarboxylic acid cycle (TCA) [35,36]. Usage of such, in combination with lactose, may result in diauxic growth and catabolite repression, which are caused by the regulatory network that is induced by glucose [37–39]. Catabolite repression results in decreased lactose uptake rates when glucose is present in excess [27,39,40]. Glycerol, first noticed in biotechnology as a by-product in the biodiesel production [41], has shown quite promising results in terms of biomass/substrate yield in *E. coli* cultivations [22,25]. To our knowledge, up to this point, no catabolic repression has been reported when glycerol was used as main carbon source (C-source) in combination with lactose [42]. In addition, mixtures of glucose, glycerol, and lactose have shown promising results for diverse products gained via autoinduction systems [20,25]. Recent studies [3,40] showed that the dependence of the inducer lactose influences the maximum IB production even on a quite low level of the specific glucose uptake rate. Low feeding rates of glucose would therefore result in the maximum inducer uptake rate, as cyclic adenosine monophosphate (cAMP) levels increase at higher glucose addition and therefore decrease the affinity for the RNA polymerase, decreasing the expression of the genes coding for the lac operon [35]. It is believed that cultivations with glycerol are able to overcome the problem of carbon catabolite repression and pave the way for usage of much higher specific C-source uptake rates, in order to increase time-space yields.

In this study, we performed cultivations with a *BL21*(*DE3*) strain, producing a recombinant protein coupled to a N-pro-fusion protein [43], expressed as IB with the goal to yield in maximum recombinant protein production. It is believed that glycerol causes positive results for the mixed-feed optimization when using lactose as an inducer, as glycerol—introduced into glycolysis but also into gluconeogenesis—yields a high amount of energy supplied to the cultivation system [42,44,45]. Couple that with increased cAMP levels throughout the whole cultivation, [35] glycerol is believed to

be beneficial over a glucose cultivation system. It is shown that the recombinant protein production is increased compared to glucose, as a result of more available energy.

2. Materials and Methods

2.1. Bioreactor Cultivations

All cultivations were carried out with the strain *E. coli BL21*(*DE3*) consisting of the pET-30a plasmid system. The eukaryotic target protein was linked to a N-pro fusion taq (size of 28.8 kDA for the fusion protein) [43]. As the given protein is currently under patenting procedure at the industrial partner no detailed information can be given on the used protein.

All bioreactor and preculture cultivations were carried out using a defined minimal medium referred to DeLisa et al. (2015) [5]. Batch media and the preculture media had the same composition with different amounts of sugars respectively. The sugar concentrations for the phases are presented in Table 1:

Table 1. Respective sugar concentrations in media composition.

	Amount of Glucose	Amount of Glycerol
Preculture	8.8 g/L	8.9 g/L
Batch-Media	22 g/L	23 g/L
Feed	either 250 g/L or 300 g/L	

As pET-30a has a Kanamycin resistance gene, antibiotic was added throughout all fermentations, resulting in a final concentration of 0.02 g/L. All precultures were performed using 500 mL high yield flasks (containing the sugar concentrations given in Table 1). They were inoculated with 1.5 mL of bacteria solution stored in cryos at −80 °C and subsequently cultivated for 20 h at 230 rpm in an Infors HR Multitron shaker (Infors, Bottmingen, Switzerland) at 37 °C.

All cultivations were either performed in a DASGIP Mini bioreactor-4-parallel fermenter system (max. working volume: 2.5 L; Eppendorf, Hamburg, Germany) or in a DASbox Mini Bioreactor 4-parallel fermenter system (max. working V.: 250 mL; Eppendorf, Hamburg, Germany). For measuring the CO_2 and O_2 flows, a DASGIP-GA gas analyser was used (Eppendorf, Hamburg, Germany). The cultivations were controlled using the provided DAS-GIP-control system, DASware-control, which logged the process parameters. During cultivation, pH was kept constant at 7.2 and controlled with base only (12.5% NH_4OH), while acid (10% H_3PO_4) was added manually, if necessary. The pH was monitored using a pH-sensor EasyFerm Plus (Hamilton, Reno, NV, USA). Base addition was monitored observing the flowrates of a DASbox MP8 Multipumpmodul. The reactors were continuously stirred at 1400 rpm.

Aeration was absolved using mixture of pressurized air and pure oxygen at 2 vvm, mixing the ratios of the airflow, so that the dissolved oxygen (dO_2) was always higher than 40%. The dissolved oxygen was monitored using a fluorescence dissolved oxygen electrode Visiferm DO 120 (Hamilton, Reno, NV, USA).

2.2. Cultivation Scheme and q_s Screening Procedure

The batch media in the DASGIP reactors always contained 1 L DeLisa medium, while the DASbox Mini bioreactors contained a volume of 100 mL.

Only static q_s-controls were performed for these experiments, as the $q_{s,C}$ was not altered during induction phase [3,27]. The procedure was always as follows: Preculture, Batch, non-induced fed-batch, and induced fed batch with an adapted $q_{s,C}$.

Inoculation was always done with one tenth of the batch media volume, resulting in 100 mL of preculture. Preculture showed an OD_{600} of approximately 7 after cultivation (described above). The batch process, performed at 37 °C, took around 6–7 h, depending on the C-source used, and was

finished, visible by a drop in the CO_2 signal. The 22 g/L of either glucose or glycerol usually resulted in a biomass of 9–10 g/L. After the batch was finished, a non-induced fed-batch was started overnight, at 35 °C and adapting the $q_{s,C}$ value to gain a biomass of approximately 30 g/L. After the non-induced fed-batch, the volume was always decreased to 1 L, in order to keep induction conditions the same. Afterwards, $q_{s,C}$ was adapted to a certain point of interest, and temperature was decreased to 30 °C and stabilized for 30 min before the inducer was added. Induction was always performed with a lactose pulse of 100 mL of a 300 g/L sterile lactose solution—resulting in a lactose concentration in the fermentation broth of approximately 30 g/L. Induction period always lasted 7 h. The q_s control used here was performed using Equation (1) according to an exponential feed forward approach to keep q_s constant [3,27,40,46]:

$$F(t) = \frac{q_{s,\,C} \times X(t) \times \rho_f}{c_f} \quad (1)$$

with F being the feed rate [g/h], $q_{s,C}$ the specific glucose or glycerol uptake rate [g/g/h], X(t) the absolute biomass [g], ρ_f the feed density [g/L], and c_f the feed concentration [g/L], respectively.

2.3. Process Analytics

Samples are always taken after inoculation, upon end of the batch-phase and after the non-induced fed-batch was finished. During the induction period, samples were either taken in 20 or 30 min intervals. Generally, biomass was measured using OD_{600} and dry cell weight (DCW), while flow cytometry analysis (FCM) was used for determination of cell-death, especially in the induction phase. Optical density (OD_{600}) was measured using a Genesys 20 photometer (Thermo Scientific, Waltham, MA, USA). Since the linear range of the used photometer is between 0.2 and 0.8 [AU], samples were diluted with dH_2O to stay within that range. The dry cell weight was determined by vortexing the sample, pipetting 1 mL of sample solution in a pre-tared 2 mL Eppendorf-Safe-Lock Tube (Eppendorf, Hamburg, Germany), and centrifuged for 10 min at 11,000 rpm at 4 °C. After centrifugation, the supernatant was used immediately for at-line high-pressure liquid chromatography (HPLC) measurement (see beneath), while the pellet was re-suspended with 1 mL of 0.9% NaCl solution and centrifuged at the same conditions. Afterwards, the pellet was dried for at least 72 h at 105 °C. Samples for FCM were diluted 1:100 with 0.9% NaCl solution, stored at 4 °C, and measured after the process was finished. The measurement was performed using the software Cube 8 (Sysmex, Partec, Görlitz, Germany) according to Langemann et al. [47] using $DiBAC_4(3)$ (bis-(1,3-dibutylbarbituricacid) trimethineoxonol) and Rh414 dye. Rh414 binds to the plasma membrane and visualizes all cells, while DiBAC is sensitive to plasma membrane potential, and therefore distinction between viable and non-viable cells can be achieved.

Product samples were taken for [P]-strain, after 2, 5 and 7 h of induction phase. They were always treated as follows: 5 mL pipetted in a 50 mL Falcon tube, centrifuged for 10 min at 4800 rpm at 4 °C. The supernatant was discarded while the pellet was frozen at −20 °C. Samples for homogenisation were disrupted as follows: The pellets were re-suspended in a Lysis buffer (0.1 M TRIS, 10 mM EDTA, pH = 7.4) according to its dry cell weight (Equation (2)):

$$\text{Volume Lysis Puffer} = \text{DCW} \times \frac{5}{4} \quad (2)$$

After suspending the cells, they were treated with an EmusiflexC3 Homogenizer (Avestin, Ottowa, ON, USA) at 1500 bar. The duration of homogenisation was always calculated to achieve ten passages through the homogenizer. After washing the pellets twice with dH_2O, the samples were measured using a HPLC method. The N-pro-fusion protein IB was measured via RP-HPLC (Thermo Scientific, Waltham, MA, USA) using a Nucleosil-column after solving in 7.5 M Guanidine Hydrochloride based buffer. The eluent was a gradient mixture of water with 0.1% TFA (tri-fluoric-acid) and Acetonitrile mixed with 0.1% TFA with a flow of 3 mL/min. Standard concentrations were 50, 140, 225, 320 and 500 mg/mL of an industrial supplied reference.

Sugar and glycerol concentrations were measured via HPLC-method (Thermo Scientific, Waltham, MA, USA) using a Supelcogel-column; Eluent: 0.1% H_3PO_4; Flow: 0.5 mL/min. Using this method, glucose or glycerol accumulation as well as the lactose decrease and the galactose accumulation could be detected. Standards had a concentration of 0.5, 1, 5, 10 and 20 g/L of every sugar used throughout all fermentations. The HPLC run lasted always for 25 min and chromatograms were analyzed using a Chromeleon Software (Dionex, Sunnyvale, CA, USA).

3. Results and Discussion

3.1. Mechanistic Correlations of Glycerol onto Specific Lactose Uptake Rate

The basic feeding rate for the induction phase for production of the recombined protein is a constant $q_{s,C}$—given by a fed-batch carried out on glucose or glycerol depending on the experiment—and by a pulse of 10 vol % high concentrated lactose feed.

In order to get comparable datasets for all experiments, a mechanistic model approach is performed. As shown in previous studies, the maximum possible specific lactose uptake rates depend on the specific glucose uptake rates which can be described by a mechanistic equation (see Equation (3)) [3,40]. The maximum $q_{s,lac}$ rates depend Monod-like on $q_{s,glu}$ until a certain maximum is reached at a respectively low feeding rate of glucose, before $q_{s,lac}$ decreases at high $q_{s,glu}$ which performs analogue to substrate inhibition [3]. Values for y = 0 correspond to the uptake rates on sole glucose/glycerol, respectively.

$$q_{s,lac} = q_{s,lac,max} \times \max\left(\left(1 - \frac{q_{s,glu}}{q_{s,glu,crit}}\right)^{n}, 0\right) \times \left(\frac{q_{s,glu}}{q_{s,glu} + K_A} + \frac{q_{s,lac,noglu}}{q_{s,lac,\ max}}\right) \quad (3)$$

with $q_{s,lac}$ being the specific lactose uptake rate [g/g/h], $q_{s,lac,max}$ the maximum specific lactose uptake rate [g/g/h], $q_{s,glu}$ the specific glucose uptake rate [g/g/h], $q_{s,glu,crit}$ the critical specific glucose uptake rate up to which lactose is consumed [g/g/h], $q_{s,lac,noglu}$ the specific lactose uptake rate at $q_{s,glu}$ = 0 [g/g/h], and K_A the affinity constant for the specific lactose uptake rate [g/g/h]. n describes the type of inhibition (non-competitive, uncompetitive, competitive).

As the model has already been established for four different products in glucose-lactose systems [40], it had to be shown if the same function fits for the given product. We fitted the model parameters as described in Wurm et al., where also a detailed description of the model derivation can be found [3]. As shown in Figure 1 and Table 2, parameters can be found to describe the experimental data for glucose and glycerol as C-source. In absence of glucose, lactose cannot be taken up, since there is not enough adenosine triphosphate (ATP) produced. Once a certain threshold of glucose is passed, enough ATP is created to metabolize the inducer [3,40]. The trend seen in the cultivations performed on glucose are explained by the well-known phenomenon of catabolite repression (CCR) [37,39], as the lactose uptake rates decrease significantly with increasing the feeding rate. As *E. coli BL21*(*DE3*) is not able to metabolize galactose due to absence of a (gal) gene, which can be referred to a deletion of the genes gal M, K, T, E [48,49], galactose should accumulate in the fermentation broth [37,50]. Hence, the galactose accumulation rate in the fermentation broth could generally be correlated to the lactose depletion rate during the cultivation (not shown).

However, the curves for glucose and glycerol are almost identical. Generally, a higher affinity for glucose is reported in literature [35], resulting in a higher μ for those cultivations, as glycerol has less affinity to the phosphotransferase system (PTS) [37]. This trend is in accordance with our data given in the value $q_{s,C,crit}$ in Table 2. Furthermore, biomass to substrate yields ($Y_{X/S}$) for glucose decrease in the induction phase from about 0.5 in the batch phase to about 0.336 $\pm$ 0.05 after the one-point lactose addition. By contrast, $Y_{X/S}$ of glycerol are generally about 0.44 $\pm$ 0.1 during the induction phase [51].

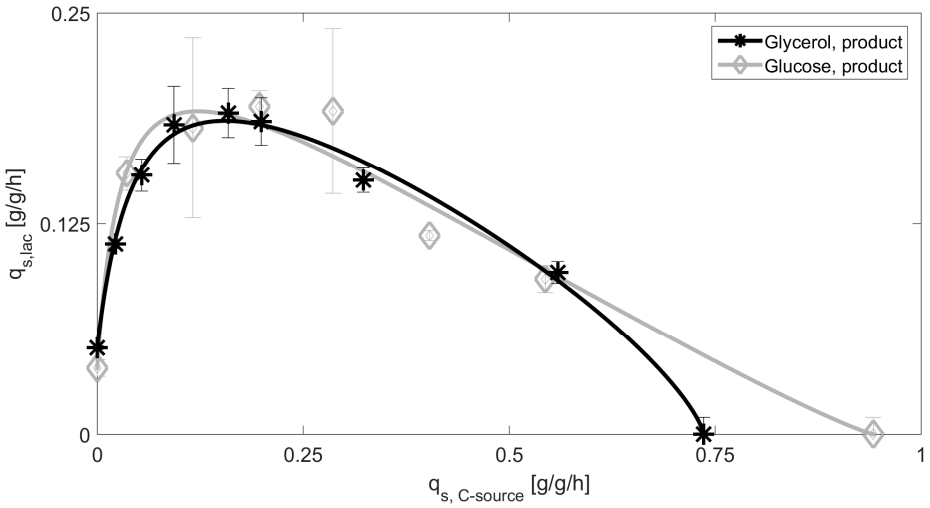

Figure 1. Extracted datapoints for q_s values including standard deviations for cultivations with glucose and glycerol in the production strain (glycerol product, glucose product). Solid lines represent the model based approach for inducer uptake rates vs. feeding rates models of glucose and glycerol.

Table 2. Model parameters and normalized-root-mean-square-error (NRMSE) for the different analysed cultivation with produced product (P).

Cultivation System	$q_{s,lac,max}$	K_A	$q_{s,C,crit}$	n	$q_{s,lac,noglu}$	NRMSE
	[g/g/h]	[g/g/h]	[g/g/h]	[-]	[g/g/h]	[%]
Glucose	0.23	0.032	0.94	1.14	0.039	6.5
Glycerol	0.23	0.053	0.74	0.74	0.051	2.6

This does not explain the very similar lactose uptake values at high $q_{s,C}$, since it is believed that carbon catabolite repression should not be present using glycerol as primary carbon source [52]. The production of the recombinant protein seems to induce stress resulting in the maximum possible activity inside the cell, which is represented by the similarity of the two curves. Therefore, the decrease of the $q_{s,lac}$ rate in the model-based approach actually referred to the CCR for glucose based systems so far ($\left(1-\frac{q_{s,glu}}{q_{s,glu,crit}}\right)^n$), may have to be reconsidered when glycerol is fed. In turn, our results would indicate that the decline cannot be attributed to carbon catabolite repression, also not for glucose. Glycerol does not interfere with the PTS transport system and no resulting change of the cAMP levels during uptake of lactose are to be believed on a first glance. Glycerol enters glycolysis as di-hydroxy-acetone-phosphate and is processed in glycolysis producing pyruvate, but also there are gluconeogenetic genes active providing the formation of glucose-6-phosphate [41,53,54]. As glycolysis seems to be running at maximum capacity, a bottleneck in the trycarboxylic acid (TCA) cycle may also be likely. Overload of the TCA cycle has already been described by Heyland et al. (2011) [55], saying that the TCA cycle cannot metabolize all the pyruvate produced in glycolysis. It has also been referred that the cells try to gain energy in alternative ways such as using acetate as a terminal electron acceptor, or the usage of oxidative phosphorylation [55,56]. However, as *E. coli BL21*(*DE3*) produces relatively low levels of acetate in general, the acetate formation is always beneath the threshold of the HPLC and may therefore not the predominant electron acceptor in this strain.

To test the observed effects, we tried a process technological method approach, rather than performing expensive and time consuming "omics" analysis. The pET-30a plasmid was transformed into the used strain *E. coli BL21*(*DE3*) without the sequence for the recombinant protein, further referred as non-producer (NP) strain. The strain was tested in the same analytical way as the used strain for recombinant protein production. HPLC raw data for lactose decrease are compared with an almost identical $q_{s,C}$ (~0,1 g/g/h) in Figure 2.

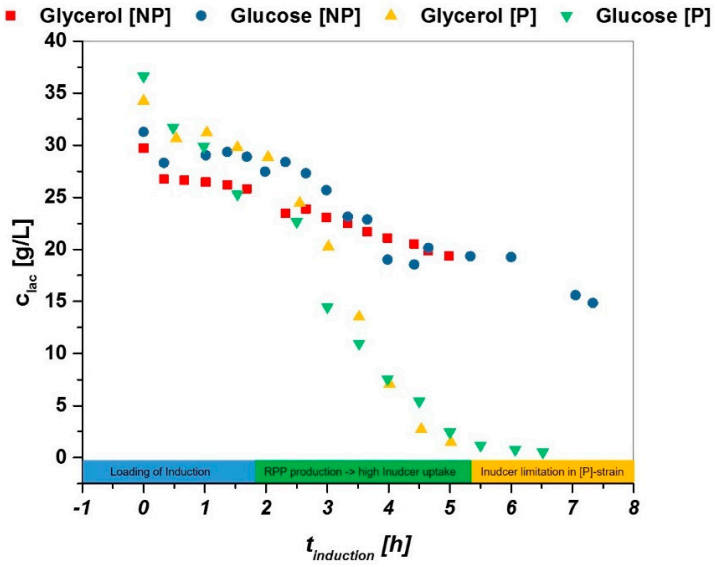

Figure 2. High-pressure liquid chromatography (HPLC)-based data for decrease of lactose in fermentation broth exhibiting very similar $q_{s,C}$ values in [g/L]. A significant decrease over the time of induction is visible in producing (P) strains, while the decrease is way slower in non-producing (NP)-strain-cultivations.

Hereby, three phases can be seen for the product producing strain in the induction phase, while only two phases can be seen in the NP strain:

(i) Adaption phase: lactose gets transferred to alloactose and loads the induction (0–2 h in induction phase).
(ii) Linear decrease of lactose as the system needs inducer for recombinant protein expression (2–5 h).
(iii) Limitation of lactose in P strain: not sufficient inducer present, need for mixed feed system (5–7 h), no inducer limitation seen in NP strain, further decrease of inducer analogue to phase 2.

Results on the model-based approach for the glucose system are given in Figure 3.

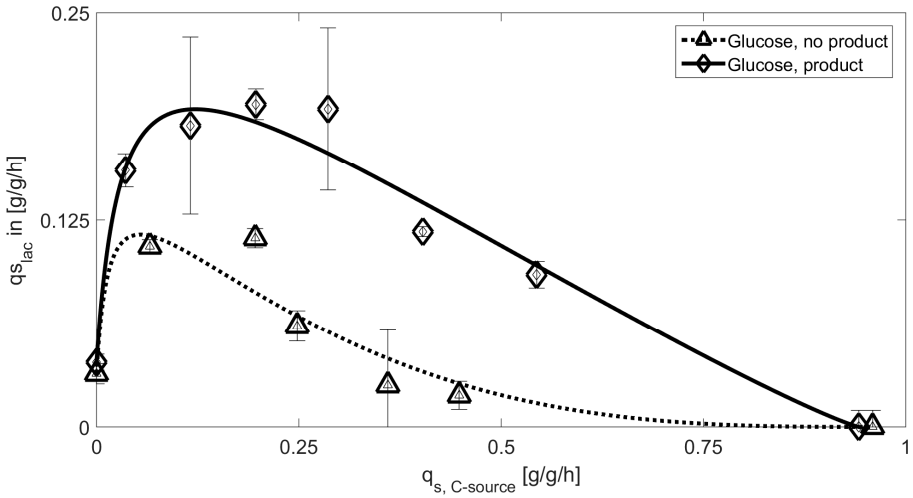

Figure 3. Extracted datapoints for $q_{s,C}$ values including standard deviations for cultivations with glucose using the product producing (glucose product) and the NP strain (glucose, no product). Solid lines represent the model based approach for inducer uptake rates vs. feeding rates models of glucose. A clearly visible difference can be observed during these cultivations.

The fermentations performed with the NP-strain showed lactose uptake rates resemble the expected carbon catabolite repression for glucose including high affinity of the PTS system at low $q_{s,glu}$ which can also be seen in Table 3. Despite the identical behavior of protein producing and NP strain, a clear difference in maximum $q_{s,lac}$ is obviously present. Higher consumption of glucose has impact on the cAMP level and decreases the specific uptake of lactose in the product producing strain. $Y_{X/S}$ stays very similar in both cases 0.37 ± 0.05 for the protein producing strain vs. 0.383 ± 0.053 for the NP strain. Given yields are a mean value over all $q_{s,C}$ values except for (lac) = 0 and (glu) = 0. So, these general deviations in $q_{s,lac,max}$ can be attributed to the increased energy demand during recombinant product production, as also the biomass yields stay the same. Lactose uptake rates on glycerol for the product producing and the NP strain are given in Figure 4. Despite the quite straightforward mechanistic explanation for glucose, glycerol biomass to substrate yields differ fundamentally for both experiments: $Y_{X/S} = 0.55 \pm 0.11$ for the NP strain, while the producing strain has a $Y_{X/S}$ of 0.44 ± 0.1. This fact may explain the much shallower uptake at low $q_{s,C}$ for the NP strain, but cannot explain the difference in the CCR term.

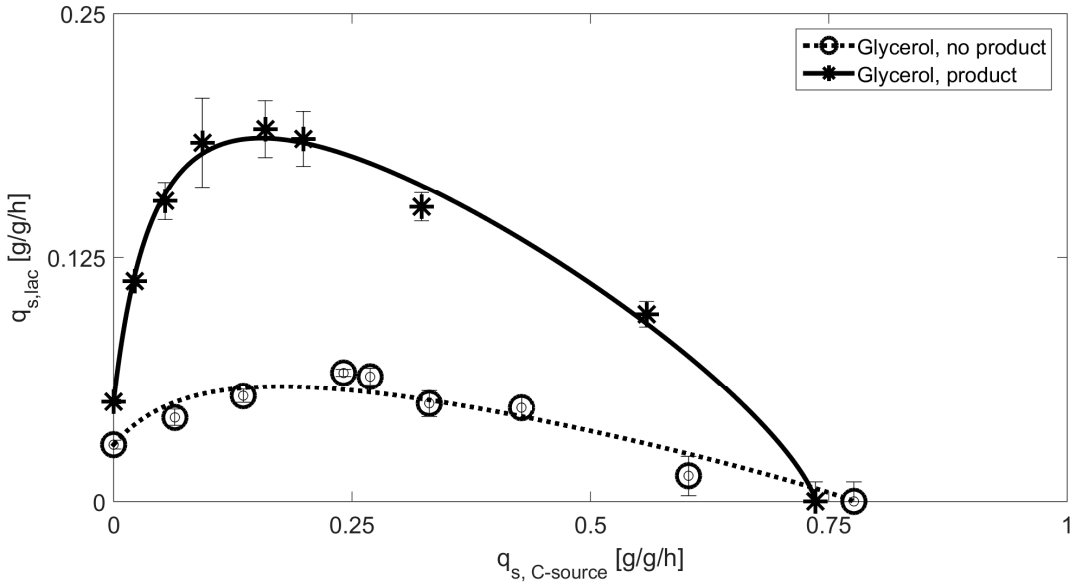

Figure 4. Extracted datapoints for $q_{s,C}$ values including standard deviations for cultivations with glycerol using the product producing (glycerol, product) and the NP strain (glycerol, no product). Solid lines represent the model based approach for inducer uptake rates vs. feeding rates models of glucose.

As a far higher biomass yield is present in the NP strain, only a reduced amount of lactose is taken up, which explains the decreased $q_{s,lac,max}$. However, the NP strain shows no pronounced substrate inhibition. The carbon catabolite repression term of the model on glycerol has only low impact (see Table 3), as the upregulation of cAMP using glycerol would also be beneficial for the lactose uptake mechanism in the PTS system [35]. Since the lactose facilitator is not considered to be the rate determining step in the glycerol metabolism, glycerol kinase closely regulated to the PTS system may cause the CCR-like effects [44,45]. As the feeding rate increases, the possibility of short-term local glucose and glycerol accumulation increases, eventually leading to diauxic growth and therefore decreased lactose rates as glucose and glycerol have higher affinity than disaccharides for *E. coli* [35,52,57,58]. The product-producing strain shows a high regulated lactose uptake at low $q_{s,C}$ values, as a result of lower biomass yield and higher energy demand in production of the recombinant protein. Higher lactose uptake results in high intracellular glucose level, which show the similar feedback mechanism like in the glucose fed cultivations.

Table 3. Model parameters and normalized-root-mean-square-error (NRMSE) for the analysed cultivation without recombinant product production (NP).

Cultivation System	$q_{s,lac,max}$ [g/g/h]	K_A [g/g/h]	$q_{s,glu,crit}$ [g/g/h]	n [-]	$q_{s,lac,noglu}$ [g/g/h]	NRMSE [%]
Glucose [NP]	0.14	0.016	0.96	2.92	0.032	12.7
Glycerol [NP]	0.10	0.13	0.78	0.90	0.029	9.7

As a result, both curves given in Figure 1 have a very similar appearance, but are expected to have a very different regulation within. To get insight into respiratory activity, qCO_2 values are compared for all four fermentations, respectively. Evaluation is given in Table 4 based on the applied $q_{s,C}$ values.

Table 4. Specific substrate uptake rate vs. specific carbon evolution rate. Product producing strains have in general increased respiratory activity. NP strains show reduced respiratory activity. Standard deviation of qCO_2 increases at higher feeding rates.

Glucose		Glucose NP		Glycerol		Glycerol NP	
$q_{s,C}$ [g/g/h]	qCO_2 [g/g/h]	$q_{s,C}$ [g/g/h]	qCO_2 [g/g/h]	$q_{s,C}$ [g/g/h]	qCO_2 [g/g/h]	$q_{s,C}$ [g/g/h]	qCO_2 [g/g/h]
0.036	2.15 ± 0.33	0.066	1.69 ± 0.25	0.022	2.91 ± 0.46	0.064	0.82 ± 0.09
0.116	3.12 ± 0.46	0.196	3.75 ± 0.44	0.054	4.41 ± 0.78	0.136	1.85 ± 0.21
0.197	3.98 ± 0.55	0.224	3.35 ± 0.42	0.093	3.88 ± 0.64	0.225	2.86 ± 0.31
0.286	5.72 ± 0.41	0.36	5.96 ± 0.26	0.159	3.12 ± 0.43	0.331	3.31 ± 0.22
0.403	6.42 ± 1.48	0.448	5.64 ± 0.47	0.199	4.14 ± 0.64	0.428	4.07 ± 0.51
0.544	7.30 ± 1.64			0.323	5.13 ± 0.48	0.603	1.75 ± 1.58
				0.559	7.18 ± 2.10		

Highly similar respiratory activity is received for the product producing strain, almost linear increasing with $q_{s,C}$. For the NP strain, a general lower respiratory activity is seen for the glycerol-fed strain. These results support the fact that lower energy demand is needed in this strain based on the general higher biomass yield and the fact that no recombinant protein is produced. In TCA, first steps of amino acid synthesis are performed, therefore the production of non-essential AA would result in the accumulation of NADH [59]. As approximately two NADH molecules can be formed to one molecule of CO_2 the enhanced respiratory activity in the product producing strain is most likely coding for the enhanced production of non-essential AA, which are essential for the recombinant product. However, further analysis on stress induced changes in the gene expression may give valuable new insights into regulation mechanism in *E. coli*.

3.2. Productivity and Physiology Using Glycerol as Primary Carbon Source

As the overall goal is an increased production rate of recombinant protein, we compare titers of the produced IBs as a function of carbon source and uptake rate. In Figure 5a, the increase in IB titer over time is presented for two cultivations. The loading of the induction, which takes about 2 h, can be clearly dedicated in these results, with no titer of the recombinant protein to be found within the first 2 h (also compare to Figure 2). Figure 5b shows product IB titers after 7 h induction time, which are plotted against the corresponding $q_{s,C}$. Only the feed rate of glucose/glycerol, adapted for the static experiment in the induced fed-batch phase, is used in this plot—as cultivations are induced with one lactose pulse only, the $q_{s,C}$ is a non-cumulative one. Generally, an increase in the feeding rate is beneficial for product formation. Cultivations carried out on glycerol tend to produce more recombinant protein with a product optimum at a q_s-glycerol-level seen around 0.3–0.35 g/g/h. It may be possible that even higher product titers can be found within the range of 0.3–0.55 g/g/h. Cultivations carried out on glucose also tend to produce more product when the feeding rate is shifted to rather high rates as well. Very similar IB titers can be obtained at high $q_{s,C}$ levels, but are far away from the observed maximum.

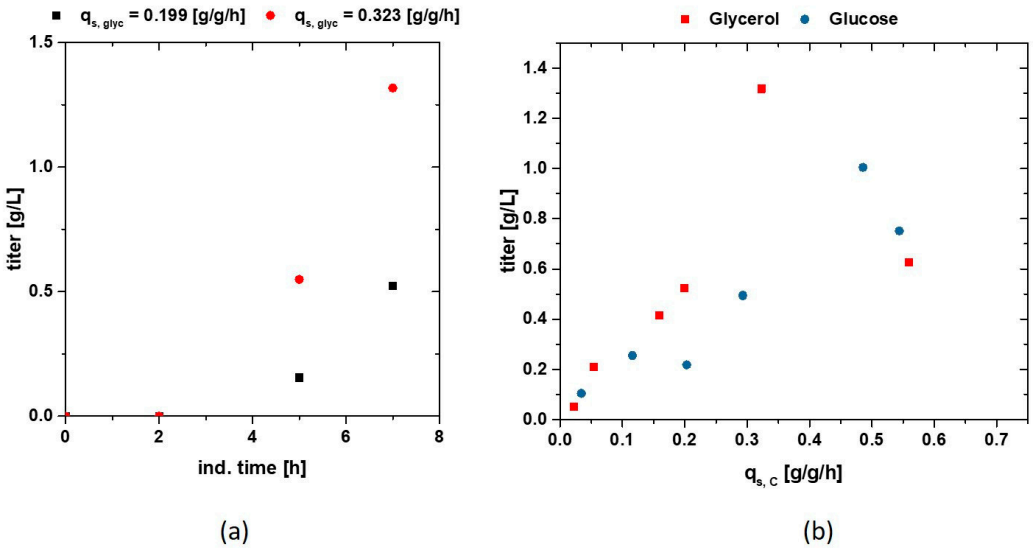

Figure 5. (**a**) Time dependence for two Inclusion Body (IB) titers starting from lactose addition to 7 h of induction; (**b**) Titers of the recombinant produced protein, after homogenisation of the inclusion bodies and a two-time washing plotted vs. the q_s of glucose and glycerol; A trend can be seen in gaining more product when cultivations are carried out on glycerol compared to glucose, respectively.

The high increase in titer as a function of $q_{s,C}$ in glycerol may be a result of the higher biomass (higher $Y_{X/S}$ during induction) usually present in glycerol fed induction phases. The phenomenon of high product formation rates at high feeding levels, was much to our surprise, as we expected to see enhanced stress reactions by the cells due to overfeeding—especially at later time stages—usually present in IPTG induced cultures. Though we see only very little levels of glucose or glycerol accumulation in our HPLC measurements (data not shown). This could be, as the fermentation conditions in the induction phase are respectively mild. Temperature is decreased to 30 °C and induction with lactose is regarded to be a softer induction than IPTG, as lactose can be metabolized by *E. coli* [22,23]. In literature, it has been reported that the catabolic repression increases with higher temperatures [60]. Altering the temperature in the induction phase would have probably led to very different results in lactose uptake rates as well as different product data. Also, we want to highlight that every induction here was only performed with a one-time lactose pulse, which is most likely an insufficient induction, as there may be too little inducer in the media, which can be seen in Figure 2. In the following development steps, mixed feeds using glycerol in combination with lactose must be established and measured as this would lead to a constant and complete induction of the system. However, the product data supports the results that most probably very different regulation mechanisms in *E. coli* lead to the same visible uptake rates in Figure 1, but have severe effects on the productivity on the different carbon sources.

Physiological analysis using flow cytometry (FCM) is presented in Figure 6a,b. The NP strain given in Figure 6a has very similar appearance for glucose and glycerol, respectively, increasing number of dead cells by increasing the feeding rate beyond a certain threshold, imposing stress to the cell. Throughout the whole experimental design, producing cells grown on glycerol exhibit a smaller cell size compared to cells grown on glucose (not shown). Since cell debris and residual particles are seen at similar cell sizes like glycerol grown cells a general higher abundance is present during those cultivations. To cope with this problem, FCM data after the non-induced fed-batch is subtracted from the subsequent measurements.

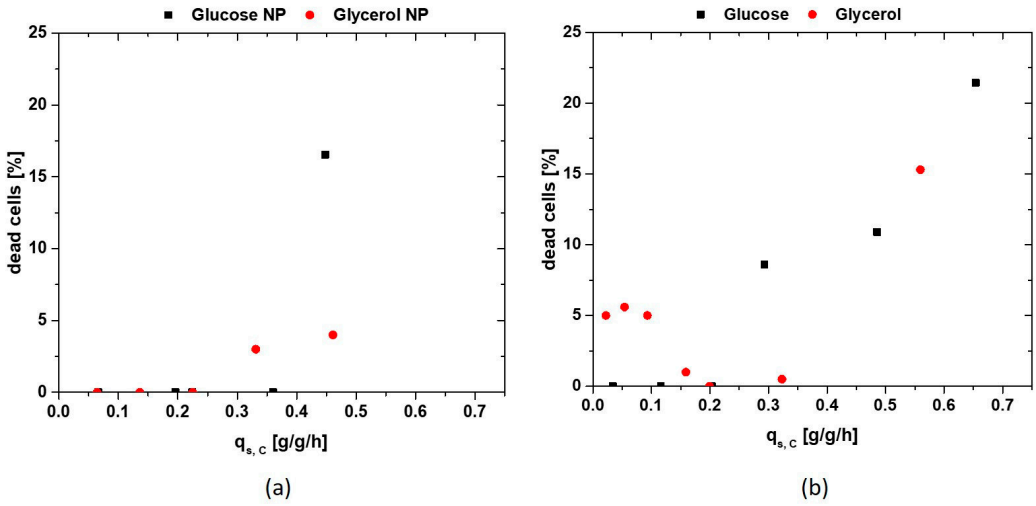

Figure 6. (**a**) Flow cytometry (FCM) analysis of NP strain 5 h after lactose pulse. As no protein data are received from these cultivations, the induction time was limited to 5 h; (**b**) FCM analysis of the product producing strain. Glycerol imposes stress at low feeding rates, while glucose shows increase in cell stress beginning at about 0.25 g/g/h.

The viability of both cultivation strategies for an induction time of 6 h—often used for IB production at industrial scale—is given in Figure 6b, with a strong contrast between glucose and glycerol. While cells fed with glucose show no cell lysis at low $q_{s,C}$ levels and are very similar to NP strain in Figure 6a, glycerol shows certain stress reaction resulting in about 5% dead cells until a 0.2 g/g/h. Afterwards, stable conditions for glycerol can be found, while stress is induced at glucose-fed systems starting at about 0.25 g/g/h. As the overnight fed-batch phase generally exhibited a q_s of 0.25 g/g/h, the switch to very low $q_{s,C}$ in the induction phase, combined with the lactose pulse, may impose the cell stress seen in 5% dead cells in Figure 6b. This corresponds well to the product data in Figure 5 with similar or even higher productivity of glucose at low $q_{s,C}$ levels, but higher productivity for glycerol at moderate to high levels. Including the fact that glycerol shows higher biomass yields during induction with lactose, glycerol may be well used as an alternative main carbon source in *E. coli* cultivations, even though glucose has high affinity to the phosphotransferase system (PTS). It has already been reported that addition of glycerol to a glucose-lactose induction system increases product formation [20,61]. As glycerol needs increased cAMP levels, which are also needed for lactose uptake [37], this might be a key function in regulating higher lactose uptake and subsequently increasing productivity and product titer.

Furthermore, as glycerol is a cheap media compared to glucose, an application of glycerol in mixed-feed system with lactose may be highly beneficial for recombinant protein production performed in industry.

4. Conclusions

In this work, the effects of glycerol or glucose on lactose uptake rates for an IB-based process using *E. coli BL21*(*DE*3) were investigated. Feeding and uptake rates are compared and evaluated in terms of productivity and physiology using FCM.

It is shown that both C-sources show identical lactose uptake rates as a function of $q_{s,C}$. The used model-based approach already performed for different products in Wurm et al. [40] can be used for description of both curves. It has been detected that glycerol is beneficial over the usage of glucose for maximising the recombinant protein production of a lactose induced system.

Glycerol and glucose most probably exhibit different regulation of the carbon catabolite repression—the reduction of lactose uptake at higher $q_{s,C}$ levels. This hypothesis is supported by cultivation and evaluation of a non-producer strain exhibiting the expected behaviour for both

C-sources, respectively. As this behaviour was not seen in the producing strain, it seems like the expression hosts are performing at maximum capacity in recombinant protein production. Additionally, glycerol is referred to different metabolic pathways [42], eventually increasing the metabolic flux [55] towards recombinant protein production.

Physiology and productivity support the hypothesis that glycerol is promising C-source for cultivations using mixed feed systems with moderate to high $q_{s,C}$ values in order to boost time-space yields. As scale-up in *E. coli* systems can be performed relatively easily [1], the much lower costs of glycerol, when compared to glucose respectively, might provide interesting options for industrial and other large scale applications.

Acknowledgments: We gratefully thank the Christian Doppler Society for the funding of this work.

Author Contributions: Julian Kopp performed and cultivations, and calculated the q_s-q_s-curves, Christoph Slouka performed the purification and the analysis of product data (These authors contributed equally to this work). Julian Kager supported during the cultivations. Sophia Ulonska is responsible for the model evaluation. Jens Fricke, Oliver Spadiut and Christoph Herwig gave valuable information for drafting this paper and helped during preparation.

Conflicts of Interest: The authors declare no conflict of interest.

References

1. Gupta, S.K.; Shukla, P. Microbial platform technology for recombinant antibody fragment production: A review. *Crit. Rev. Microbiol.* **2017**, *43*, 31–42. [CrossRef] [PubMed]
2. Walsh, G. Biopharmaceutical benchmarks 2010. *Nat. Biotechnol.* **2010**, *28*, 917–924. [CrossRef] [PubMed]
3. Wurm, D.J.; Veiter, L.; Ulonska, S.; Eggenreich, B.; Herwig, C.; Spadiut, O. The *E. coli* pET expression system revisited-mechanistic correlation between glucose and lactose uptake. *Appl. Microbiol. Biotechnol.* **2016**, *100*, 8721–8729. [CrossRef] [PubMed]
4. Meuris, L.; Santens, F.; Elson, G.; Festjens, N.; Boone, M.; Dos Santos, A.; Devos, S.; Rousseau, F.; Plets, E.; Houthuys, E.; et al. GlycoDelete engineering of mammalian cells simplifies N-glycosylation of recombinant proteins. *Nat. Biotechnol.* **2014**, *32*, 485–489. [CrossRef] [PubMed]
5. DeLisa, M.P.; Li, J.; Rao, G.; Weigand, W.A.; Bentley, W.E. Monitoring GFP-operon fusion protein expression during high cell density cultivation of Escherichia coli using an on-line optical sensor. *Biotechnol. Bioeng.* **1999**, *65*, 54–64. [CrossRef]
6. Berlec, A.; Strukelj, B. Current state and recent advances in biopharmaceutical production in *Escherichia coli*, yeasts and mammalian cells. *J. Ind. Microbiol. Biotechnol.* **2013**, *40*, 257–274. [CrossRef] [PubMed]
7. Baeshen, M.N.; Al-Hejin, A.M.; Bora, R.S.; Ahmed, M.M.; Ramadan, H.A.; Saini, K.S.; Baeshen, N.A.; Redwan, E.M. Production of Biopharmaceuticals in *E. coli*: Current Scenario and Future Perspectives. *J. Microbiol. Biotechnol.* **2015**, *25*, 953–962. [CrossRef] [PubMed]
8. Spadiut, O.; Capone, S.; Krainer, F.; Glieder, A.; Herwig, C. Microbials for the production of monoclonal antibodies and antibody fragments. *Trends Biotechnol.* **2014**, *32*, 54–60. [CrossRef] [PubMed]
9. Studier, F.W.; Moffatt, B.A. Use of bacteriophage T7 RNA polymerase to direct selective high-level expression of cloned genes. *J. Mol. Biol.* **1986**, *189*, 113–130. [CrossRef]
10. Steen, R.; Dahlberg, A.E.; Lade, B.N.; Studier, F.W.; Dunn, J.J. T7 RNA polymerase directed expression of the Escherichia coli rrnB operon. *EMBO J.* **1986**, *5*, 1099–1103. [PubMed]
11. Studier, F.W.; Rosenberg, A.H.; Dunn, J.J.; Dubendorff, J.W. Use of T7 RNA polymerase to direct expression of cloned genes. *Methods Enzymol.* **1990**, *185*, 60–89. [PubMed]
12. Dubendorff, J.W.; Studier, F.W. Controlling basal expression in an inducible T7 expression system by blocking the target T7 promoter with lac repressor. *J. Mol. Biol.* **1991**, *219*, 45–59. [CrossRef]
13. Neubauer, P.; Hofmann, K. Efficient use of lactose for the lac promoter-controlled overexpression of the main antigenic protein of the foot and mouth disease virus in Escherichia coli under fed-batch fermentation conditions. *FEMS Microbiol. Rev.* **1994**, *14*, 99–102. [CrossRef] [PubMed]
14. Lyakhov, D.L.; He, B.; Zhang, X.; Studier, F.W.; Dunn, J.J.; McAllister, W.T. Pausing and termination by bacteriophage T7 RNA polymerase. *J. Mol. Biol.* **1998**, *280*, 201–213. [CrossRef] [PubMed]

15. Jeong, H.; Barbe, V.; Lee, C.H.; Vallenet, D.; Yu, D.S.; Choi, S.H.; Couloux, A.; Lee, S.W.; Yoon, S.H.; Cattolico, L.; et al. Genome sequences of *Escherichia coli* B strains REL606 and BL21(DE3). *J. Mol. Biol.* **2009**, *394*, 644–652. [CrossRef] [PubMed]
16. Jeong, H.; Kim, H.J.; Lee, S.J. Complete Genome Sequence of *Escherichia coli* Strain BL21. *Genome Announc.* **2015**, *3*, e00134-15. [CrossRef] [PubMed]
17. Tseng, T.T.; Tyler, B.M.; Setubal, J.C. Protein secretion systems in bacterial-host associations, and their description in the Gene Ontology. *BMC Microbiol.* **2009**, *9* (Suppl. 1), S2. [CrossRef] [PubMed]
18. Marbach, A.; Bettenbrock, K. Lac operon induction in *Escherichia coli*: Systematic comparison of IPTG and TMG induction and influence of the transacetylase LacA. *J. Biotechnol.* **2012**, *157*, 82–88. [CrossRef] [PubMed]
19. Keiler, K.C. Biology of trans-translation. *Annu. Rev. Microbiol.* **2008**, *62*, 133–151. [CrossRef] [PubMed]
20. Viitanen, M.I.; Vasala, A.; Neubauer, P.; Alatossava, T. Cheese whey-induced high-cell-density production of recombinant proteins in *Escherichia coli*. *Microb. Cell Fact.* **2003**, *2*, 2. [CrossRef] [PubMed]
21. Marisch, K.; Bayer, K.; Cserjan-Puschmann, M.; Luchner, M.; Striedner, G. Evaluation of three industrial *Escherichia coli* strains in fed-batch cultivations during high-level SOD protein production. *Microb. Cell Fact.* **2013**, *12*, 58. [CrossRef] [PubMed]
22. Ukkonen, K.; Mayer, S.; Vasala, A.; Neubauer, P. Use of slow glucose feeding as supporting carbon source in lactose autoinduction medium improves the robustness of protein expression at different aeration conditions. *Protein Expr. Purif.* **2013**, *91*, 147–154. [CrossRef] [PubMed]
23. Neubauer, P.; Hofmann, K.; Holst, O.; Mattiasson, B.; Kruschke, P. Maximizing the expression of a recombinant gene in *Escherichia coli* by manipulation of induction time using lactose as inducer. *Appl. Microbiol. Biotechnol.* **1992**, *36*, 739–744. [CrossRef] [PubMed]
24. Marschall, L.; Sagmeister, P.; Herwig, C. Tunable recombinant protein expression in *E. coli*: Enabler for continuous processing? *Appl. Microbiol. Biotechnol.* **2016**, *100*, 5719–5728. [CrossRef] [PubMed]
25. Blommel, P.G.; Becker, K.J.; Duvnjak, P.; Fox, B.G. Enhanced bacterial protein expression during auto-induction obtained by alteration of lac repressor dosage and medium composition. *Biotechnol. Prog.* **2007**, *23*, 585–598. [CrossRef] [PubMed]
26. Dvorak, P.; Chrast, L.; Nikel, P.I.; Fedr, R.; Soucek, K.; Sedlackova, M.; Chaloupkova, R.; de Lorenzo, V.; Prokop, Z.; Damborsky, J. Exacerbation of substrate toxicity by IPTG in *Escherichia coli* BL21(DE3) carrying a synthetic metabolic pathway. *Microb. Cell Fact.* **2015**, *14*, 201. [CrossRef] [PubMed]
27. Wurm, D.J.; Herwig, C.; Spadiut, O. How to Determine Interdependencies of Glucose and Lactose Uptake Rates for Heterologous Protein Production with *E. coli*. *Methods Mol. Biol.* **2017**, *1586*, 397–408. [PubMed]
28. García-Fruitós, E.; Vázquez, E.; Díez-Gil, C.; Corchero, J.L.; Seras-Franzoso, J.; Ratera, I.; Veciana, J.; Villaverde, A. Bacterial inclusion bodies: Making gold from waste. *Trends Biotechnol.* **2012**, *30*, 65–70. [CrossRef] [PubMed]
29. Palmer, I.; Wingfield, P.T. Preparation and extraction of insoluble (inclusion-body) proteins from *Escherichia coli*. *Curr. Protoc. Protein Sci.* **2012**. [CrossRef]
30. Ramón, A.; Señorale-Pose, M.; Marín, M. Inclusion bodies: Not that bad . . . . *Front. Microbiol.* **2014**, *5*, 56. [CrossRef] [PubMed]
31. Villaverde, A.; Corchero, J.L.; Seras-Franzoso, J.; Garcia-Fruitós, E. Functional protein aggregates: Just the tip of the iceberg. *Nanomedicine (Lond.)* **2015**, *10*, 2881–2891. [CrossRef] [PubMed]
32. Wingfield, P.T.; Palmer, I.; Liang, S.M. Folding and Purification of Insoluble (Inclusion Body) Proteins from *Escherichia coli*. *Curr. Protoc. Protein Sci.* **2014**. [CrossRef]
33. Wingfield, P.T. Preparation of Soluble Proteins from *Escherichia coli*. *Curr. Protoc. Protein Sci.* **2014**, *78*, 6.2.1–6.2.22. [PubMed]
34. Postma, P.W.; Lengeler, J.W.; Jacobson, G.R. Phosphoenolpyruvate:carbohydrate phosphotransferase systems of bacteria. *Microbiol. Rev.* **1993**, *57*, 543–594. [PubMed]
35. Deutscher, J.; Francke, C.; Postma, P.W. How phosphotransferase system-related protein phosphorylation regulates carbohydrate metabolism in bacteria. *Microbiol. Mol. Biol. Rev.* **2006**, *70*, 939–1031. [CrossRef] [PubMed]
36. Ronimus, R.S.; Morgan, H.W. Distribution and phylogenies of enzymes of the Embden-Meyerhof-Parnas pathway from archaea and hyperthermophilic bacteria support a gluconeogenic origin of metabolism. *Archaea* **2003**, *1*, 199–221. [CrossRef] [PubMed]

37. Bettenbrock, K.; Fischer, S.; Kremling, A.; Jahreis, K.; Sauter, T.; Gilles, E.D. A quantitative approach to catabolite repression in *Escherichia coli*. *J. Biol. Chem.* **2006**, *281*, 2578–2584. [CrossRef] [PubMed]
38. Kremling, A.; Bettenbrock, K.; Laube, B.; Jahreis, K.; Lengeler, J.W.; Gilles, E.D. The organization of metabolic reaction networks. III. Application for diauxic growth on glucose and lactose. *Metab. Eng.* **2001**, *3*, 362–379. [CrossRef] [PubMed]
39. Stülke, J.; Hillen, W. Carbon catabolite repression in bacteria. *Curr. Opin. Microbiol.* **1999**, *2*, 195–201. [CrossRef]
40. Wurm, D.J.; Hausjell, J.; Ulonska, S.; Herwig, C.; Spadiut, O. Mechanistic platform knowledge of concomitant sugar uptake in *Escherichia coli* BL21(DE3) strains. *Sci. Rep.* **2017**, *7*, 45072. [CrossRef] [PubMed]
41. Martínez-Gómez, K.; Flores, N.; Castañeda, H.M.; Martínez-Batallar, G.; Hernández-Chávez, G.; Ramírez, O.T.; Gosset, G.; Encarnación, S.; Bolivar, F. New insights into *Escherichia coli* metabolism: Carbon scavenging, acetate metabolism and carbon recycling responses during growth on glycerol. *Microb. Cell Fact.* **2012**, *11*, 46. [CrossRef] [PubMed]
42. Lin, E.C. Glycerol dissimilation and its regulation in bacteria. *Annu. Rev. Microbiol.* **1976**, *30*, 535–578. [CrossRef] [PubMed]
43. Achmüller, C.; Kaar, W.; Ahrer, K.; Wechner, P.; Hahn, R.; Werther, F.; Schmidinger, H.; Cserjan-Puschmann, M.; Clementschitsch, F.; Striedner, G.; et al. N(pro) fusion technology to produce proteins with authentic N termini in *E. coli*. *Nat. Methods* **2007**, *4*, 1037–1043. [CrossRef] [PubMed]
44. Zwaig, N.; Kistler, W.S.; Lin, E.C. Glycerol kinase, the pacemaker for the dissimilation of glycerol in *Escherichia coli*. *J. Bacteriol.* **1970**, *102*, 753–759. [PubMed]
45. Voegele, R.T.; Sweet, G.D.; Boos, W. Glycerol kinase of *Escherichia coli* is activated by interaction with the glycerol facilitator. *J. Bacteriol.* **1993**, *175*, 1087–1094. [CrossRef] [PubMed]
46. Slouka, C.; Wurm, D.J.; Brunauer, G.; Welzl-Wachter, A.; Spadiut, O.; Fleig, J.; Herwig, C. A Novel Application for Low Frequency Electrochemical Impedance Spectroscopy as an Online Process Monitoring Tool for Viable Cell Concentrations. *Sensors (Basel)* **2016**, *16*, 1900. [CrossRef] [PubMed]
47. Langemann, T.; Mayr, U.B.; Meitz, A.; Lubitz, W.; Herwig, C. Multi-parameter flow cytometry as a process analytical technology (PAT) approach for the assessment of bacterial ghost production. *Appl. Microbiol. Biotechnol.* **2016**, *100*, 409–418. [CrossRef] [PubMed]
48. Xu, J.; Banerjee, A.; Pan, S.H.; Li, Z.J. Galactose can be an inducer for production of therapeutic proteins by auto-induction using *E. coli* BL21 strains. *Protein Expr. Purif.* **2012**, *83*, 30–36. [CrossRef] [PubMed]
49. Studier, F.W.; Daegelen, P.; Lenski, R.E.; Maslov, S.; Kim, J.F. Understanding the differences between genome sequences of *Escherichia coli* B strains REL606 and BL21(DE3) and comparison of the *E. coli* B and K-12 genomes. *J. Mol. Biol.* **2009**, *394*, 653–680. [CrossRef] [PubMed]
50. Daegelen, P.; Studier, F.W.; Lenski, R.E.; Cure, S.; Kim, J.F. Tracing ancestors and relatives of *Escherichia coli* B, and the derivation of B strains REL606 and BL21(DE3). *J. Mol. Biol.* **2009**, *394*, 634–643. [CrossRef] [PubMed]
51. Korz, D.J.; Rinas, U.; Hellmuth, K.; Sanders, E.A.; Deckwer, W.D. Simple fed-batch technique for high cell density cultivation of *Escherichia coli*. *J. Biotechnol.* **1995**, *39*, 59–65. [CrossRef]
52. Inada, T.; Kimata, K.; Aiba, H. Mechanism responsible for glucose-lactose diauxie in *Escherichia coli*: Challenge to the cAMP model. *Genes Cells* **1996**, *1*, 293–301. [CrossRef] [PubMed]
53. Larson, T.J.; Ye, S.Z.; Weissenborn, D.L.; Hoffmann, H.J.; Schweizer, H. Purification and characterization of the repressor for the sn-glycerol 3-phosphate regulon of *Escherichia coli* K12. *J. Biol. Chem.* **1987**, *262*, 15869–15874. [PubMed]
54. Iuchi, S.; Cole, S.T.; Lin, E.C. Multiple regulatory elements for the glpA operon encoding anaerobic glycerol-3-phosphate dehydrogenase and the glpD operon encoding aerobic glycerol-3-phosphate dehydrogenase in *Escherichia coli*: Further characterization of respiratory control. *J. Bacteriol.* **1990**, *172*, 179–184. [CrossRef] [PubMed]
55. Heyland, J.; Blank, L.M.; Schmid, A. Quantification of metabolic limitations during recombinant protein production in *Escherichia coli*. *J. Biotechnol.* **2011**, *155*, 178–184. [CrossRef] [PubMed]
56. Glick, B.R. Metabolic load and heterologous gene expression. *Biotechnol. Adv.* **1995**, *13*, 247–261. [CrossRef]
57. Weissenborn, D.L.; Wittekindt, N.; Larson, T.J. Structure and regulation of the glpFK operon encoding glycerol diffusion facilitator and glycerol kinase of *Escherichia coli* K-12. *J. Biol. Chem.* **1992**, *267*, 6122–6131. [PubMed]

58. Hogema, B.M.; Arents, J.C.; Bader, R.; Postma, P.W. Autoregulation of lactose uptake through the LacY permease by enzyme IIAGlc of the PTS in *Escherichia coli* K-12. *Mol. Microbiol.* **1999**, *31*, 1825–1833. [CrossRef] [PubMed]
59. Berg, J.M.; Tymoczko, J.L.; Stryer, L. *Biochemistry*, 5th ed.; W. H. Freeman: New York, NY, USA, 2002.
60. Marr, A.G.; Ingraham, J.L.; Squires, C.L. Effect of the temperature of growth of *Escherichia coli* on the formation of beta-galactosidase. *J. Bacteriol.* **1964**, *87*, 356–362. [PubMed]
61. Mayer, S.; Junne, S.; Ukkonen, K.; Glazyrina, J.; Glauche, F.; Neubauer, P.; Vasala, A. Lactose autoinduction with enzymatic glucose release: Characterization of the cultivation system in bioreactor. *Protein Expr. Purif.* **2014**, *94*, 67–72. [CrossRef] [PubMed]

chemosensors

MDPI

Article

Low-Frequency Electrochemical Impedance Spectroscopy as a Monitoring Tool for Yeast Growth in Industrial Brewing Processes

Christoph Slouka [1,*], Georg Christoph Brunauer [2], Julian Kopp [1], Michael Strahammer [1], Jens Fricke [1], Jürgen Fleig [3] and Christoph Herwig [1]

1 Christian Doppler Laboratory for Mechanistic and Physiological Methods for Improved Bioprocesses, Institute of Chemical, Environmental and Biological Engineering, TU Wien, Vienna 1060, Austria; julian.kopp@aon.at (J.K.); michael.strahammer@stud.fh-campuswien.ac.at (M.S.); jens.fricke@tuwien.ac.at (J.F.); christoph.herwig@tuwien.ac.at (C.H.)

2 Institute for Energy Systems and Thermodynamics, TU Wien, Vienna 1060, Austria; georg.brunauer@tuwien.ac.at

3 Research Division Electrochemistry, Institute of Chemical Technology and Analytics, TU Wien, Vienna 1060, Austria; juergen.fleig@tuwien.ac.at

* Correspondence: christoph.slouka@tuwien.ac.at; Tel.: +43-699-1267-1472

Received: 24 May 2017; Accepted: 1 August 2017; Published: 3 August 2017

Abstract: Today's yeast total biomass and viability measurements during the brewing process are dependent on offline methods such as methylene blue or florescence dye-based staining, and/or the usage of flow cytometric measurements. Additionally, microscopic cell counting methods decelerate an easy and quick prediction of yeast viability. These processes are time consuming and result in a time-delayed response signal, which not only reduces the knowledge of the performance of the yeast itself, but also impacts the quality of the final product. Novel approaches in process monitoring during the aerobic and anaerobic fermentation of *Saccharomyces cerevisiae* are not only limited to classical pH, dO_2 and off-gas analysis, but they also use different in situ and online sensors based on different physical principles to determine the biomass, product quality and cell death. Within this contribution, electrochemical impedance spectroscopy (EIS) was used to monitor the biomass produced in aerobic and anaerobic batch cultivation approaches, simulating the propagation and fermentation unit operation of industrial brewing processes. Increases in the double-layer capacitance (C_{DL}), determined at frequencies below 1 kHz, were proportional to the increase of biomass in the batch, which was monitored in the online and inline mode. A good correlation of C_{DL} with the cell density was found. In order to prove the robustness and flexibility of this novel method, different state-of-the-art biomass measurements (dry cell weight—DCW and optical density—OD) were performed for comparison. Because measurements in this frequency range are largely determined by the double-layer region between the electrode and media, rather minor interferences with process parameters (aeration and stirring) were to be expected. It is shown that impedance spectroscopy at low frequencies is not only a powerful tool for the monitoring of viable yeast cell concentrations during operation, but it is also perfectly suited to determining physiological states of the cells, and may facilitate biomass monitoring in the brewing and yeast-propagating industry drastically.

Keywords: brewing; *S. cerevisiae*; electrochemical impedance spectroscopy; fermentation technology; inline sensors

1. Introduction

Microbial cultivations play a key role in many different fields, such as in food, drug and bulk chemical production, as well as in waste-to-value concepts [1]. Process monitoring, such as pH, dissolved oxygen (dO_2) and off-gas analysis, is state of the art in today's industrial cultivations for guaranteeing product quality and safety. However, the most important parameter in bioprocesses, the biomass, can only be determined using offline methods or complex soft-sensor applications [2]. These control systems are often dependent on inline/online/at-line detection systems, such as high-performance liquid chromatography (HPLC) for metabolites, off-gas balance, and/or dielectric spectroscopy measurements. The use of accurate and reliable biomass measurement systems [3,4], especially of viable cell concentrations (VCCs), enables proper process control tools, which lead subsequently to more robust and reliable bioprocesses. The VCC is measured using offline measurement principles including marker proteins or fluorescence probes, such as flow cytometry or confocal microscopy [5,6]. Because these control and analytical tools are cost intensive, classical bulk food products—such as yeast and beer—are produced in rather uncontrolled environments. Not only the complex raw material, but especially growth conditions of the yeast (propagation and fermentation) are of high importance for the quality of the final product. The implementation of online vitality measurements in the brewing industry has historically been hindered by affordable, simple, robust and reproducible tests [7].

In general, online and inline biomass measurement approaches are rather scarce and are based on physical measurement principles. One principle generally applied is high-frequency alternating current (AC) impedance spectroscopy with high field amplitudes, used on the basis of the ß-dispersion [8,9]. Cells with an integer cell membrane affect the relative permittivity between two electrodes and, therefore, this signal is used for the estimation of VCCs. A detailed description of the measurement principles can be found in [10–13].

The model organism for the application of AC measurements in the ß-dispersion range is yeast, being a very important expression host for recombinant proteins [14–16]. Additionally, approaches towards more complex expression systems, such as filamentous fungi and Chinese hamster ovary (CHO) cells, are already performed [17–19]. These measurements show a strong dependence upon physical process parameters (such as aeration and stirring—causing gas bubbles, temperature shifts and pH gradients), and are furthermore highly affected by changes in the media's composition during cultivation.

However, not only high-frequency impedance spectroscopy in the ß-range can be used for the determination of biomass, but changes of the electrical double layer by the adsorption/desorption of cells at the electrode surface (detectable at low frequencies in the mHz range; α-dispersion) can also provide valuable information. Besides the cell type itself (cell wall/membrane compositions, size and shape), many physical parameters, especially in the media (pH and ion concentrations), can influence the potential distribution in the double layer [20,21]. Furthermore, the given method via α-dispersion detection is capable of detecting even very small numbers of bacteria in soil, food and feces-polluted water using interdigitated microelectrode designs [22–27]. These studies were only performed at a very small scale and with a low cell concentration. In general, a threshold in the measurement was present at low cell concentrations. Exceeding this limitation, over time, very stable signals were achieved in these studies. Besides direct measurements in the broth, a modified electrode system in an interdigitated design can be used [28–30]. First approaches towards process monitoring were shown by Kim et al. [31], who worked with an inline sensor used in the lower frequency range between 40 Hz and 10 kHz for the real-time monitoring of biomass. Kim et al. showed the feasibility for measuring changes in the double-layer capacitance (C_{DL}), but no analysis of the C_{DL} itself was performed; only discrete extracted values for distinct frequency values were used. Recent studies on *Escherichia coli* showed reasonable results for VCC determination not only in the batch phase, but also in the fed-batch approaches, leading to far higher cell densities [32].

In this study, impedance measurements in the α-dispersion range were performed during the batch-based cultivation of *Saccharomyces cerevisiae* aimed for usage in brewing applications. Different

state-of-the-art methods were applied for determination of the corresponding total biomass—dry cell weight (DCW) and optical density (OD_{610}) offline. Flow cytometry (FCM) in combination with the fluorescence dye (bis-(1,3-dibutylbarbituricacid)trimethineoxonol) (DiBAC) was used for a cell physiology evaluation to account for changes in the viability during cultivation. With this knowledge, we were able to correlate the total biomass to the extracted C_{DL}.

A prototype inline probe was designed and built for easy plug-in measurements of the biomass. Online and new inline probes were tested using defined media with glucose and maltose in different concentrations and with malt extract as the complex base material in brewing.

2. Materials and Methods

2.1. Expression Host and Cultivation

All cultivations were performed using the *S. cerevisiae* strain, supplied by Brauerei GUSSWERK (Salzburg, Austria). For the preculture, 500 mL of sterile Delft medium was inoculated from frozen stocks (1.5 mL; −80 °C) and incubated in a 2500 mL High-Yield shake flask for 20 h (230 rpm; 28 °C). Batch cultivations were performed in a stainless-steel Sartorius Biostat Cplus bioreactor (Sartorius, Göttingen, Germany) with a 10 L working volume, and in an Infors Techfors-S bioreactor (Infors HT; Bottmingen, Switzerland) with a 20 L working volume. Aerobic batches were cultivated using 1000 to 1400 rpm stirrer speeds with an aeration of 2 vvm. Anaerobic batches were cultivated at 600 rpm and with a 2 to 4 L/min N_2 flow. The composition of the defined Delft medium used was as follows: 7.5 g/L $(NH_4)_2SO_4$, 14.4 g/L KH_2PO_4, 0.5 g/L $MgSO_4 \cdot 7H_2O$, 2 mL of trace metal stock, 1 mL of vitamins, 50 µL of polypropylenglycol (PPG) as Antifoam, and maltose and glucose in different concentrations as a carbon source. For the malt extract-based fermentation, a preculture with Delft media was cultivated, which was afterwards inoculated into the malt extract solution (150 g/L malt extract in deionized water; Weyermann, Bavarian Pilsner, Bamberg, Germany).

2.2. Analytical Procedures

For the DCW measurements, 1 mL of the cultivation broth was centrifuged at about 9000 g, subsequently washed with 0.9% NaCl solution, and centrifuged again. After drying the cells at 105 °C for 48 h, the pellet was evaluated gravimetrically. DCW measurements were performed in five replicates and the mean error for DCW was about 3%. Offline OD_{610} measurements were performed in duplicates in a UV/VIS photometer, Genisys 20 (Thermo Scientific, Waltham, MA, USA).

Verification of the cell viability in defined medium samples was performed using FCM measurements. After the addition of DiBAC (Thermo Scientific, Waltham, MA, USA), the diluted cultivation broth was measured using a CyFlow Cube 8 flow cytometer (Sysmex-Partec, Bornbach, Germany). DiBAC is sensitive to the plasma membrane potential, and therefore a distinction between viable and non-viable cells can be achieved. Detailed information on the viability assay can be found elsewhere [33]. The overall errors for this method were in the range of 0.5% to 1%.

Sugar concentrations in the fermentation broth were determined using a Supelco C-610H HPLC column (Supelco, Bellefonte, PA, USA) on an Ultimate 300 HPLC system (Thermo Scientific, Waltham, MA, USA) using 0.1% H_3PO_4 as a running buffer at 0.5 mL/min. Ethanol concentrations were determined using an Aminex HPLC column (Biorad, Hercules, CA, USA) on an Agilent 1100 System (Agilent Systems, Santa Clara, CA, USA) with 40 mM H_2SO_4 as a running buffer at 0.6 mL/min.

Cultivation off-gas was analyzed by gas sensors: IR for CO_2 and ZrO_2-based for O_2 (Blue Sens Gas analytics, Herten, Germany).

2.3. Impedance Measurements

Physical analysis of VCCs in state-of-the-art capacitance probes, which rely on β-dispersion (10^7–10^4 Hz), show a high dependence on process parameters (e.g., stirring, temperature, pH, salt and substrate concentration, etc.) and the cultivation phase (exponential growth phase, starvation phase,

etc.) [12,33]. We focused the measurement on a different physical phenomenon (α-dispersion), which yields valuable information mainly regarding the biomass concentration. The "α-dispersion effect", at frequencies below 10 kHz, which is most likely a result of deformation of ionic species around the cell membranes, was used for these measurements. The dielectric response was therefore proportional to the ionic charge gathered around the membrane of adsorbed cells on the electrode [20,21]. Impedance measurements were recorded in the range of 10^6 to 10^{-1} Hz with amplitudes of 100 to 250 mV using the Alpha-A high-resolution dielectric analyzer (Novocontrol, Montabaur, Germany). Because measurements in this frequency range are largely determined by the double-layer region between the electrode and the media, rather minor interferences with the process parameters (aeration and stirring) were to be expected. Online flow cells showed the benefit of a laminar flow through the cell and minor turbulence, but they generally had the problems of differences in the process state (side stream) and of performing sterilization procedures. Inline probes should overcome these problems, but they may be strongly affected by the process parameters. Details on the fitting procedure and data evaluation are given in [32].

2.4. Inline Probe Construction

As online probes are not directly situated inside the reactor but are often supplied by a side stream of the fermentation broth, changes in the metabolism in this time interval may be highly possible, but less disruption of the signal is also observed by the stirring and aeration of the system. Furthermore, online probes always pose the danger of contaminating the process, as the sterile barrier is not kept inside the fermenter. Therefore, for sterile processes without constant streams of broth, the assembly of an inline probe prototype used a commonly used 25 mm B. Braun safety port with O-ring (Ingold connector). Materials were chosen to be permanently stable at 130 °C, and could easily sustain in situ autoclavation procedures. The physical analysis of VCCs was monitored and investigated by the inline probe sketched in Figure 1.

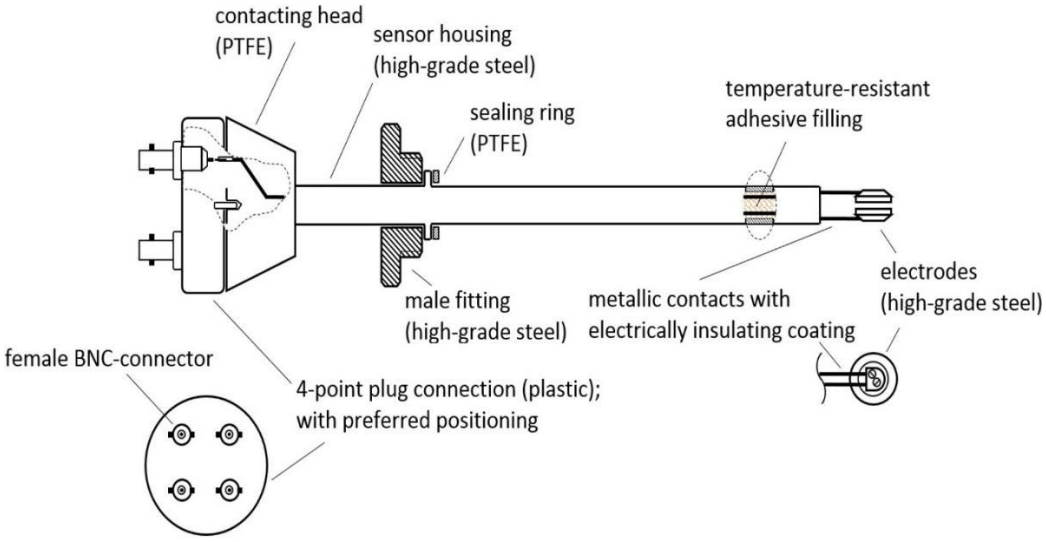

Figure 1. Sketch of the inline probe prototype indicating used materials and wiring. Connection to the impedance analyzer was performed using a four-point BNC (Bayonet Neill–Concelman) connector.

The body as well as the electrodes of the inline probe consist of high-grade steel, that is, austenitic stainless steel, which is approximately 140 mm in length and at least 12 mm in diameter. Each electrode has a diameter of 10 mm. The gap between the electrodes is approximately 2 mm.

3. Results and Discussion

3.1. Aerobic and Anaerobic Batch Cultivations in Defined Media Monitored in Online Mode

Yeast, as a well-known host for diauxic growth, was cultivated aerobically and anaerobically using different carbon sources, preliminarily present in malted barley and wheat grain. A batch-based design was used in both cultivations. Growth rates of corresponding cultivations in Figure 1 are given in Table 1. The specific growth rate describes the increase of biomass in a given time interval normalized to the biomass inside the reactor (dx/dt*1/x(t), with x being the biomass).

Table 1. Specific growth rate μ of batch phases determined by offline dry cell weight (DCW) measurements (given in Figure 1).

Cultivation	μ (1/h)
Aerobic	0.345 ± 0.04
Anaerobic	0.150 ± 0.02

3.1.1. Raw Data and General Considerations

The measured impedance raw data were analyzed by a resistance R_{DL} in parallel to a non-ideal capacitance (constant phase element) CPE_{DL} (parameter Q, n). These elements most likely originate from the double-layer region close to the electrode and can be expressed by Equation (1):

$$Z_{DL} = 1/({R_{DL}}^{-1} + (i\omega)^n \times Q_{DL}) \quad (1)$$

where ω is the arc frequency and i is the imaginary number; n and Q are obtained from a fit to experimental data. In principle, these parameters can be used to calculate the C_{DL} according to $C_{DL} = ({R_{DL}}^{1-n} \times Q_{DL})^{1/n}$.

The aerobic growth of yeast results in partial aerobic metabolism and partial fermentation, well known as the Crabtree effect. During anaerobic growth, sugars are solely fermented to ethanol. The corresponding DCW and OD of two cultivations are given in Figure 2a. During growth on a high concentration of glucose, the respiratory capacity was generally too low, and ethanol was produced simultaneously. The sugar decrease and ethanol production are given in Figure 2b, which includes the Q value of the online impedance probe. Upon sugar depletion in the fermentation broth at t = 12 h, a strong decrease in the impedance signal is observed, which corresponds to the growth on ethanol. Anaerobic growth on glucose yielded much higher ethanol concentrations (about 1.5 vol % in this run), as shown in Figure 2c. The impedance signal increased over time with a maximum upon the complete glucose depletion. Because ethanol cannot be metabolized anaerobically and accumulates in the supernatant, no change in cell metabolism, but rather a shift from exponential growth into the stationary phase, was expected. Therefore, no steep drop in the impedance signal, but a smooth decrease over several hours, was observed.

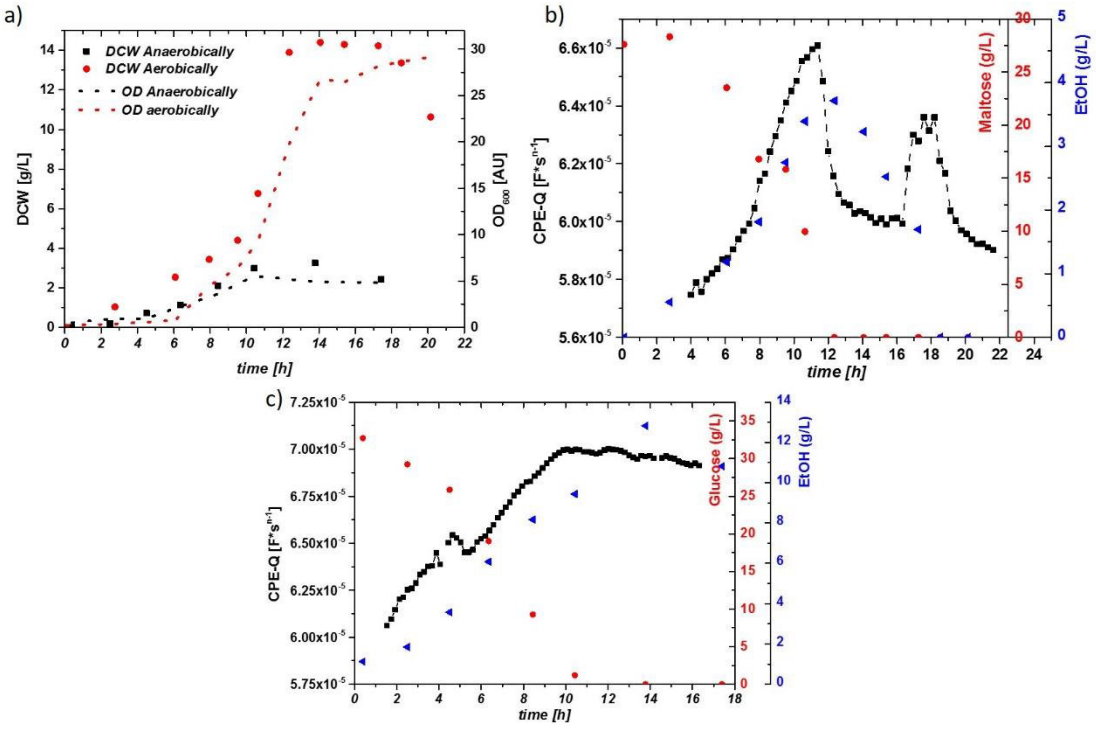

Figure 2. (**a**) Time courses of the dry cell weight (DCW; g/L) and optical density (OD; AU) for the aerobically and anaerobically cultivated *S. cerevisiae.* Corresponding μ values are given in Table 1. (**b**) Impedance signal (constant phase element-Q: CPE-Q) and maltose/ethanol concentrations over time during the aerobic cultivation. A drop in the impedance signal is visible after depletion of maltose (change in metabolism). A further small increase upon ethanol uptake can be observed, until the second carbon source was depleted. (**c**) Impedance Signal (here, CPE-Q) and glucose/ethanol concentrations during the anaerobic cultivation. No sudden decrease of the impedance signal is spotted after depletion of glucose in the media; rather, a constant decrease in the signal can be observed.

3.1.2. Aerobic Cultivations

The double-layer resistance (R_{DL}) could not be fitted accurately [32] (especially for the inline probe) as a result of the high overall fitting error, as already observed for cultivations with *E. coli.* Furthermore, n values, received from fittings with CPE elements, showed deviations dependent on the cultivation state (aerobic/anaerobic) and especially on the type of probe (inline/online). These changes in the n values made a comparison of runs difficult. For a better description of the different metabolic states, the fitting procedure was modified. For easier comparability of the performed runs, n was fixed to be 1 in the following data analysis, reflecting the idealized capacitance (C_{ideal}) of the sample.

Measured values for biomass determination (OD_{610} and DCW) were correlated to the received idealized impedance signal referred to as C_{ideal}. The corresponding data for aerobic cultivations on glucose as well as on maltose are given in Figure 3a for OD and in Figure 3b for the DCW measurement.

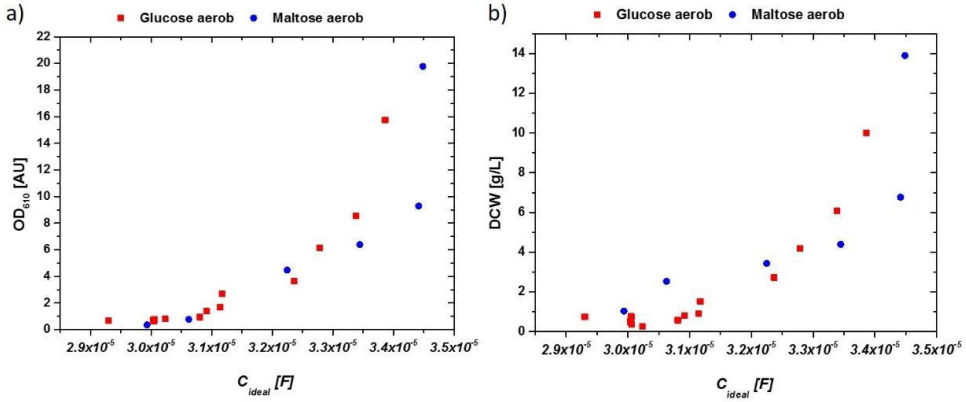

Figure 3. (**a**) OD_{610} vs. extracted capacitance of the impedance signal in aerobic cultivations with glucose and maltose. (**b**) DCW vs. extracted capacitance of the impedance signal in aerobic cultivations. Very similar responses are obtained for both cultivations, irrespective of the used C-source.

The late stage during the end of the batch cultivation showed deviations in the impedance signal as a result of metabolic changes in the system (compared to Figure 2b). Deviations between glucose and maltose may have been a result of a different sugar transportation through the membrane. Because maltose uptake is mediated by a proton-mediated symporter, a change in the counterion-cloud and therefore changes in the overall impedance would be very likely [34]. Furthermore, changes in the overall membrane structure, producing maltose-transporting proteins (maltose permease), not present in glucose-grown cells, may have changed the magnitude of the impedance signal in these cultivations. However, the impedance signal, especially at the end of the aerobic batch-phase, held valuable information on the present metabolism of *S. cerevisiae*.

3.1.3. Anaerobic Cultivations

Ethanol production may have had further effects on the impedance signal, holding information on the physiological state of the system. Sugar concentrations of up to 200 g/L showed no effect on the magnitude of the impedance signal [32]. However, growth conditions of *S. cerevisiae* may have impacted on the impedance signal. To test the impact of growth conditions, different anaerobic cultivations (ANA) were performed, according to Table 2. Oxygen from air was eliminated with a flow of nitrogen at 4 L/min through the fermenter. Gas analysis of the off-gas confirmed the absence of oxygen throughout the entire batch.

Table 2. Starting sugar concentrations in different anaerobic batch runs (ANA) extracted by high-pressure liquid chromatography (HPLC) measurements.

Cultivation	Maltose (g/L)	Glucose (g/L)
ANA1	—	32.7
ANA2	44.4	54.2
ANA3	—	22.5

Raw data for cultivations with a different sugar concentration (compared to Figure 2c), including maltose and glucose grown anaerobically, showed high ethanol concentrations, which reached a maximum of about 3 vol % in these cultivations (ANA2).

Anaerobic growth could be well described, except for very early time points, when cell densities were below the threshold of about 0.3 g/L. For inline OD measurements, very similar results could be obtained (not shown). Generally, the fits for aerobic and anaerobic cultivations are used to estimate biomass in real-time for the aerobic and anaerobic runs. As a very good linear description can

be obtained in anaerobic runs, the real-time estimation of biomass is straightforward, as shown in Figure 4a,b, after normalization to the threshold of the impedance signal.

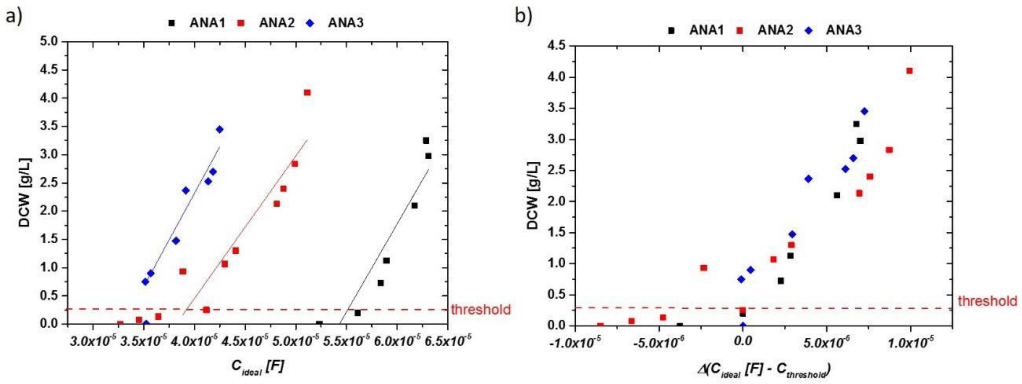

Figure 4. (**a**) Idealized capacitances of anaerobic runs exhibiting sugar concentrations of up to 100 g/L in the fermentation broth (mixture of maltose and glucose). Ethanol concentrations reached 3 vol %. Different absolute values could be found in these cultivations, but the increase of the impedance signal with DCW is very similar. (**b**) DCW vs. delta of impedance signal (ideal capacity) in the anaerobic runs. Normalization to the threshold value of about 0.3 g/L resulted in very reproducible signals for very different fermentation runs.

Using these results, DCW (half-filled circles) values are well described by the impedance signal over the process time (Figure 5a). A general quality of the fit is given in Figure 5b. The calculated DCW versus the measured DCW is situated close to the first median. Values not situated along the first median indicate the overall error in the fitting routine, compared to a residual analysis. As cell densities were very low during these cultivations, errors during the DCW measurement were about 10% of the actual mean value (highlighted for ANA2 in Figure 5b). When comparing the accuracy and threshold to those of *E. coli* cultivations, *S. cerevisiae* cultivations had a very good reproducibility for aerobic and anaerobic growth using the online impedance probe, even in the low-biomass concentration regime. A threshold of about 0.3 g/L DCW also gives a strong benefit for monitoring highly dynamic systems.

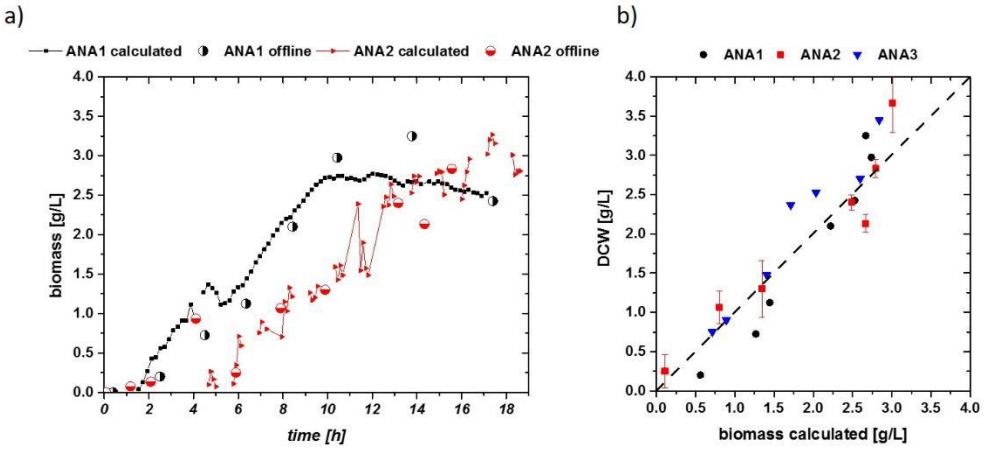

Figure 5. (**a**) Biomass calculated from the impedance signal fit extracted in Figure 4a, including offline-measured DCW values as circles. Flow cytometric measurements confirmed that no dead population is visible; thus, DCW can be compared to the viable cell concentration (VCC) in these runs. (**b**) Residual analysis of the three anaerobic runs. Despite the low cell densities, a very accurate correlation can be found in all cultivations. Error bars are exemplarily plotted for the ANA2 cultivation.

3.2. Aerobic and Anaerobic Cultivations in Defined Media Using the New Inline Probe

The impedance signal in the online mode could be used to estimate the viable cell concentrations in the aerobic and anaerobic cultivations. The newly built inline probe prototype was measured alternating to the online probe in two cultivation runs (one aerobic and the other anaerobic). Impedance raw data of the aerobic run are given in Figure 6a. Two very distinct features are visible. At higher frequencies, a shift to negative differential resistances is visible. Similar phenomena have already been observed in *E. coli* fermentations, even before inoculation of the system [32]. Further, a reduction of the capacity by an order of magnitude is observed between the online probe and the inline probe, compared to Figure 6a.

The capacitance of our almost-ideal plate capacitor design, as built in the inline and online probe, is proportional to

$$C = \varepsilon \cdot d / A \quad (2)$$

where C is the capacity (F), d the distance between the plates, ε is the dielectric constant ($\varepsilon_R \cdot \varepsilon_0$), and A is the area of the electrode. For an electrode with half the diameter, the capacitance signal should decrease by a factor of 4. Stirring and aeration of the system may have effects on the used electrode area, and may reduce the measured capacitance even more.

The extracted idealized capacitance of an aerobic run measured using the inline probe is given in Figure 6b, including process values of glucose consumption and ethanol production. Gaps in the time scale were caused by alternating measurements of the inline and online probes during the cultivation. After 1 h, an increasing signal in the capacitance was found, in accordance with measurements using the online probe. However, higher fluctuations in the signal were visible, making a smoothing of the raw capacitance signal beneficial. Smoothing was performed in the aerobic fermentation using the OriginPro 9 (Northampton, MA, USA) five-point fast fourier transformation (FFT) smoothing procedure.

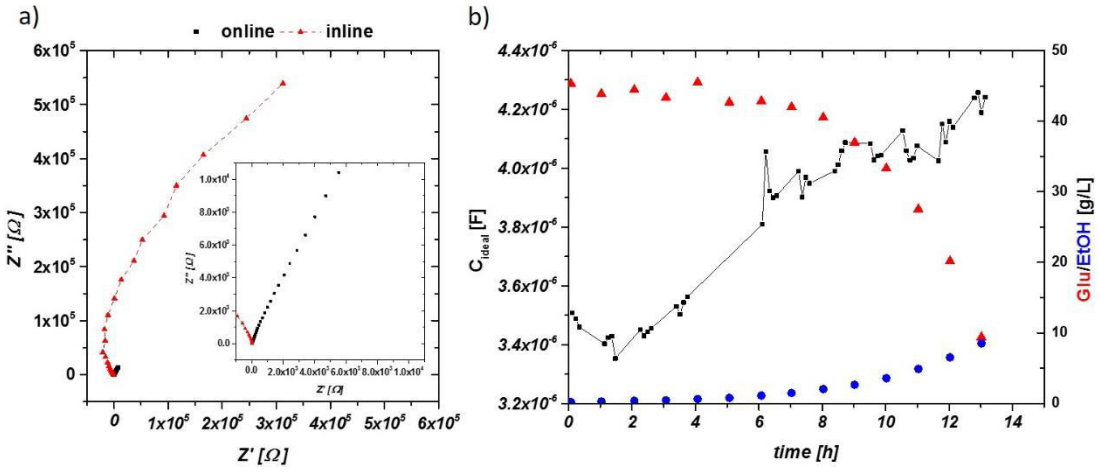

Figure 6. (**a**) Impedance raw data in the Nyquist plot for an aerobic cultivation. Black squares represent the signal from the online probe—enlarged in the inlay—and red triangles, the inline probe at similar time stages. Capacitance of the inline probe is one order of magnitude lower (as a result of smaller electrode areas). (**b**) The dependence of the impedance signal (not smoothed), glucose consumption and ethanol production in an aerobic cultivation using the inline probe.

The smoothed signals—especially for the aerobic run—were then used for fitting the biomass data. The corresponding results are given in Figure 7a. Clearly, a higher threshold for accurate data acquisition was found for the inline probe, it having the lower limit of 1 g/L DCW biomass (compared to about 0.3 g/L for the online probe). Exceeding the threshold, a good linear trend can generally be seen for the aerobic and anaerobic fermentation in both samples.

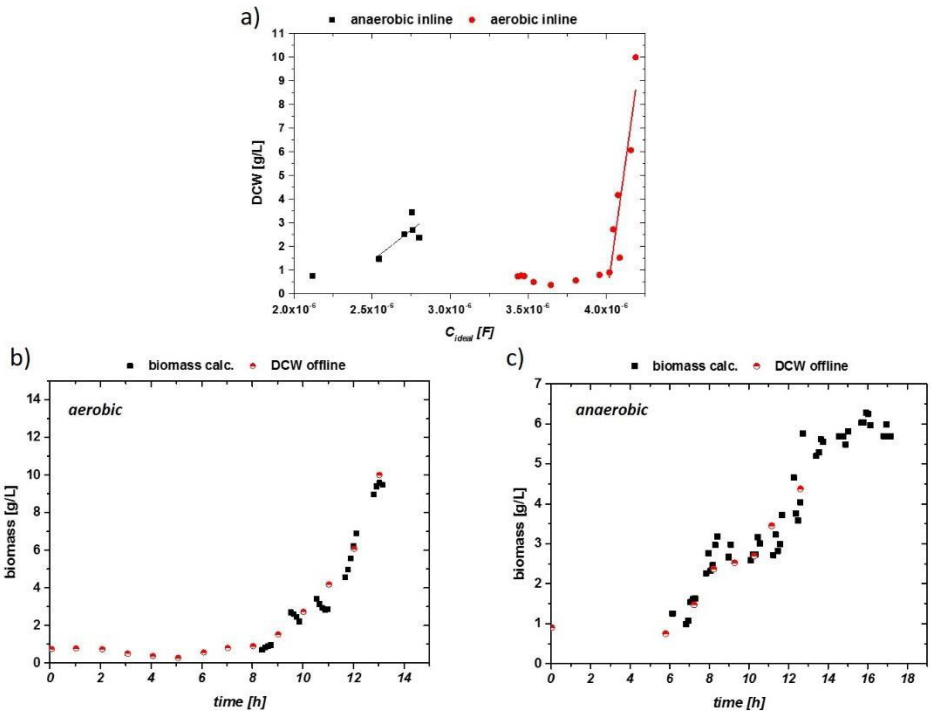

Figure 7. (**a**) Impedance signal vs. offline DCW for aerobic (circles) and anaerobic (squares) cultivations with linear fits beyond a threshold of 1 g/l DCW. (**b**) Impedance signal of aerobic run (smoothed), calculated via a linear fit into a viable biomass. This is correlated to the offline DCW. (**c**) Impedance signal vs. DCW of the anaerobic run.

The correlations of the calculated biomass compared to the offline biomass are given in Figure 7b,c. Early stages without pronounced growth could not be monitored during the cultivation. The exponential growth could be described accurately with the inline probe, despite high aeration and stirring rates. Promising results were also obtained for the anaerobic cultivation, despite higher fluctuations in the signal. For defined minimal media, the measurement with the inline probe showed reproducible, stable results in the used systems (Sartorius and Techfors with 10 to 20 L as the maximum volume of the fermenter).

Larger systems in the brewing industry, including longer residual times in the side stream, may affect the online signal and change the absolute impedance signal and slopes of the DCW versus capacitance curves. Furthermore, larger tank reactors may include inhomogeneities within the system, which have effects on the signal and have to be taken into account. As residual times in the different bypasses may result in high variations, online probes therefore should be calibrated within the measurement system. Signals of the assembled inline probe are affected by process conditions such as stirring and aeration, which results in higher fluctuations of the signal in general. An increase in the electrode area may have a beneficial impact on the stability of the signal, as absolute capacitance values are one order of magnitude lower, compared to the online probe.

3.3. Aerobic Growth of Yeast on Complex Malt Extract Medium

Defined media have the advantage of good reproducibility and easy analytics, such as OD for biomass determination and HPLC for sugar/ethanol analytics, and are therefore perfectly suited for the first development steps. However, because defined media are scarce in their use in industrial processes for yeast production, malt extract for the production of pilsner beer was used for this cultivation run. Complex media such as malt extract and molasses often have the drawback that OD measurements generally show a very high blank adsorption (especially in the IR range), and cannot easily be used online in those cultivations for the determination of the total biomass.

The performed cultivation was analyzed by HPLC and off-gas analytics to determine the end of the batch phase. HPLC data for sugar and ethanol are given in supplementary Figure S1. A mixture of different mono- and poly-saccharides was consumed during fermentation. This led to 10.6 g/L DCW and 3.2 vol % ethanol after the batch phase, at about t = 16 h. Online and inline impedance measurements were performed in the alternating mode for one cultivation. Raw data for the online impedance signal is given in Figure 8a, including information on the ethanol concentration during the cultivation. A steep increase is followed by a shoulder at about 13 h of the cultivation time, which may indicate a change in the sugar metabolism at the end of the batch phase. At process time t = 16 h, a decrease of the impedance signal is visible, generally observed for growth on ethanol. However, the decrease in the signal is rather smooth, compared to the distinct drop in defined media (Figure 2b). Interpolation of the signal and five-point FFT smoothing was performed to reduce the noise in the signal. The same procedure was performed for the inline impedance signal, given in Figure 8b. For the inline signal, a distinct decrease of the capacitance can be spotted after the end of the batch phase, which is accompanied by an increase of ethanol growth at a later process time.

The obtained smoothed and interpolated data are compared to the DCW taken and plotted in Figure 8c for the online probe and in Figure 8d for the inline probe. The slopes of the signals are very similar to extracted values for defined media samples (red/blue dots). However, an obvious shift in the signal intensity can be observed for both probes.

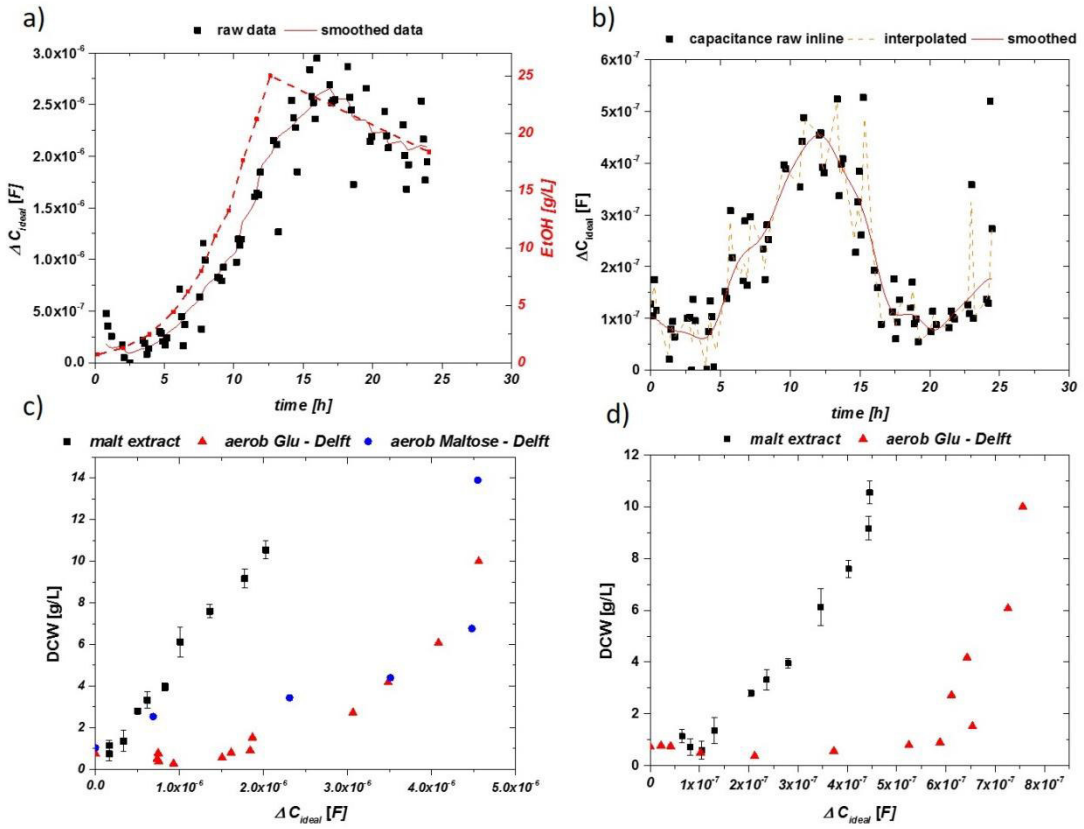

Figure 8. (**a**) Impedance signal over the cultivation time for the online probe using only malt extract as growth media. The line (orange) shows the interpolation procedure. As for related aerobic cultivation, a drop in the impedance is observed after consumption of sugars. (**b**) Impedance signal raw data, interpolated and smoothed for the inline probe. (**c**) Normalized impedance signal vs. DCW for the online probe using malt extract compared to defined media. (**d**) Normalized impedance signal vs. DCW for the inline probe using malt extract and defined media with glucose.

A linear fitting was applied to the impedance versus DCW plot in Figure 8c, and DCW was calculated through the impedance signal and compared to the offline measured signal in Figure 9. Beyond the given threshold of 1 g/L, a good description of the process could be achieved by the usage of the inline probe.

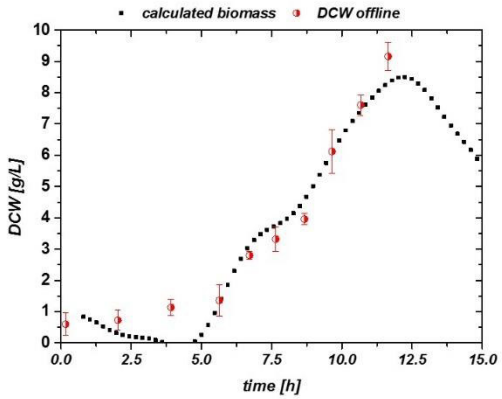

Figure 9. Impedance signal vs. DCW for the inline probe in complex medium: malt extract. A good description is found beyond 1 g/L DCW in this experiment.

On the basis of these first measurements in complex media, impedance spectroscopy at frequencies in the kHz to mHz range seems to be a promising tool for online process monitoring in yeast production processes, and possibly even in anaerobic refining processes in brewing applications. The present decrease in the signal upon complete sugar consumption is a powerful feature in terms of a stop criterion in these cultivations. An optimization of the signal-to-noise ratio, especially for the inline probe, would be beneficial for increasing the accuracy of the biomass estimation. However, tower-type reactors rather than stirred tank reactors are generally used in brewing applications because of aroma compound reasons [35]. Hence, the stirring and aeration rates used for the development were much harsher compared to those used in the industry, and therefore a much more stable signal is to be expected. Calibration of the probe may be performed once within the used system and growth media, and it should remain stable for forthcoming measurements.

4. Conclusions

New online and inline probes based on EIS at low frequencies for the measurement of VCCs for *S. cerevisiae* were tested. First, cultivations were monitored using a formerly developed online probe for pharmaceutical *E. coli* fed-batch cultivations. Batch cultivations on defined media for aerobic and anaerobic growth showed stable results, irrespective of the carbon source or concentrations. A newly assembled inline probe was tested in aerobic and anaerobic cultivations in defined media and was compared to the online probe. A good description of the biomass growth during the process was achieved. Besides the determination of the biomass during the cultivation, physiological states could be determined, depending on the respiratory condition of the cells. This measurement setup for biomass is highly beneficial, especially in complex media such as malt extract or molasses, as optical online methods cannot be used in such optically dense media. The developed system therefore shows high potential for monitoring cell growth and harvest time points for yeast- and beer-producing industries.

Supplementary Materials: The following are available online at www.mdpi.com/2227-9040/5/3/24/s1. Figure S1: HPLC data of the used pilsner malt extract at different time stages. Increase of ethanol is applicable due to late retention time in the chromatogram. Glucose and Galactose are first, afterwards the disaccharides are consumed by the cells. After consumption of all easy accessible sugars, growth on ethanol starts leading to a decrease in ethanol concentration overnight.

Acknowledgments: The authors thank the Christian Doppler Gesellschaft (CDG) for funding.

Author Contributions: C. Slouka, J. Kopp and M. Strahammer performed cultivation. G. Brunauer assembled the online and inline probes and helped during cultivation. J. Fricke, J. Fleig and C. Herwig helped with data evaluation and gave valuable input for the manuscript. C. Slouka, G. Brunauer and J. Fricke prepared the manuscript.

Conflicts of Interest: The authors declare no conflict of interest.

Abbreviation

dO_2	dissolved oxygen
C_{DL}	double layer capacitance
EIS	electrochemical impedance spectroscopy
DCW	dry cell weight
OD	optical density
VCC	viable cell concentration
AC	alternating current
CHO	Chinese hamster ovary (cells)
DiBAC	(bis-(1,3-dibutylbarbituricacid)trimethineoxonol)
HPLC	high-pressure liquid chromatography
BNC	Bayonet Neill Concelman
Z	general impedance
R	resistance
ω	arc frequency
CPE	constant phase element
ε	dielectric constant

References

1. Gavrilescu, M.; Chisti, Y. Biotechnology—A sustainable alternative for chemical industry. *Biotechnol. Adv.* **2005**, *23*, 471–499. [CrossRef] [PubMed]
2. Sagmeister, P.; Wechselberger, P.; Jazini, M.; Meitz, A.; Langemann, T.; Herwig, C. Soft sensor assisted dynamic bioprocess control: Efficient tools for bioprocess development. *Chem. Eng. Sci.* **2013**, *96*, 190–198. [CrossRef]
3. Clarke, D.; Blake-Coleman, B.; Carr, R.; Calder, M.; Atkinson, T. Monitoring reactor biomass. *Trends Biotechnol.* **1986**, *4*, 173–178. [CrossRef]
4. Kiviharju, K.; Salonen, K.; Moilanen, U.; Eerikäinen, T. Biomass measurement online: The performance of in situ measurements and software sensors. *J. Ind. Microbiol. Biotechnol.* **2008**, *35*, 657–665. [CrossRef] [PubMed]
5. Davey, H.M.; Kell, D.B. Flow cytometry and cell sorting of heterogeneous microbial populations: The importance of single-cell analyses. *Microbiol. Rev.* **1996**, *60*, 641–696. [PubMed]
6. Veal, D.; Deere, D.; Ferrari, B.; Piper, J.; Attfield, P. Fluorescence staining and flow cytometry for monitoring microbial cells. *J. Immunol. Methods* **2000**, *243*, 191–210. [CrossRef]
7. Lodolo, E.J.; Kock, J.L.; Axcell, B.C.; Brooks, M. The yeast Saccharomyces cerevisiae–the main character in beer brewing. *FEMS Yeast Res.* **2008**, *8*, 1018–1036. [CrossRef] [PubMed]
8. Schwan, H.P. Electrical and acoustic properties of biological materials and biomedical applications. *IEEE Trans. Biomed. Eng.* **1984**, *31*, 872–878. [CrossRef] [PubMed]
9. Schwan, H.P.; Foster, K.R. RF-field interactions with biological systems: Electrical properties and biophysical mechanisms. *Proc. IEEE* **1980**, *68*, 104–113. [CrossRef]
10. Yardley, J.E.; Kell, D.B.; Barrett, J.; Davey, C.L. On-line, real-time measurements of cellular biomass using dielectric spectroscopy. *Biotechnol. Genet. Eng. Rev.* **2000**, *17*, 3–36. [CrossRef] [PubMed]
11. Dabros, M.; Dennewald, D.; Currie, D.J.; Lee, M.H.; Todd, R.W.; Marison, I.W.; von Stockar, U. Cole–Cole, linear and multivariate modeling of capacitance data for on-line monitoring of biomass. *Bioprocess Biosyst. Eng.* **2009**, *32*, 161–173. [CrossRef] [PubMed]
12. Soley, A.; Lecina, M.; Gámez, X.; Cairo, J.; Riu, P.; Rosell, X.; Bragos, R.; Godia, F. On-line monitoring of yeast cell growth by impedance spectroscopy. *J. Biotechnol.* **2005**, *118*, 398–405. [CrossRef] [PubMed]
13. Carvell, J.P.; Dowd, J.E. On-line measurements and control of viable cell density in cell culture manufacturing processes using radio-frequency impedance. *Cytotechnology* **2006**, *50*, 35–48. [CrossRef] [PubMed]

14. Gerngross, T.U. Advances in the production of human therapeutic proteins in yeasts and filamentous fungi. *Nat. Biotechnol.* **2004**, *22*, 1409–1414. [CrossRef] [PubMed]
15. Buckholz, R.G.; Gleeson, M.A.G. Yeast Systems for the Commercial Production of Heterologous Proteins. *Nat. Biotechol.* **1991**, *9*, 1067–1072. [CrossRef]
16. Cereghino, G.P.L.; Cregg, J.M. Applications of yeast in biotechnology: Protein production and genetic analysis. *Curr. Opin. Biotechnol.* **1999**, *10*, 422–427. [CrossRef]
17. Konakovsky, V.; Yagtu, A.C.; Clemens, C.; Müller, M.M.; Berger, M.; Schlatter, S.; Herwig, C. Universal Capacitance Model for Real-Time Biomass in Cell Culture. *Sensors* **2015**, *15*, 22128–22150. [CrossRef] [PubMed]
18. Ehgartner, D.; Sagmeister, P.; Herwig, C.; Wechselberger, P. A novel real-time method to estimate volumetric mass biodensity based on the combination of dielectric spectroscopy and soft-sensors. *J. Chem. Technol. Biotechnol.* **2015**, *90*, 262–272. [CrossRef]
19. Ferreira, A.P.; Vieira, L.M.; Cardoso, J.P.; Menezes, J.C. Evaluation of a new annular capacitance probe for biomass monitoring in industrial pilot-scale fermentations. *J. Biotechnol.* **2005**, *116*, 403–409. [CrossRef] [PubMed]
20. Poortinga, A.T.; Bos, R.; Norde, W.; Busscher, H.J. Electric double layer interactions in bacterial adhesion to surfaces. *Surf. Sci. Rep.* **2002**, *47*, 1–32. [CrossRef]
21. Bot, C.; Prodan, C. Probing the membrane potential of living cells by dielectric spectroscopy. *Eur. Biophys. J.* **2009**, *38*, 1049–1059. [CrossRef] [PubMed]
22. Radke, S.M.; Alocilja, E.C. Design and fabrication of a microimpedance biosensor for bacterial detection. *IEEE Sens. J.* **2004**, *4*, 434–440. [CrossRef]
23. Yang, L.; Li, Y.; Griffis, C.L.; Johnson, M.G. Interdigitated microelectrode (IME) impedance sensor for the detection of viable Salmonella typhimurium. *Biosens. Bioelectron.* **2004**, *19*, 1139–1147. [CrossRef] [PubMed]
24. Liu, J.; Li, H.; Zhang, F.; Li, X.; Wang, L.; Chen, Y. Online impedance monitoring of yeast cell culture behaviors. *Microelectron. Eng.* **2011**, *88*, 1711–1713. [CrossRef]
25. Lei, K.F. Review on impedance detection of cellular responses in micro/nano environment. *Micromachines* **2014**, *5*, 1–12. [CrossRef]
26. Yang, L.; Ruan, C.; Li, Y. Detection of viable Salmonella typhimurium by impedance measurement of electrode capacitance and medium resistance. *Biosens. Bioelectron.* **2003**, *19*, 495–502. [CrossRef]
27. Gonzalez, J.; Santana, A.F.; Mirza-Rosca, J. Effect of bacterial biofilm on 316 SS corrosion in natural seawater by EIS. *Corros. Sci.* **1998**, *40*, 2141–2154. [CrossRef]
28. Bayoudh, S.; Othmane, A.; Ponsonnet, L.; Ouada, H.B. Electrical detection and characterization of bacterial adhesion using electrochemical impedance spectroscopy-based flow chamber. *Colloids Surf. A* **2008**, *318*, 291–300. [CrossRef]
29. Wu, J.; Ben, Y.; Chang, H.-C. Particle detection by electrical impedance spectroscopy with asymmetric-polarization AC electroosmotic trapping. *Microfluid. Nanofluid.* **2005**, *1*, 161–167. [CrossRef]
30. K'Owino, I.O.; Sadik, O.A. Impedance spectroscopy: A powerful tool for rapid biomolecular screening and cell culture monitoring. *Electroanalysis* **2005**, *17*, 2101–2113. [CrossRef]
31. Kim, Y.-H.; Park, J.-S.; Jung, H.-I. An impedimetric biosensor for real-time monitoring of bacterial growth in a microbial fermentor. *Sens. Actuators B* **2009**, *138*, 270–277. [CrossRef]
32. Slouka, C.; Wurm, D.J.; Brunauer, G.; Welzl-Wachter, A.; Spadiut, O.; Fleig, J.; Herwig, C. A Novel Application for Low Frequency Electrochemical Impedance Spectroscopy as an Online Process Monitoring Tool for Viable Cell Concentrations. *Sensors* **2016**, *16*, 1900. [CrossRef] [PubMed]
33. Langemann, T.; Mayr, U.B.; Meitz, A.; Lubitz, W.; Herwig, C. Multi-parameter flow cytometry as a process analytical technology (PAT) approach for the assessment of bacterial ghost production. *Appl. Microbiol. Biotechnol.* **2016**, *100*, 409–418. [CrossRef] [PubMed]
34. Weusthuis, R.A.; Pronk, J.T.; Van Den Broek, P.; Van Dijken, J. Chemostat cultivation as a tool for studies on sugar transport in yeasts. *Microbiol. Rev.* **1994**, *58*, 616–630. [PubMed]
35. Okabe, M.; Katoh, M.; Furugoori, F.; Yoshida, M.; Mitsui, S. Growth and fermentation characteristics of bottom brewer's yeast under mechanical stirring. *J. Ferment. Bioeng.* **1992**, *73*, 148–152. [CrossRef]